METAL-BASED COMPOSITE MICROCAPSULE SHELLS: DEVELOPMENT OF NEW SYNTHESIS METHODS AND CHARACTERISATION OF TRANSPORT PROPERTIES

Assim Fiaz

Submitted in accordance with the requirements for the degree of

DOCTOR OF PHILOSOPHY

The University of Leeds

School of Chemical and Process Engineering

March 2019

The candidate confirms that the work submitted is his/her/their own, except where work which has formed part of jointly authored publications has been included. The contribution of the candidate and the other authors to this work has been explicitly indicated below. The candidate confirms that appropriate credit has been given within the thesis where reference has been made to the work of others.

The following publication has been a result of this research and formed part of the following chapter to the Thesis.

Chapter 4:

Stark, K., Hitchcock, J. P., **Fiaz, A.**, White, A. L., Baxter, E., Biggs, S. R., & Cayre, O. J. (2019). Encapsulation of emulsion droplets with metal shells for subsequent remote, triggered release. ACS applied materials & interfaces.

Acknowledgements

I would like to start by firstly thanking my supervisor Dr Olivier Cayre for giving me this opportunity to work on this fascinating project, for his guidance, support and feedback throughout my PhD. Additionally, I would like to thank the EPSRC and Procter & Gamble for the funding towards the project, without which it would not have been possible.

Additionally, I would like to thank a number of people within the School of Chemical and Process Engineering, including those within the Colloids and Polymer Engineering group, LEMAS and Energy. In particular, I would like to express my gratitude towards all the people I have met along the way that I have become privileged enough to call my friends.

Finally, I would like to thank all my family and friends, especially my mum and dad for providing me with the opportunity to attain the best education possible, for supporting me throughout my PhD and for always being there.

Abstract

In this study platinum nanoparticles (Pt-NPs) and silica/platinum composite (Si/Pt) stabilised oil-in-water emulsions (low molecular weight oil core) have been investigated for the reduction, catalytic activity and deposition of a secondary metal film via electroless plating, resulting in gold coated emulsion droplets. Colloidal silica stabilised emulsion droplets have been coated in poly(dopamine) (PDA) resulting in core-shell microcapsules where the shell is a binary mixture of polymer and particles. Subsequently the PDA microcapsule surface has been used for the deposition of a silver shell on the surface via electroless plating of silver ions initially adsorbed to the PDA microcapsule shells.

The microcapsules have been tested for active core retention and shell permeability, by introducing the microcapsules to a continuous phase of ethanol/water (volume ratio 4:1) in which the active core is completely soluble and measuring the core release by utilising gas chromatography. The gold coated emulsion droplets (Pt-NPs and Si/Pt) completely retained the active core for over 30 days at 40^{o}C, demonstrating the retention of the core and permeability of the gold shell. The silver coated PDA microcapsules released most of the core after 1 hour due to the in-sufficient coverage of the PDA surface with silver.

The microcapsules were also tested for encapsulating phase change materials (PCM) resulting in MicroEncapsulated PCM (MEPCMs). The MEPCMs were tested for thermal energy storage and release for home comfort. Analysis on the MEPCMs properties such as supercooling, encapsulation efficiency and thermal conductivity was also carried out. Gold coated emulsion droplet (Pt-NPs and Si/Pt), demonstrated good encapsulation efficiencies and ratios, which demonstrated the good ability of the

MEPCMs to store and release thermal heat. The gold coated emulsion droplets also demonstrated reduced supercooling and enhanced thermal conductivity.

Abbreviations

ELP Electroless plating

GC Gas chromatography

IFT Interfacial tension

MEPCMs Microencapsulated phase change material

NP nanoparticles

PCMs Phase change materials

PDA Polydopamine

Pt-NPs Polyvinypyrrolidone stabilised platinum nanoparticles

PVP Polyvinylpyrrolidone

SEM Scanning electron microscopy

Si/Pt Silica platinum composites

TEM Transmission electron microscopy

UV-vis Ultraviolet-visible

Nomenclature

A Surface area (nm^2)

β Shape factor (-)

C Active concentration (mM)

D Diffusion coefficient ($cm^2.s^{-1}$)

g Gravitational constant ($m^3 \cdot kg^{-1} \cdot s^{-2}$)

H Partition coefficient (-)

k Boltzmann constant ($J \cdot K^{-1}$)

n Viscosity ($Pa \cdot s$)

Φ Oil volume fraction (-)

P_c Polymer chain length (nm)

r Particle radius (nm)

R_g Radius of gyration (nm)

T Temperature (°C)

y Interfacial tension (mN/m)

ΔP Pressure (Pa)

P_{in} Pressure Internal (Pa)

P_{out} Pressure External (Pa)

θ Contact Angle (^{O})

ΔE Detachment Energy (J)

ΔH Enthalapy/energy (J/g)

Contents

List of Figures

1 Introduction

Microencapsulation of functional or non-functional materials and chemically or biologically active ingredients is of a great interest to chemical industries ranging from home and personal care, pharmaceuticals, energy and construction. [1-3]

Microencapsulation is described as a process of enclosing micron-sized particles of solids or droplets of liquids or gasses in a shell, which in turn isolates and protects them from the external environment.[4] The material inside the microcapsule is referred to as the core, internal phase, or fill, whereas the wall is sometimes called a shell, coating, or membrane. Most microcapsules have diameters between a few micrometres and a few millimetres.[5] The main role of the microcapsule is to isolate its core material from its surrounding and act as a barrier between the core and exterior environments. This is done:

- To protect reactive substances from the environment such as vitamins from oxygen and moisture.[3]
- To prevent the evaporation of volatile actives, such as fragrances.[6]
- To mask undesired properties of actives, such as undesirable smells.[7]
- To protect the environment from the actives, such as having an enzyme or an initiator as the active.[8]
- To control the release of the active, such as fragrance capsules in laundry for fresh lasting clothes.[9]
- To improve efficacy and reduce toxicity in drug delivery.[10]

Microencapsulation allows the controlled release and targeted delivery of the encapsulate. The trigger for release varies from mechanical rupture for polymer microcapsules containing fragrance, temperature change for phase change materials, to electrolyte concentration and pH change for drug delivery.

The driving force behind this project is the challenging task that remains unsolved, with current technologies of encapsulation and full retention of small volatile active ingredients. The focus of this project will be on microencapsulating low molecular weight oils/fragrances for use in perfumes. Perfumes consist of ~70% alcohol and ~30% low molecular weight oils/fragrance. Due to their volatility fragrances will evaporate in a matter of minutes. For this reason, it is desired to encapsulate low molecular weight oils/perfumes to delay the release of these volatile components.

When attempting to encapsulate in difficult environments (alcohols) where the continuous phase is able to fully dissolve the encapsulated active (low molecular weight oils/fragrances), will result in the full release of the core over a much shorter time, significantly reducing the lifetime of the product. This is due to the porosity of polymeric membranes, across which small volatile actives are able to diffuse. Polymer membranes are also soluble in alcohols resulting in the full release of the microcapsule content in the continuous phase.

Fickian law of diffusion is used to describe the diffusion rate of an active ingredient across a membrane as a function of time. Equation 1.1, can be used to describe the parameters effecting the retention of low molecular weight/fragrance oils. [11]

$$d_c/_{d_t} = A * H * D \frac{C_{int} - C_{ext}}{x} \quad 1.1$$

Where:

A = surface area

H = Partition coefficient

D = Diffusion coefficient

C = Active concentration

x = Shell thickness

The partition coefficient H, defines the solubility of the core in the shell material, and diffusion coefficient D, describes the diffusion of the core phase through the shell material. When encapsulating low molecular weight oils/perfumes with polymer membranes the high partition coefficient and high diffusion coefficient, result in most techniques inappropriate to achieve full retention of perfumes.[11] For highly volatile actives polymer membranes produce diffusion coefficients in the order of 10^{-8} $cm^2.s^{-1}$, with the addition of the solubility of the core in the continuous phase renders it impossible to retain the core material, such as low molecular weight oils/perfumes.[12] Upon storage highly volatile components are loss over time thus reducing the olfactory performance.[9] To overcome these disadvantages the microcapsule walls require, being impermeable to small volatile components, such as low molecular weight oils/perfumes, this can be done by lowering the diffusion coefficient and partition coefficient to drastically slow down the leaching in these condition.

To overcome these undesired properties metal coated microcapsules are of a particular interest. Metal encapsulated low molecular weight oils/fragrances can have an improved shelf life. A shell consisting of a continuous metal barrier can provide reduced permeability, greater barrier properties as metal permeability is much lower

than that of polymers due to their crystalline structure. The diffusion coefficient for highly volatile actives is very low when using metals (10^{-15} $cm^2.s^{-1}$ for hydrogen atoms diffusing across a metal membrane). It is possible for atomic species to permeate across a metal membrane, but larger hydrocarbon chains are unable to permeate through the lattice.[13]

At the University of Leeds metal microcapsules have been synthesised containing low molecular weight oils/fragrance which are impermeable to small volatile molecules offering improved protection. Metal NPs stabilised with PVP have been applied to stabilise an emulsion (o/w), absorbing at the interface and catalysing the deposition of a continuous metal film. This has resulted in greater barrier properties of metals compared to polymers, resulting in metal films preventing the permeation of small volatile components and increasing shelf life.[11, 13]

My project aims to build on this work, by analysing the parameters and procedure steps effecting the metal microcapsule formation and properties. To optimise the process in terms of efficiency, applications and cost effectiveness. The project will concentrate initially on microcapsules for use in personal care, as additives to perfumes. The microcapsules need to be robust and stable over time. They need to withstand harsh environments such as alcohol carrier phases and also release their content only when required on the skin.

The project will also analyse microencapsulated phase change materials (MEPCMs) for energy storage and release in building material applications. The heat transfer properties of metal-shell microcapsules will be analysed and quantified.

This project will also aim to remove the use of intermediate NPs, due to strict EU regulations on uses of NPs in personal care. Other methods or techniques will be required to deposit metallic shells without metal NP intermediates. Other areas of interest include:

1. The deposition and reduction of metal ions onto silica surfaces, which in turn can be used to stabilise a Pickering emulsion and used to catalyse/nucleate the growth of a metallic film.
2. The synthesis of polydopamine (PDA) on silica stabilised Pickering emulsions, resulting in PDA microcapsules. Inherently the PDA surface can be used to deposit metal shells via electroless plating on the poly dopamine microcapsules due to its metal binding ability.

1.1 Thesis Structure

Chapter 2 provides a background, literature review, aim and objectives. Chapter 3 contains the materials and methodologies section. Chapter 4 focuses on synthesising and characterising gold coated Pt-NP stabilised emulsions and analysing the parameters affecting the gold microcapsule formation and properties. Chapter 5 will focus on removing the Pt-NP intermediates by forming Si/Pt composites which will be used to stabilise Pickering emulsions and subsequently gold coated via electroless plating. Chapter 6 will focus on completely removing nanoparticle intermediates by synthesising PDA microcapsules which will inherently be used to deposit a silver shell via electroless plating on the PDA microcapsules due to its metal binding ability. Chapter 7 will give an introduction and literature review on PCMs and Microencapsulated PCMs (MEPCMs) for thermal energy storage and release. The different methods described in chapter 4, 5 and 6 to synthesise metal coated microcapsules will be used to encapsulate PCMs (hexadecane) resulting in MEPCMs, which will be compared for thermal energy storage/release for home comfort/building applications.

2 Principles of microencapsulation systems and literature review

The following section will consist of describing emulsions, factors effecting emulsion stability and how to stabilise emulsions via surfactants, polymeric stabilisers and colloids. These steps are very important in forming and maintaining a stable emulsion for metal electroless plating. This will be followed by describing microcapsules and the possible microcapsule morphologies followed by methods of encapsulation including chemical, physical and mechanical. The final section will consist of a description of low molecular weight oils/fragrances followed by a description on available microencapsulated low molecular weight oils/fragrances.

2.1 Emulsions

An emulsion can be described as a mixture of two or more liquids, which are immiscible, where one immiscible liquid is dispersed as fine droplets in another. Emulsions can also be described as colloidal dispersion, which contain a continuous phase normally water and a dispersed phase normally oil. From systems consisting of water and oil, it is possible to form three types of emulsions: oil in water (O/W), water in oil (W/O) and a multiple emulsion which consists of smaller droplets inside the dispersed phase such as water in oil in water (W/O/W) or oil in water in oil (O/W/O).[14] The following chapter will initially consist of describing how to form emulsions and emulsion stability, as stable emulsion are required to form colloidosomes or microcapsules which will be described later in this chapter.

2.1.1 Emulsion Stability

Emulsion stability greatly influences the process of forming colloidosomes or microcapsules, without stable emulsions the process of forming colloidosomes or microcapsules would not be possible. Emulsions are thermodynamically unstable systems, this is due to the energetically unfavourable contact between the immiscible liquid interfaces which needs to be minimised.[15, 16] Destabilisation of the emulsion can result from creaming, sedimentation, flocculation, coalescence, phase inversion and Ostwald ripening, these processes can be kinetically slowed with the addition of stabilisers.

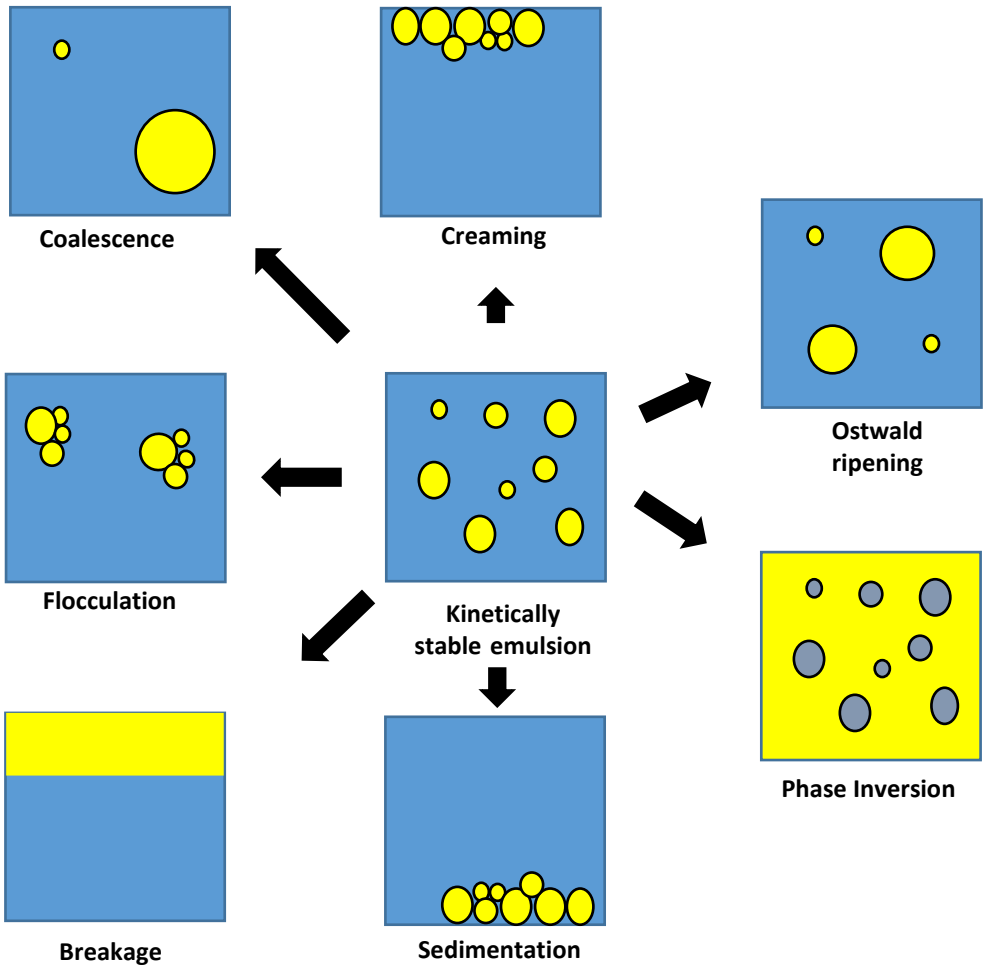

Figure 2.

Figure 2. 1: Schematic illustration of processes that cause instabilities in emulsions.

2.1.2 Creaming and sedimentation

Creaming and sedimentation is due to the density differences between the emulsion droplets compared to the continuous phase liquid surrounding them. When thermal motion forces (Brownian motion) acting on the droplet are exceed by the gravitational forces, this will result in the emulsion either to cream (if the density is lower than the continuous phase) or sediment (if the density is higher than the continuous phase).[17] The creaming and sedimentation rate can be controlled by matching the density of the immiscible liquids, or increasing the viscosity of the dispersed phase or by reducing the average droplet size resulting in an increase in Brownian motion.

The relationship between the creaming or sedimentation rate can be defined by the Stokes law (dilute systems) as shown in Equation 2.1:[18]

2.1

$$U_{stokes} = -\frac{2gr^2\ (p_2 - p_1)}{9n_1}$$

where U_{stokes} is the creaming or sedimentation velocity, (if the value is positive the emulsion droplets will cream and if negative the emulsion will sediment), g is the gravitational acceleration (9.81 ms^{-2}), r is the particle radius, n is the viscosity of the continuous phase, p_1 is the density of the continuous phase and p_2 is the density of the dispersed phase. In concentrated emulsions, Stokes law can only be used as an approximation, as the sedimentation/creaming is hindered and influenced by the motion of the surrounding droplet and is not independent.

2.1.3 Flocculation and Coalescence

Droplet flocculation and coalescence result from the collisions between emulsion droplets. Droplets collide with each other, as they are in constant motion due to external mechanical forces, Brownian motion (thermal energy) and gravitational separation. As the droplets collide with each other, they either move away or remain together aggregated due to the attractive and repulsive forces acting on them. Flocculation is the direct result when droplets collide and the van der Waals attractive forces overcome the repulsive forces resulting in droplet aggregates to form.[19]

Coalescence results from the merging of two droplets with each other upon colliding, to form a single large droplet. As the droplets collide the contact zone deforms and flattens, resulting in the droplets to merge as the interstitial film between the two phases interact via van der waals forces, which cause the film to drain and become unstable due to thermal fluctuations.[20] The interaction forces acting over the contact area are known as the disjoining pressure. A negative disjoining pressure will lead to the film rupturing, causing the droplets to merge whilst a positive disjoining pressure will lead to a stable film. This results as it is thermodynamically favourable to decrease the contact area between the oil and water phases.

2.1.4 Ostwald ripening

Ostwald ripening is an observed phenomenon, which is thermodynamically driven and results due to the chemical potential differences between small and large droplets. Larger droplets grow at the expense of smaller droplets as larger droplets are more energetically favoured over smaller droplets.[21]

The Ostwald ripening process is driven by the difference in Laplace pressure,ΔP, between droplets of different radii, Equation 2.2:

2.2

$$\Delta P = P_{in} - P_{out} = \frac{2_y}{r}$$

Where P_{in} denotes the pressure inside the droplet, P_{out} the pressure outside the droplet, y is the interfacial tension and r is the droplet radius.

The pressure difference is higher in smaller droplets, resulting in the oil phase being forced out to join larger droplets. Ostwald ripening can be controlled by

- controlling the droplet size and size distribution
- reducing the interfacial tension
- controlling the composition of the droplet to limit large differences in chemical potential (solubility)

2.2 Emulsifiers

Immiscible liquids do not mix together; emulsifiers are surface active agents which are kinetically used to stabilise emulsions. Emulsifiers adsorb onto the interface between the two immiscible liquids and form a protective membrane which prevents the droplets from aggregation and coalescence. The main type of emulsifiers for stabilising emulsions are surfactants polymers and particles (Pickering emulsions).[19]

2.2.3 Surfactants

Surfactants are usually organic compounds that are amphiphilic, containing both hydrophobic and hydrophilic properties. The hydrophilic head interacts with polar solvents (water) and the hydrophobic tail interacts with non-polar solvents (oil). Surfactants stabilise emulsions by diffusing to the interface, adsorbing onto the interface and lowering the interfacial tension at the oil-water interface forming a barrier, which prevents the droplets from coalescence for a reasonable period of time.[22]

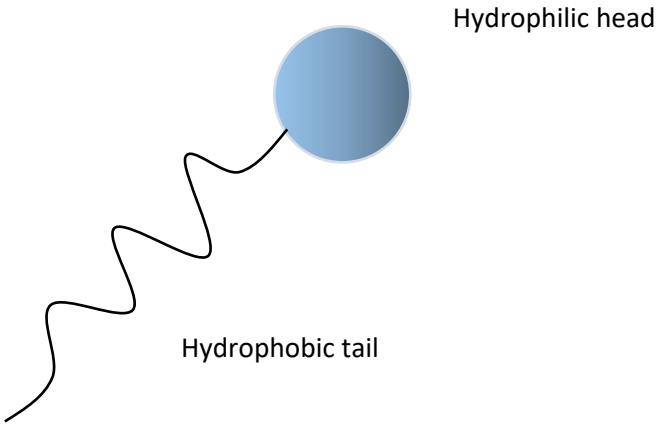

Figure 2.

Figure 2. 2: Illustration of a surfactant molecule consisting of a hydrophilic head and a hydrophobic tail.

2.2.4 Polymeric stabilisers

Polymers are able to stabilise emulsions both sterically and electrostatically. To effectively provide steric stabilisation the polymer must be amphiphilic having both hydrophobic and hydrophilic segments which can bind strongly at the interface and segments which protrude into the surrounding liquids, forming a physical barrier which prevents contact and coalescence. For example, high-molecular-weight polymers can adsorb at emulsion interfaces and extend significantly into the continuous phase, providing a physical barrier for emulsion droplet interactions. Some polymeric stabilisers are charged and are also able to electrostatically stabilise emulsions.[23, 24]

2.2.5 Colloidal particles

Colloidal particles can also be used as emulsifiers, by behaving similarly to surfactants and adsorbing onto the interface. The relative parameter of particles at the interface is thought to be the three phase contact angle θ. The contact angle is measured between the tangents to the solid particle surface and the interface. The Young's equation describes the contact angle, Equation 2.3:[25]

2.3

$$cos\theta = \frac{\gamma_{po} - \gamma_{pw}}{\gamma_{ow}}$$

γ_{po} = interfacial tension at the particle-oil interface

γ_{pw} = interfacial tension at the particle- water interface

γ_{ow} = interfacial tension at the oil-water interface

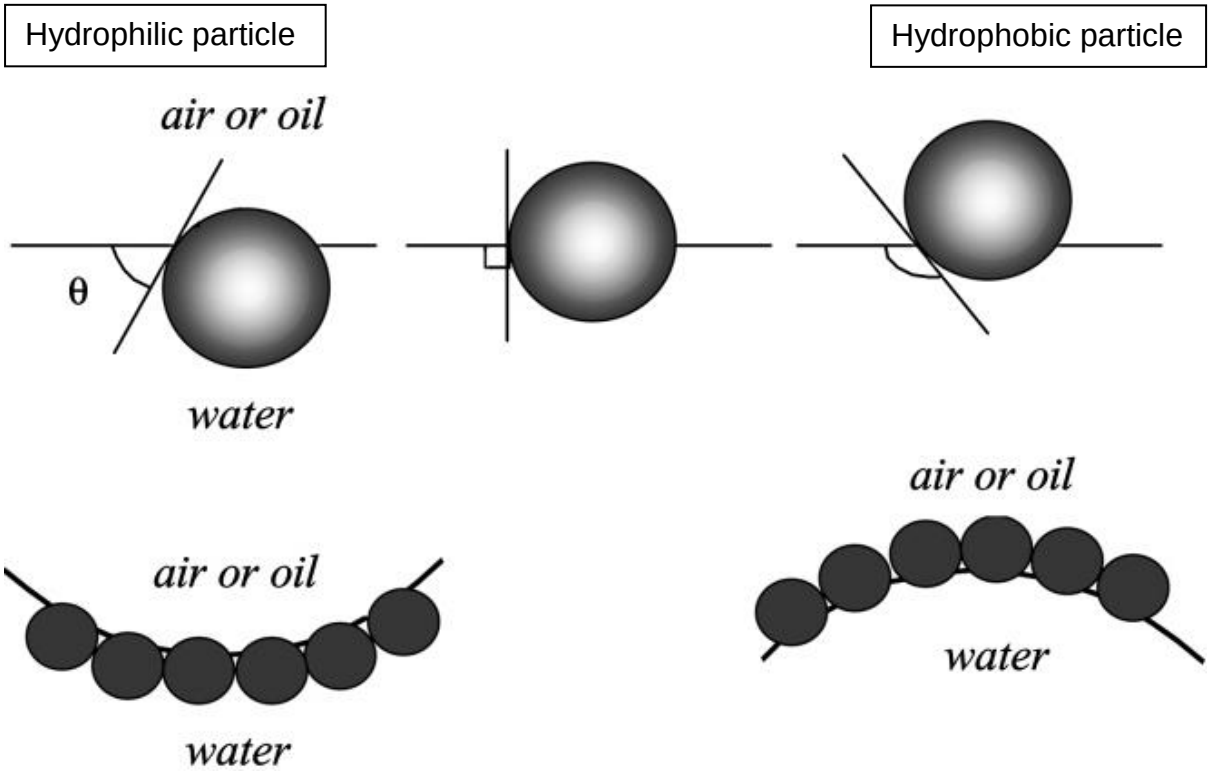

Figure 2. 3: (Upper) Position of silica spherical particles at a planar fluid-water interface for a contact angle, less than 90° (left), equal to 90° (centre) and greater than 90° (right). (Lower) Corresponding probable positioning of particles at a curved fluid-water interface. For $\boldsymbol{\theta}$ < 90° solid-stabilised aqueous foams or oil in water emulsions may form (left). For $\boldsymbol{\theta}$ > 90° solid-stabilised aerosols or water in oil emulsions may form (right). [25]

For hydrophilic particles which will be wetted by the water ($\gamma_{po} > \gamma_{pw}$) the contact angle will be <90°, for hydrophobic particles wetted by oil ($\gamma_{po} < \gamma_{pw}$) the contact angle will be >90°.[26]

Once adsorbed at the interface colloidal particles are trapped due to the large adsorption energy for particles at the oil water interface and require a high energy input to remove them from the interface (desorption). Equation 5.2 describes the detachment energy ΔE required to remove the particle from the interface:

$$\Delta E = \pi a^2 y_{ow}(1 \pm cos\theta)^2$$

2.4

a = the radius of the particle

y_{ow}= the oil-water interfacial tension

θ= the three phase contact angle

Once a particle is adsorbed at the oil water interface, a certain area of the interface is substituted by an equivalent area of the particle (cross-sectional area). The energy required to remove the particle from the interface is related to the particle contact angle θ, the particle radius a and the oil-water interfacial tension y_{ow}. The sign inside the bracket is negative for particle removal into a water phase and positive for particle removal into the air or oil phase. [26] For a micrometre sized particle at the oil-water interface with a contact angle of ~90°, the detachment energy is on the order of 10^7 k_BT.[27]

From equation 5.2 apart from the contact angle (wettability) the detachment energy ΔE is also effected by the particle radius. Assuming the y_{ow} = 50mN m^{-1} and θ = 90º, the relationship between desorption energy and particle radius is shown in figure 5.2, with increasing particle radius results in an increase in the energy of detachment. In chapter 4 Pt-NPs 2.9 nm (+/-0.4) were used to stabilise oil in water emulsions, the detachment of the particles from the interface compared to larger particles ~100nm would acquire less energy, resulting in less stable emulsions.

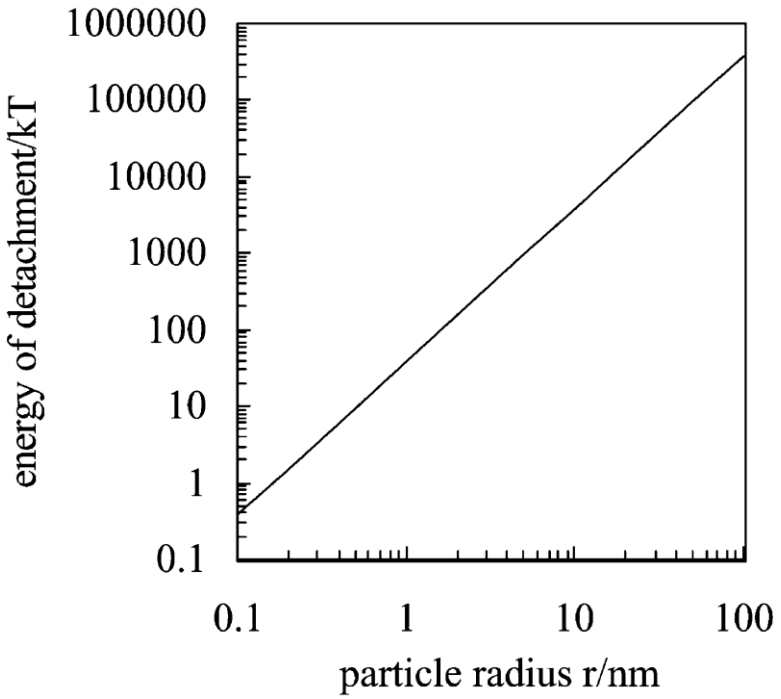

Figure 2. 4: Variation of energy required to remove a single spherical particle ($\boldsymbol{\theta}$ = 90°) from a planar oil-water interface ($\boldsymbol{y_{ow}}$ = 50mN m^{-1}) with particle radius at 298 K.[26]

2.3 Microcapsules

Microencapsulation is described as a process of enclosing micron-sized particles of solids or droplets of liquids or gasses in an inert shell, which in turn isolates and protects them from the external environment.[4] The material inside the microcapsule is referred to as the core, internal phase, or fill, whereas the wall is referred to as the shell, coating, or membrane. Most microcapsules have diameters between a few micrometres and a few millimetres.[5]

The following sections will describe different methods of encapsulation, the chemical/physical and mechanical properties of the resulting microcapsules and their morphologies. In particular, a brief summary describing the methods used to encapsulate low molecular weight oil and fragrances will be provided along with a description of their advantages and disadvantages.

2.3.1 Morphologies of microcapsules

The morphology of microcapsules is dependant mainly on the core material and deposition process of the shell. The three main basic type of microcapsule morphologies (figure 2.4) are mononuclear (core shell) microcapsules, polynuclear microcapsules have many cores entrapped within the microcapsule shell and matrix microcapsules which have the core material distributed homogenously into the shell material. It is also possible to have variations of mononuclear microcapsules, with multiple shells or clusters of microcapsules.[4]

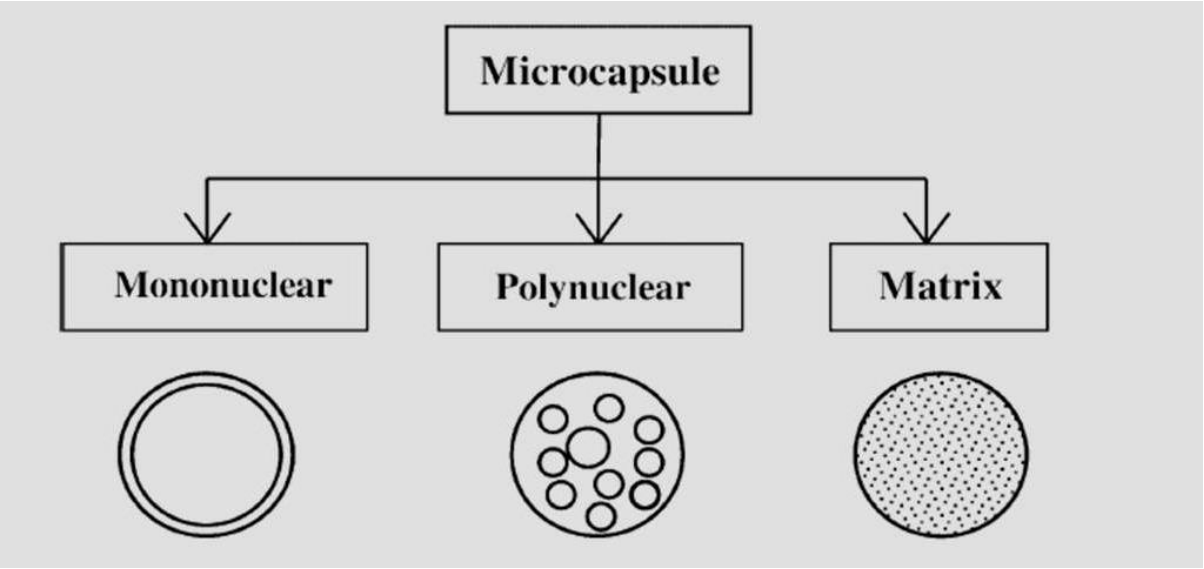

Figure 2. 5: Morphologies of microcapsules

2.4 Methods of Encapsulation

2.4.1 Chemical and Physical Methods of Encapsulation

2.4.1.1 Coacervation

Coacervation is the separation into two liquid phases in colloidal systems. The phase more concentrated in colloid component is known as the coacervate and the other phase is the equilibrium solution. If there is an electrostatic attraction this will cause associative phase separation of the two polymers in water. Complex coacervation is

caused by the interaction of two oppositely charged colloids. The gum arabic-gelatine system has been studied extensively and was first applied in the patent on carbon-less copying paper.[28] Coacervation can be simple or complex. Simple coacervation involves only one type of polymer with the addition of strongly hydrophilic agents to the colloidal solution and for complex coacervation; two or more types of polymers are used.[29]

Coacervation process consists of: formation of an aqueous solution of gelatine (simple coacervation), gum arabic (complex coacervation) and NaOH and maintained at 50^{o}C. The pH is gradually lowered to 4.5 and the core material (oil) is added. Coacervates form microcapsules around the core material (positively charged gelatine and negatively charged gum arabic) depositing around the oil droplets. The microcapsules are cooled which harden and are cross-linked with glutaraldehyde. Kruif, Veis, Overbeek and Piacentine described the coacervation process.[30-32]

The main uses of the coacervation technique are to encapsulate essential oils containing pigments and dyes. Essential oils are not very volatile such as fragrances oils, so are more suited to this technique. The main uses of the microcapsules produced are for visual effects, such as for uses in body lotion to give an overall appeasing look.

Coacervation process has its disadvantages when encapsulating fragrances and low molecular weight oils. In the formation process volatile components of the fragrance will be lost. The barrier properties of the capsules are poor. The capsules also have a short shelf life and are prone to bacterial growth. And also harmful residual of the

crosslinking agent glutaraldehyde can be present. Coacervation process also has ethical issues raised, as it applies the usage of animal derivatives such as gelatine.

2.4.1.2 Polymerisation induced phase separation (PIPS)

PIPS require a monomer and initiator (most likely oil soluble) added and dispersed to the oil phase of the oil/water emulsion. Initiation is most likely caused by a heat source. As the polymerisation proceeds, the increasing molecular weight of the polymer chain results in the polymer chains becoming less soluble in the oil phase/monomer. As the polymer chains grow, polymer rich regions are present in the oil phase which precipitates to the interface resulting in shell formation. The build-up of interfacial tension decreases the permeability of the continuous phase/water into the core.[33]

Mistry, *et al.,* described the process of producing cationized hydrogel microcapsules using the PIPS technique. Mistry, *et al.,* [34] produced cationic amine based polymer shelled microcapsules with an oil/fragrance core. As the microcapsules carried a cationic charge this increased their attraction towards fabrics, hence increasing the amount of capsules depositing on clothes during the washing cycle. The release mechanism for these microcapsules was physically rupture.

When applying the PIPS method to encapsulate fragrance, undesired side reaction can occur, such as side reactions between monomers with several reactive functionalities of fragrances components. Also as monomers and initiators are used in the process, residual monomer and initiator and also harmful by products can be present in the final product.[35]

2.4.1.3 Internal phase separation- Solvent extraction and evaporation

In the solvent extraction method, microcapsules are produced by phase separation of the polymer from within the oil in water emulsion. The oil phase consists of the polymer which forms the shell, dissolved in a volatile solvent (good) and a non-volatile solvent (poor). As the volatile substance evaporates, the polymer precipitates and forms polymer rich regions. Gradually if the balance of interfacial tension is correct the polymer rich regions precipitate to the interface forming a shell.[36]

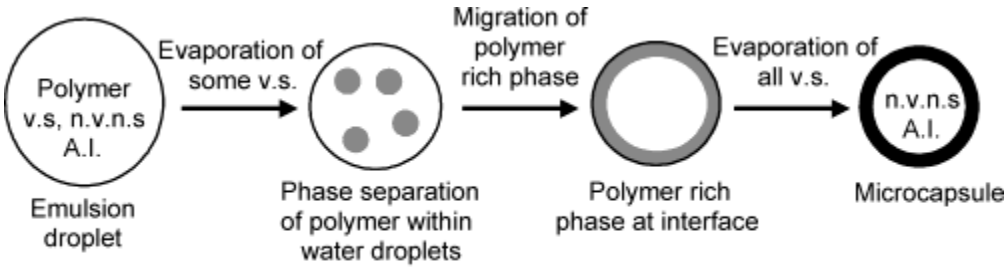

Figure 2. 6: Schematic diagram of internal phase sepaeratio process, n.v.n.s- non-volatile non-solvent, v.s- volatile solvent and A.I- active ingredient. [36]

Loxley, *et al.,* [36] studied poly (methylmethacrylate) (PMMA) microcapsules with oil cores using the solvent and evaporation process. It was concluded size distribution and morphologies of the microcapsules was dependant on the emulsifier used and the concentration of PMMA.

When applying the solvent extraction and evaporation technique to encapsulate low molecular weight oils and fragrances, volatile fragrances are lost during the process, also the polymeric shells are not able to with stand harsh conditions, releasing the core.

2.4.1.4 Interfacial polymerisation

In the interfacial polymerisation method, monomers in the continuous phase of an emulsion react with a second monomer in the dispersed phase. As the polymerisation proceeds a thin shell forms at the interface and the reaction rate decreases.[37]

Morgan, *et al.,* [37] demonstrated interfacial polymerisation, diamine monomers dissolved in water, aqueous phase was dispersed in the oil phase. The second monomer (oil soluble) diacid chloride was then added, which reacted at the interface with the first monomer diamine forming a membrane.

When applying the interfacial method to encapsulate fragrance, undesired side reaction can occur between monomers with several reactive functionalities of fragrances components.[35] Also as monomers and initiators are used in the process, residual monomer and initiator and also harmful by products can be present in the final product.

2.4.2 Mechanical Methods of Encapsulation

2.4.2.1 Spray drying

Spray-drying is one of the most common and cheapest techniques to produce microencapsulated food materials. Spray drying has been used for decades to encapsulate food ingredients such as flavours, lipids, and carotenoids.[38]

Spray drying process entraps active materials within a protective matrix, which is inert to the active material being encapsulated. It is a continuous processing operation involving a combination of several stages namely atomisation, mixing of spray and air, evaporation and product separation.[39]

Actives dispersed within a protective matrix (fluid form) are fed into a hot drying chamber and atomized into a powder. The feed can be in the form of a solution, emulsion or a suspension, the solid content is preferred to be around 10%. The microcapsules produced range from a very fine powder (10–50 um) or large size particles (2–3 mm).[40]

Spray drying technique is not used to encapsulate fragrances due to their volatility, but microencapsulated low molecular weight oils and fragrance microcapsule slurries have been spray dried to give powdered microcapsules. Rosenburg, *et al.,* analysed the factors affecting retention of volatile materials in microcapsules using the spray drying technique. It was concluded the main factors affecting the retention were the wall material, wall material thickness and the spray drying temperature.[41]

Spray drying technique also produces microcapsules with a wide range of sizes, shell thickness and structures, and thus offers poor control of their release properties.

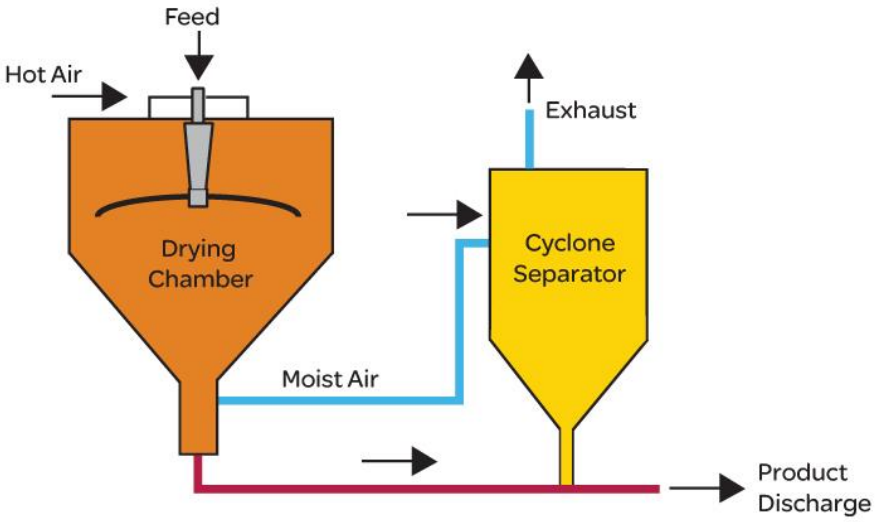

Figure 2. 7: Schematic diagram of process of spray diagram[39]

2.4.2.2 Extrusion

The simple extrusion process involves the dispersion of the core material in a matrix polymer at high temperature. The resulting mixture is forcefully passed through a die

and plunged into a desiccant liquid, resulting in the hardening of the extruded material and trapping the active. As high temperature are used this method is not suitable for encapsulating fragrances.[42]

From describing the encapsulating process above, non are suited to encapsulate low molecular weight oils and fragrances. Due to several reasons, including harsh preparation conditions such as high temperatures which result in the loss of volatiles, polymeric membranes which are porous and prone to diffusion, side reactions between monomers and fragrances components and also the inability of microcapsules to retain the core within the final formulation such as alcohol. The poor control over microcapsules produced resulting in a wide range of sizes, shell thickness and structures, and thus offering poor control of their release properties.[35, 40]

2.5 Low molecular weight oils/fragrances

In the previous section methods of encapsulation were described, in the following section fragrance will be described in depth and the main method of encapsulating low molecular weight oils/fragrances will be described in-depth. Fragrances mainly consist of low molecular weight components, resulting in high diffusivity.

Fragrances have become an intrinsic part of our lives. From when we wake up till we go to bed, we are in contact with fragrances in many different forms. From the fragrances on our bed sheets to the fragrances in our tooth paste to the fragrances we apply in the form of perfume. Fragrances bring a feel of comfort and cleanliness. Demands have increased for fragrances, to improve them by making them more effective and longer lasting.[43]

Fragrances can be divided into two categories, fragrance oils and essential oils. Essential oils are natural, exhibit medicinal and therapeutically properties and have

greater depth and character than fragrance oils. Essential oils do not contain as many carcinogens and other toxin as fragrance oils.[44]

Fragrance oils can be purely synthetic or a mixture of synthetic and essential oils. Fragrance oils contain synthetic components which are synthesised to mimic natural oils. Fragrance oils are cheaper than essential oils, are more in variety, have stronger scents and will last longer than essential oils. Fragrances mainly consist of low molecular weight components, resulting in high diffusivity.

As the cost of some essential oils can be very high, essential oils are only applicable to personal applications due to their chemical stability. With the growth of organic chemistry, the use of synthetic chemicals has grown in fragrances. Synthetic fragrances are mostly derived from alcohol, aldehydes, esters and ketones. Benzyl acetate is an example of synthetic chemicals used in fragrances. It is naturally found in flowers but is synthesised by the condensation of benzyl alcohol and acetic acid. It has a sweet aroma reminiscent of jasmine.[45]

When describing fragrance, three notes can be used to define fragrance, top notes, middle notes and base notes. Top notes consist of small, light and volatile components which are perceived immediately when smelling the fragrance and evaporate of quickly setting an initial impression. Middle notes emerge as the top notes evaporate of; they are the main body of the perfume and mask the unpleasant initial impression of base notes which with time become pleasant. Base notes emerge as the middle notes fade away; base notes and middle notes combine to give the main theme of the perfume. Base notes are typical rich and deep scented and are not perceived until prolonged exposure.

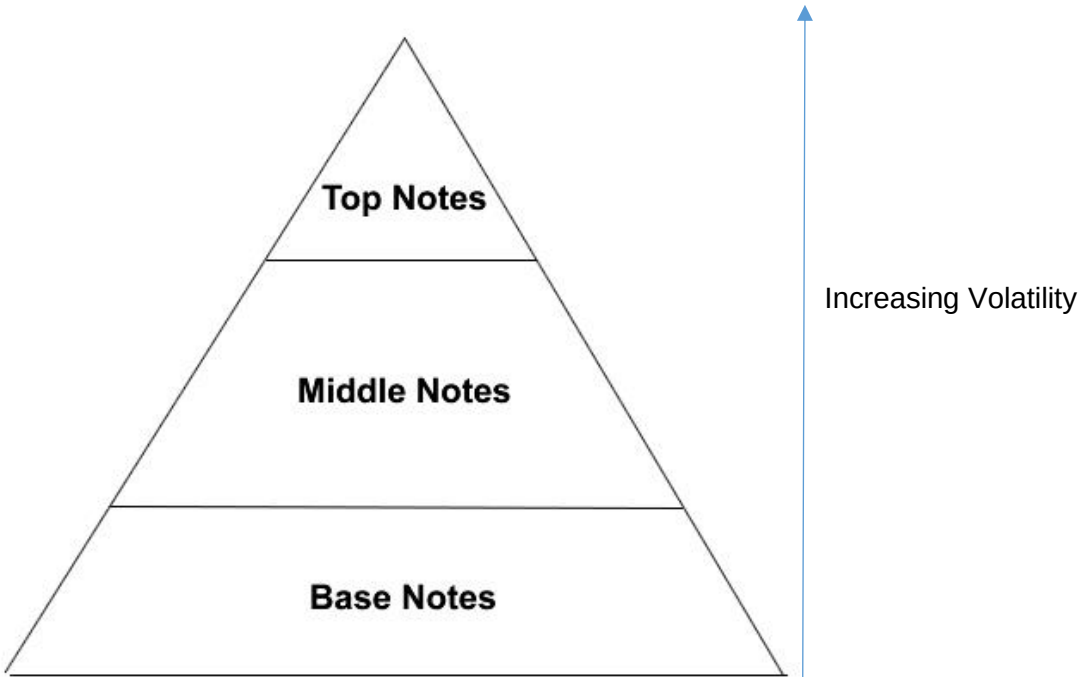

Figure 2. 8: Schematic illustration describing fragrance component volatility.

The main reason for encapsulating low molecular weight oils/fragrances is to prolong the release, increase efficiency and increase the exposure time of the scent. As fragrances are volatile, handling and encapsulating fragrances becomes an issue. Top notes are easily lost reducing the efficacy of the fragrance when first exposed. Encapsulation methods acquiring high temperatures and harsh conditions cannot be used to encapsulate fragrances.[46]

2.5.1 Encapsulated low molecular weight oils/fragrances

The main uses of encapsulated low molecular weight oils/fragrance are in home care; Melamin Formaldehyde microcapsules are used in fabric base softeners.[9] When added to laundry, microcapsules attach to fibres during the wash cycle. After drying the laundered items, applying pressure such as rubbing breaks the capsules releasing the fragrance giving a sense and feel of freshness.

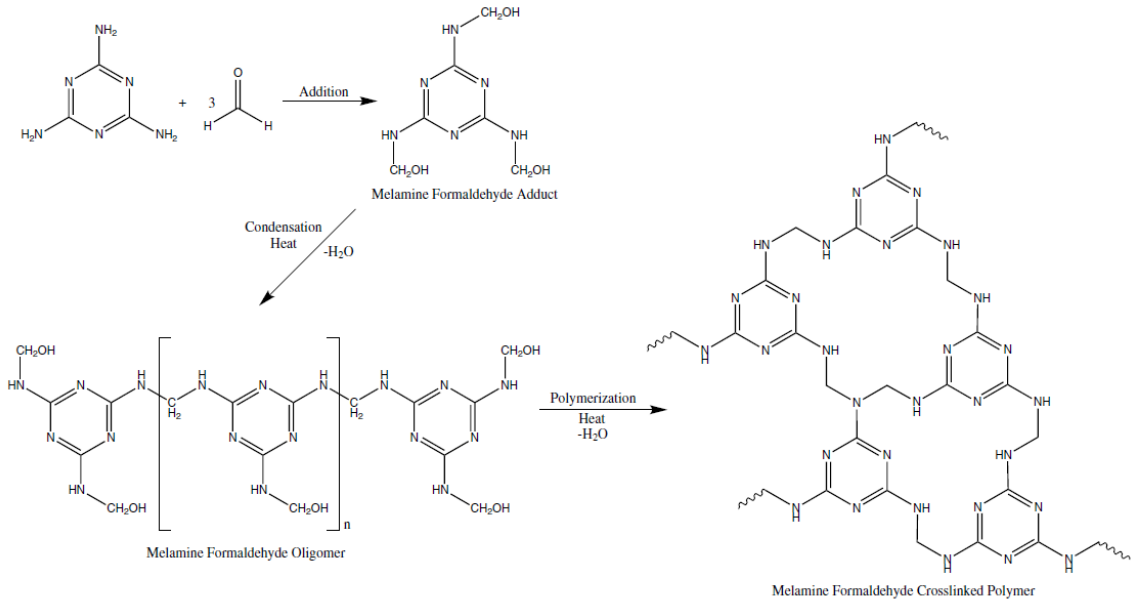

Figure 2. 9: Reaction schmeme of Melamin Formaldehyde Polycondensation.[9]

2.5.2 Melamin Formaldehyde polycondensation

The procedure for making melamin formaldehyde microcapsules (MF) involves three steps. Step 1 requires the formation of an emulsion by mixing the perfume with the aqueous phase containing the monomers (melamin formaldehyde precondensate). Step 2 requires the activation of the polycondensation by adjusting the pH, the reaction mixture is held at low temperature for several hours to enable the formation of the pre-polymer which deposits at the interface. The final step consists of ramping up the temperature to crosslink the polymer shell.[9]

MF microcapsules are not without their disadvantages, as they contain residual formaldehyde and the porous polymer shell is prone to diffusion of the core. These capsule cannot also withstand alcohol containing formulation which will result in the microcapsules releasing their cores.

The main reason for encapsulating low molecular weight oils/fragrances is to prolong the release, increase efficiency and increase the exposure time of the scent. As fragrances are volatile, handling and encapsulating fragrances becomes an issue. Top notes are easily lost reducing the efficacy of the fragrance when first exposed. Encapsulation methods acquiring high temperatures and harsh conditions cannot be used to encapsulate fragrances.

It is known that controlling the volatilization rate and degradation is the key to prolonging the sensory characteristics and improving the stability of fragrance materials. Many techniques have been studied to improve the encapsulation process and the robustness of the microcapsules.

So why do microcapsules leak over time and are not able to completely retain their core (low molecular weight volatile actives). This is due to the inherent porosity of the polymeric membrane used to encapsulate the actives in current technologies. Harsh product formulations and continuous phases which are able to dissolve the encapsulated actives, force microcapsules to release the core content in a fraction of the intended lifetime of the product.

Low molecular weight/small and volatile actives are able to diffuse across the permeable membrane. Fickian law of diffusion is used to describe the diffusion rate of an active ingredient permeating across a membrane. For the diffusion of an

encapsulated active through a membrane into an immiscible liquid the following equation can be applied, Equation 2.4. [11]

$$d_c/d_t = A * H * D \frac{C_{int} - C_{ext}}{x} \quad 2.4$$

Where:

A = surface area

H = Partition coefficient

D = Diffusion coefficient

C = Active concentration

x = Shell thickness

From the above equation the diffusion rate can be controlled through a series of parameters. Reducing the surface area can be done by increasing the microcapsule size which results in the reduction of diffusion. Increasing the shell thickness also reduces the rate of diffusion, but would result in smaller cores and a reduced payload. Minimizing the relative solubility of the dispersed phase within the continuous phase and reducing the concentration difference between the capsule core and continuous phase can also reduce the rate of diffusion.[11]

When encapsulating with polymeric materials the diffusion coefficient is in the order of 10^{-8} $cm^2 .s^{-1}$ for highly volatile small molecules hence making it impossible to achieve full retention of highly volatile small molecules.[12]

Industrially the MF technology is used to encapsulate low molecular weight oils/fragrances. Other polymer technologies are also used but the MF technology is

the leader in encapsulating low molecular weight oils/fragrances. The current challenges with these technologies consist of the following. Volatile actives/low molecular weight oils/fragrances are lost in the encapsulation process. Polymer shells leak due to their porosity. Side reaction between monomers and reactive functionalities of oil/fragrances components. Harmful residuals of e.g. monomers, formaldehyde, initiator and by products. Stability of microcapsules, such as creaming and leakage of core in harsh formulations. Ununiformed distribution of microcapsule size. Compatibility of the core with shell material.[11, 34, 35]

2.6 Literature Review

In the previous section emulsion stability and methods of encapsulating low molecular weight oils/fragrances and challenges arising from these methods were discussed. The following section will consist of what has been done to overcome these challenges and how these techniques can be used within the project.

2.6.1 Techniques for improving microcapsule stability

Zieringer, *et al.,*[47] described a microfluidic approach for fabricating PFPE-based microcapsules that showed enhanced retention of encapsulated cargo. PFPE (perfluoropolyethers) consist of repeating small units of perfluorinated aliphatic oxide. PFPE are known of their remarkable properties including low surface tension, excellent spreading, high fluidity, antifriction, thermally and chemically stable as well as biologically inert. PFPE are also hydrophobic and lipophobic enabling the encapsulation of hydrophilic and hydrophobic cargos. Zieringer, *et al.,*[47] formed water-fluorinated-water (W/F/W) double emulsions to encapsulate hydrophilic compounds within a PFPE dimethacrylate middle layer in a combined coflow and flow-focusing

microfluidic device. Retention of a water soluble dye was demonstrated over a trial period of four weeks and also the retention of small ions. It was also demonstrated the encapsulation of an organic compound and the retention of the encapsulated cargo. Due to the combination of the microfluidic device and the properties of PFPE control was demonstrated over microcapsule sizes, shell thickness, structure, release properties, payload and core-shell ratio. However the production rate was very low, resulting in the procedure not being suitable for many applications.

Lee, *et al.,*[48] combined the bulk and microfluidic emulsification process to demonstrate stable fragrance in water emulsions incorporated within polymeric membranes resulting in polymeric microcapsules. From the combination of the two methods, retention of the fragrance core was enhanced to 50% after 5 days in an ethanol continuous phase.

Yang, *et al.,*[49] to increase the mechanical, thermal and retention properties of microcapsules, incorporated the use of $Si0_2$ nanoparticles into the stabilisation of the emulsion (o/w). This was followed by interfacial reaction and in situ polymerisation. The oil core consisted of EPA, isophorone diisocyante (IPDI) and tolylene 2, 4-diisocyante-terminated poly (propylene glycol) (PPG_TDI) which reacted with MF prepolymer (pre-MF) dissolved in the oil phase. Yang, *et al.,*[49] demonstrated the capsules displayed excellent thermal stability with little weight loss when exposed to 150°C for 2h. The microcapsules also showed extra low shell permeability and enhanced mechanical stability. Sun, *et al.*, [50] studied the effects of incorporating $Si0_2$ at the interfaces of emulsions (w/o). The study demonstrated enhanced mechanical stability with incorporation of $Si0_2$ at the interface. Delcea, *et al.,* [51] analysed the effect of incorporating $Si0_2$ into PDADMAC microcapsules, Delcea, *et al.,*[51] was able to demonstrate an increase in mechanical strength of the microcapsules by using the

AFM technique to analyse the microcapsules. Mistry, *et al.,*[34] demonstrated, improved microcapsule shell permeability by crosslinking the microcapsule polymer shell, reducing the pore sizes in the shell.

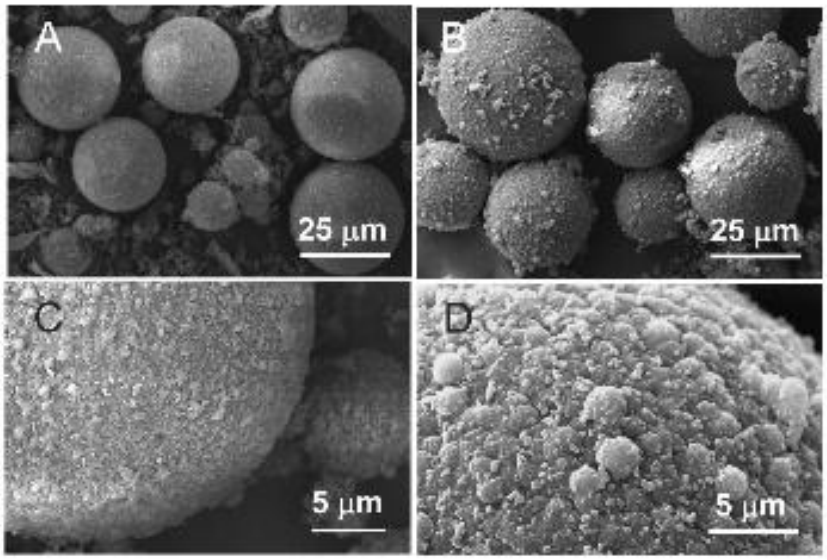

Figure 2. 10: SEM images of EPA-loaded hybrid microcapsules with PU/ PMF double-walled shells: (A) low amplification and (C) high amplification; (B) low amplification and (D) high amplification. [49]

The techniques discussed above have been used to enhance the retention of microcapsule core, but no technique has demonstrated the complete retention of the core material, or is practical. Other techniques such as electroless plating (ELP) have been utilised to apply metallic coatings on microcapsules to reduce permeability of the shells.

Electroless plating (ELP) was first discovered by Brenner and Riddell [52] in 1946 and is also termed as controlled autocatalytic (self-containing) reduction. ELP is a chemical technique employed for the metallization of non-conductive substrates, such as plastics, glasses, and ceramics without the use of external electricity. ELP has become

increasingly attractive because of its cost saving and low energy thin metal film deposition capabilities. ELP requires the aid of a reducing agent in solution to deposit a coating to a surface without the application of an electric current. The electrochemical deposition of a metal from a solution of the metal salt occurs via an electrochemical redox reaction, where electrons are transferred between the reacting chemical species.[52]

ELP is an electrochemical process which involves donor/acceptor electron reactions. The redox reaction consists of transfer of electrons between the oxidizing and reducing agent. Metal ions in the aqueous solution react with electrons from the reducing agent converting them to metallic coatings. Chemical reducing agents used in the ELP process consist of borohydrides, formaldehyde, hydrazine and amine boranes.[53]

2.6.2 Metal deposition onto substrate surfaces- Nanoparticle catalysed metal film

In the following section processes using ELP to deposit metal films onto substrate surfaces will be described. Methods involving various metal NPs used as catalysis and also varying deposition metals will be described.

ELP had been used to deposit a wide range of metals. Horiuchi, *et al.,* studied the ELP process producing gold thin films with strong adhesion to various polymer films. Horiuchi, *et al.,* synthesized Pt, Au and Pd colloids by the reduction of a metal salt ($HAuCl_4.4H_20$, $H_2PtCl_6.6H_20$ or $PdCl_2$) by $NaBH_4$ in the presence of polyvinylpyrrollidone (PVP) at room temperature for one day to from an aqueous stable suspension. The substrates were dipped into the Pt aqueous colloidal solution, immobilizing the Pt colloidal nanoparticles onto the substrates surface. The substrate

then was immersed into a cyanide-free gold electroless plating solution composed of chloroauric acid and hydrogen peroxide, resulting in gold deposition onto the Pt-catalyzed surface. PVP-Pt colloidal nanoparticles were observed by EFTEM. TEM was used to observe gold deposition onto PVP-Pt catalyzed surface.[54]

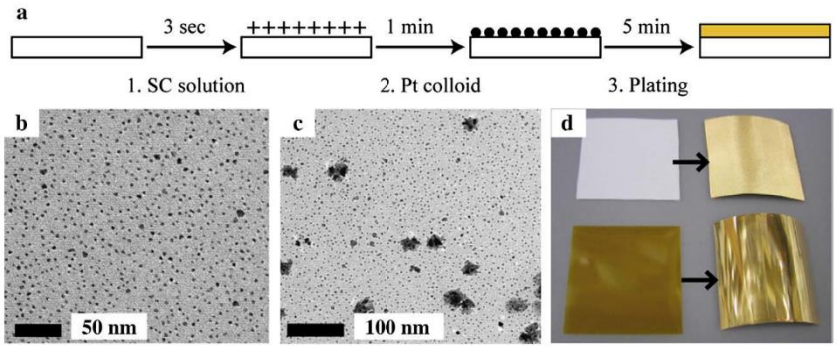

Figure 2. 11: (a) Illustration showing the process of the electroless gold plating using the Pt colloid as catalyst. (b) and (c) TEM micrographs showing the Pt nanoparticles immobilized on a 100 nm thick spin-cast PS thin film, and the gold deposits on the Pt-catalyzed surface after the plating for 10 s, (above) and on Kapton film (below) for 5 min.[54]

Fujiwara, *et al.,* [55] studied Ag nanoparticles as catalyst for the electroless deposition of Cu and promotion of its adsorption onto epoxy substrates. Fujiwara, *et al.,* synthesized Ag nanoparticles by adding $AgNO_3$ solution to a Sn(II)-citrate complex solution. UV-vis spectrometer was used to analyze the Ag nanoparticles. To promote the adsorption of the Ag nanoparticles onto the substrates, the substrates were dipped into a cationic surfactant solution at 50^{o}C for 5 mins. After conditioning the substrates were rinsed in water, and dipped into the Ag nanoparticle suspension at 25^{o}C. Cu was deposited onto the Ag nanoparticle catalyzed epoxy substrate by immersing the epoxy substrate into proprietary plating bath containing formaldehyde as the reducing agent and ethylenediaminetetraacetate as a complexing reagent for Cu^{2+}.

Dinderman, *et al.,*[56] studied the deposition of Fe onto Pd/Sn- catalyzed substrates at room temperature. Dinderman, *et al.,* described in his study, the electroless iron bath containing Fe^{2+} as the metal source, citrate as the metal chelator, boric acid buffer as the pH controller, and sodium borohydride as the reductant. Pd/Sn-catalysed cellulose fibers were added to the bath under agitation at room temperature, resulting in the deposition of Fe onto the Pd/Sn- catalysed cellulose fibres. To analyze the deposition of Fe onto the cellulose fibers, a minimum of 200 fibers coated and uncoated were observed under the LeitzWetzlar optical microscope and photographed. Uncoated fibers appeared translucent brown and the Fe coated cellulose fibers appeared black.

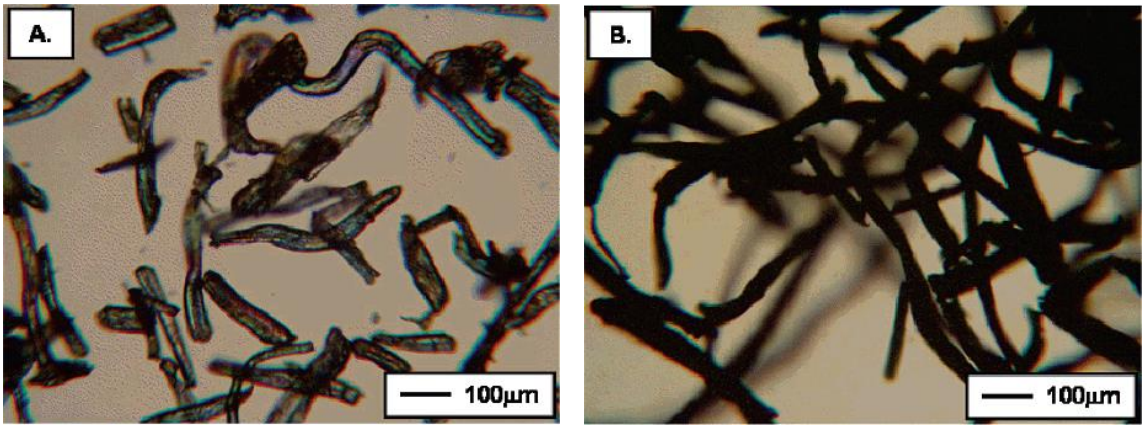

Figure 2. 12: Optical micrographs (20×) of cellulose fibers: (A) catalysed, unplated fibers, (B) dried, plated fibers. [56]

2.6.3 Metal Coated Microcapsules

In the previous section methods to deposit metal films onto surfaces via electroless plating were reviewed. In the following section methods to deposit metal films to synthesize metal coated microcapsules will be reviewed.

Patchan, *et al.*,[57] demonstrated in his study a facile method of producing liquid filled metal microcapsules in large quantities. The synthesis consisted of deposition of a thin metallic shell onto polymeric microcapsules containing an oily core. The process combined a few steps of emulsification, interfacial polymerization and electroless plating (figure 2.12).

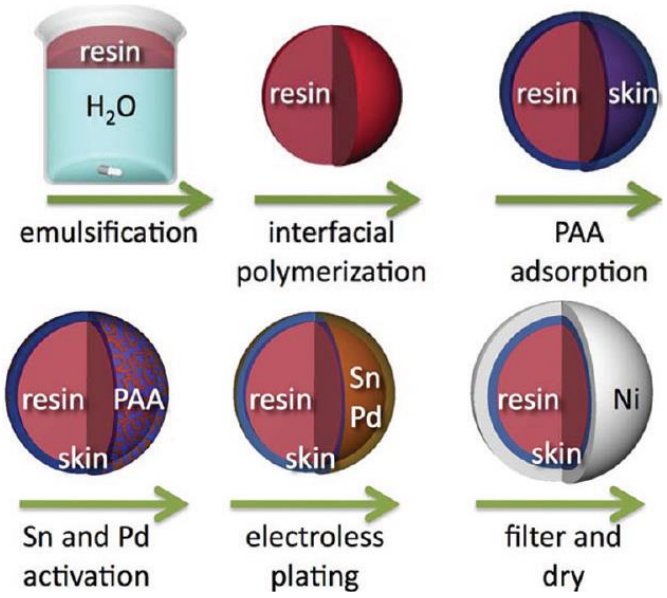

Figure 2. 13: Diagram illustrating the Synthesis of Liquid-Filled Metal Microcapsules.[57]

Synthesized polymeric microcapsules were immersed in $SnCl_2$ solution followed by a rinse three times with Milli-Q water. Microcapsules were then immersed in $PdCL_2$ solution for two minutes. The microcapsules were washed two times with Milli-Q water followed by immersion into an electroless Nickel plating bath, resulting in the deposition of Nickel onto the microcapsules. The microcapsules were analysed using a Hitachi S4700 scanning electron microscope (SEM) with an EDAX energy dispersive X-ray spectroscopy (EDS) system.

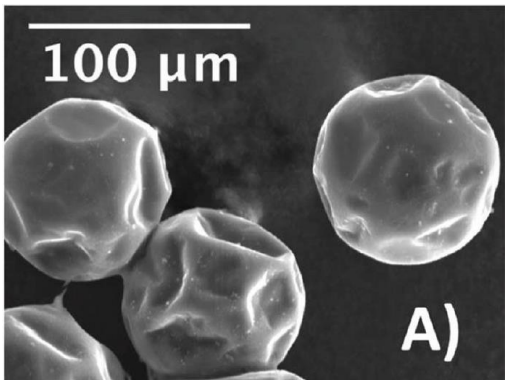

Figure 2. 14: SEM micrograph of nickel coated microcapsules.[57]

Tsuneyoshi, *et al.,*[58] demonstrated metal coated polymeric microcapsules which could be transferred to a target site by applying external magnetic fields. Cross-linked Melamin formaldehyde microcapsules were prepared. The microcapsules were placed in an acidic $PdCl_2$ solution for 2 minutes, stirred and washed with water. The activated microcapsules were placed into an electroless Ni plating bath and stirred for 1 hour, resulting in nickel coated Melamin formaldehyde microcapsules. Tsuneyoshi, *et al.,*[58] demonstrated the magnetic behaviour of the metal coated microcapsules by applying a magnetic.

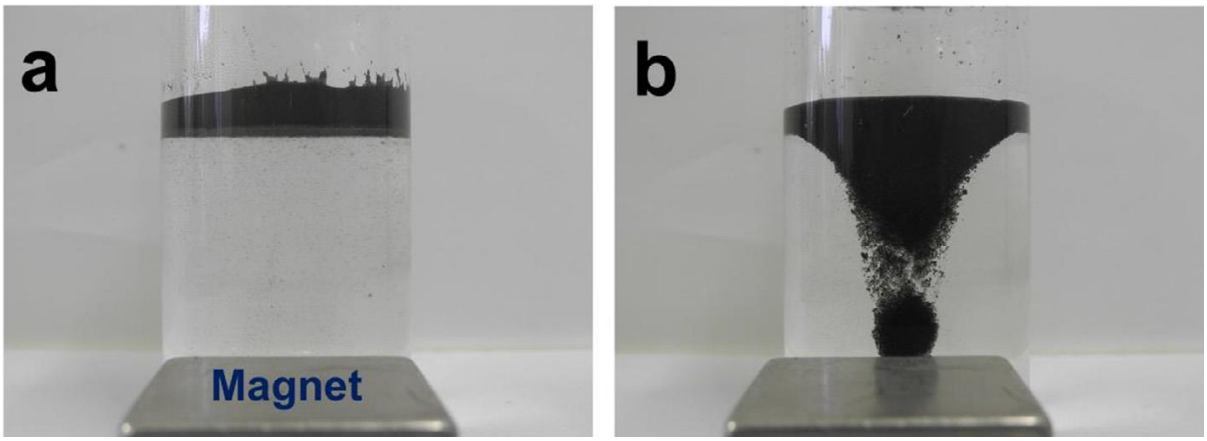

Figure 2. 15: Magnetic behaviour of metal-coated microcapsules. [58]

Tasker, *et al.*,[13] demonstrated electroless gold plating on Poly(methyl methacrylate) (PMMA) microcapsules containing a hexyl salicylate core. In the study it was concluded the arrangement of the platinum nanoparticle layer on the PMMA surface determined the final shell thickness. Lower surface coverage of nanoparticles resulted in thicker metal shells compared to higher surface coverage of nanoparticles, this was due to lower concentrations of nanoparticles, resulted in gold growth as a clusters before fusing to form a continuous shell.

Hitchcock, *et al.,*[11] reported and demonstrated the metal coating of polymeric microcapsules followed by the complete retention of the core (hexyl salicylate) in the impermeable metallic shell. Polymeric microcapsules were synthesised (PMMA), containing a fragrance core, added to a suspension of Pt-PVP NPs, which resulted in the Pt-NPs adsorbing onto the surface of the polymeric microcapsules. The Pt-NPs at the surface were used to deposit a gold shell on the polymeric membrane. The gold coated microcapsule were able to completely retain the encapsulated core in an ethanol continuous phase after 40 days.

In the above section methods using ELP to deposit metal films on polymeric microcapsule surface were described. All the methods described are not without disadvantages. All the methods described above incorporate the use of polymeric microcapsules, this in return reduces the core payload and increases the process time. The methods described by Patchan, *et al.,* [57] and Tsuneyoshi, *et al.,* [58] both incorporate the use of harsh chemicals and conditions. Both methods result in the nickel coated microcapsules, nickel is known to effect the environment and also human health. Nickel is listed by the National Toxicology Program as carcinogenic and also known to irritate the skin. Nickel inhibits and damages the growth of plants on

land and algae on surface water. The method described by Hitchcock, *et al.,* [11] and Tasker, *et al.,* [13] utilises expensive metals such as Platinum as a catalysis and Gold as the shell material, hence occurring huge costs for the encapsulation of a small payload and also incorporating a polymer shell, followed by electroless plating of the polymeric microcapsules, hence reducing the payload and also inhibiting the initial problems of microencapsulating with polymeric shells as described previously.

The methods described for electroless metal plating, with their coupling metal NP catalysis and deposition metal will be used in this project to form a protective metal barrier around a small volatile core. In the following section methods of producing metallic NPs for use as catalysis will be described. Various NP system will be used in this project with the end goal of achieving a system with high catalytic activity for the depositing metal and cost effectiveness.

2.6.4 Metal nanoparticle background/synthesis

Metal Nanoparticles (NPs) have attracted great interest due to their catalytic properties. At low temperatures colloidal dispersions of metal nanoparticles are able to operate as catalysts. Due to their size they offer high surface to volume ratio, better dispersion ability and lower loading amount. These properties contribute to more active sites on the surface. The size of metal nanoparticles greatly influences the catalytic reactivity.[59]

Metal NPs can be synthesised using physical and chemical techniques. Metal NPs synthesised using the chemical technique tend to have a narrower size distribution.[60] As nanoparticles can aggregate, steric or charge stabilisation have been used to overcome this. Polymers (PVP), borohydride or citrate ions can be used to prevent the

metal NPs aggregating.[61] Metal NPs are able to form catalytic nuclei on a variety of surfaces such as polymers and ceramics.[62]

Lin, *et al.,* [63] prepared gold nanoparticles (Au NPs) ranging in size from 1.7 to 8.2nm. $HAuCL_4$ was reduced with $NaBH_4$ to synthesise Au-NPs. The Au-NPs size was controlled by adjusting the amount of $NaBH_4$ used during the synthesis.

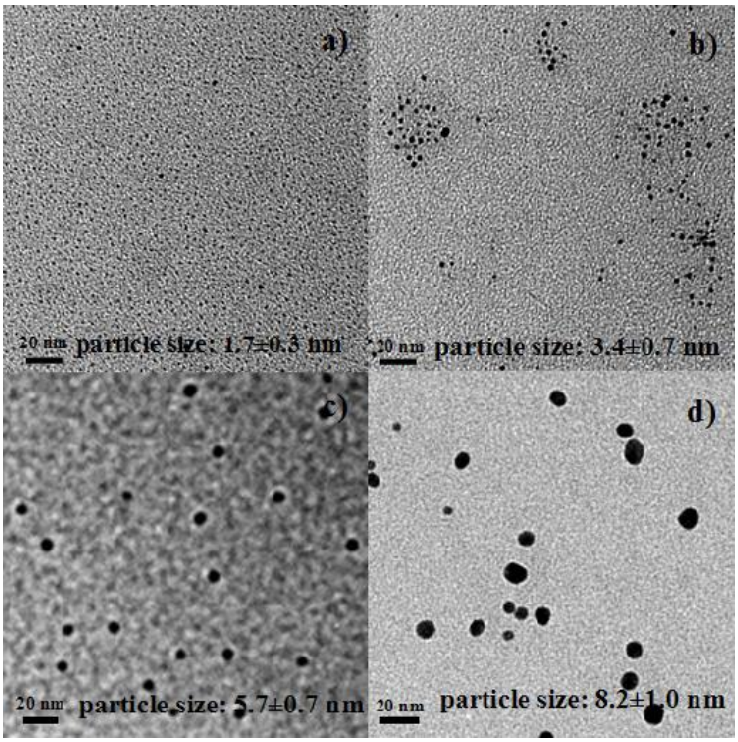

Figure 2. 16: TEM images of Au NPs synthesized by mixing 0.06 mmol $HAuCl_4$ with different amounts of $NaBH_4$. (a) 0.4 mmol; (b) 0.5 mmol; (c) 1.0 mmol; and (d) 1.1 mmol, $NaBH_4$. Scale bars are 20 nm. [63]

Lin, *et al.,* [63] reported Au NPs were used in the catalytic reduction of p-Nitrophenol with $NaBH_4$, the catalytic activity increased as the Au-NPs average size decreased. The catalytic activity was highest when the average size was 3.4 nm. From the reaction it was calculated the ratio of Au to PVP was 1.13 to 1. The concentration of Au NPs was calculated to be 0.0113%. The concentration of Au NPs was very low and the amount of PVP was very high, nearly equalling the amount of Au.

Using this method to synthesise Au NPs, would result in oil in water emulsions with very low amounts of Au NPs absorbed at the interface and high amounts of PVP at the interface. This in turn would reduce the amount of catalytic activity of Au NPs to attract the deposit a metallic coating.

Solomon, *et al.,* [64] synthesised Ag NPs (yellow colloidal silver), estimated their particle size using visible spectroscopy and studied their aggregation effects. A large excess of sodium borohydride was used to reduce the ionic silver and to stabilise the silver nanoparticles that formed, Reaction equation 2.1:

2.1

$$AgNO_3 + NaBH_4 \longrightarrow Ag + \tfrac{1}{2} H_2 + \tfrac{1}{2} B_2H_6 + NaNO_3$$

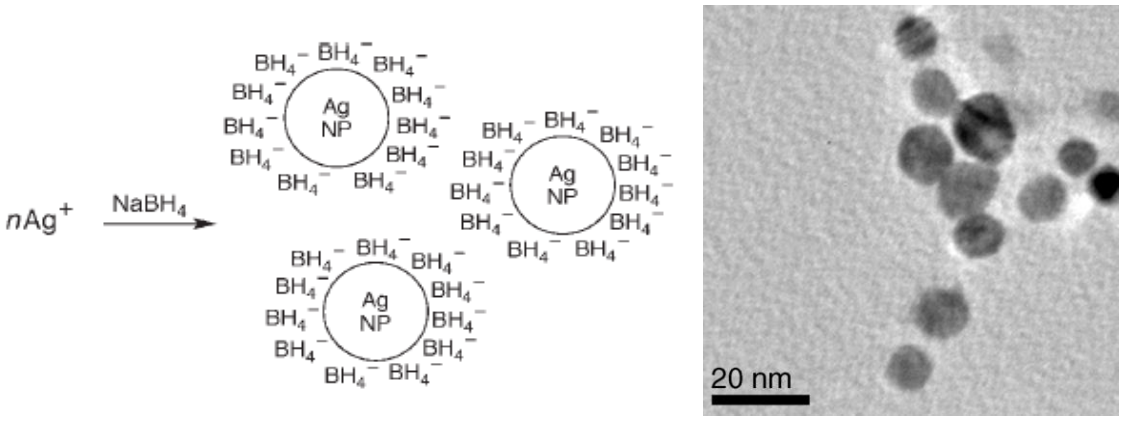

Figure 2. 17: a) Repulsive forces separate Ag nanoparticles (NP) with adsorbed borohydride and b) TEM image of silver nanoparticles.[64]

Adsorption of borohydride onto the Ag NPs stabilized the Ag NPs by providing a particle surface charge as shown above.

Pastoriza-Santos and Liz-Marzan [61] synthesise Au-NPs stabilised with varying PVP molecular weight. Increasing the PVP molecular weight/concentration resulted in the mean core particle size of the Au-NPs to decrease.

Above methods for producing metallic NPs as catalysis was described. The section describing the ELP techniques and section on metal NP synthesis will be used to find couples of metal NPs and deposition metals for use in this project. Below a description of how ELP and NPs have been used to overcome problems related with encapsulating small volatile actives and permeability problems of polymers is described.

Hitchcock and Tasker, [11] demonstrated a method for producing microcapsules with metallic coatings. These microcapsules were prone to undesired loss of encapsulated actives when under extreme conditions. The method consisted of three steps, producing oil core microcapsules using the co-solvent extraction method to precipitate a polymeric shell around the oil core, followed by physically absorbance of metallic Pt-NPs onto the polymeric shell, and finally these metal Pt-NPs acted as catalysis for the growth of a secondary metallic film.

ELP can be used to coat microcapsules with metallic shells, this would result in enhanced barrier properties with reduced permeability of the shell and increased mechanical strength. But current problems which exist with encapsulating the core with polymer would still arise, as the microcapsule would have to be produced before coating them with a metallic shell. Also the use of metallic NPs would cause issues when regarding EU regulations.

To overcome these problems, work in the group has been carried on this project. Metallic gold (Au) coatings have been deposited on Pt-NP stabilized emulsions, removing the undesired polymer coating and hence increasing the oil core ratio. But still this does not achieve the challenge of removing intermediate steps involving NPs. To overcome this challenge, methods which employ the use of metallic NPs by

depositing them directly onto a substrate can be achieved to overcome this. In the following section a process will be described of depositing metals onto silica surface for use as catalysis for a metallic deposition and also for use as emulsion stabilizers.

2.6.5 Metal deposition that does not involve nanoparticles – metal ions in particular

Zidki, *et al.,*[65] deposited silver nanoparticles on silica nanoparticles in aqueous medium to form silver-silica nanocomposites. Silica dispersed in water to give a 2.25 wt% solution, 1.25 mM of $AgClO_4$ was added dropwise to the stirred silica suspension. The suspension was stirred for 5 hours resulting in the silver ions, homogenously dispersed on the silica particles. $NaBH_4$ (1.25 mM) ice cold aqueous solution was very slowly added to the silver-silica suspension to reduce the silver. The suspension was centrifuged until all the solid was precipitated and suspended in a portion of the supernatant.

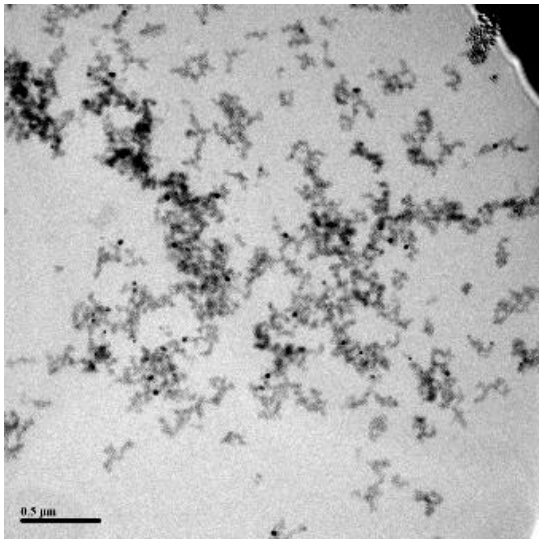

Figure 2. 18: TEM micrograph of SiO_2-Ag NPs.[65]

The silver NPs supported on the silica NPs with no bridging molecule. The advantage of not using a bridging molecule was that no undesirable side reactions occur between

the bridging molecule and any reagent present in the solution. Also no stabilizer was required to keep the suspension stable.

Zidki, *et al.,*[65] method could be used to synthesize Si/metal nanocomposites which could in turn stabilize an emulsion and catalyze a secondary metallic coating without the use of metallic NPs.

Lee, *et al.,* [66] demonstrated the coating of inorganic and organic materials with polydopamine PDA by dip coating the objects in an aqueous solution of dopamine, resulting in the self-polymerization of dopamine to PDA. The metal binding ability of the catechol groups present in the PDA coating were exploited to deposit metal coatings via electroless plating. The PDA coated objects were coated in silver and copper films.

Luo, *et al.,*[67] demonstrated the self-polymerisation of dopamine by synthesizing PDA sub-micrometer spheres. The metal binding ability of the catechols groups were exploited to deposit silver nanoparticles on the PDA spheres resulting in Ag-PDA spheres.

Wang, *et al.,* [68-70] utilized the ability of dopamine to self-polymerise and deposit on inorganic and organic substrates by depositing thin uniform layers of PDA on silica, aluminum and poly styrene microspheres. The ability of the catechols group on the PDA surface was utilized as a chelating agent for silver ions and as a reducing agent for the formation of catalytic sites, resulting in Si-PDA-Ag, Al-PDA-Ag and PS-PDA-Ag core shell microspheres. The silver coating was deposited via electroless plating, glucose was used as the reducing agent.

The ability of dopamine to self-polymerise and deposit on organic and inorganic materials could be utilized to synthesis PDA microcapsules, which inherently could be

used by exploiting the ability of the catechols group to chelate/complex silver ions, reducing the silver ions on the surface of PDA, resulting in silver coated PDA microcapsules.

The polymerisation mechanism of dopamine in solution is still not fully understood, nevertheless, a general scheme can be drawn. The proposed mechanism for the self-polymerisation of dopamine is shown in figure 6.2. The mandatory requirements for the reaction to proceed are a basic medium (Tris-HCl buffer solution 10mM, pH=8.5) and an O_2 rich environment. The initial reaction involves the slow oxidation of dopamine (A) to dopamine quinone (C), via dopamine semiquinone (B). Dopamine quinone (C) rapidly undergoes cyclisation through a Michael type cycloaddition forming leucodopaminechrome (D). The oxidation and subsequent rearrangement of leucodopaminechrome (D) results in the formation of 5,6-Dihydroxyindoline DHI (E) and its oxidised product 5,6-indolequinone (F). 5,6-Dihydroxyindoline DHI (E) and 5,6-indolequinone (F) are the building block of PDA, and many chemical pathways are proposed leading to PDA through covalent polymerization and non-covalent self-assembly. [66, 68, 70-77]

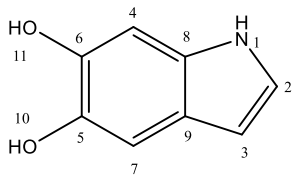

Figure 2. 19: Structure of 5,6-Dihydroxyindoline DHI, with numbering.

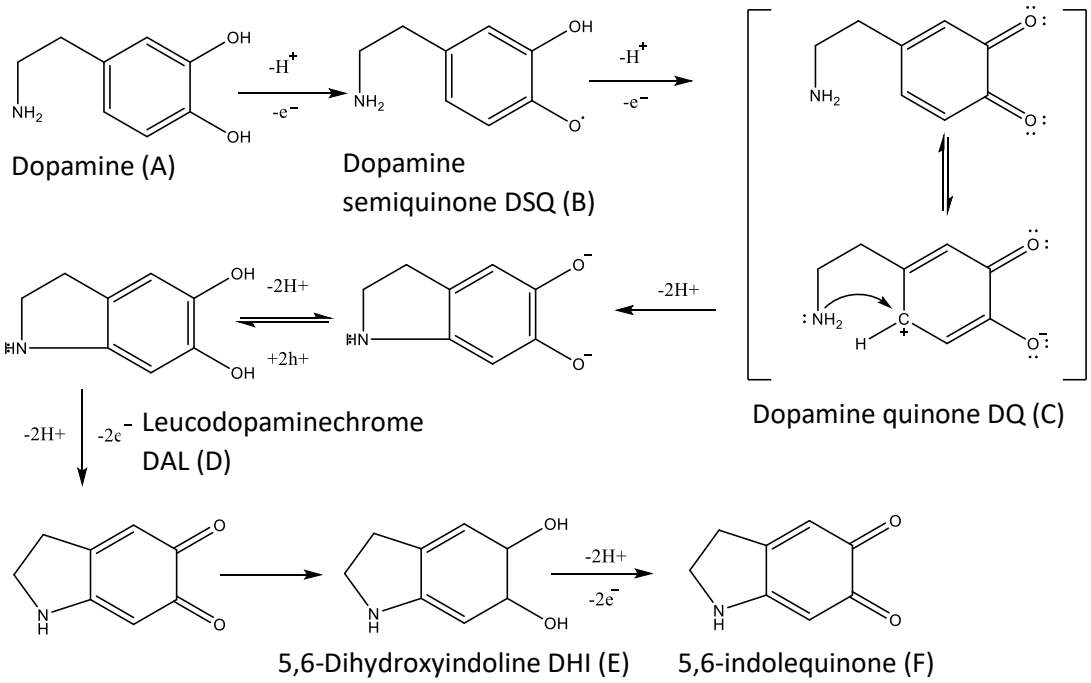

Figure 2. 20: Dopamine self-assembly (Tris buffer pH~8.5) proposed mechanism (A-F).

Okuda, *et al.,* [68, 70, 77, 78] proposed the formation of a linear polymer through covalent bonds governed by electron-transfer-controlled reaction. It is suggested the process involves the nucleophilic attack of DHI (C3) to one of the two-electron-oxidants (C4, C7) as an electrophile, resulting in DHI homotrimers (3 and 4). This is followed by the nucleophilic attack of the C4 position (3) to the C4 position (4) leading to the formation of PDA (figure 6.3).

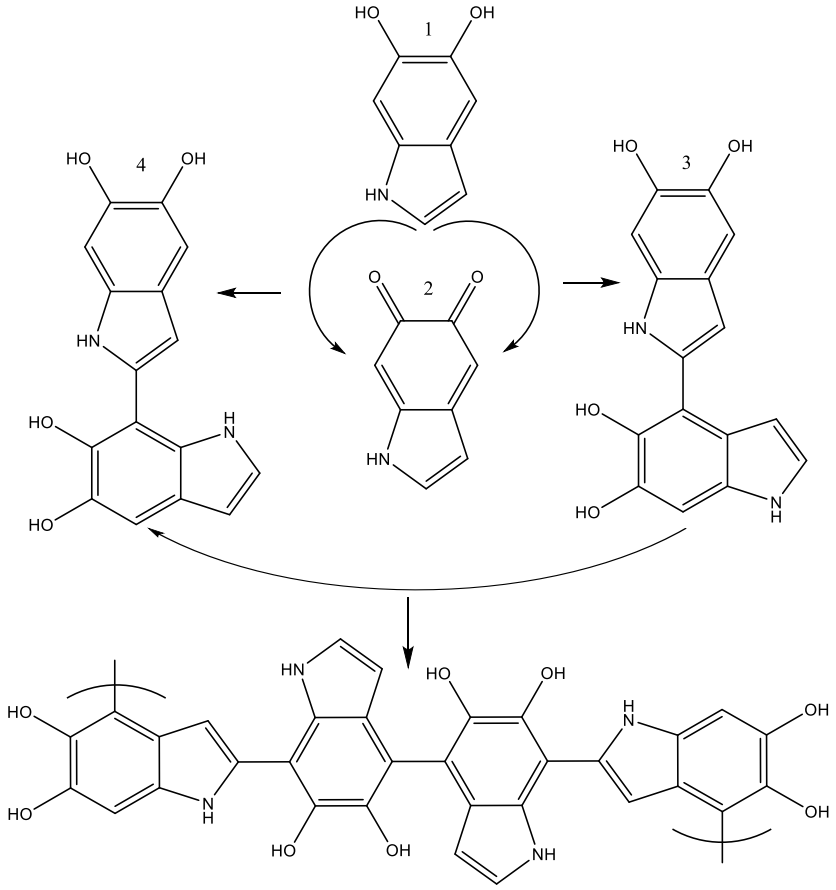

Figure 2. 21: Dopamine self-polymerisation, (Tris buffer pH~8.5) PDA proposed polymer structure.

Della Vecchia, *et al.,* [79] proposed the formation of PDA as a supramolecular aggregate of monomers (consisting primarily of 5,6-dihydroxyindoline (E) and its dione derivative 5,6-indolequinone (F), held together through a combination of charge transfer, π - stacking, and hydrogen-bonding interactions (figure 6.4).

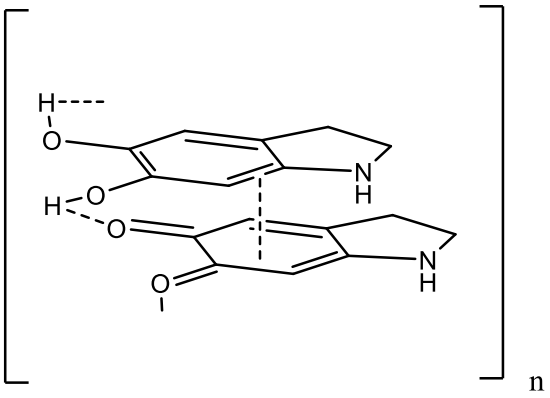

Figure 2. 22: PDA structure held together through a combination of charge transfer, π - stacking, and hydrogen-bonding interactions. [79]

PDA formation has also been proposed through combined covalent bonding and self-assembly via a combination of charge transfer, π- π stacking and H bonds (figure 6.5). [69, 75, 80-82]

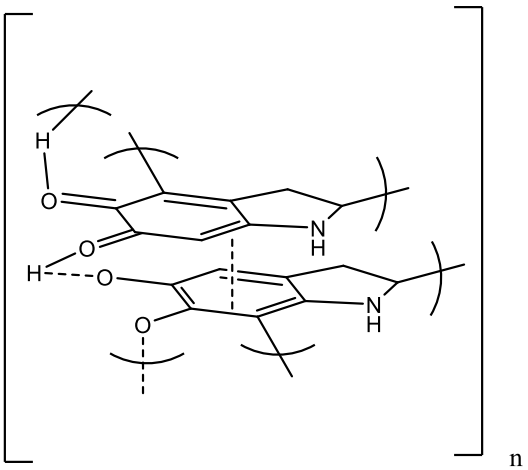

Figure 2. 23: PDA structure proposed through combined covalent bonding and self-assembly via a combination of charge transfer, π- π stacking and H bonds.

Once self-polymerised, PDA is able to deposit on inorganic and organic materials through strong covalent and non-covalent interactions with substrates.[66] PDA is able to deposit and bind to the silica through strong hydrogen-bonding between the catechol groups and the silanol groups on the silica surface.[83]

From the literature review not much information is present on ways of overcoming the retention problems related to fragrance microcapsules. Studies described in the previous section either have used techniques such as crosslinking polymer shell or increasing shell thickness which do not provide adequate retention and can be only applied to polymer techniques. Ziegler, *et al.,* method of using fluorinated polymers has provided a process of retaining small volatile actives, but not in non-aqueous phases, where-as Hitchcook and Tasker method does describe a way of overcoming the problem related with retention of small volatile components by using a metallic shell on a polymer capsule.

The main objective for this project is to build up on the work that has been documented by Hitchcock and Tasker by continuing working on the metallic deposition on emulsion stabilized by Pt-NPs. And particular focusing to find cheaper alternatives for Au and Pt and alternative methods not using nanoparticles. This can be done by applying Zidki, *et al.,* method producing Si/metal nanocomposite, which in turn could be used to stabilize and emulsion and directly deposit a metallic coating onto the emulsion. And also using the ability of dopamine to self-polymerise on colloidal silica stabilized emulsions, resulting in PDA microcapsules, which could inherently be coated in silver by utilizing the ability of the PDA surface to complex/chelate metal ions.

2.7 Aim and objectives

The aim of this project is to build up on previous work in the group on metallic microcapsules, by reproducing the work and developing a reliable route to the production of nonporous microcapsules which are able to retain the small volatile core molecules. The specific objectives of this project are described below:

- Synthesise and characterise Au coated Pt-NP stabilised emulsions, analyse parameters affecting the metal microcapsule formation and properties.

- Synthesise metal coated microcapsules without the use of metal nanoparticles intermediates, by synthesising Si/metal composites for use as stabilisers for Pickering emulsions followed by metal coating via electroless plating.

- Synthesise metal coated microcapsules with reduced costs by replacing Pt-NPs and finding alternative coatings to Au.

- Demonstrate the metal coated microcapsules ability to encapsulate and retain small volatile actives within a continuous phase that is able to fully dissolve the core.

- Find alternative applications for metal coated microcapsules.

2.8 References chapter 1 and 2

1. Gouin, S., *Microencapsulation: industrial appraisal of existing technologies and trends.* Trends in Food Science & Technology, 2004. **15**(7-8): p. 330-347.
2. Illesova, A., et al., *Encapsulation as a useful tool for a biotechnological production of natural aromas.* Current Opinion in Biotechnology, 2013. **24**: p. S59-S60.
3. Manu Arora Nikita Agnihotri, R.M.C.G., *Microencapsulation- A novel approach in drug delivery: A Review.* Indo Global Journal of Pharmaceutical Sciences, 2012. **2**(1).
4. Ghosh, S.K., *Functional coatings : by polymer microencapsulation*. xiv, 357 pages.
5. Avalani Gunjan, N.S., Mahesh Gupta, Mahveer Prasad Khinchi , RiteshVerma , Subhendu S. Mishra, *An review of microencapsulation as novel drug delivery.* Asian Journal of Pharmaceutical Education and Research 2012. **1**(2): p. 53-66.
6. Meyer, A., *Perfume Microencapsulation by Complex Coacervation.* Chimia, 1992. **46**(4): p. 101-102.
7. Klaypradit, W. and Y.W. Huang, *Fish oil encapsulation with chitosan using ultrasonic atomizer.* Lwt-Food Science and Technology, 2008. **41**(6): p. 1133-1139.
8. Tsuji, K., *Microencapsulation of pesticides and their improved handling safety.* Journal of Microencapsulation, 2001. **18**(2): p. 137-147.
9. Bone, S., et al., *Microencapsulated fragrances in melamine formaldehyde resins.* Chimia (Aarau), 2011. **65**(3): p. 177-81.
10. San Miguel, A., et al., *Smart colloidosomes with a dissolution trigger.* Soft Matter, 2010. **6**(14): p. 3163-3166.
11. Hitchcock, J.P., et al., *Long-Term Retention of Small, Volatile Molecular Species within Metallic Microcapsules.* ACS Appl Mater Interfaces, 2015. **7**(27): p. 14808-15.
12. Ponitsch, M., et al., *Diffusion of small molecules in glassy polymers.* Journal of Polymer Science Part B-Polymer Physics, 1997. **35**(15): p. 2397-2408.
13. Tasker, A.L., et al., *Understanding the Mechanisms of Gold Shell Growth onto Polymer Microcapsules to Control Shell Thickness.* Chem Asian J, 2017. **12**(13): p. 1641-1648.
14. Dickinson, E., *An introduction to food colloids*. 1992, Oxford ; New York: Oxford University Press. viii, 207 p.
15. Israelachvili, J.N., *Intermolecular and surface forces*. 3rd ed. 2011, Burlington, MA: Academic Press. xxx, 674 p.
16. Walstra, P., *Principles of Emulsion Formation.* Chemical Engineering Science, 1993. **48**(2): p. 333-349.

17. Schroder, V., O. Behrend, and H. Schubert, *Effect of dynamic interfacial tension on the emulsification process using microporous, ceramic membranes.* Journal of Colloid and Interface Science, 1998. **202**(2): p. 334-340.
18. Yuan, Q.C., et al., *Manufacture of controlled emulsions and particulates using membrane emulsification.* Desalination, 2008. **224**(1-3): p. 215-220.
19. Vladisavljevic, G.T. and R.A. Williams, *Recent developments in manufacturing emulsions and particulate products using membranes.* Advances in Colloid and Interface Science, 2005. **113**(1): p. 1-20.
20. Thompson, K.L., S.P. Armes, and D.W. York, *Preparation of Pickering emulsions and colloidosomes with relatively narrow size distributions by stirred cell membrane emulsification.* Langmuir, 2011. **27**(6): p. 2357-63.
21. Zhu, J. and D. Barrow, *Analysis of droplet size during crossflow membrane emulsification using stationary and vibrating micromachined silicon nitride membranes.* Journal of Membrane Science, 2005. **261**(1-2): p. 136-144.
22. Aryanti, N., et al., *Performance of rotating membrane emulsification for o/w production.* Desalination, 2006. **200**(1-3): p. 572-574.
23. McClements, D.J., *Food Emulsions: Principles, Practices, and Techniques.* 1999: CRC Press LLC, United States of America. .
24. Claesson, P.M., et al., *Protein Interactions at Solid-Surfaces.* Advances in Colloid and Interface Science, 1995. **57**: p. 161-227.
25. Zhao, T. and L. Jiang, *Contact angle measurement of natural materials.* Colloids Surf B Biointerfaces, 2018. **161**: p. 324-330.
26. Binks, B.P., *Particles as surfactants - similarities and differences.* Current Opinion in Colloid & Interface Science, 2002. **7**(1-2): p. 21-41.
27. Xu, J., et al., *Janus-like Pickering emulsions and their controllable coalescence.* Chemical Communications, 2013. **49**(92): p. 10871-10873.
28. Pieter Bos, B.T., *Beijerinck and the delft school of microbiology*. 1995: Delft University Press.
29. Baldwin, E.A., R.D. Hagenmaier, and J. Bai, *Edible coatings and films to improve food quality*. Second edition. ed. 1 online resource (xii, 448 pages).
30. de Kruif, C.G., F. Weinbreck, and R. de Vries, *Complex coacervation of proteins and anionic polysaccharides.* Current Opinion in Colloid & Interface Science, 2004. **9**(5): p. 340-349.
31. Overbeek, J.T. and M.J. Voorn, *Phase separation in polyelectrolyte solutions; theory of complex coacervation.* J Cell Physiol Suppl, 1957. **49**(Suppl 1): p. 7-22; discussion, 22-6.

32. Veis, A. and C. Aranyi, *Phase Separation in Polyelectrolyte Systems .1. Complex Coacervates of Gelatin.* Journal of Physical Chemistry, 1960. **64**(9): p. 1203-1210.
33. Bahadur, B., *Liquid Crystals Application and Uses.* Journal of the SID, 1995. **2**(1): p. 364.
34. Mistry, K.K., *Hydrogel Microcapsules*, Ashland, Editor. 2013: UK.
35. Sansukcharearnpon, A., et al., *High loading fragrance encapsulation based on a polymer-blend: preparation and release behavior.* Int J Pharm, 2010. **391**(1-2): p. 267-73.
36. Loxley, A. and B. Vincent, *Preparation of Poly(methylmethacrylate) Microcapsules with Liquid Cores.* J Colloid Interface Sci, 1998. **208**(1): p. 49-62.
37. Poncelet, C.P., *Interfacial Polymerisation Versus Cross-Linking Microencapsulation.* Bioencapsulation Innovations, 2013: p. 1-28.
38. Gharsallaoui, A., et al., *Applications of spray-drying in microencapsulation of food ingredients: An overview.* Food Research International, 2007. **40**(9): p. 1107-1121.
39. Re, M.I., *Microencapsulation by spray drying.* Drying Technology, 1998. **16**(6): p. 1195-1236.
40. Madene, A., *Flavour encapsulation and controlled release – a review.* International Journal of Food Science and Technology 2006. **41**(1): p. 1-21.
41. Rosenberg, M., Y. Talmon, and I.J. Kopelman, *The Microstructure of Spray-Dried Microcapsules.* Food Structure, 1988. **7**(1): p. 15-23.
42. Risch, S.J., *Encapsulation of Flavors by Extrusion.* Acs Symposium Series, 1988. **370**: p. 103-109.
43. Pybus, D., C. Sell, and Royal Society of Chemistry (Great Britain), *The chemistry of fragrances*. RSC paperbacks. 1999, Cambridge: Royal Society of Chemistry. xvi,276p.
44. Sell, C., *The Chemistry of Fragrances-From Perfumer to Consumer.* RSC Publishing, 2006: p. 33-51.
45. Hongjie, L.Z., L. , *An overview on synthetic methods of Benzyl Acetate.* European Chemical Bulletin, 2013. **2**(5): p. 272-274.
46. Boh, B., & Frere, Y, *Microencapsulation by Chemical Methods: A solution for the Past or Future.* Bioencapsulation Innovations, 2013: p. 1-28.
47. Zieringer, M.A., et al., *Microcapsules for Enhanced Cargo Retention and Diversity.* Small, 2015. **11**(24): p. 2903-9.
48. Lee, H., et al., *Encapsulation and Enhanced Retention of Fragrance in Polymer Microcapsules.* ACS Appl Mater Interfaces, 2016. **8**(6): p. 4007-13.

49. Yang, Y., et al., *Versatile fabrication of nanocomposite microcapsules with controlled shell thickness and low permeability.* ACS Appl Mater Interfaces, 2013. **5**(7): p. 2495-502.
50. Sun, B.J., et al., *Microfluidic melt emulsification for encapsulation and release of actives.* ACS Appl Mater Interfaces, 2010. **2**(12): p. 3411-6.
51. Delcea, M., et al., *Anisotropic multicompartment micro- and nano-capsules produced via embedding into biocompatible PLL/HA films.* Chemical Communications, 2011. **47**(7): p. 2098-2100.
52. Petro, R. and M. Schlesinger, *Direct Electroless Deposition of Nickel Boron Alloys and Copper on Aluminum Containing Magnesium Alloys.* Electrochemical and Solid State Letters, 2011. **14**(4): p. D37-D40.
53. Satas, D. and A.A. Tracton, *Coatings technology handbook*. Second edition, revised and expanded. ed. xvi, 902 pages.
54. Horiuchi, S. and Y. Nakao, *Platinum colloid catalyzed etchingless gold electroless plating with strong adhesion to polymers.* Surface & Coatings Technology, 2010. **204**(23): p. 3811-3817.
55. Fujiwara, Y., et al., *Ag nanoparticle catalyst for electroless Cu deposition and promotion of its adsorption onto epoxy substrate.* Journal of the Electrochemical Society, 2008. **155**(5): p. D377-D382.
56. Dinderman, M.A., et al., *Electroless plating of iron onto cellulose fibers.* Chemistry of Materials, 2006. **18**(18): p. 4361-4368.
57. Patchan, M.W., et al., *Liquid-Filled Metal Microcapsules.* Acs Applied Materials & Interfaces, 2012. **4**(5): p. 2406-2412.
58. Tsuneyoshi, T. and T. Ono, *Metal-coated microcapsules with tunable magnetic properties synthesized via electroless plating.* Materials Science and Engineering B-Advanced Functional Solid-State Materials, 2017. **222**: p. 49-54.
59. Toshima, N., *Metal Nanoparticles for Catalysis.* Nanoscale Materials, 2003. **35**(34): p. 79-96.
60. Moshfegh, A.Z., *Nanoparticle catalysts.* Journal of Physics D-Applied Physics, 2009. **42**(23).
61. Pastoriza-Santos, I. and L.M. Liz-Marzan, *Formation of PVP-protected metal nanoparticles in DMF.* Langmuir, 2002. **18**(7): p. 2888-2894.
62. Zhu, S.L., et al., *Preparation of copper-coated beta-SiC nanoparticles by electroless plating.* Surface & Coatings Technology, 2011. **205**(8-9): p. 2985-2988.
63. Lin, C., et al., *Size effect of gold nanoparticles in catalytic reduction of p-nitrophenol with NaBH4.* Molecules, 2013. **18**(10): p. 12609-20.

64. Solomon, S.D., *Synthesis and Study of Silver Nanoparticles.* Journal of Chemical Education, 2007. **84**(2): p. 322-325.
65. Zidki, T., Cohen, H., Meyerstein, D.,, *Direct deposition of silver nanoparticles on silica nanoparticles in aqueous suspensions. .* The Optimization of Composition, Structure and Properties of Metals, Oxides, Composites, Nano and Amorphous Materials, 2014: p. 175-179.
66. Lee, H., et al., *Mussel-inspired surface chemistry for multifunctional coatings.* Science, 2007. **318**(5849): p. 426-30.
67. Luo, H.Y., et al., *Facile synthesis of novel size-controlled antibacterial hybrid spheres using silver nanoparticles loaded with poly-dopamine spheres.* Rsc Advances, 2015. **5**(18): p. 13470-13477.
68. Wang, W., et al., *Fabrication of silver-coated silica microspheres through mussel-inspired surface functionalization.* J Colloid Interface Sci, 2011. **358**(2): p. 567-74.
69. Wang, W., et al., *Preparation and characterization of polystyrene/Ag core-shell microspheres--a bio-inspired poly(dopamine) approach.* J Colloid Interface Sci, 2012. **368**(1): p. 241-9.
70. Wang, W.C., et al., *Dopamine-Induced Surface Functionalization for the Preparation of Al-Ag Bimetallic Microspheres.* Journal of the Electrochemical Society, 2011. **158**(4): p. D228-D233.
71. Ball, V., *Polydopamine films and particles with catalytic activity.* Catalysis Today, 2018. **301**: p. 196-203.
72. Ito, S., *A chemist's view of melanogenesis.* Pigment Cell Research, 2003. **16**(3): p. 230-236.
73. Yin, X.B. and D.Y. Liu, *Polydopamine-based permanent coating capillary electrochromatography for auxin determination.* Journal of Chromatography A, 2008. **1212**(1-2): p. 130-136.
74. d'Ischia, M., A. Napolitano, and A. Pezzella, *5,6-Dihydroxyindole Chemistry: Unexplored Opportunities Beyond Eumelanin.* European Journal of Organic Chemistry, 2011(28): p. 5501-5516.
75. Hong, S., et al., *Non-Covalent Self-Assembly and Covalent Polymerization Co-Contribute to Polydopamine Formation.* Advanced Functional Materials, 2012. **22**(22): p. 4711-4717.
76. Chen, C.T., et al., *Excitonic effects from geometric order and disorder explain broadband optical absorption in eumelanin.* Nature Communications, 2014. **5**.
77. Perrot, D., C. Croutxe-Barghorn, and X. Allonas, *Towards mussel-like on-demand coatings: light-triggered polymerization of dopamine through a photoinduced pH jump.* Polymer Chemistry, 2016. **7**(15): p. 2635-2638.

78. Okuda, H., et al., *Possible Oxidative Polymerization Mechanism of 5,6-Dihydroxyindole from A Initio Calculations.* Journal of Physical Chemistry A, 2008. **112**(44): p. 11213-11222.
79. Della Vecchia, N.F., et al., *Building-Block Diversity in Polydopamine Underpins a Multifunctional Eumelanin-Type Platform Tunable Through a Quinone Control Point.* Advanced Functional Materials, 2013. **23**(10): p. 1331-1340.
80. Postma, A., et al., *Self-Polymerization of Dopamine as a Versatile and Robust Technique to Prepare Polymer Capsules.* Chemistry of Materials, 2009. **21**(14): p. 3042-3044.
81. Dreyer, D.R., et al., *Elucidating the Structure of Poly(dopamine).* Langmuir, 2012. **28**(15): p. 6428-6435.
82. Dreyer, D.R., et al., *Perspectives on poly(dopamine).* Chemical Science, 2013. **4**(10): p. 3796-3802.
83. Qu, Y.N., et al., *Interfacial Polymerization of Dopamine in a Pickering Emulsion: Synthesis of Cross-Linkable Colloidosomes and Enzyme Immobilization at Oil/Water Interfaces.* Acs Applied Materials & Interfaces, 2015. **7**(27): p. 14954-14964.

3 Materials and Method

3.1 Materials

The following material were used as obtained: Polyvinlypyrrolidone (PVP, 360kDa, Sigma Aldrich, CAS: 9003-39-8), Polyvinlypyrrolidone (PVP, 40kDa, Sigma Aldrich, CAS: 9003-39-8), Polyvinlypyrrolidone (PVP, 10 kDa, Sigma Aldrich, CAS: 9003-39-8), (NaBH4), (Sigma Aldrich, CAS: 26023-84-7), Choroplatinic acid hydrate, ($H_2Cl_6Pt.x\ H_2O$), (Sigma Aldrich, CAS: 26023-84-7), Gold (III) chloride hydrate ($HAuCl_4.H_20$), (Sigma Aldrich, CAS:27988-77-8), Silver Nitrate, ($AgNO_3$), (Sigma Aldrich, CAS: 7761-88-8), Hexadecane, ($CH_3(CH2)_{14}CH_3$), Sigma Aldrich, CAS: 544-76-3), Hexyl Salicylate, ($C_{13}H_{18}O_3$), Sigma Aldrich, CAS: 6259-76-3) Hydrogen Peroxide, (H_2O_2), Sigma Aldrich, CAS: 7722-84-1) and Glucose, ($C_6H_{12}O_6$), Sigma Aldrich, CAS: 50-99-7.

3.2 Methodology

3.2.1 Synthesis of Platinum nanoparticles

Platinum nanoparticles were synthesised in situ, stabilised with PVP for use as catalysis for the deposition of gold film growth. H_2Cl_6Pt .6 H_2O (0.23 g, 5.61 mM) was dissolved in a solution (100 ml) of PVP (0.0067 wt %). $NaBH_4$ (2 ml, 1.1 mM) was added to the solution under vigorous stirring (1000rpm, 250ml conical flask, magnetic stirrer bar), resulting in a dark brown/black suspension. After 5 minutes of vigorous stirring the nanoparticle suspension was filtered with a PTFE filter (0.2 µm) and stored in the fridge.

3.2.2 Effect of varying molecular weight of PVP

Platinum nanoparticles were synthesised as described above with H_2Cl_6Pt .6 H_2O (0.23g, 5.61 mM), $NaBH_4$ (2 ml, 1.1 mM), and PVP (10, 40, 56, 360 kDa) resulting in PVP solutions ($1.675x10^{-3}$, $6.7x10^{-3}$, $9.38x10^{-3}$, $6x10^{-2}$ wt %) respectively, containing an equal number of polymer chains.

3.2.3 Pt-NP stabilised emulsions

Emulsions were stabilised using 10 ml Pt-NPs dispersion (0.56 mM H2Cl6Pt .6 H2O) to which 0.4 ml Hexadecane was added and emulsified using sonic dismembrator ultrasonic processor for 1 min (40% amplitude, 3.1mm micro-tip, in a 40 ml glass vial) in a water bath. The resulting emulsion was placed on the carousel for 10 mins and washed with Milli-Q water after the emulsion had creamed.

3.2.4 Effect of varying oil fraction on Pt-NP stabilised emulsions

Emulsions were stabilised as described above using 10ml Pt-NPs dispersion (0.56 mM H_2Cl_6Pt .6 H_2O) to which hexadecane was added (0.4, 0.55, 0.7, 1.2 and 1.6 ml), corresponding to oil volume fractions ϕ 0.04, 0.05, 0.07, 0.1 and 0.14.

3.2.5 Gold film growth at emulsion interface

Microcapsules were prepared from a hexadecane (0.4 ml) and Pt-NPs (10 ml) emulsion homogenised with an ultrasonic probe at 40% amplitude for 1 minute. Following the washing cycle, the emulsion (0.5 ml) was placed in a plating solution consisting of PVP (5 ml, 0.2 wt%), gold (III) chloride hydrate (1ml 40 mM) and hydrogen peroxide (1ml 60 mM) as a reducing agent in a 40 ml vial. The microcapsules

were mixed for 10 minutes and subsequently washed after sedimentation by removing the supernatant and replacing with Milli-Q water.

3.2.6 Effect of H202 concentration on shell thickness

Microcapsules were synthesised as described above, emulsion (0.5 ml), plating solution consisted of PVP (5 ml, 0.2 wt%), gold (III) chloride hydrate (1ml 40 mM), and the hydrogen peroxide concentration was varied (1ml) (60mM, 180mM, 300 mM and 600 mM).

3.2.7 Effect of Oil volume fraction and gold (III) chloride hydrate concentration on shell thickness

Microcapsules were prepared from a hexadecane oil volume fractions ϕ (0.04, 0.05, and 0.07) and Pt-NPs (10 ml) emulsion homogenised with an ultrasonic probe at 40% amplitude for 1 minute. Following the washing cycle, the emulsion (0.5ml) was placed in a plating solution consisting of PVP (5 ml, 0.2 wt%), gold (III) chloride hydrate (0.5, 1 and 1.5 ml 40 mM) and hydrogen peroxide (0.5, 1 and 1.5 ml 60 mM) as a reducing agent in a 40 ml vial. The microcapsules were mixed for 10 minutes and subsequently washed after sedimentation by removing the supernatant and replacing with Milli-Q water.

3.2.8 Synthesis of Si/Pt Composites

Pt-NPs synthesised as described in section 3.1.1, (3.3 ml) were added to a silica suspension (0.1g) and left to stir over 4 hours. The Si/Pt composite was centrifuged after settling, the continuous phase was removed and the composite was re-dispersed in Milli-Q water resulting in a Si/Pt composite suspension (0.1 wt% silica).

3.2.9 Effect of Pt-NPs on Si surface coverage

As described above Pt-NPs (8.25, 16.5 and 33 ml) were added to a silica suspension (0.1g) and left to stir over 4 hours. The Si/Pt composite was centrifuged after settling, the continuous phase was removed and the composite was re-dispersed in Milli-Q water resulting in a composite suspension (0.1 wt% silica).

3.2.10 Si/Pt stabilised emulsions

Emulsions were stabilised using 9ml Si/Pt composite suspensions (10, 25, 50 and 100% theoretical surface coverage of silica with Pt-NPs) to which 1.0 ml hexadecane was added and emulsified using sonic dismembrator ultrasonic processor for 1 min (40% amplitude, 3.1 mm micro-tip, in a 40 ml glass vial) in a water bath. The resulting emulsion was placed on the carousel for 10 minutes and washed with Milli-Q water after the emulsion had creamed.

3.2.11 Si/Pt composite stabilised emulsions-effect of oil volume fraction

Si/Pt stabilised emulsion (100% theoretical surface coverage of silica with Pt-NPs) were prepared with varying oil volume fractions of hexadecane (ϕ 0.1, 0.18 and 0.25) by using sonic dismembrator ultrasonic processor for 1 min (40 % amplitude, 3.1 mm micro-tip, in a 40 ml glass vial) in a water bath. The resulting emulsion was placed on the carousel for 10 minutes and washed with Milli-Q water after the emulsion had creamed.

3.2.12 Gold film growth on Si/Pt stabilised emulsion droplets

Microcapsules were prepared from a hexadecane (1ml, oil volume fraction ϕ 0.1) and Si/Pt (9 ml) (10, 25, 50 and 100% theoretical surface coverage with Pt-NPs) emulsion

homogenised with an ultrasonic probe at 40% amplitude for 1 minute. Following the washing cycle, the emulsion (0.5 ml) were placed in a plating solution consisting of PVP (5 ml, 0.2 wt%), gold (III) chloride hydrate (1ml 40 mM) and hydrogen peroxide (1ml 60 mM) as a reducing agent in a 40 ml vial. The microcapsules were mixed for 10 minutes and subsequently washed after creaming by removing the supernatant and replacing with Milli-Q water.

3.2.13 Preparation of Tris(hydroxymethyl)aminomethane tris-buffer solution

Tris(hydroxymethyl)aminomethane (tris) (10 mM) solution was prepared by adding tris (1.2114g) into Milli-Q water (900 ml), HCl was added dropwise until the pH was stable at 8.5. The solution was transferred to a measuring cylinder (1000 ml) and filled up to the mark with Milli-Q water.

3.2.14 Dispersing Silica

Silica 100nm (0.1 g) was dispersed in the tris buffer (9 ml) using sonic dismembrator ultrasonic processor for 1 min (x3) (40% amplitude, 3.1mm micro-tip, in a 40 ml glass vial) in a water bath.

3.2.15 PDA self-polymerisation on Silica particles

The silica suspension, as described above (10 ml, 1wt% Si) was added to 290 ml of tris-buffer (10 mM pH8.5) under agitation using an overhead stirrer with a paddle shift stirrer (300 rpm), to which different concentrations of dopamine was added (mass of dopamine/total surface area 0.04 and 0.22 g/m^2) and left to stir for 24 hours. After 24 hours the Si-PDA composites was centrifuged out, re-dispersed in Milli-Q, this was repeated to remove any PDA in the continuous phase.

3.2.16 Silica stabilised emulsions

Emulsions were stabilised using Si suspension (9ml) to which hexadecane (1 ml) was added and emulsified using sonic dismembrator ultrasonic processor for 1 min (40% amplitude, 3.1mm micro-tip, in a 40 ml glass vial) in a water bath. The resulting emulsion was placed on the carousel for 10 mins and washed with Milli-Q water after the emulsion had creamed.

3.2.17 Synthesis of PDA microcapsules stabilised via silica (Pickering emulsions)

Silica stabilised emulsion (10 ml) as described above were added to a tris buffer (10mM, pH 8.5) (290 ml) under agitation using an overhead stirrer with a paddle shift stirrer (300 rpm), to which varying concentrations of dopamine was added (mass of dopamine/total emulsion surface area 0.09, 0.19, and 0.28 g/m^2) and left to stir for 24 hours. After 24 hours the PDA microcapsules was left to cream and the supernatant was replaced with Milli-Q water.

3.2.18 Silver plating bath

Silver nitrate (10mM) 0.17g was added to Milli-Q water (90ml) and PVP (40 kDa 0.1g 0.5 wt%), to which under agitation NH_4OH (33 wt%) was added drop-wise until the solution went clear. To the solution NaOH was added dropwise until the pH was stable at 11, the solution totalled 100 ml.

3.2.19 Silver plating of PDA microcapsules

Silver coated microcapsules were prepared from PDA microcapsules (1 ml) suspended in silver plating solution 10 ml ($[Ag(NH_3)_2]^+$, 10 and 20 mM) and left stirring for 1 hour in a 10 ml glass vial, to which 2ml glucose (100, 200 mM) was added

resulting in silver coated PDA microcapsules. The microcapsules were mixed for 10 minutes and subsequently washed after creaming by removing the supernatant and replacing with Milli-Q water.

3.3 Characterisation methods

3.3.1 Transmission electron microscopy TEM

Characterisations of Pt-NPs, Si/Pt composites and Si-PDA composites

Pt-NPs, Si/Pt composites and Si-PDA composites were analysed using a FEI Tecnai TF20 field emission transmission gun electron microscope (FEGTEM) fitted with a HAADF detector Gatan Orius SC600A CCD camera. An Oxford Instruments INCA 350 EDX (energy dispersive x-ray) system/80mm X-Max SDD detector was used for elemental mapping. Samples were dispersed on TEM grids (holey carbon film, 400 Cu Mesh from Agar Scientific) and allowed to dry. Particle size was determined using ImageJ software, from this the nanoparticle core size can be determined, by analysing a 1000 nanoparticle and taking an average mean diameter.

3.3.2 Zetasizer

DLS was used to measure the changes in hydrodynamic diameter of Pt-NPs stabilised with PVP 10, 40, 56 and 360 kDa. The zetasizer Nano ZS (Malvern Nano-ZS) was used for the measurements. The zetasizer uses helium-neon laser with a wavelength of 633 nm and utilises a non-invasive back-scatter (NIBS) technology. The zetasizer uses a backscatter angle of 173^{o} compared to the conventional 90^{o} angle used in most DSL measurements. The zetasizer consists of a laser, detector and a focusing lens. The focusing lens allows the positioning of the beam to maximise the scatter

information depending on the size of the particles measured. The laser shinning on the particles in the solution undergoing Brownian motion, causes a Doppler shift to slightly higher or lower frequencies, this is dependent on whether the particle is moving away or towards the detector, resulting in the shifts producing a Doppler frequency broadening peak. A pattern of beat frequencies is produced when the incident light and broadened scattered signal is mixed, which allows the calculation of the particle diffusion coefficient which is used to calculate the hydrodynamic diameter (D_H) using the Stokes-Einstein equation 3.1:

$$D_H = \frac{k\ x\ T}{3\pi\ x\ \eta\ x\ D_{sol}}$$

Where k is the Boltzmann constant, T is the absolute temperature, η is the viscosity of the solvent and D_{sol} is the diffusion coefficient of the object in the solution.

3.3.3 UV-Vis spectroscopy

Pt-NP concentration was determined with a Perkin Elmer Lambda 950 UV-Vis spectrophotometer in order to analyse the absorption concentration on the surface of silica. Samples were analysed from 200-1000 nm. A calibration curve was plotted between the ranges 0 - 0.04 mM Pt-NPs, from this the concentration of Pt-NPs adsorbed on the silica surface was determined.

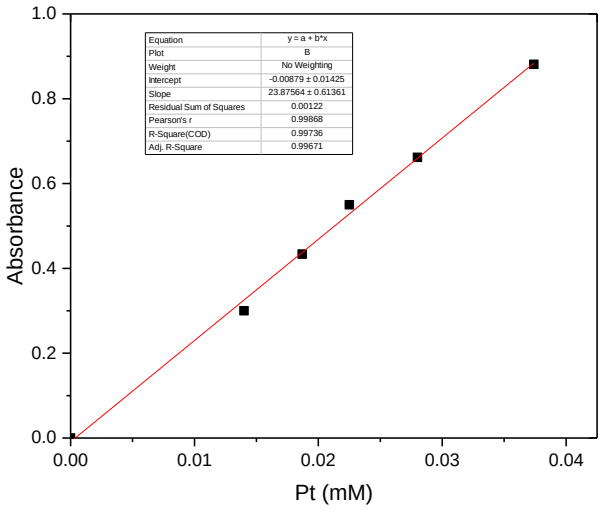

Figure 3. 1: UV-Vis Absorbance calibration as a function of Pt-NP concentration.

3.4 Characterisation of oil-water interface

3.4.1 Pendant drop tensiometer

Pendant drop tensiometry offers a simple and convenient solution to determine surface and interfacial tension. To analyse the emulsion properties and adsorption of Si/Pt composites at the oil-water interface, interfacial tension was recorded using a Theta Optical tensiometer with a USB3 difital camera and LED based background lighting. The surface tension measurement was taken by injecting a droplet of Si/Pt composite (0.1 wt%) into hexadecane and obtaining the largest drop possible. The surface tension was then calculated based on the Young-Laplace equation. A 22GA needle was used for the measurements. The shape of a droplet hanging from a syringe is determined from the balance of forces, including the surface tension. The interfacial tension can be related to the drop shape through equation 3.2.

3.2

$$y = \Delta pxgxRo/\beta$$

y = surface tension

Δp = difference in density between fluids at the interface

β = shape factor

g =gravitational constant

Ro =radius of drop

To determine the shape factor,β, the Young-Laplace equation coupled as a set of dimensionless differential equations can be applied.

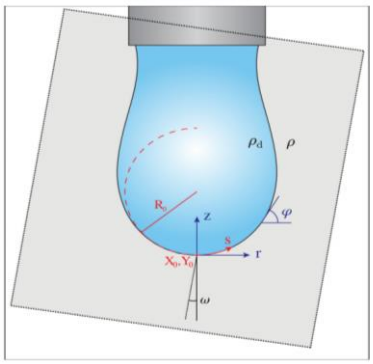

$$\frac{d\varphi}{d\bar{s}} = 2 - Bo\,\bar{z} - \frac{\sin\varphi}{\bar{r}}$$
$$\frac{d\bar{r}}{d\bar{s}} = \cos\varphi$$
$$\frac{d\bar{z}}{d\bar{s}} = \sin\varphi$$

Figure 3. 2: Schematic of pendant drop below a needle with associated variables used to detremine the shape factor, $\boldsymbol{\beta}$.

Computational routine consisting of two steps is used for the pendant drop analysis. The drop profile is extracted from an experimental image followed by the iterative approximation of the Young-Laplace equation.

3.4.2 Three phase contact angle wettability

To measure the three phase contact angle θ (solid/water/air), glass slides were coated in Si-Pt composites by dipping the glass slides in Si-Pt composite suspension and left to air dry. A water droplet was placed on the surface of the Si-Pt coated glass slide and the 3 phase contact angle θ was measured. Importantly, we believe that these measurements do not accurately represent the contact angles of the actual particles, but more represents a modified glass slide contact angle. Information may correlate, but with caution.

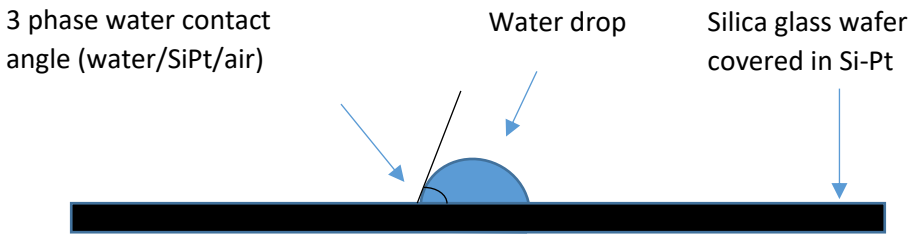

Figure 3. 3: Schematic diagram representing measurement of 3 phase contact angle $\boldsymbol{\theta}$ (water/Si-Pt/air).

3.5 Characterisation of emulsion

3.5.1 Mastersizer

A Malvern hydro 2000SM Mastersizer was used in conjunction with a Malvern 'Small Volume Sample Dispersion Unit' to measure size distributions of microcapsules via low angle laser light scattering (LALLS).

3.5.2 Optical light microscope

The emulsions were visualised using an Olympus BX51 optical microscope with a digital camera. Cell D imaging software was used to record the images.

3.6 Characterisation of microcapsules

3.6.1 Scanning electron microscope SEM

Microcapsules were added to a SEM specimen stub and left to air dry. Dried microcapsules were analysed using The Hitachi SDD detector, operating at 2kV. Dried microcapsules were also imaged using the TM3030 Tabletop SEM at 15 kV.

3.6.2 Cryo-SEM FIB

Cryo-Sem was used to visual Si/Pt stabilised emulsions in order to study the Si/Pt arrangement at the oil/water interface (via Focussed ion beam FIB). The samples were frozen by dipping them in slushed nitrogen and transferred under vacuum to the FEI Helios G4 CX and analysed at 2 kV (FIB 30kV). All samples were coated in Pt 5uA for 45 seconds prior to analysis.

3.6.3 Energy-dispersive X-ray spectroscopy EDX

Samples were dispersed on TEM grids (holey carbon film, 400 Cu Mesh from Agar Scientific) and allowed to dry and elemental analysis was carried out using the FEI Titan Themis Cubed 300 TEM EDX.

3.6.4 Microtoming

The samples were air dried and mixed with an epoxy resin to harden the samples. A diatome diamond knife was used to section the samples on a Reichert-Jung Ultracut-E Ultramicrotome. The thickness of the cut section was 90 nm thick and picked up on a 200 mesh, thin bar, copper grid coated with formvar. The samples were analysed under TEM.

3.6.5 Optical microscope

The gold coated microcapsules were visualised using an Olympus BX51 optical microscope with transmitted and reflected light with a digital camera. Cell D imaging software was used to record the image.

3.6.6 Differential scanning calorimetry DSC

Perkin Elmer Differential scanning calorimetry analysis 8000 (DSC) was used to analyse the thermal properties of PCM and MEPCMs. From the DSC thermograms curve, energy storage (latent heat), supercooling and thermal conductivity can be deduced. The DSC technique measures the heat flow and the temperature associated with phase change as a function of temperature. The sample and reference material is heated and cooled, while the furnace keeps the temperature of both equal, the difference in the electrical power utilised by the furnace is monitored and used to determine the amount of energy absorbed or release in the sample. The temperature heating and cooling programme was set at 2°C /min (0-30°C). Prior analysis MEPCMs were washed with ethanol and dried in the oven at 100°C.

3.6.7 Gas chromatography

Release of the hexadecane core from the microcapsules was analysed using gas chromatography (Perkin Elmer Clarus 580GC). The microcapsules (1 ml) were added to ethanol (4 ml). The microcapsules were dispersed and 1ml sample was taken and centrifuged on an Eppendorf Mini Spin plus at 8000 rpm for 1 minute to remove the microcapsules. The remaining sample was placed in a water bath at 40°C. 1 ml sample was taken after 10 and 30 days and centrifuged. All supernatant from samples after centrifuging was added to a GC sample vial for GC analysis.

Samples were analysed on a Perkin Elmer Clarus 580GC, the column temperature was programmed from 50°C to 300°C at 20°C/min at a flow rate of 2 ml/min. The data was compared to a calibration curve plotted of hexadecane.

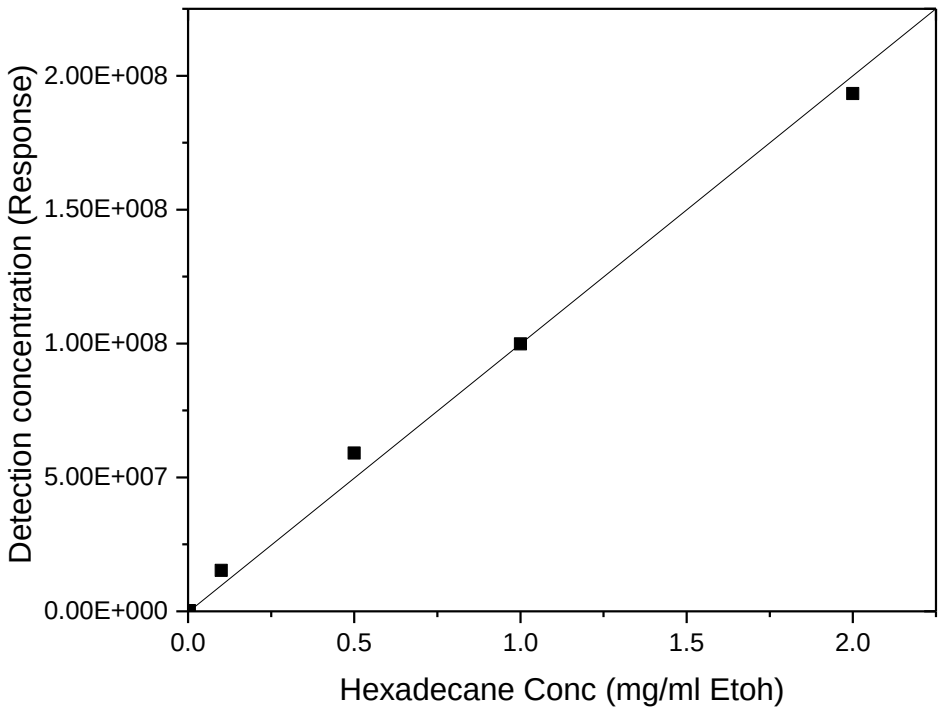

Figure 3. 4: GC calibration as a function of hexadecane/Ethanol (mg/ml) concentration.

3.6.8 TGA analysis

Thermal gravimetric analysis mettler Toledo TGA/DSC was used to analyse the shell thickness of gold coated microcapsules. A known concentrated Microencapsulation sample was placed in an aluminium crucible and closed with a lid containing a hole to release any pressure build up. The crucible was sealed using a press machine and placed in the TGA tray to conduct the experiment. The microcapsule sample was heated from 35°C to 105°C (rate 10°C /min) and held for 10 mins at 105°C to remove water present in sample. The sample temperature was ramped up to 500°C (rate 10 °C /min) to remove the hexadecane core and the sample temperature was cooled back down to room temperature, resulting in only the gold shell material mass remaining. The shell thickness analysis is demonstrated in chapter 3.7.1.

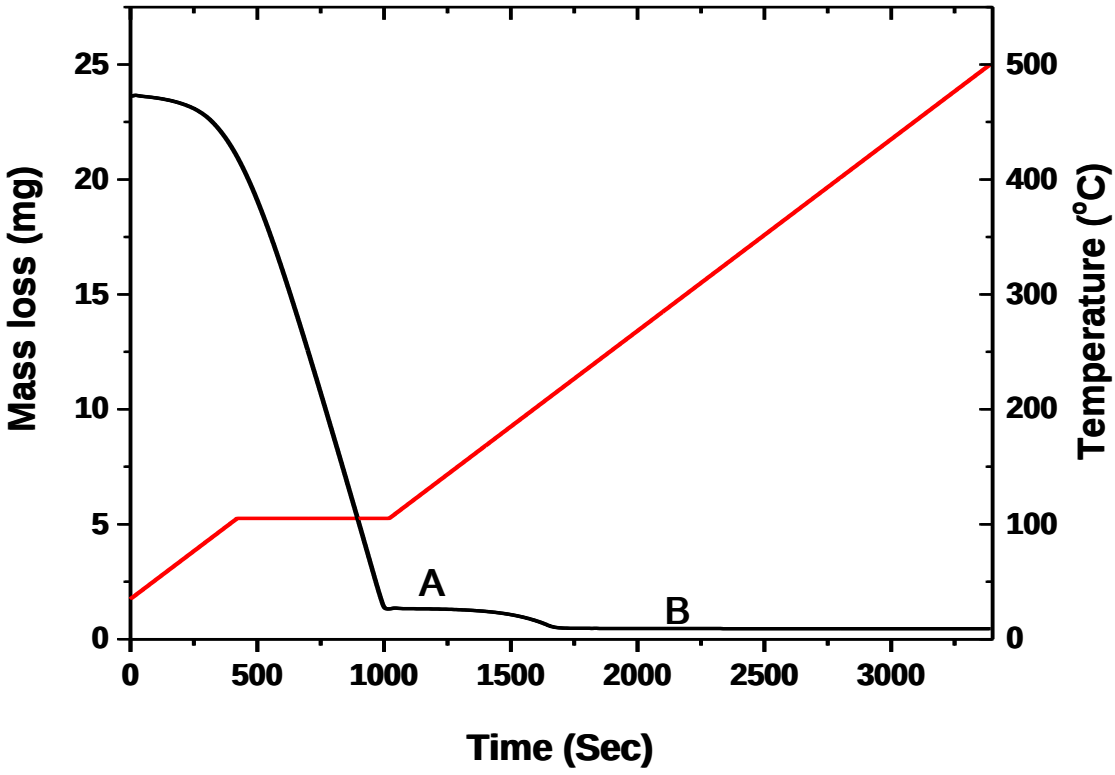

Figure 3. 5: Mass loss (mg) and temperature (°C) plotted against time (sec).The oil loss mass (A) (Hexadecane) and remaining mass (B) (Au) are used to calculate the shell thickness of AU microcapsules.

3.7 Calculations

3.7.1 Theoretical and TGA Shell thickness calculations

The thickness of metal coated microcapsules shell can be theoretically calculated from the emulsion size distribution obtained from the mastersizer, the volume of hexadecane core and the Au salt. The thickness of the shell is calculated from the total surface area which is based on the bin limits of the emulsion size distribution, from which a mean size is obtained for each bin limit and the surface area is calculated at each bin limit. The total amount of Au salt added to the system is divided by the total surface area on the emulsion to obtain the shell thickness. Equation 3.3, describe he theoretical shell thickness calculations.

$$S_{tot} = S_{drop}\ x\ N$$

$$V_{drop} = \frac{4}{3}\pi r^3$$

$$N = \left(\frac{V_{oil}}{V_{drop}}\right)$$

$$S_{drop} = 4\pi r^2$$

3.3

S_{tot}= Total surface area of emulsion droplets

S_{drop}= Surface area of single emulsion droplet

N = Number of droplets in emulsion

V_{drop}= Volume of single emulsion droplet

r = Radius of emulsion droplet

V_{oil}= Volume of oil (hexadecane)

The actual thickness of metal coated microcapsules shell can be calculated from the emulsion size distribution obtained from the mastersizer, the volume of hexadecane core and the gold from the TGA analysis. The thickness of the shell is calculated from the total surface area which is based on the bin limits of the emulsion size distribution, from which a mean size is obtained for each bin limit and the surface area is calculated at each bin limit. The total amount of gold and hexadecane obtained from the TGA is substituted into equation 3.4 and 3.5 to obtain the actual shell thickness.

$$T_E = \frac{M_S}{M_O} x\, S_{tot}$$

$$S_T = \frac{V_{Au}}{T_E}$$

3.4

T_E = Total surface of emulsion used

M_S= Oil mass in sample

M_O = Total mass of oil used in emulsion sample

S_T = Theoretical shell thickness nm

V_{Au} = Volume of Au used in the electroless deposition process

$$T_{TGA} = \frac{M_{TGA}}{M_O} x\, S_{tot}$$

$$T_{shell} = \frac{V_{Au}}{T_{TGA}}$$

3.5

T_{TGA} = Total surface area of Au coated emulsion in TGA crucible

M_{TGA} = Mass of oil detected by TGA in Au coated emulsion sample (in TGA crucible)

T_{shell} = Shell thickness nm

T_{TGA} = Total surface area of Au coated emulsion in TGA crucible

The total number of emulsion droplets in the system can be calculated from the density and mass of hexadecane:

$$Volume\ of\ Hexadecane = \frac{Mass\ of\ hexadecane}{Density\ of\ hexadecane} = \frac{0.4}{0.77} = 0.52\ cm^3$$

$$Volume\ of\ single\ emulsion\ droplet = \frac{4}{3}\pi r^3 = \frac{4}{3}\pi\ x\ (500nm^3) = 5.2\ x\ 10^8\ nm^3$$
$$= 5.2\ x\ 10^{-13}\ cm^3$$

$$Number\ of\ droplets\ in\ emulsion\ N = \frac{Total\ Volume\ of\ oil\ in\ emulsion}{Volume\ of\ single\ emulsion\ droplet} = \frac{0.52}{5.2\ x\ 10^{-13}}$$
$$= 1x\ 10^{12}$$

$$Surface\ area\ of\ single\ emulsion\ droplet\ S_{drop} = 4\pi r^2 = 4\pi x500^2 = 3.14\ x\ 10^6\ nm^3$$

$$The\ total\ surface\ area\ S_{tot} = 1x\ 10^{12}\ x\ 3.14\ x\ 10^6 = 3.1\ x\ 10^{18}\ nm^2$$

The total surface area is based on one bin limit and is repeated for all bin limits to get the sum of total surface area based on bin limits.

$$Bin\ limit\ 1 = S_{tot}\ x\ \frac{Volume\ \%}{100}$$

$$Total\ surface\ area\ (bin\ limits) = Sum\ of\ bin\ limits\ Surface\ area$$

$$Theoretical\ Shell\ thickness\ T_{shell} = \frac{V_{Au}}{T_E}$$

$$Volume\ of\ Au = \frac{mass\ of\ Au}{Density\ 19.32\ gcm^3}$$

3.7.2 Ratio of polymer chains to Platinum nanoparticles

From the number of NPs and polymer chains in the system the ratio between the two can be calculated. For the nanoparticle synthesis 0.11 wt% Pt and 0.0067wt% PVP was used (100 ml).

For the number of polymer chains in the system the following equation was applied: (Equation 3.6)

$$N_{PVP} = \frac{M_{PVP}}{M_W} . N_A \qquad 3.6$$

Where M_{PVP} is the mass of PVP (g), MW is the molecular weight of PVP (g mol^{-1}) and N_A is the Avogadro's constant (6.022140857 $x10^{23}$ mol^{-1}. The number of PVP chains calculated was 1.01 $x10^{17}$.

For the number of Pt-NPs in the system the following equation was applied: (Equation 3.7)

$$N_{PtNPs} = (\frac{M}{D})/V$$

$$V = \frac{4}{3} n r^3 \qquad 3.7$$

Where M is the mass of Pt (g), D is the density of Pt (g/cm^3) and V is the volume of a single Pt NP (cm^3). The number of Pt NPs calculated was 4.03 $x10^{17}$.

Table 3. 1: Ratio of Pt-NP core diameter to PVP chain length (PVP 10, 40, 55, 380 kDa) and ratio of PVP chains (PVP 10, 40, 55, 380 kDa) to Pt NPs.

Mean Core diameter of Pt NPs (nm)	PVP MW kDa	Number of PVP chains ($x10^{17}$)	Number of NPs ($x10^{17}$)	Ratio PVP:Pt NPs
3.9	10	1.01 (1.7mg)	1.66	0.6
2.9	40	1.01 (6.7mg)	4.03	0.25
2.7	55	1.01 (11.7mg)	4.99	0.2
2.2	360	1.01 (60.3mg)	9.23	0.1

From the ratio of PVP: Pt it could be concluded no excess PVP was present in the system.

3.7.3 PVP radius of gyration

The radius of gyration of the PVP chain can be calculated using the following equation: (Equation 3.8)

$$R_g = bN^{1/2} \quad 3.8$$

Where:

R_g Radius of gyration

N Number of monomers

b Inter-monomer spacing

This equation assumes the dissolved polymer chain takes up a free random confirmation.

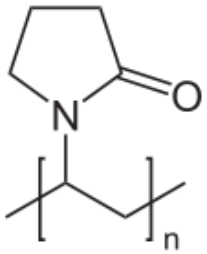

Figure 3.6: PVP molecular structure

For the 10 KDa PVP chains, *N* (number of monomers) is the total molecular mass divided by the mass of the monomer:

$$\frac{10000}{111} = 90$$

The length of a c-c bond (*b* inter-monomer spacing) in a hydrocarbon is 0.15 nm:

$$2\ x\ 0.15 = 0.3\ nm$$

$$R_g = 0.3x\ \sqrt{90}$$

$$R_g = 2.8\ nm$$

3.7.4 PVP chain length

The PVP polymer chain length P_c can be calculated using the following equation: (Equation 3.9)

$$P_c = bN \qquad 3.9$$

P_c Polymer chain length
N Number of monomers
b Inter-monomer spacing

This equation assumes the PVP chain is uncoiled and completely rolled out into a straight line configuration. For the 10 KDa PVP chains:

$$P_c = 0.3x90$$

$$P_c = 27\ nm$$

Table 3. 2: Describes the effect of PVP molecular weight (PVP 10, 40, 58, 380 kDa) on the radius of gyration *Rg*, and polymer chain length *Pc*.

PVP MW kDa	Number of monomers N	Radius of gyration R_g nm	Polymer chain length P_c nm
10	90	2.8	27
40	360	5.7	108
56	495	6.7	149
360	3243	17	973

3.7.5 Calculation of total surface area of silica particles

To work out the surface area of silica equation 3.10 was applied.

3.10

$$S_{tot} = S_{silica}\ x\ N$$

$$S_{silica} = 4\pi r^2$$

$$V_{silica} = \frac{4}{3}\pi r^3$$

$$N = \left(\frac{VT_{silica}}{V_{silica}}\right)$$

S_{tot}= Total surface area of silica particles

S_{silica}= Surface area of single silica particle

N = Number of silica particles

V_{silica}= Volume of single silica particle

r = Radius of silica particle

VT_{Silica}= Volume of total silica particles

Table 3. 3: Calculated total surface area of silica particles

Silica Conc	Density of silica g/cm^3	Radius of silica nm	Volume of one silica particle nm^3 x10^{-16}	Surface area of single silica particle nm^2	Number of silica particles x10^{13}	Total surface area silica particles nm^2 x10^{18}
0.1g	2.65	50	5.2	31400	7.2	2.3

3.7.6 Calculations of Pt-NP coverage of silica surface

To work the coverage of silica surface with Pt-NPs the total surface area of Pt-NPs on a flat surface in a hexagonal packing arrangement was calculated, the silica surface area was also calculated and the surface coverage was worked out from the numbers in table 3.4

Total surface area of silica particles = 2.3 x10^{18} nm^2

Table 3. 4: Calculated surface coverage of silica with Pt-NPs.

Sample No.	Total surface area of silica particles x10^{18} nm^2	Pt-NPs (ml)	Total Theoretical surface area Pt-NPs can cover (x10^{18}nm^3)	Maximum surface coverage of Si (%) by Pt-NPs
1	2.3	3.3	0.23	10
2	2.3	8.25	0.575	25
3	2.3	16.5	1.15	50
4	2.3	33	2.3	100

3.7.7 Calculations of silica packing gaps

To work out the packaging gaps in between the silica particles the following calculations were applied.

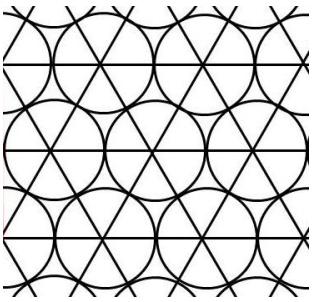

Figure 3. 6: Packing arrangement of silica particles in a hexagonal arrangement at the interface.

Figure 3. 7: Surface area of single silica particle.

$$A = \pi r^2$$

A = Surface area of silica particle 100nm

A= 7855 nm^2

A= 7855/6= 1309

Surface area of triangle T= 100^2/2 = 5000 nm^2

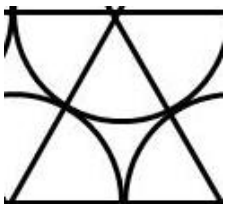

Figure 3. 8: Surface area of triangle and the packing gap between the silica particles.

Gap in between silica particles = 3x 1309-5000 = 1072.4 nm^2

$$\sqrt{1072.4} = \frac{32.75}{2} = 16.4 \text{ nm}$$

3.7.8 Theoretical PDA thickness on silica stabilised emulsions

To work out the PDA shell thickness on silica stabilised emulsions the density of melanin (1.6 g/m^2) was used as the density of PDA is not known. The conditions are illustrated in table 3.5 and calculations are demonstrated in chapter 3.7.1.

Table 3. 5: Calculated PDA thickness on silica stabilised emulsion

Total emulsion surface area nm^2 x10^{18}	Mass of dopamine/total emulsion surface area g/m^2	Assumed density of PDA g/cm^3	Total volume of PDA cm^3	Theoretical shell thickness nm
1.08	0.09	1.6	0.0625	58

3.7.9 Theoretical silver thickness on PDA microcapsules

To work out the theoretical shell thickness on PDA microcapsules the conditions are illustrated in table 3.6 and demonstrated in figure 3.7.1.

Table 3. 6: Calculated silver thickness on PDA microcapsules

Total emulsion surface area nm^2 x10^{18}	Mass of silver mg	Silver density g/cm^3	Total volume of silver cm^3	Theoretical shell thickness nm
0.11	10.8	10.5	0.001	10
0.11	21.6	10.5	0.002	19

4 Step by step approach to the synthesis of gold coated, Pt PVP stabilised emulsions

4.1 Synopsis

This chapter will focus on the synthesis and characterisation of poly(vinyl pyrrolidone) (PVP) stabilised platinum nanoparticles (Pt-NPs) and the effect of PVP chain length on the synthesis of the nanoparticles. The Pt-NPs will subsequently act both as an emulsifier for stabilising oil-in-water emulsions and as a catalyst for the electroless plating deposition of gold films onto the emulsion droplets, resulting in the synthesis of gold-shell microcapsules. This chapter will also focus on the parameters that influence the microcapsule shell thickness and demonstrate its accurate measurement via an indirect method and the retention of the microcapsule core as a result of the gold shell impermeability.

4.2 Preparation of PVP- stabilised platinum nanoparticles (Pt-NPs)

Metal nanoparticles have attracted great interest due to their catalytic properties. At low temperatures colloidal dispersions of metal nanoparticles are able to operate as catalysts.[1] Due to their size they offer high surface to volume ratio, better dispersion ability and long term stability due to their smaller size, which enhances their effectiveness as catalysts when compared to larger crystals of the same mass.[2, 3] Steric or charge stabilisation has generally been used to confer colloidal stability to the nanoparticles in order to preserve the large surface area they provide.

It is well documented that PVP acts as an effective stabiliser for metal nanoparticles, in particular complexing and stabilising Ag, Au, Pt, Pd and Cu nanoparticles.[4-7] PVP is also known to contribute towards the reduction, final particle size, stability and morphology of the metal nanoparticle systems.[6] PVP contributes towards

nanoparticle reduction by providing sites for complexation with the metal ions, reduction of the metal ion takes place, which then nucleate, and finally these nuclei act as seeds for further growth.[8] Longer molecular weight of the PVP chain results in more sites for VP metal ion complexes, hence resulting in more reduction/nucleation sites for the metal ions which in-turn effects the metal nanoparticle size, stability and morphology. PVP also contributes to the reduction process as the two kind of coordinative types can effectively decrease the chemical potential and further enable the PVP-bound metal ion to be reduced more easily as shown in figure 4.1.[9] Jiang, *et al.,* demonstrated in their study that PVP was able to complex silver ions and in turn affected the morphology and size of the silver nanoparticles synthesised. The different coordinative complexes between PVP and the metal ions, the solvent used and synthesis technique, induced different nucleation which resulted in either cubic, triangular or hexagonal morphologies.[9] Pastoriza-Santos and Liz-Marzan [6] in their study of PVP and silver ions demonstrated that higher PVP molecular weight and lower metal ion concentration were found to lead to more stable colloids with smaller particle size. The concentrations used in the study equated to 0.076-0.76wt% PVP and 4.8mM silver salt, whereas the concentrations of PVP 0.0067wt% PVP and 5.6mM Pt salt for our studies is lower than the lowest concentration used by Pastoriza-Santos and Liz-Marzan. This was done to demonstrate the low PVP concentrations we are working at for the purpose of not introducing excess polymer for the subsequent emulsification step (to maximise the NPs density on the surface of the droplets). [6]

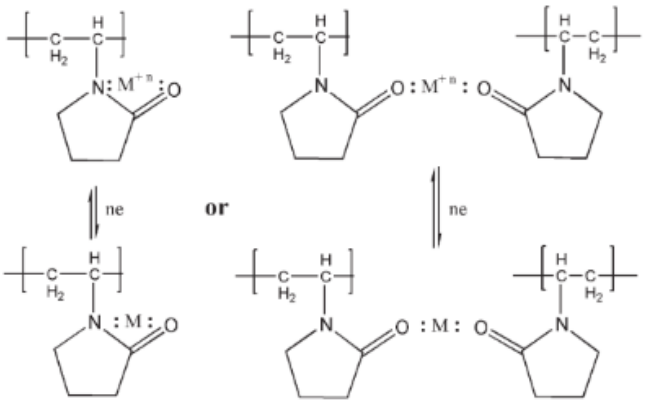

Figure 4. 1: Possible coordination and reaction process for PVP and metal ions.[6]

The stabilisation effect of PVP and metal ion arises initially from the lone pair of electrons from the nitrogen and oxygen atoms in the polar groups of PVP repeating units, which can be donated into two *sp* hybrid orbitals of the metal ions, forming a complex between PVP and metal ion. It is believed that after the reduction of metal ions, the bonding between PVP and metal atoms remains hence resulting in strong bonding between the polymer and the metal colloid particle.[10] Figure 4.1 describes the two different coordination complexes and reduction processes possible.

4.3 Synthesis of PVP-stabilised platinum nanoparticles (Pt-NPs)

The mechanism for the synthesis of colloidal metal nanoparticles is described as a two-step process, the metal precursor is reduced to zero-valent metal atoms, followed by the growth of nanoparticles from the metal atoms, initially reduction of the metal ion takes place, which then nucleate, and finally these nuclei act as seeds for further growth.[8] The chemical reduction of hexachloroplatinic acid by sodium borohydride proceeds via the following overall reaction in aqueous solution (Reaction equation 4.1). [11]

$$NaBH_4 + H_2PtCl_6 + 3H_2O \rightarrow Pt + H_3BO_3 + 5HCl + NaCl + H_2 \qquad 4.1$$

The formation of Pt-NPs was described by Gharibshahi and Saion and the following reaction scheme applies for this reaction: [12]

$$[Pt^{+IV}Cl_6]^{2-}(aq) + BH_4^-(aq) + 3H_2O \rightarrow$$

$$Pt^0 + H_2BO_3^-(aq) + 6Cl^-(aq) + 4H^+(aq) + 2H_2(g) \qquad 4.2$$

Initial experiments were conducted with evaluating the literature to determine the lowest PVP concentration required to stabilise Pt-NPs, for the purpose of not introducing excess polymer for the subsequent emulsification step (to maximise the NPs density on the surface of the droplets). From Pastoriza-Santos and Liz-Marzan study the lowest PVP concentration to stabilise Ag-NPs was 0.076 wt% to 4.8 mM silver salt.[8] From our initial experimental data we were able to further reduce the PVP concentration to 0.0067 wt% to stabilise 5.6mM platinum salt, resulting in 10 fold decrease in the PVP concentration compared to concentrations used by Pastoriza-Santos and Liz-Marzan.[6]

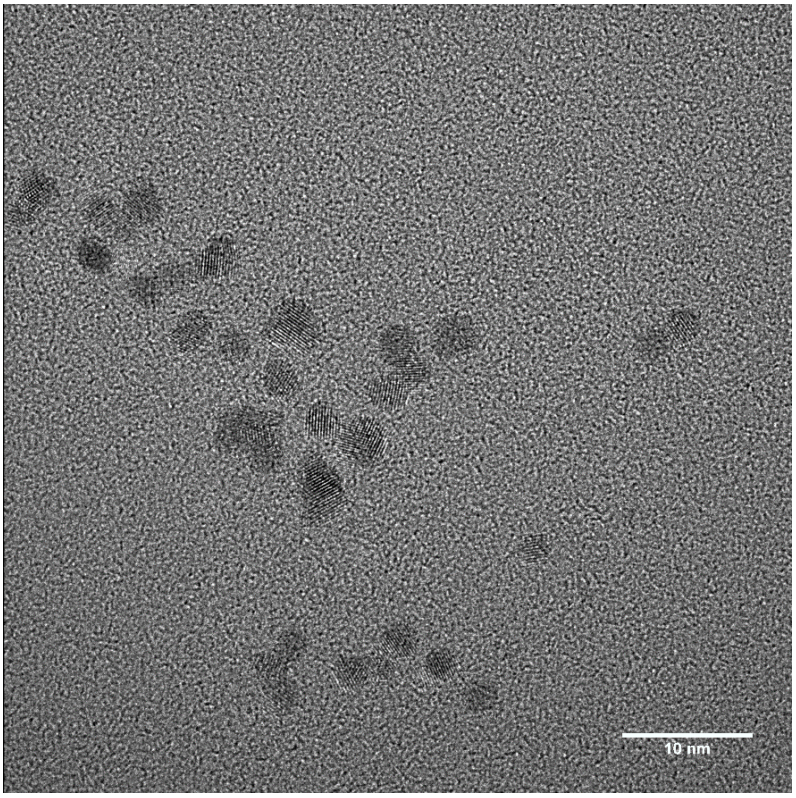

Figure 4. 2: Transmission electron micrographs of Pt-NPs deposited on TEM grids 24 hours after synthesis conducted using the following conditions: (5.6 mM) $PtCl_6H_2$, (1.1 mM) $NaBH_4$ and (0.0067wt% 40kDa) PVP.

Figure 4.2 demonstrates TEM image of Pt-NPs stabilised with 40kDa PVP and indicates well dispersed Pt-NPs. The mean core particle size of Pt-NPs as determined from analysing a 1000 Pt-NPs using image J was 2.9nm (+/-0.4).

4.4 Effect of PVP chain length on Pt-NP synthesis

The aim of this experiment was to determine the effect of the PVP molecular weight (chain length) on the number, size and stability of Pt-NPs synthesised. From the size of nanoparticles, we can determine the number of nanoparticles and also the ratio of nanoparticles to number of polymer chains. From this we will determine if the polymer chains are in excess or if the polymer chains can accommodate more than one

nanoparticle. This experimental data will demonstrate that we have no excess PVP in the system, and the PVP concentration has been optimised to stabilise the Pt-NPs, therefore the Pt-NPs will not compete with PVP chains to stabilise the interface. Also from the size of the nanoparticle's we will be able to theoretically calculate the total interface the nanoparticles will be able to adsorb at. Pt-NPs were synthesised with varying PVP chain length (10, 40, 55, 380 kDa) in the bulk aqueous phase. The number of polymer chains was kept constant and only the chain length was varied. The resulting data is shown below in figure 4.3

.

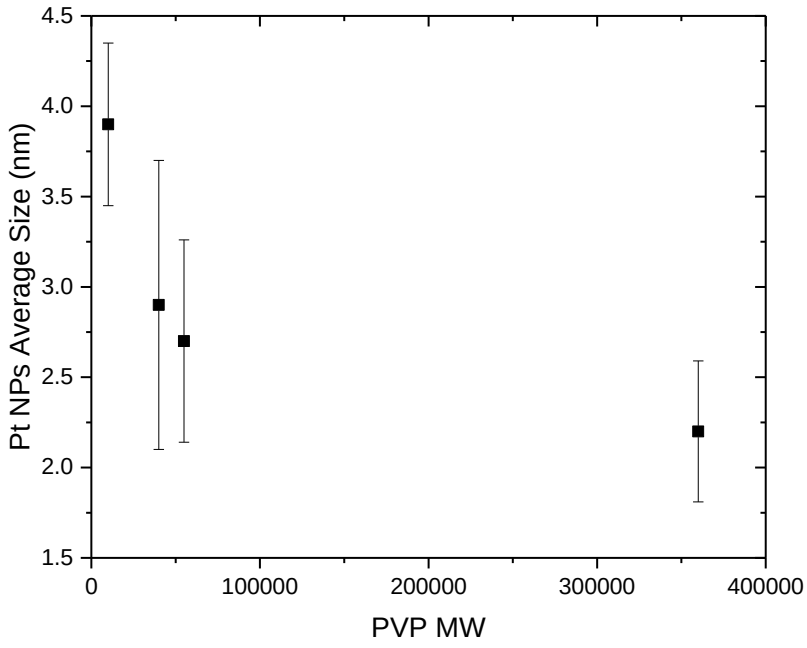

Figure 4. 3: Mean core Pt-NP size obtained from Image J analysis at different PVP molecular weight, (PVP 10, 40, 55, 380 kDa) the concentration of $PtCl_6H_2$ and $NaBH_4$ was kept constant at (5.6 mM,) and (1.1 mM) respectively. Error bars represent the standard deviation of the mean. The average size of Pt-NPs was collected from analysing 1000 Pt-NPs from Transmission electron micrographs using image J, the method is described in chapter 3.3.1.

From figure 4.3 it can be noted with the increasing PVP molecular weight resulted in the mean core particle size of the Pt-NPs to decrease, this effect was also seen and explained by Pastoriza-Santos and Liz-Marzan and is due to more coordination/complexes sites availble at higher molecular weight PVP than lower molecular weight PVP for the metal ions to complexes at.[6]

4.5 Ratio of polymer chains to Platinum nanoparticles

The following section will combine the data from the previous section on the average Pt-NP size to determine the number of Pt-NPs. From the number of Pt-NPs the ratio of Pt-NPs to PVP chains will be calculated. The calculated ratios of PVP: Pt-NPs are based on the assumption that all the platinum is reduced and no platinum is lost in the filtering process. The calculations for the number of PVP chains is shown in chapter 3.7.2.

Table 4. 1: Details of components within the nanoparticle synthesis and resulting ratios of PVP chains to Pt-NPs synthesised in the final nanoparticle suspension for different PVP molecular weights (PVP 10, 40, 55, 380 kDa). Concentrations of $PtCl_6H_2$ and $NaBH_4$ in the synthesis was kept constant at (5.6 mM, 0.11wt%) and (1.1 mM) respectively.

Mean Core diameter of Pt NPs (nm)	PVP MW kDa	Number of PVP chains ($x10^{17}$)	Number of NPs ($x10^{17}$)	Ratio PVP:Pt NPs
3.9	10	1.01 (1.7mg)	1.66	0.6
2.9	40	1.01 (6.7mg)	4.03	0.25
2.7	55	1.01 (11.7mg)	4.99	0.2
2.2	360	1.01 (60.3mg)	9.23	0.1

The number of PVP chains was kept constant throughout the experiment. From the ratio of PVP: Pt-NPs the Pt-NPs are in excess in comparison to number of PVP chains therefore we can hypothesize that more than one Pt-NP is interacting with a single PVP chain. As the molecular weight of the PVP chain is increased, the size of the Pt-NPs synthesised decreases. The reduction in the Pt-NP size can be explained in terms of the interaction between the Pt and PVP described in Figure 4.1. As the length of the PVP chain increases, there are more sites for the interaction between Pt ions and VP. This effect was also described by Shimmin *et al*., who studied the effect of polymer molecular weight on gold nanoparticle synthesis and concluded that increasing the polymer molecular weight results in a decrease in gold nanoparticle size.[13] Longer polymer chains are able to stabilise more nanoparticle interface than smaller polymer chains therefore the nanoparticle size decreases resulting in an overall increase in the total interfacial area in the system.

4.6 Predicted conformations for systems of different Pt-NPs and PVP stabiliser ratios

When the Pt-NPs are adsorbed onto the interface immobilising the catalyst, if any excess polymer is available in the bulk it can compete for surface adsorption and therefore reduce the efficiency of the process and final catalyst density at the interface.[14] As the ratios indicate (table 4.1), the polymer use is maximised as a stabiliser to the extent no polymer chains are left unused by the nanoparticle's, the assumption can be made that Pt-NPs do not have to compete with PVP chains at the interface.

Table 4.2 describes the properties Pt-NPs to PVP stabiliser ratios. Figure 4.4, 4.5, 4.6 and 4.7 demonstrate the predicted conformations based on the calculated ratio of PVP

chains (chapter 3.6.4) to Pt-NPs and the measured hydrodynamic diameter of the Pt PVP NPs (chapter 3.6.2), the procedure for measuring the hydrodynamic diameter using the Malvern-zetasizer is described in chapter 3.5.1. The ratio of PVP: Pt NPs is the number of Pt NPs per polymer chain.

Table 4. 2: Ratio of Pt-NP core diameter to PVP chain length (PVP 10, 40, 55, 380 kDa) and ratio of PVP chains (PVP 10, 40, 55, 380 kDa) to Pt NPs.

PVP MW kDa	Polymer chain length P_c nm	Ratio of Pt NP core diameter to PVP chain length	Ratio PVP: Pt-NPs
10	27	6.9	0.6
40	108	37.2	0.25
55	149	55.2	0.2
360	973	442.3	0.1

PVP 10KDa

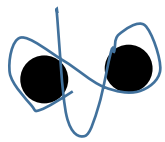

a)

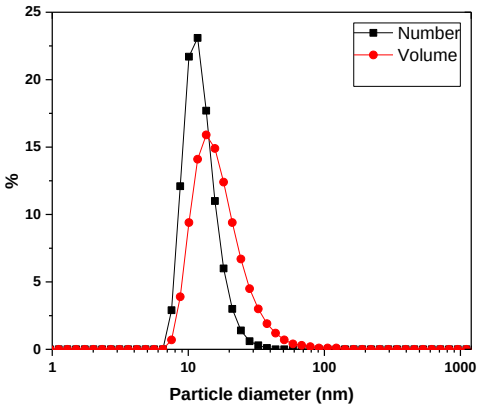

b)

Figure 4. 4: (a) Schematic diagram of Pt PVP NP predicted from the ratio of Pt NPs to PVP (10kDA) and hydrodynamic diameter, (b) Pt PVP NP (10kDa) hydrodynamic diameter size distribution measured as number and volume % using the Zetasizer.

PVP 40KDa

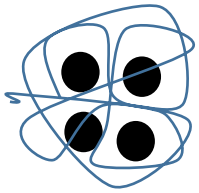

a)

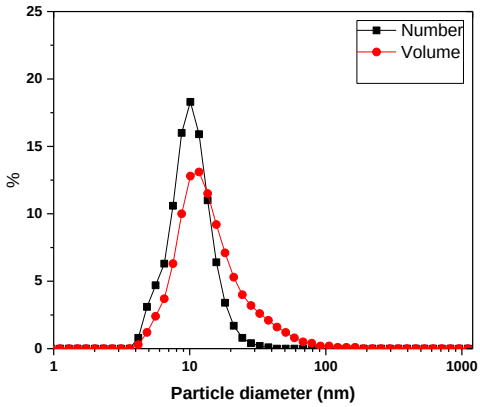

b)

Figure 4. 5: (a) Schematic diagram of Pt PVP NP predicted from the ratio of Pt NPs to PVP (40kDA) and hydrodynamic diameter, (b) Pt PVP NP (40kDa) hydrodynamic diameter size distribution measured as number and volume % using the Zetasizer.

PVP 58KDa

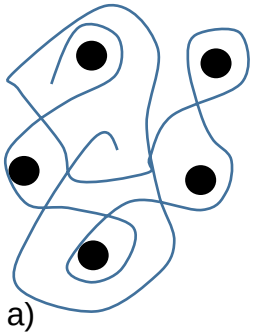

a)

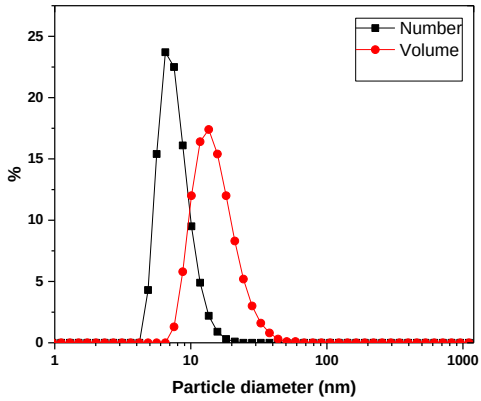

b)

Figure 4. 6: (a) Schematic diagram of Pt PVP NP predicted from the ratio of Pt NPs to PVP (55kDA) and hydrodynamic diameter, (b) Pt PVP NP (55kDa) hydrodynamic diameter size distribution measured as number and volume % using the Zetasizer.

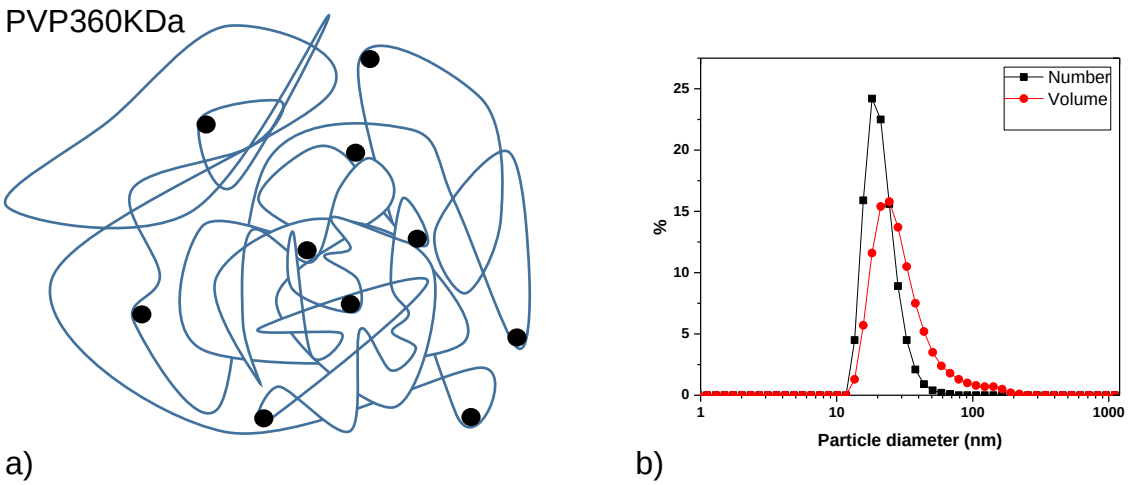

Figure 4. 7: (a) Schematic diagram of Pt PVP NP predicted from the ratio of Pt NPs to PVP (360kDA) and hydrodynamic diameter, (b) Pt PVP NP (360kDa) hydrodynamic diameter size distribution measured as number and volume % using the Zetasizer.

From table 4.2 and figure 4.4, 4.5, 4.6 and 4.7 it can be concluded as the ratio of Pt-NPs to PVP decreased with increasing PVP molecular weight the hydrodynamic diameter also increased. This was expected due to the longer polymer chain length accommodating more Pt-NPs due to more VP sites available for platinum ion interaction as was described by Pastoriza-Santos, *et al.,* and shown in figure 4.1.[6] This can also be explained in terms of the concentration of platinum salt used in the synthesis. As this is kept constant, more growing nuclei are accommodated on longer PVP chains, therefore if the platinum salt is constant the nuclei will grow into smaller nanoparticles.

The Pt-NP stabilised emulsions will subsequently be used as templates for the growth of gold impermeable metal shells. The Pt-NPs at the interface will be used as catalysts for gold reduction and also provide a nucleation site for the electroless deposition of gold. The gold reduction is limited to the Pt-NP sites, so it is important no excess Pt-NP remains in the bulk and also the Pt-NP do not have to compete with PVP and are

at the interface so the gold growth is limited at the interface resulting in a gold metal shell.

4.7 Pt-NP Stabilised emulsions

The following section will describe the stabilisation of oil in water emulsions with Pt-NPs and investigate some key parameters in order to optimise and demonstrate the control of the emulsion system. The oil chosen for the emulsification process was hexadecane, as it has a low molecular weight and is easily detectable on gas chromatography due to its simple structure.

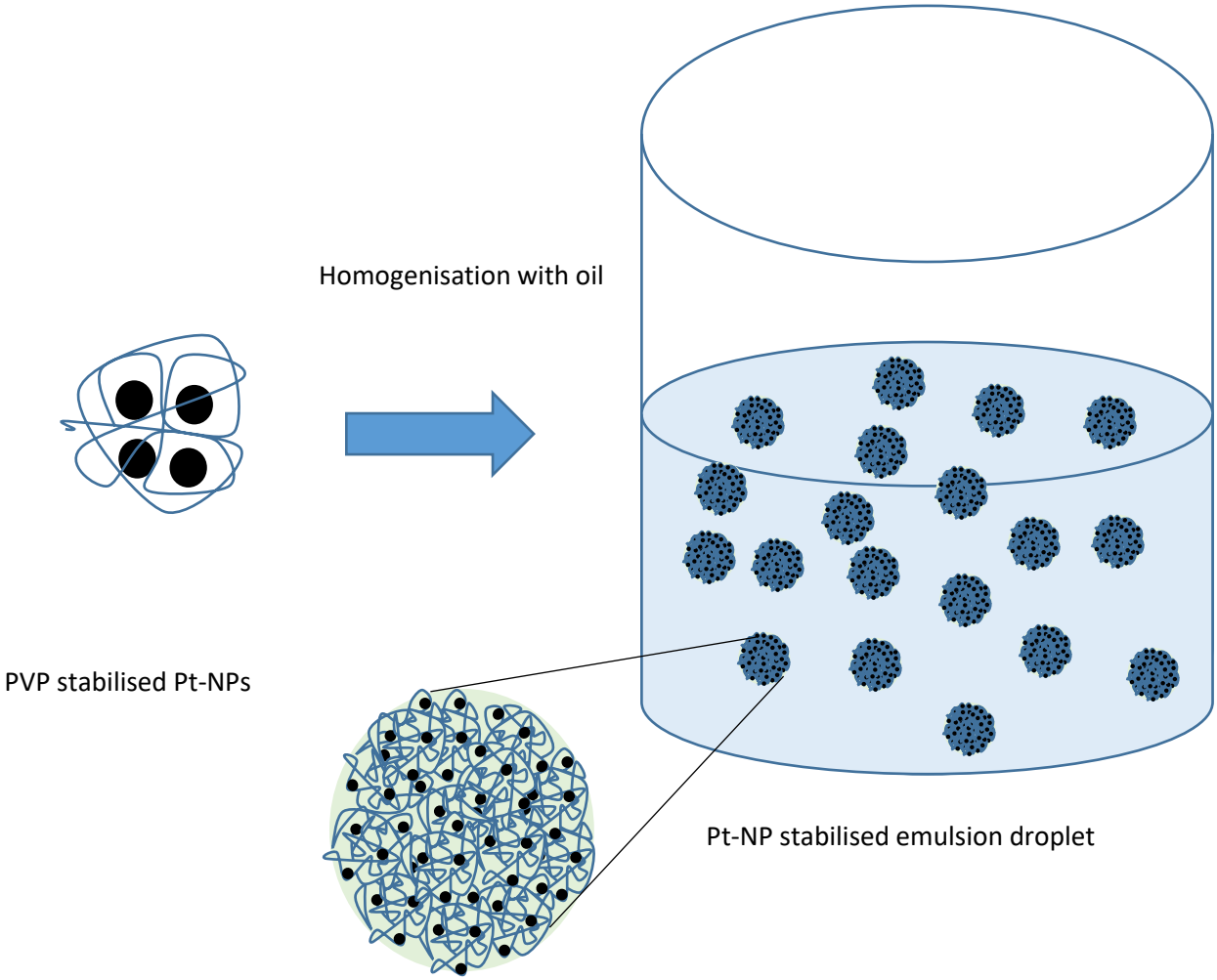

Figure 4. 8: Schematic representation of process of emulsifying oil in water emulsions by adsorbing Pt-NPs at oil water interface, (10 ml Pt-NPs 5.6mM, 0.4ml hexadecane, sonicated for 1 minute at 40% amplitude).

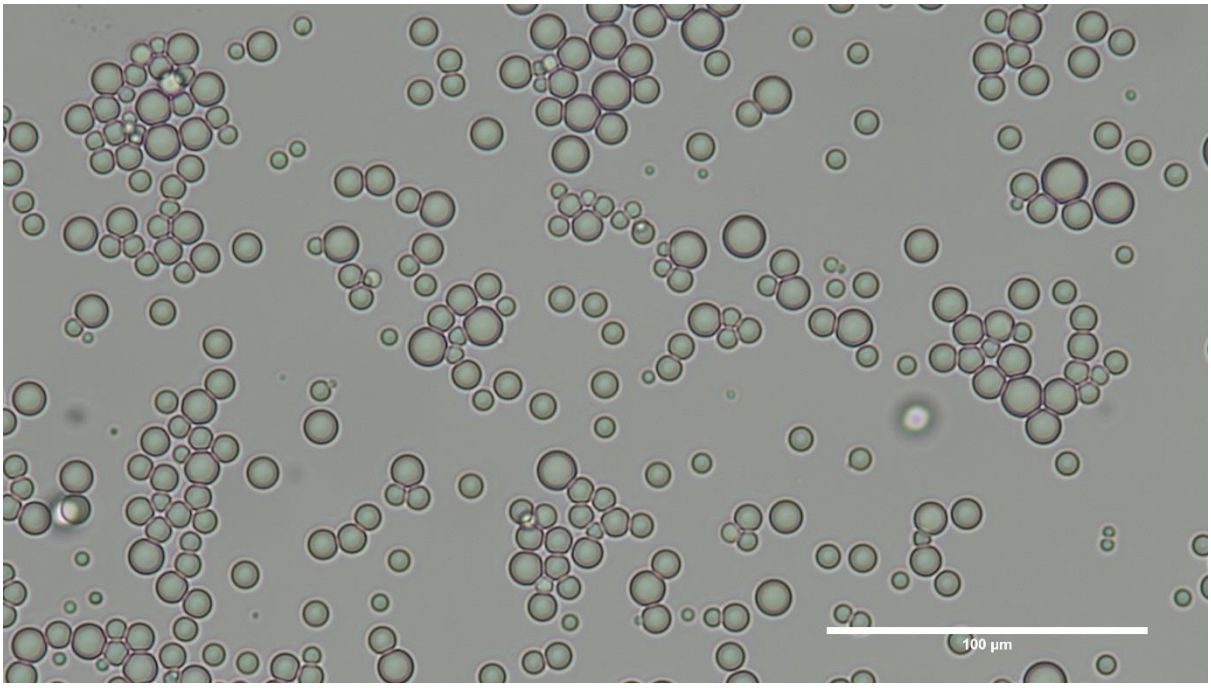

Figure 4. 9: Optical micrograph of emulsion prepared from a hexadecane (0.4ml) and Pt PVP NPs (10ml) emulsion homogenised at 40% amplitude for 1 minute.

Figure 4.9 demonstrates an oil in water emulsion stabilized with Pt-NPs.

4.8 Effect of varying oil fraction on Pt-NP stabilised emulsions

The following section describes the effect of increasing the oil volume fraction, whilst keeping the concentration of Pt-NPs constant, on the emulsion droplets average size and surface area. In theory the Pt-NPs should consistently cover the same surface area of the emulsion oil droplets (if the oil is in excess) and should be independent of the oil volume fraction. With increasing the oil volume fraction we should measure an increase in oil droplet size.

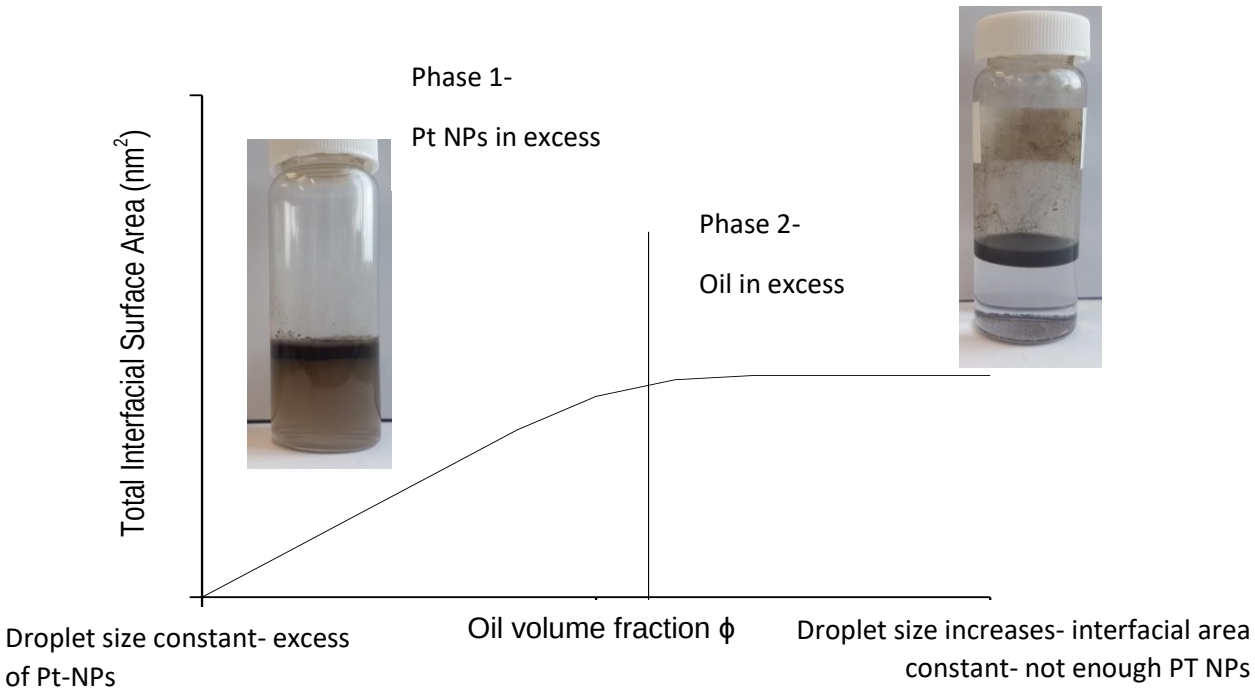

Figure 4. 10: Effect of oil volume fraction on total surface area stabilised by Pt-NPs, at low oil volume fractions Pt-NPs are in excess as the emulsion creams the continuous phase is still cloudy as Pt-NPs are in excess. At high oil volume fractions, the oil is in excess and the Pt-NPs are all adsorbed onto the oil water interface, as the emulsion creams the continuous phase is clear demonstrating all the Pt-NPs are at the oil water interface.

Figure 4.10 describes the effect of oil volume fraction on total interfacial surface area, as the concentration of Pt-NPs is consistent and the oil volume fraction is increased. At low oil volume fraction all the nanoparticles do not adsorb onto the interface as they are in excess, as the oil volume fraction is increased this results in an increase in total interfacial surface area initially as the nanoparticles are in excess and can adsorb onto more interface created. A point is reached when the nanoparticle and oil concentration are in sync and all the nanoparticles are at the oil water interface, as the oil volume fraction is increased the interfacial surface area will stay the same as the nanoparticles cannot stabilise any more surface area and the oil droplets size will increase, as the oil is in excess, this is demonstrated in figure 4.12.

Resulting data is shown in figure 4.11, the average emulsion size was measured against varying the oil volume fraction ϕ (0.04, 0.05, 0.07, 0.1 and 0.14). From the emulsion size distribution (bin limits) the Total Interfacial Surface Area (nm^2) was calculated.

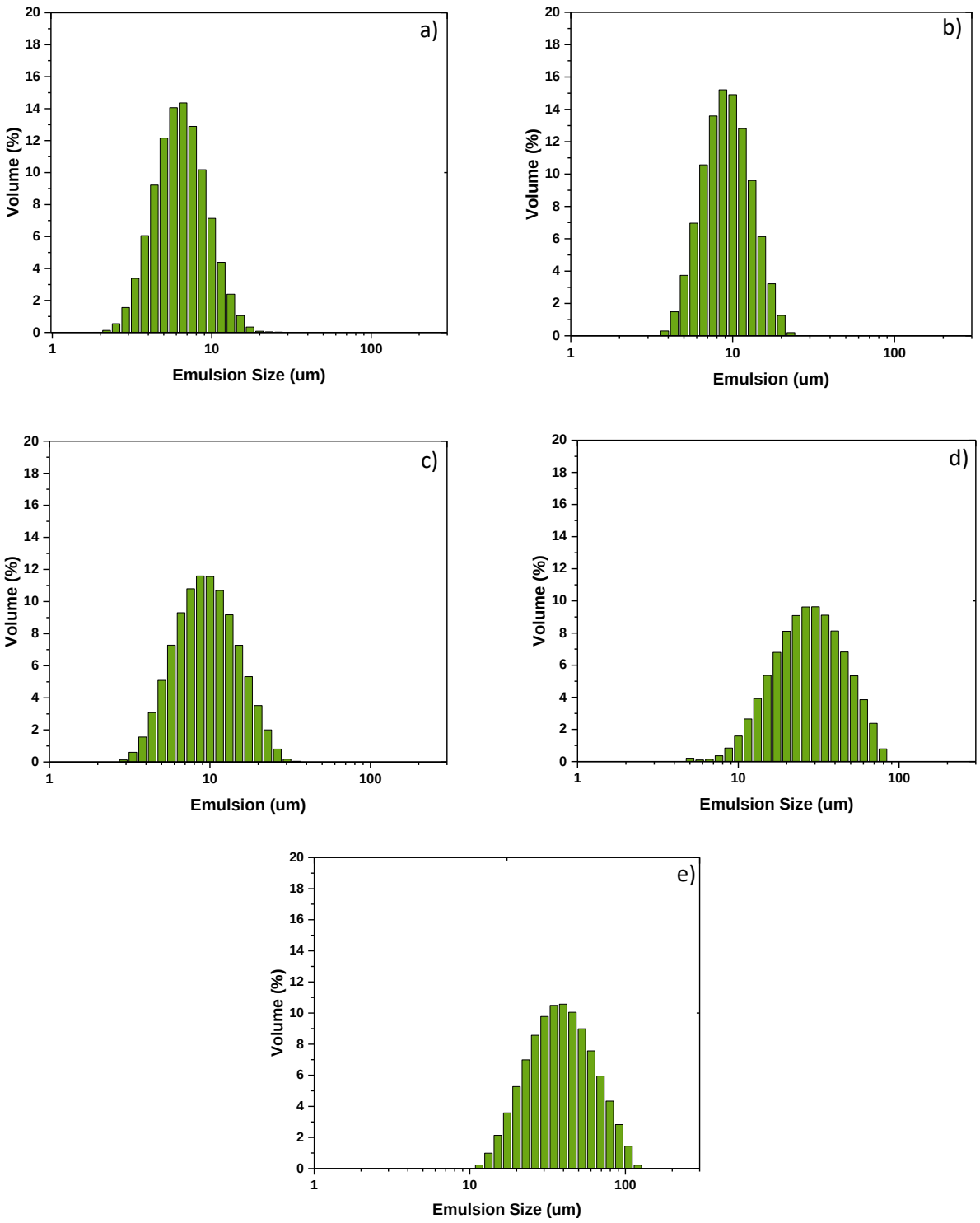

Figure 4. 11: Average emulsion size distributions measured using the mastersizer at varying oil volume fractions ϕ, (a) 0.04, (b) 0.05, (c) 0.07, (d) 0.1 and (e) 0.14) the Pt-NPs were kept constant at (10 ml Pt-NPs 5.6mM) and sonicated for 1 minute at 40% amplitude to form emulsions.

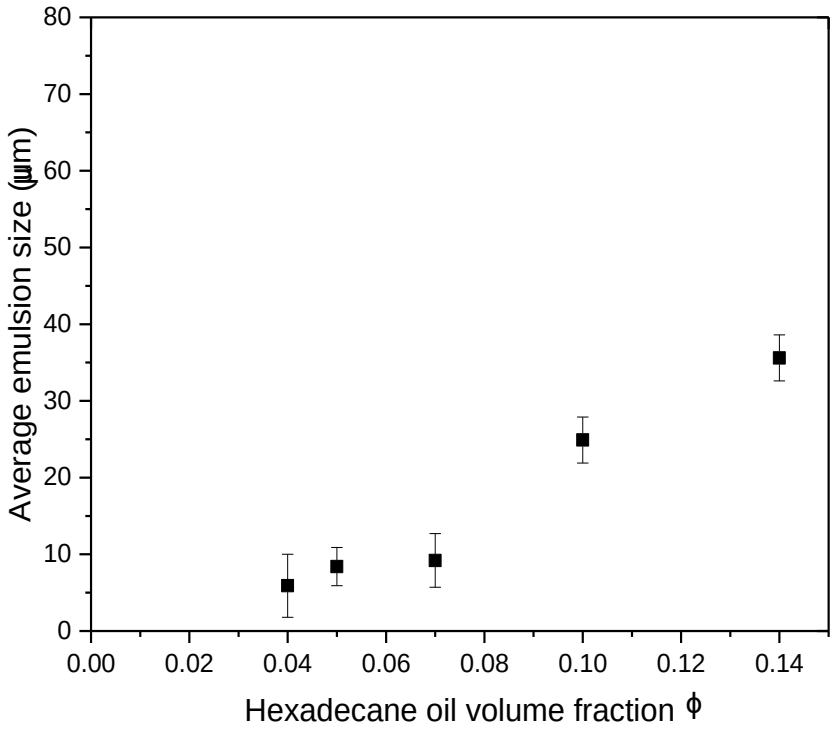

Figure 4. 12: Effect of oil volume fractions ϕ (0.04, 0.05, 0.07, 0.1 and 0.14 wt %) on the average emulsion size. Error bars represent the standard deviation of the mean.

Figure 4.12 demonstrates the average emulsion droplet size from figure 11 plotted against the hexadecane oil volume fraction ϕ, at the lower oil volume fraction the emulsion droplet size are similar, this could be explained in terms of the Pt-NPs and hexadecane oil being at a fine balance where neither are in excess and as the oil volume fraction ϕ is increased above 0.08 the average emulsion droplet size increases as the oil is in excess and no free Pt-NPs are available to adsorb onto and create more interface and in turn the droplets merge to form larger droplets.

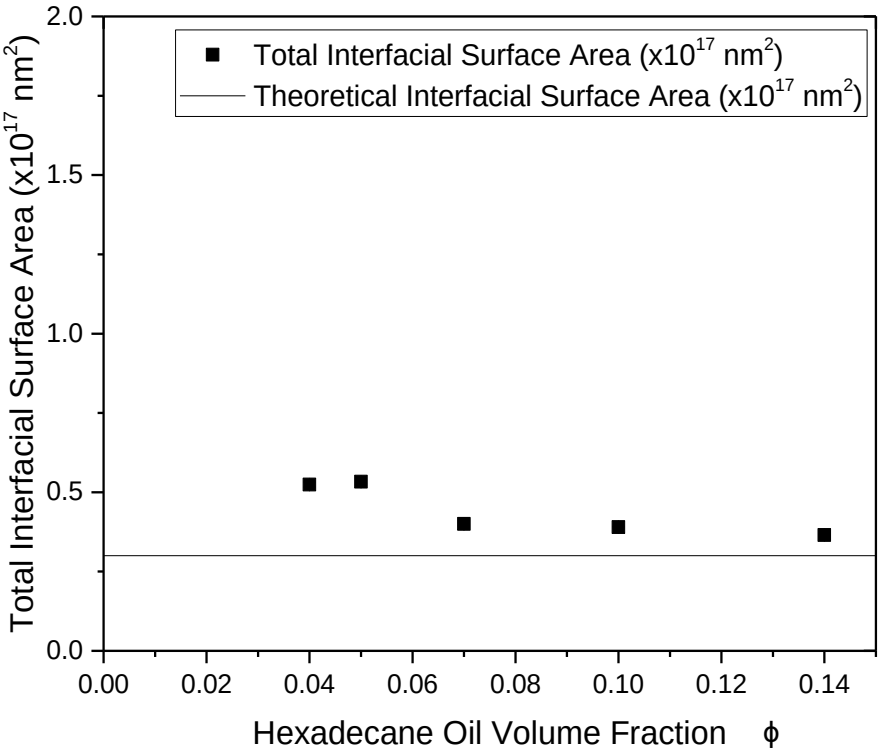

Figure 4. 13: Total interfacial surface area calculated from the average emulsion size distribution (bin limits) figure 4.11, a, b, c, d, and e. The black line represents the total surface area the Pt-NPs (10 ml 0.56mM) can cover based on hexagonal packing.

Figure 4.13 demonstrates the total interfacial surface area plotted against the Hexadecane oil volume fraction ϕ, the total interfacial surface area for all the emulsions is very similar as the Pt-NPs concentration was consistent, hence resulting in the stabilisation of the similar interfacial surface area for each emulsion. For all the oil volume fractions of hexadecane, the Pt-NPs were not in excess as seen from the emulsion droplet size and total surface area.

The theoretical interfacial surface area coverage is calculated by the number of Pt-NPs and the diameter of the Pt-NPs (diameter 2.9nm, number of NPs 4.03×10^{16}) based on hexagonal packing. From figure 4.13 the total surface interfacial area (nm^2)

scale is based on the total surface interfacial area (nm^2) of the highest hexadecane the oil volume fraction ϕ (0.14) at an average emulsion size of 5.9nm (lowest average emulsion size).

4.9 Metal Coating of Pt-NP stabilised emulsion droplets

In the following section the emulsions stabilised with Pt-NPs which were discussed in the previous section will be coated with a metallic shell, resulting in metal coated emulsion droplets.

The Pt-NP stabilised emulsions were subsequently coated by the deposition of gold onto the droplet surface, hence resulting in the encapsulation of the oil core, as the Pt-NPs can catalyse gold reduction/nucleation and also stabilise the oil/water (Pickering) emulsion as demonstrated.[4] As demonstrated in figure 4.12 and 4.13 above no excess Pt-NPs are present in the system and are only absorbed onto the oil/water interface, resulting in the electroless deposition of gold at the oil/water interface. Reaction equation 4.3 explains the reduction of $HAuCl_4$ by H_2O_2 and Pt as a catalyst and nucleation site for gold growth.

$$2HAuCl_4 + 3H_2O_2 \xrightarrow{Pt} 2Au + 3O_2 + 8HCl$$

4.3

$HAuCl_4$ and H_2O_2 were used to deposit the gold film, where H_2O_2 reduced the Au^{3+} ions to Au^0, whilst Pt-NPs catalysed the reaction and provided an active site for the reduction and deposition of gold.

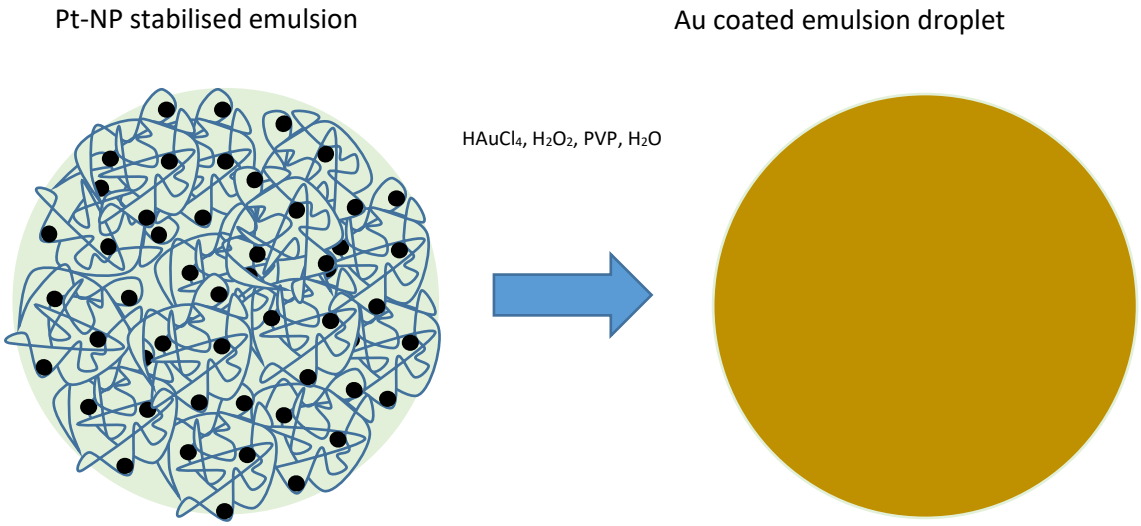

Figure 4. 14: Schematic diagram demonstrating the reduction of $HAuCl_4$ by H_20_2 and platinum as a catalyst and nucleation site for gold growth on the emulsion surface.

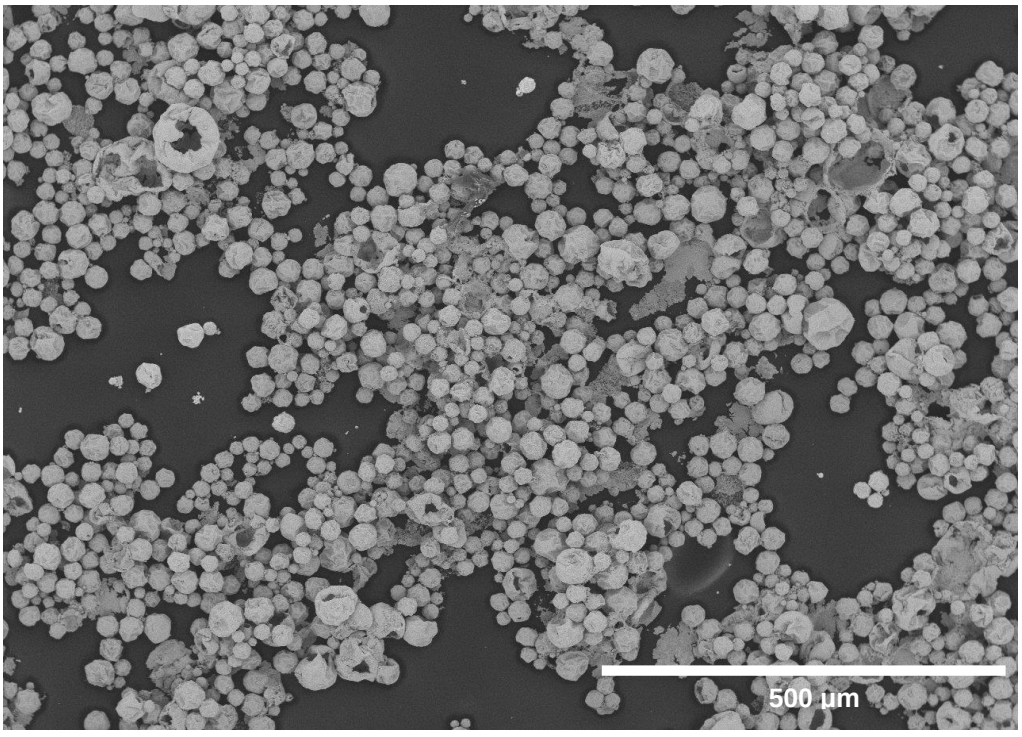

Figure 4. 15: Bench top Scanning Electron micrographs of gold microcapsules stabilised with 40 kDa PVP and 40mM $HAuCl_4$ (1ml).

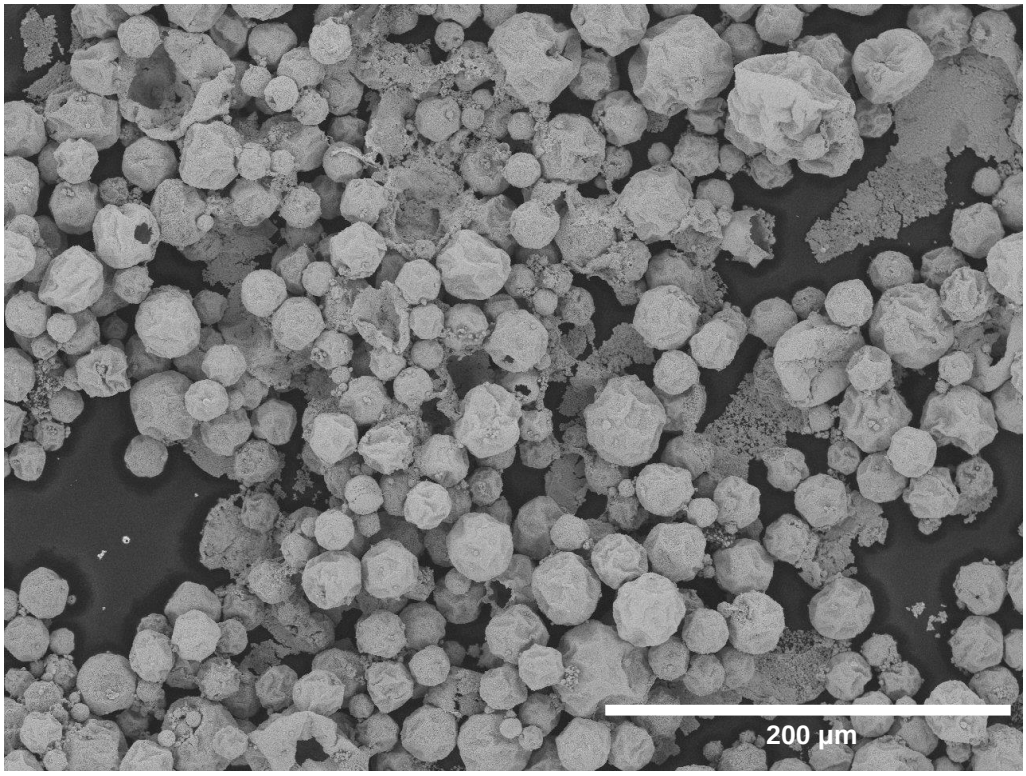

Figure 4. 16: Bench top Scanning Electron micrographs of gold microcapsules stabilised with 40 kDa PVP and 40mM $HAuCl_4$ (1ml).

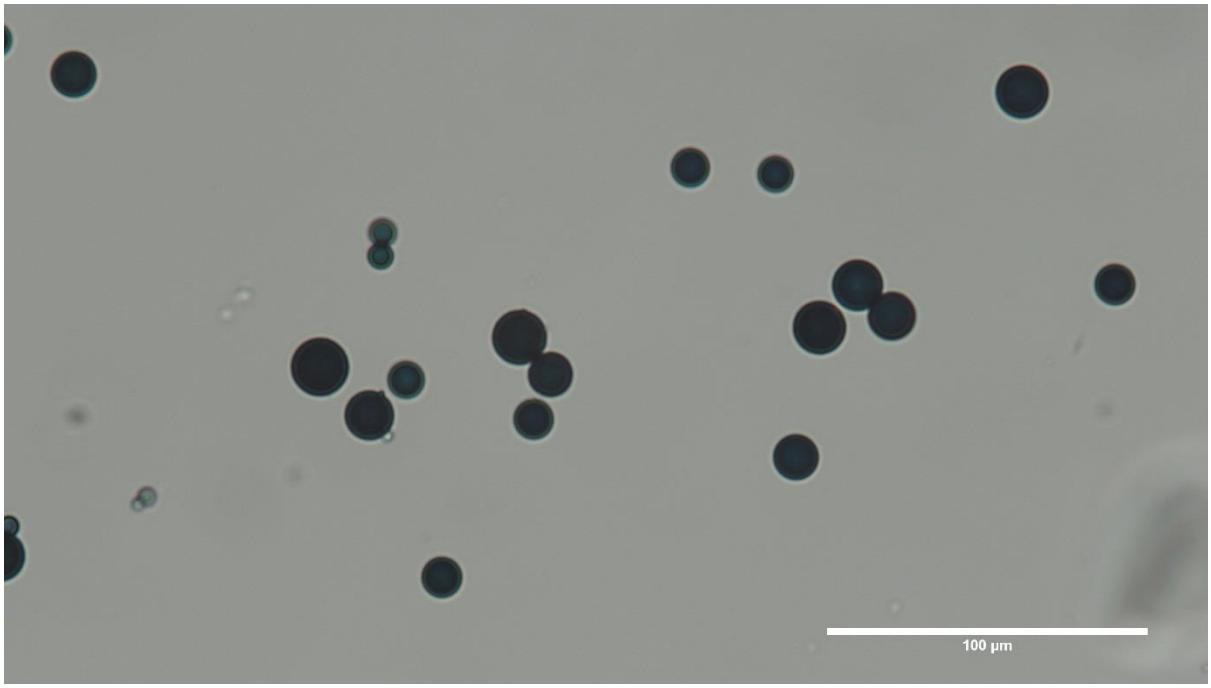

Figure 4. 17: Optical micrographs of PVP (40kDA) stabilised gold microcapsules in suspension of water, transmitted light.

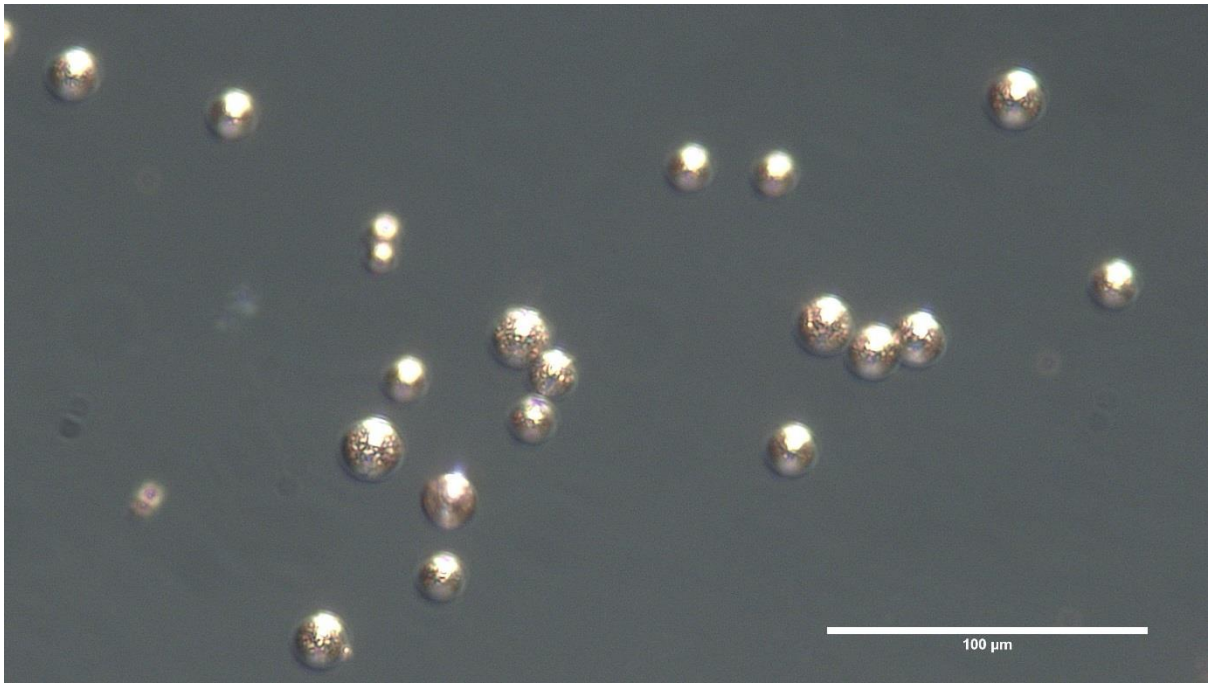

Figure 4. 18: Optical micrographs of PVP (40kDA) stabilised gold microcapsules in suspension of water, reflected light.

Figure 4.15 and 4.16 demonstrate SEM micrographs of gold coated microcapsules at different magnifications. Figure 4.17 and 4.18 demonstrate optical micrographs of gold coated microcapsules under transmitted and reflected light. All the gold coated microcapsules remain stable and no aggregation is seen, also the emulsion droplets seem to be coated in a full continuous gold metal shell.

As demonstrated by Hitchcock, Horiuchi and Nakao [4, 15] and from the resulting data in this chapter, Pt-NPs are able to catalyse the growth of gold films and provide a nucleation site for the deposition of gold. Previously we demonstrated no excess Pt-NPs are present in the continuous phase and are adsorbed onto the interface. Initially the gold salt is reduced by hydrogen peroxide and the reaction is catalysed by the Pt-

NPs at the droplet interface. A plating solution consists of hydrogen peroxide, polymer stabiliser (PVP), gold salt and water.

4.9.1 Gold Shell Thickness Measurements

In the previous section it was demonstrated the gold coating on emulsion droplets stabilised with Pt-NPs. This section will consist of demonstrating the measurement of the gold shell thickness on the emulsion droplets.

To analyse the microcapsule shell thickness, the method described by Hitchcook, *et al*., was applied. The microcapsule samples were air dried and mixed with an epoxy resin and hardened. A diatome diamond knife was used to section the samples on a Reichert-Jung Ultracut-E Ultramicrotome. The thickness of the cut section was 90nm thick and picked up on a 200mesh, thin bar, copper grid coated with formvar. The samples were analysed under TEM.

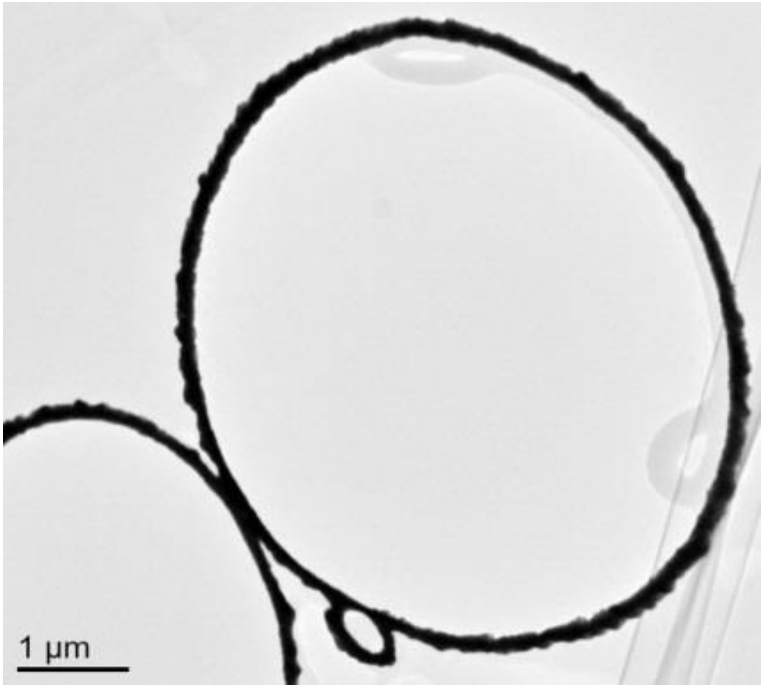

Figure 4. 19: Cross section of a gold coated polymer microcapsules. [15]

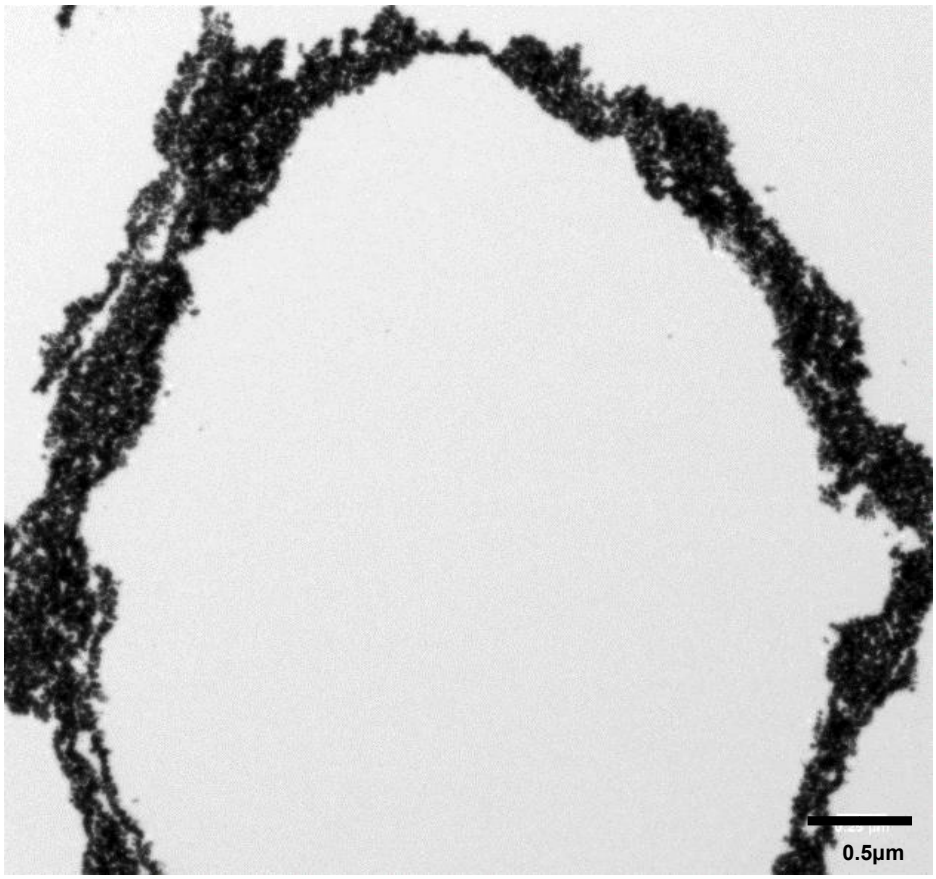

Figure 4. 20: Cross section of a gold coated Pt-NP stabilised emulsion droplet.

After analysing the cross section of gold coated Pt-NP emulsions under TEM, it could be noted the gold shell did not remain completely intact when preparing for cross sectioning. This could be explained in terms of the microcapsules prepared by Hitchcock, *et al*., had a polymer template on which the gold was deposited, hence giving greater stability to the microcapsule shell, whereas the gold shell grown on the emulsion template had no skeletal support, hence when under stress the shell did not remain intact.

To measure the microcapsule shell thickness a new approach was taken, initially theoretical shell thickness was calculated followed by actual shell thickness measurements using data from TGA, this method will be described and demonstrated in the following section.

4.9.2 TGA analysis of Gold coated emulsion microcapsule shell thickness

The following section will consist on analysing the effect of H_2O_2 reducing agent on the shell thickness. This was initially done to demonstrate the consistency of H_2O_2 when reducing the gold salt.

TGA analysis was applied to analyse the effect of reducing agent H_2O_2 on microcapsule shell thickness. The ratio of $HAuCl_4$ to H_2O_2 was varied from 1:1.5 to 1:15: all other parameters were kept constant.

Table 4. 3: Experimental condition, all the parameters were kept constant except the H_2O_2 concentration which was varied. The error bar represents the standard deviation of the measured emulsion size distributions from the mastersizer.

Volume of H_20_2 1ml	60mM	180mM	300mM	600mM
Volume of $HAuCl_4$ (40 mM)	1ml	1ml	1ml	1ml
Molar ratio ($HAuCl_4$:H_20_2)	1 : 1.5	1 : 4.5	1 : 7.5	1 : 15
Shell Thickness (nm)	31 +/- 0.2nm	30 +/- 0.2nm	33 +/- 0.2nm	32 +/- 0.2nm

To predict and control the shell thickness, a two-step approach was taken on the assumption a consistent amount of Au is reduced onto the emulsion droplets.

1. Theoretically calculate shell thickness

- Measure droplet size distribution using light diffraction (Mastersizer)
- Calculate total surface area of emulsion droplets-based on bin limits
- Calculate theoretical shell thickness from surface area and volume of oil used as the emulsion dispersed phase.

2. Shell thickness calculation from TGA data
    - Analyse Au coated emulsion droplets using TGA
    - Calculate oil mass loss and Au Mass
    - Revert back to surface area and calculate actual shell thickness

Calculations are shown in chapter 3.7.1.

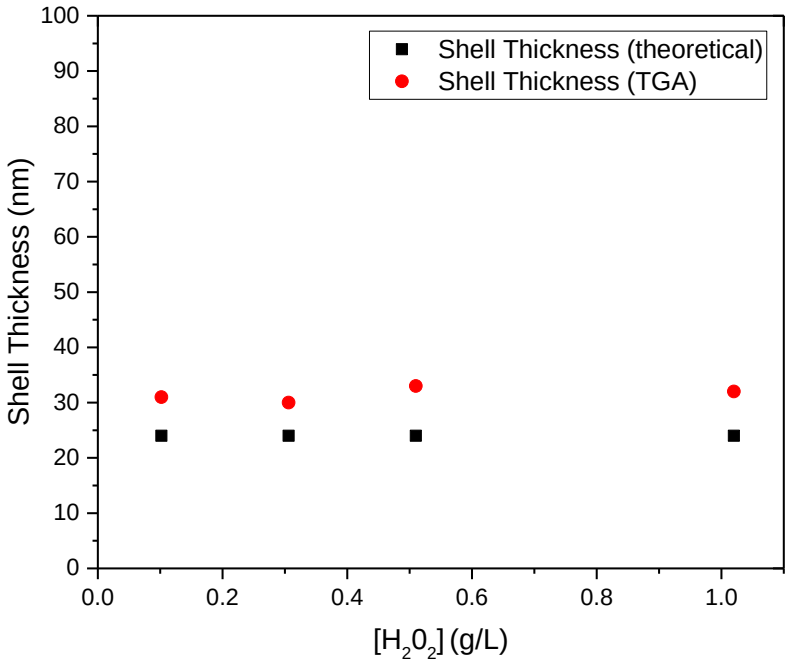

Figure 4. 21: Demonstrates the theoretical and measured (TGA) shell thickness results from analysing the effects of H_2O_2 on gold shell thickness.

From figure 4.21 the ratio of reducing agent H_2O_2 did not affect the reduction of $HAuCl_4$ as the measured shell thickness (TGA) was constant for all measured samples.

$$2HAuCl_4 + 3H_2O_2 \xrightarrow{Pt} 2Au + 3O_2 + 8HCl$$

4.3

Figure 4.21 demonstrates the measured shell thickness (TGA) and theoretical shell thickness are very close and a similar trend is observed across the different concentrations of reducing agent. The ratio of $HAuCl_4$ to H_2O_2 was kept at 1:1.5 in all experiments, also from equation 4.3, the ratio of $HAuCl_4$ to H_2O_2 required is 1:1.5. From this we can assume the concentration of $HAuCl_4$ reduced remained constant in each experiment.

4.9.3 Effect of Oil weight fraction on shell thickness

Previously it was demonstrated the ratios of Au salt to H_2O_2 1:1.5 was adequate and consistent at reducing the Au salt. In this section it will be demonstrated the effect of oil volume fraction ϕ on the Au metal shell thickness. From the emulsion size distribution (bin limits) the total surface area was calculated and compared against the measured shell thickness (TGA).

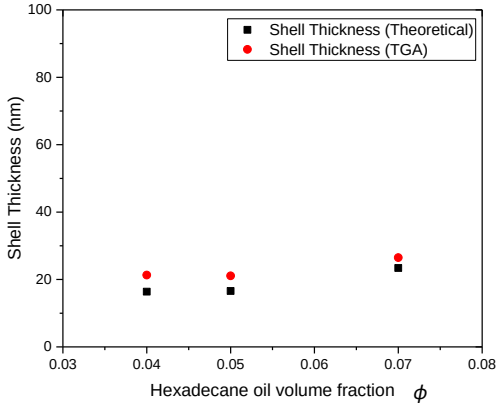

Figure 4. 22: Demonstrates and compares the theoretical shell thickness against the actual measured shell thickness of Au coated emulsion droplets. The Au concentration was kept constant at 7.9mg and the hexadecane oil volume fraction ϕ was varied (0.04, 0.05, 0.07).

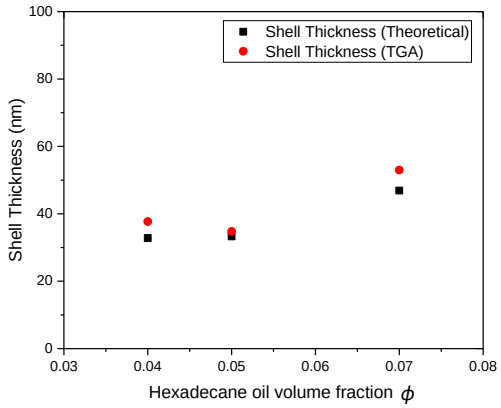

Figure 4. 23: Demonstrates and compares the theoretical shell thickness against the actual measured shell thickness of Au coated emulsion droplets. The Au concentration was kept constant at 15.8mg and the hexadecane oil volume fraction ϕ was varied (0.04, 0.05, 0.07).

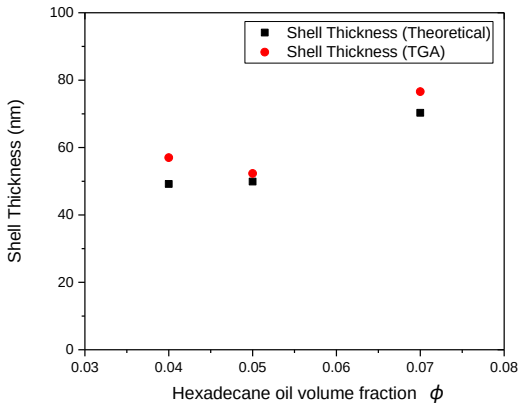

Figure 4. 24: Demonstrates and compares the theoretical shell thickness against the actual measured shell thickness of Au coated emulsion droplets. The Au concentration was kept constant at 23.6mg and the hexadecane oil volume fraction ϕ was varied (0.04, 0.05, 0.07).

The total surface area of the emulsions was consistent over the oil volume fraction ϕ increase as demonstrated in figure 4.13. The theoretically calculated and actual

measured (TGA) shell thickness were all in good agreement, as expected with a reduction in total surface area as seen with the higher oil volume fractions resulted in thicker shells as there was less surface area to cover than with the lower oil volume fractions which had a slightly higher total surface area (figure 4.13) hence resulting in slightly thinner shell thickness compared to, at higher oil volume fractions, this is demonstrated in figure 4.22, 4.23 and 4.24.

4.9.4 Effect of $HAuCl_4$ concentration on shell thickness

In this section it will be demonstrated the effect of $HAuCl_4$ concentration on the Au metal shell thickness.

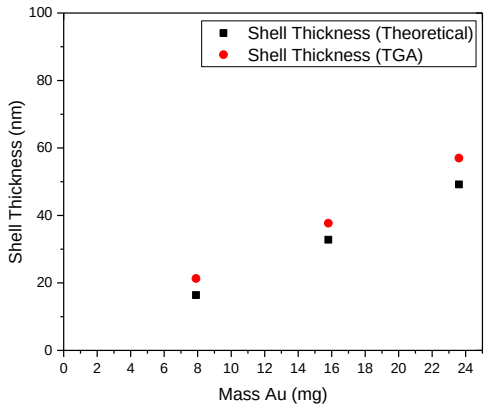

Figure 4. 25: Demonstrates and compares the theoretical shell thickness against the actual measured shell thickness of Au coated emulsion droplets. The Hexadecane oil volume fraction ϕ was kept constant at 0.04 and the Au concentration was varied (7.9, 15.8 and 23.6mg).

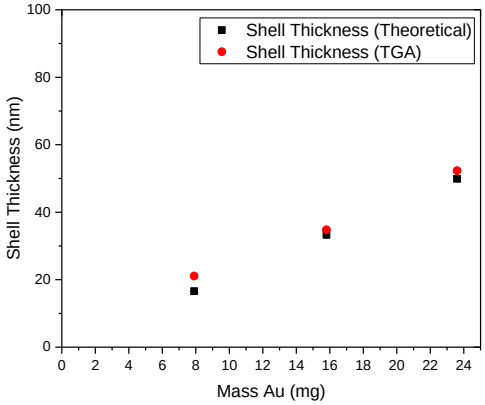

Figure 4. 26: Demonstrates and compares the theoretical shell thickness against the actual measured shell thickness of Au coated emulsion droplets. The Hexadecane oil volume fraction ϕ was kept constant at 0.05 and the Au concentration was varied (7.9, 15.8 and 23.6mg).

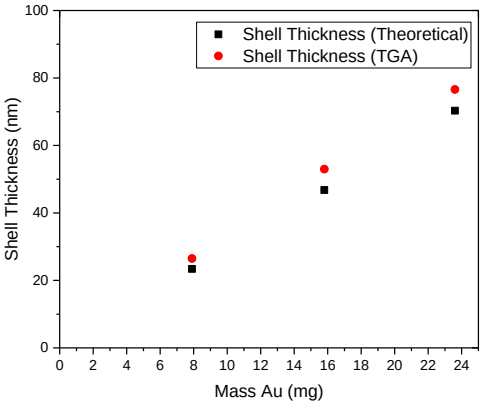

Figure 4. 27: Demonstrates and compares the theoretical shell thickness against the actual measured shell thickness of Au coated emulsion droplets. The Hexadecane oil volume fraction ϕ was kept constant at 0.07 wt% and the Au concentration was varied (7.9, 15.8 and 23.6mg).

Figure 4.25, 4.26 and 4.27 demonstrate we can predict and control the shell thickness accurately by manipulating the emulsion size distribution by varying the oil weight

fraction, and the shell thickness by varying the Au concentration. All the data for shell thickness TGA measured and theoretical are in good agreement.

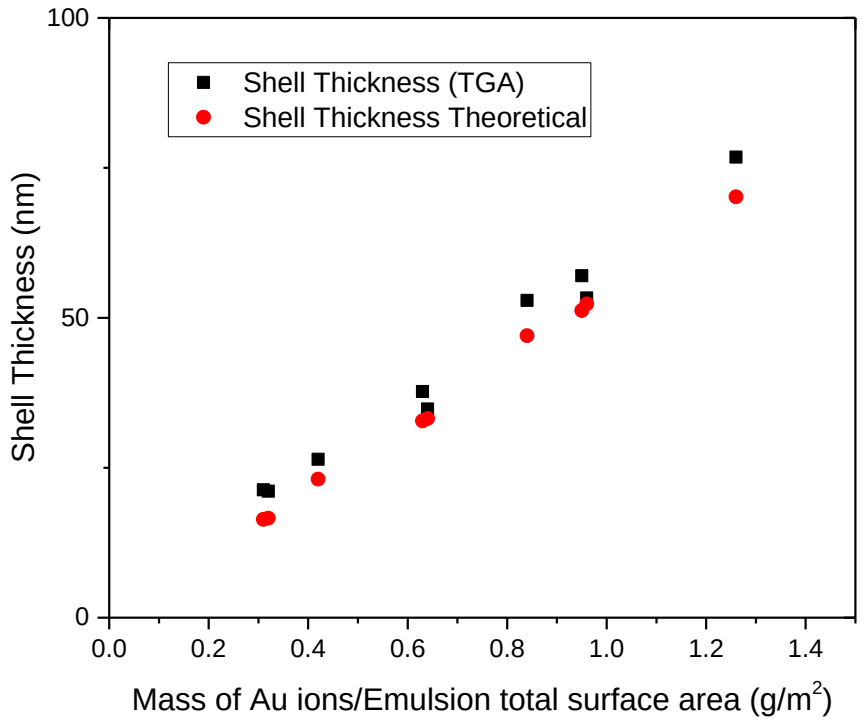

Figure 4. 28: Combined data from figure 4.22, 4.23, 4.24, 4.25, 4.26 and 4.27 plotted as shell thickness vs Mass of Au ions/Emulsion total surface area (g/m^2).

Figure 4.28 demonstrates the combined theoretical and measured shell thickness from the TGA, plotted as shell thickness against Mass of Au ions/Emulsion total surface area (g/m^2). As expected the theoretical shell thickness increases linearly and the shell thickness measured from the TGA is very close to the theoretical calculated shell thickness and consistent as expected.

As mentioned previously figure 4.25, 4.26 and 4.27 assume a constant amount of Au is reduced consistently in each experiment and the theoretical calculated shell thickness assumes all the Au salt is reduced onto the emulsion template, which

justifies the liner relationship between Au salt concentration and microcapsule shell thickness. Previous studies suggest this is not the case for electroless deposition of metals onto surfaces and contradicts our theory. It is suggested the film growth takes place in two steps: [16-18]

1. Rapid initial growth until the surface is covered with metal
2. Slower growth, plateauing over time

To experimentally verify the claims, Au concentration was increased whilst keeping the hexadecane oil volume fraction ϕ consistent. The resulting data is demonstrated in figure 4.29.

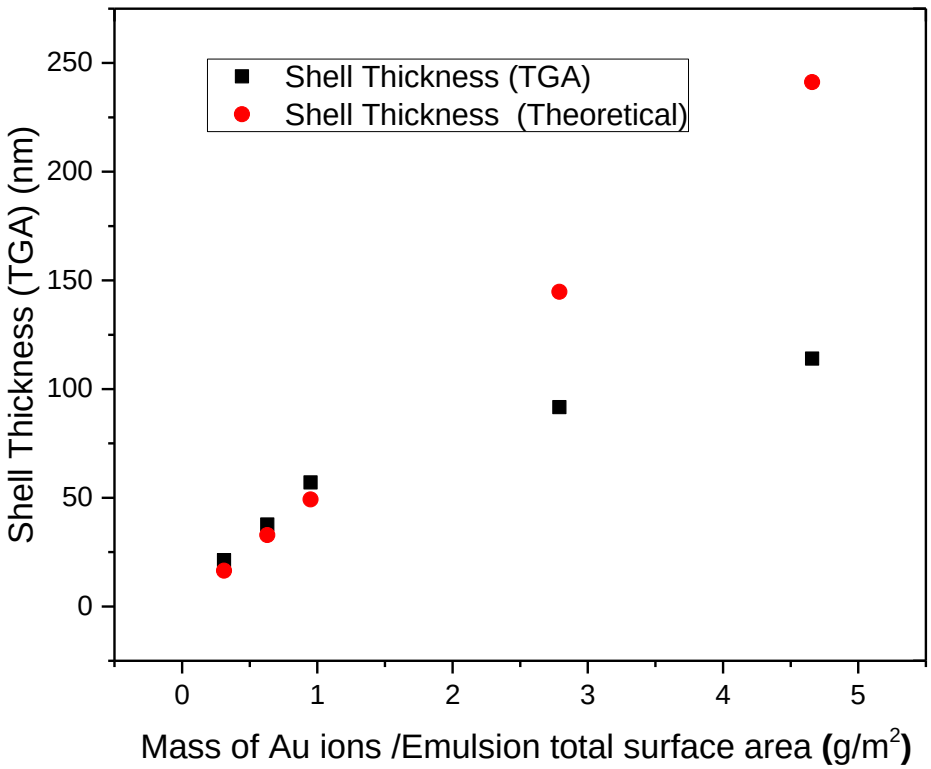

Figure 4. 29: Demonstrates the theoretical shell thickness and the measured shell thickness of Au coated emulsion droplets. Hexadecane oil volume fraction was kept constant at 0.04 and the Au concentration was varied (0.31, 0.63, 0.95 2.79 and 4.7 g/m^2).

As expected from figure 4.29, at the lower concentrations of Mass of Au ions/Emulsion total surface area (g/m^2) the data agrees with the statement that rapid growth takes place, but with increasing Mass of Au ions/Emulsion total surface area (g/m^2) the measured shell thickness does not agree with the theoretical shell thickness, hence agreeing with the assumption that at higher concentration of Mass of Au ions/Emulsion total surface area (g/m^2), initially rapid growth takes place followed by slower growth which plateaus over time.

Figure 4.29 demonstrates the Au growth on Pt-NP stabilised emulsions, initially at lower concentrations of Au, the Au shell thickness is as anticipated but with increasing the concentration of Au at the higher concentrations, the shell thickness is less than anticipated, this is due to the thickness of Au shell, as it grows the influence of Pt is reduced (figure 4.32) and resulting in Au on Au growth and also Au-NP growth in the bulk, which was observed.

4.9.5 Demonstrating impermeability

In the previous section it was demonstrated we could accurately predict the shell thickness theoretically and then measure the actual shell thickness by utilising TGA and both are in good agreement. The microcapsule shell thickness ranged from 21nm to 114nm. In this section we will demonstrate the retention of the hexadecane core of the microcapsule and also demonstrate the effect of shell thickness on the permeability of the microcapsules. The microcapsules were placed in a 4:1 (volume ratio) ethanol/water continuous phase, this was done as the hexadecane core is completely soluble in ethanol and any hexadecane residue present or released from the microcapsules would be solubilised in the ethanol. Microcapsules were dispersed

in an ethanol/water 4:1 ratio and kept suspended at 40°C for 30 days. The microcapsules samples were taken at different time intervals and centrifuged to remove the microcapsules; the resulting sample was measured for hexadecane concentration using gas chromatography (GC). After 30 days the microcapsules were sonicated to break the microcapsules and measured for hexadecane, this was done to demonstrate the microcapsules core contained hexadecane. The resulting data from this experiment is shown in figure 4.30.

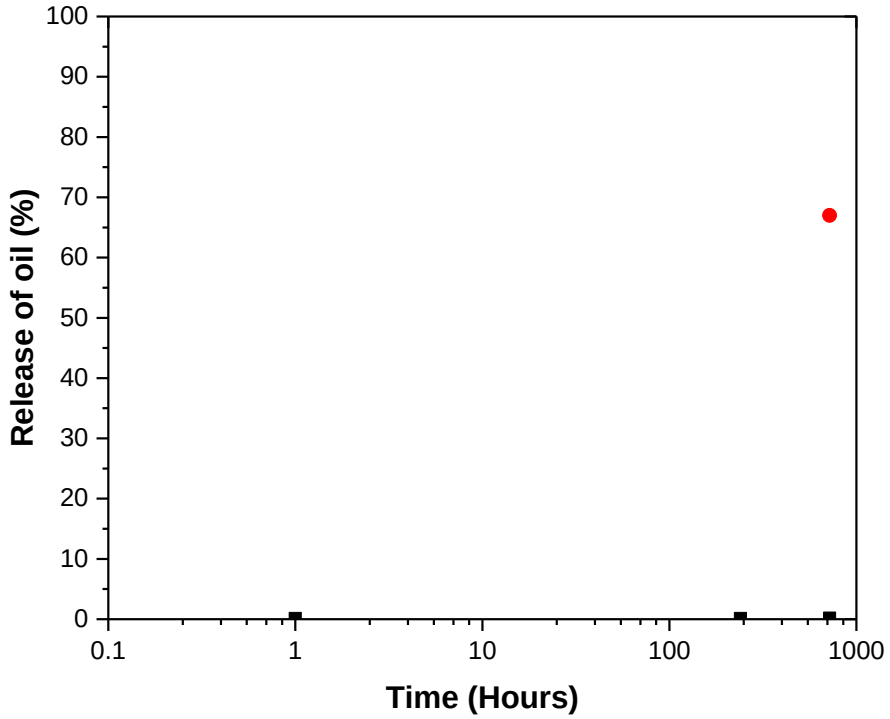

Figure 4. 30: Release of oil core from microcapsules (21nm shell thickness) over time in a 4:1 ethanol/water continuous phase at 40°C. Black square represents Hexadecane release after 1 Hour, release after 10 days and release after 30 days and red circle shows complete release after microcapsules are sonicated to break metal shells.

Figure 4.30 demonstrates the microcapsules (shell thickness 21nm) are able to fully retain the hexadecane core for over 30 days. After 30 days the microcapsules were sonicated to break the shells and the hexadecane concentration was measured and 68% of the initial hexadecane core was recovered.

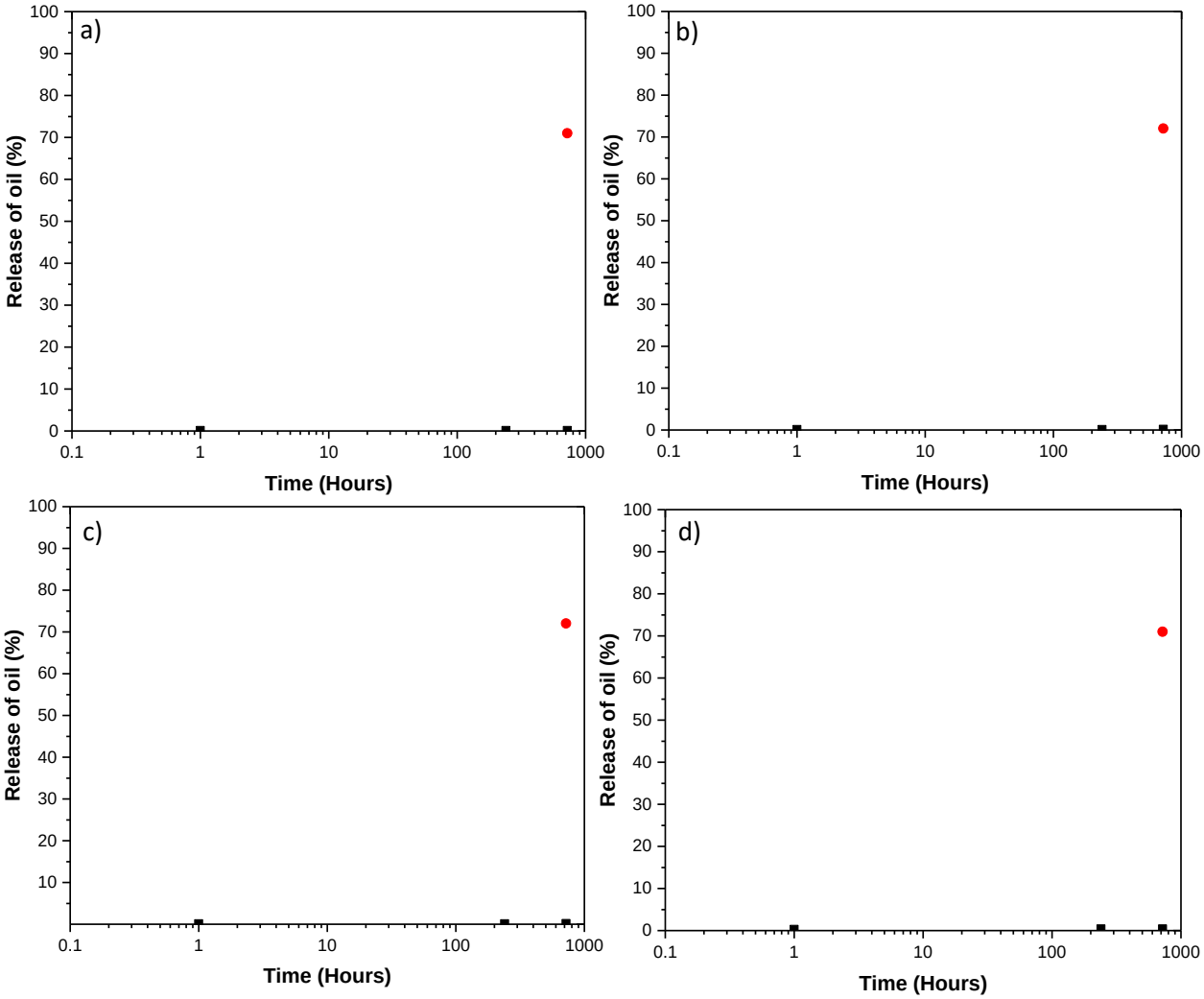

Figure 4. 31: Release of oil core from microcapsules, a-37nm, b-57nm, c-91nm and d-114nm shell thickness, over time in a 4:1 ethanol/water continuous phase at 40ºC. Black square represents Hexadecane release after 1 Hour, release after 10 days and release after 30 days and red circle shows complete release after microcapsules are sonicated to break metal shells (1 min 40% amplitude).

All the microcapsules with shell thickness above 21nm demonstrated complete retention of the hexadecane core for over 30 days.

Figure 4. 32: Schematic representation of Au growth on Pt-NP at the interface at varied Au concentrations 40mM (0.5, 1, 1.5, 3 and 5ml), with increasing growth results in increasing separation distance from Pt-NP.

Figure 4.32 demonstrates the Au growth on the Pt-NPs at the interface at different concentrations, it has been demonstrated at the lowest concentration of gold (0.5ml $HAuCl_4$ 40mm) resulting in 21nm shell thickness sufficiently covered the Pt-NP stabilised emulsion resulting in a complete and impermeable metal shell as demonstrated in figure 4.30. Figure 4.32 also demonstrates as the shell thickness increases the Pt influence is reduced.

4.10 Conclusion

In this chapter we have demonstrated the reduction of H_2PtCl_6 with $NaBH_4$, resulting in Pt-NPs stabilised with PVP. It was also demonstrated the control of the size of Pt-NPs by varying the molecular weight of PVP. The Pt-NPs were chosen for their ability to act as a catalyst for metal film growth via electroless plating. The Pt-NPs in-turn have been used to stabiles oil in water emulsions by adsorbing onto the interface and forming stable emulsions. The surface of the Pt-NP stabilised emulsions has been coated in a gold shell resulting in gold coated emulsion droplets. The Pt-NPs at the interface catalyse the reaction and also provide a nucleation site for the deposition of gold. We have combined theoretical calculations and data from the TGA to accurately predict and control gold shell thickness on Pt-NP stabilised emulsion droplets. We have also demonstrated a continuous shell thickness of 21nm is sufficient to completely retain the hexadecane core over 30 days at 40^oC, in an ethanol/water (4:1) continuous phase by utilising the GC.

The following chapter will demonstrate electroless plating of gold on Si/Pt composite stabilised emulsion, the purpose of moving away from Pt-NPs is due to the regulatory

issues involved with nanoparticle use in personal care products, as the main use of the microcapsules would be for personal care products i.e. fragrances.

4.11 References

1. Moshfegh, A.Z., *Nanoparticle catalysts.* Journal of Physics D-Applied Physics, 2009. **42**(23).

2. Hvolbaek, B., T.V.W. Janssens, B.S. Clausen, H. Falsig, C.H. Christensen, and J.K. Norskov, *Catalytic activity of Au nanoparticles.* Nano Today, 2007. **2**(4): p. 14-18.

3. Roldan Cuenya, B., *Metal Nanoparticle Catalysts Beginning to Shape-up.* Accounts of Chemical Research, 2013. **46**(8): p. 1682-1691.

4. Horiuchi, S. and Y. Nakao, *Platinum colloid catalyzed etchingless gold electroless plating with strong adhesion to polymers.* Surface & Coatings Technology, 2010. **204**(23): p. 3811-3817.

5. Koczkur, K.M., S. Mourdikoudis, L. Polavarapu, and S.E. Skrabalak, *Polyvinylpyrrolidone (PVP) in nanoparticle synthesis.* Dalton Transactions, 2015. **44**(41): p. 17883-17905.

6. Pastoriza-Santos, I. and L.M. Liz-Marzan, *N,N-Dimethylformamide as a Reaction Medium for Metal Nanoparticle Synthesis.* Advanced Functional Materials, 2009. **19**(5): p. 679-688.

7. Sarkar, A., T. Mukherjee, and S. Kapoor, *PVP-stabilized copper nanoparticles: A reusable catalyst for "Click" reaction between terminal alkynes and azides in nonaqueous solvents.* Journal of Physical Chemistry C, 2008. **112**(9): p. 3334-3340.

8. Pastoriza-Santos, I. and L.M. Liz-Marzan, *Formation of PVP-protected metal nanoparticles in DMF.* Langmuir, 2002. **18**(7): p. 2888-2894.

9. Jiang, P., S.Y. Li, S.S. Xie, Y. Gao, and L. Song, *Machinable long PVP-stabilized silver nanowires.* Chemistry-a European Journal, 2004. **10**(19): p. 4817-4821.

10. Dandapat, A., A. Mitra, P.K. Gautam, and G. De, *A Facile Synthesis of Pt Nanoflowers Composed of an Ordered Array of Nanoparticles.* Nanomaterials and Nanotechnology, 2013. **3**.

11. Vanrheenen, P.R., M.J. Mckelvy, and W.S. Glaunsinger, *Synthesis and Characterization of Small Platinum Particles Formed by the Chemical-Reduction of Chloroplatinic Acid.* Journal of Solid State Chemistry, 1987. **67**(1): p. 151-169.

12. Gharibshahi, E. and E. Saion, *Influence of dose on particle size and optical properties of colloidal platinum nanoparticles.* Int J Mol Sci, 2012. **13**(11): p. 14723-41.

13. Shimmin, R.G., A.B. Schoch, and P.V. Braun, *Polymer size and concentration effects on the size of gold nanoparticles capped by polymeric thiols.* Langmuir, 2004. **20**(13): p. 5613-20.

14. Hitchcock, J.P., A.L. Tasker, K. Stark, A. Leeson, E.A. Baxter, S. Biggs, and O.J. Cayre, *Adsorption of Catalytic Nanoparticles onto Polymer Substrates for Controlled Deposition of Microcapsule Metal Shells.* Langmuir, 2018. **34**(4): p. 1473-1480.

15. Hitchcock, J.P., A.L. Tasker, E.A. Baxter, S. Biggs, and O.J. Cayre, *Long-Term Retention of Small, Volatile Molecular Species within Metallic Microcapsules.* ACS Appl Mater Interfaces, 2015. **7**(27): p. 14808-15.

16. Quintanilla, A., S. Garcia-Rodriguez, C.M. Dominguez, S. Blasco, J.A. Casas, and J.J. Rodriguez, *Supported gold nanoparticle catalysts for wet peroxide oxidation.* Applied Catalysis B-Environmental, 2012. **111**: p. 81-89.

17. Vasileva, P., B. Donkova, I. Karadjova, and C. Dushkin, *Synthesis of starch-stabilized silver nanoparticles and their application as a surface plasmon resonance-based sensor of hydrogen peroxide.* Colloids and Surfaces a-Physicochemical and Engineering Aspects, 2011. **382**(1-3): p. 203-210.

18. Zayats, M., R. Baron, I. Popov, and I. Willner, *Biocatalytic growth of Au nanoparticles: From mechanistic aspects to biosensors design.* Nano Letters, 2005. **5**(1): p. 21-25.

5 Emulsions stabilised by Silica/Platinum composite particles as templates for gold film deposition

5.1 Synopsis

This chapter will focus on a method for the synthesis of gold-coated microcapsules that does not involve free nanoparticles in the main fabrication process. Instead here, the necessary Pt nanoparticles will be adsorbed onto carrier silica particles, thus resulting in composite silica/platinum particles that can be used for stabilising the emulsion templates. The reason for removing free Pt-NPs from the main manufacturing process relates to regulatory issues against the use of nanoparticles in formulated products. In this chapter the focus will be on synthesising the Si/Pt composite particles, developing suitable emulsion templates stabilised by the composite particles and finally optimising the subsequent electroless plating of gold films onto the emulsion templates to form gold-shell microcapsules.

5.2 Background and literature review on Pickering emulsions and influence of rough particles

In chapter 4 we demonstrated the ability of Pt-NPs to stabilise oil in water Pickering emulsion and investigated and demonstrated the properties of Pt-NPs to catalyse the reduction of gold and provide a nucleation/deposition site for gold resulting in Pt-NP stabilised emulsion droplets gold coated. In this chapter we will study the effect of silica colloidal particles and their wettability on stabilising oil in water Pickering emulsions. The wettability of the silica particles will be analysed by changing the surface roughness by adsorbing Pt-NPs onto the silica surface. The following section will consist of a background and literature review on silica stabilised Pickering emulsions and the effect of surface roughness on the wettability of the silica particles.

5.2.1 Pickering emulsions

Colloidal particles are able to spontaneously partition to interface of two immiscible liquids and thereby stabilize and disperse emulsions and foams.[1, 2] Emulsions solely stabilised by solid particles are referred to as Pickering emulsions.[3-5] Pickering emulsions show high stability against coalescence, due to the particles adsorbed at the interface of the emulsion droplet creating a physical barrier preventing the droplets from coalescences.[6, 7]

Colloidal particles act in many ways similar to surfactants, they can adsorb at a fluid-fluid interface to produce Pickering emulsions. The wettability of the particle is used to justify to quantify the water or oil liking tendency of the particles.[4] The wettability is quantified in terms of the contact angle of the particle. The contact angle is measured between the tangents to the solid particle surface and the interface. The Young's equation (equation 5.1) describes the contact angle:

$$cos\theta = \frac{\gamma_{po} - \gamma_{pw}}{\gamma_{ow}} \qquad 5.1$$

γ_{po} = interfacial tension at the particle-oil interface

γ_{pw} = interfacial tension at the particle- water interface

γ_{ow} = interfacial tension at the oil-water interface

For hydrophilic particles which will be wetted by the water ($\gamma_{po} > \gamma_{pw}$) the contact angle will be <90°, for hydrophobic particles wetted by oil ($\gamma_{po} < \gamma_{pw}$) the contact angle will be >90°.

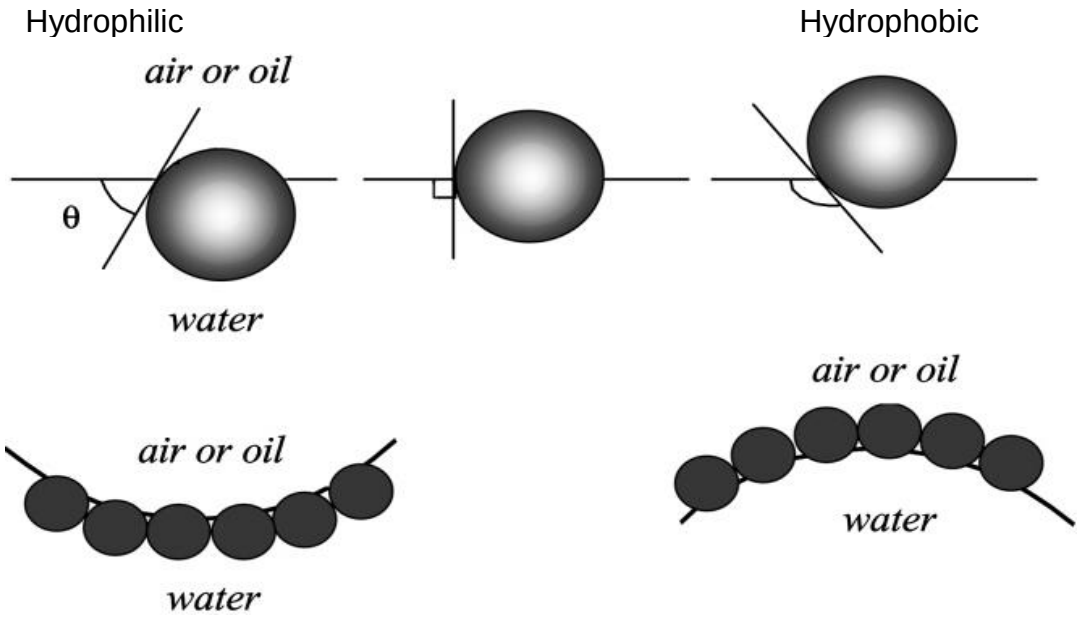

Figure 5. 1: (Upper) Position of silica spherical particles at a planar fluid-water interface for a contact angle, less than 90° (left), equal to 90° (centre) and greater than 90° (right). (Lower) Corresponding probable positioning of particles at a curved fluid-water interface. For $\boldsymbol{\theta}$ < 90° solid-stabilised aqueous foams or oil in water emulsions may form (left). For $\boldsymbol{\theta}$ > 90° solid-stabilised aerosols or water in oil emulsions may form (right)

Once adsorbed at the interface colloidal particles are trapped due to the large adsorption energy for particles at the oil water interface and require a high energy input to remove them from the interface (desorption). Equation 5.2 describes the detachment energy ΔE required to remove the particle from the interface:

$$\Delta E = \pi a^2 y_{ow}(1 \pm cos\theta)^2 \qquad 5.2$$

a = the radius of the particle

y_{ow}= the oil-water interfacial tension

θ= the three phase contact angle

Once a particle is adsorbed at the oil water interface, a certain area of the interface is substituted by an equivalent area of the particle (cross-sectional area). The energy required to remove the particle from the interface is related to the particle contact angle θ, the particle radius a and the oil-water interfacial tension y_{ow}. The sign inside the bracket is negative for particle removal into a water phase and positive for particle removal into the air or oil phase. [4] For a micrometre sized particle at the oil-water interface with a contact angle of ~90°, the detachment energy is on the order of 10^7 k_BT.[8]

From equation 5.2 apart from the contact angle (wettability) the detachment energy ΔE is also effected by the particle radius. Assuming the y_{ow} = 50mN m^{-1} and θ = 90º, the relationship between desorption energy and particle radius is shown in figure 5.2, with increasing particle radius results in an increase in the energy of detachment. In chapter 4 Pt-NPs 2.9 nm (+/-0.4) were used to stabilise oil in water emulsions, the detachment of the particles from the interface compared to larger particles ~100nm would acquire less energy, resulting in less stable emulsions.

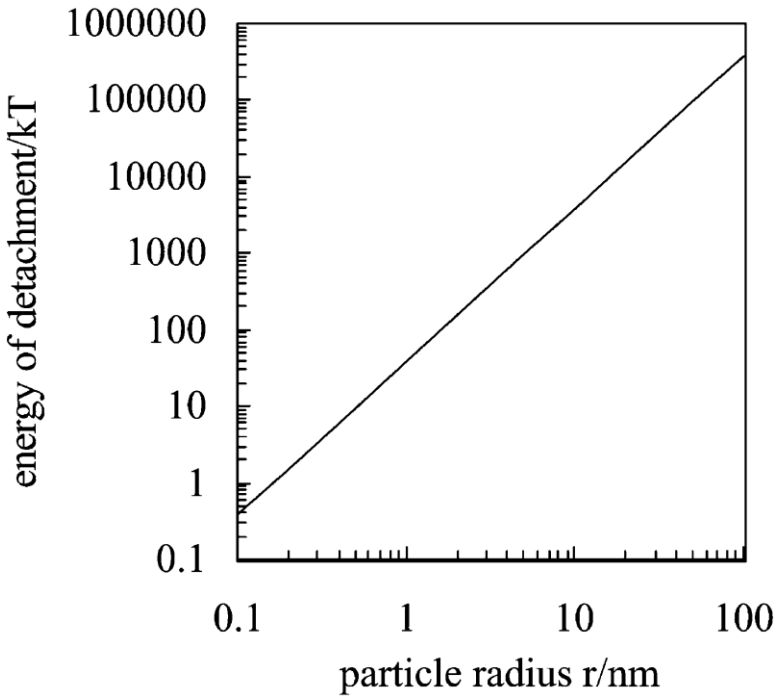

Figure 5. 2: Variation of energy required to remove a single spherical particle ($\boldsymbol{\theta}$ = 90°) from a planar oil-water interface ($\boldsymbol{\gamma_{ow}}$ = 50mN m^{-1}) with particle radius at 298 K.[4]

5.2.2 Silica stabilised Pickering emulsions

In this section a review of silica stabilised emulsion will be carried out. A number of authors demonstrated the stabilisation of Pickering emulsions with different hydrophobicity of silica particles, emulsions were formed by shaking equal volumes of octane and water in the presence of silica, less hydrophobic particles (θ=65°) resulted in oil in water emulsions, whereas hydrophobic particles (θ=152°) resulted in water in oil emulsions.[6, 9, 10] Vignati and Piazza demonstrated the stabilisation of oil in water emulsions with hydrophilic silica particles. The oil cores consisted of either isooctane or octanol dispersed in an aqueous phase, resulting in long term stability.[11] Kaganayuk and Mohraz investigated the effect of particle volume fraction of colloidal silica particles on emulsion size and bridging over time, it was concluded increasing particle volume fraction resulted in larger emulsion droplets with increased bridging.[12]

Ridel, *et al*., demonstrated the use of hydrophilic Ludox silica nanoparticles (30nm) for stabilising (diisopropyl adipate oil) oil in water emulsions. Stable emulsions could be prepared up to 60 vol% oil.[13] Frelichowska, *et al*., demonstrated the use of un-modified hydrophilic fumed silica nanoparticles (100nm), stabilising oil in water emulsions, it was concluded polar oils were favoured over non-polar oils due to enhanced emulsion stability with polar oils.[14] All the papers reviewed above demonstrated the fabrication and stabilisation of oil in water Pickering emulsions (mostly polar oils).

5.3 Influence of rough particle surface on wettability of particles and stabilisation of Pickering emulsions

5.3.1 Cassie-Baxter and Wenzel States

In our studies the Pt-NPs will be adsorbed onto the surface of silica resulting in Si/Pt composites (~100nm), with increasing the adsorption of Pt-NPs to the silica surface will result in an increase of surface roughness, which effects the wettability of the particles. The surface wettability affects the stability of the Pickering emulsion. This is known as the Cassie-Baxter state, in which the liquid does not penetrate into the hollows of the corrugated surface, resulting in a composite interface consisting of both solid and vapour as demonstrated in figure 5.3 A.[15]

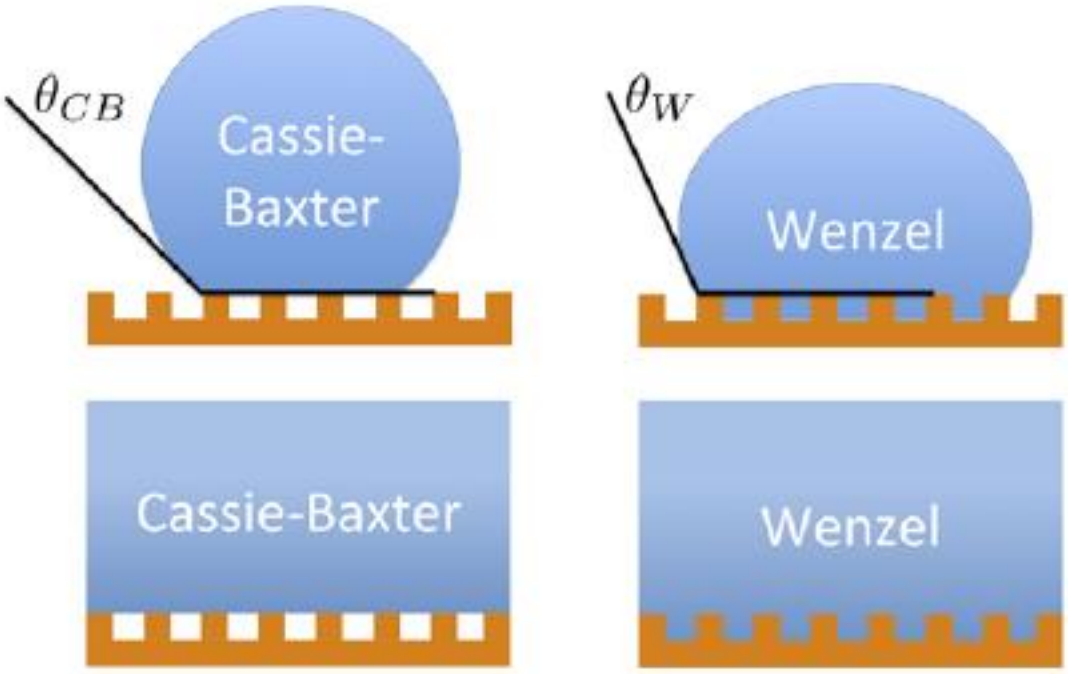

Figure 5. 3: A- Schematic of Cassie-Baxter state in drop (top) and bulk liquid (bottom): the liquid does not wet the entire surface but remains suspended on top of the surface. B- Schematic of Wenzel state in drop (top) and bulk liquid (bottom): the liquid remains in contact with entire exposed surface in drop and bulk liquid. $\boldsymbol{\theta_{CB}}$ and $\boldsymbol{\theta_W}$ denote the contact angles on a rough substrate in a Casssie-Baxter and Wenzel state, respectively.[15]

Another state exists, in which the liquid is in contact with the entire exposed surface of the rough particle, known as the Wenzel state as demonstrated in figure 5.3 B. For hydrophobic states both the Cassie-Baxter and Wenzel state results in an increase in the contact angle. [15]

5.3.2 Particle surface modification through physical adsorption and chemical anchoring

Surface modification by physiosorbed small particles has attracted significant interest due to its simple preparation and efficacy. Hydrophilic silica particles have been modified to enhance the hydrophobicity of the particles, by adsorption of small particles, to form stable emulsions. Modified silica particles have been used to demonstrate the stabilisation of non-polar oils.[16, 17] This was the reason for choosing un-modified silica particles and modifying the surface to stabilise our oil in water emulsions with the oil phase consisting of hexadecane. In chapter 4 we demonstrated, characterised and analysed the stabilisation of Pt-NPs with PVP and also explained the interactions between Pt-NPs and PVP. As PVP is able to stabilise and complex Pt-NPs it was also demonstrated the ability of Pt to catalyse and provide a deposition for a secondary metal, it was decided to use Pt-NPs for adsorption on to the silica surface.

There are two main approaches to adjusting the surface wettability of particles, physical adsorption and chemical anchoring of small molecules or polymers. Frith, *et al*., demonstrated surface modification through the adsorption of cations La^{3+} onto hydrophilic colloidal silica particles, retendering the particles more hydrophobic.[18] Haase, *et al*., stabilised oil in water Pickering emulsions, with hydrophilic silica particles with 8-hydroquinoline adsorption on the surface, the oil core consisted of diethyl phthalate. The 8-hydroquinoline adsorption on the surface rendered the silica particles more hydrophobic improving the stability of the emulsion.[19] Binks and Yin, demonstrated the hydrophobization of hydrophilic silica particles in situ by the adsorption of dissolved oil molecules (dialkyl adipate) in the aqueous phase, enabling

the particles to stabilise oil in water emulsions efficiently.[20] Yang, *et al*., demonstrated the chemical anchoring of organosilanes to hydrophilic silica particles by covalent linkages leading to triamine–octyl bi-functionalized hairy silica microsphere, with increasing hydrophobicity of the silica particles. Stable oil in water (toluene) Pickering emulsions were fabricated with the modified silica particles which demonstrated good stability compared to emulsions stabilised with bare silica particles. [21] Bjorkegren, *et al*., demonstrated chemical anchoring of hydrophobic organosilanes to hydrophilic silica rendering them hydrophobic. It was concluded functionalised silica particles with hydrophobic groups produced emulsions with smaller droplets compared to using unmodified silica. In the above section we described physical absorption and chemical anchoring methods for adjusting the wettability of silica particles.

In addition to surface chemistry, the surface topology such as roughness also affects the wetting behaviour of colloidal particles and the adsorption of the particles at the oil/water interface. The roughness of the particle surface increases the surface area, resulting in an increase in the adsorption energy of the particle at the oil water interface, which is described by equation 5.3:

$$\Delta E = \pi a^2 y_{ow}(1 \pm \alpha \, cos\theta)^2 \qquad 5.3$$

Where α is the surface area magnification factor.[22]

In the following section, studies investigating particles adsorption onto silica particles and their properties for stabilising oil in water emulsions will be described. Zanini, *et al*., fabricated rough particles through electrostatic absorption of negatively charged silica nanoparticles onto larger positively charged silica nanoparticles. To further increase the surface roughness a modified Stober process was used, in which silica was heterogeneously nucleated on the surface of the particles, resulting in a broad

range of particle surface roughness. It was concluded particles with specific roughness could stabilise both oil in water and water in oil emulsions.[23]

San-Miguel and Berens, investigated the effect of surface roughness on the wetting ability of silica particles. Poly(methacrylic acid-*co*-methyl methacrylaye) nanoparticles (50nm) were electrostatically adsorbed onto silica particles. The surface roughness was further tuned by exposing the polymer nanoparticles to aqueous solution of ethanol and or acetone at different concentrations. It was concluded emulsion stability was enhanced further with increasing surface roughness. [24]

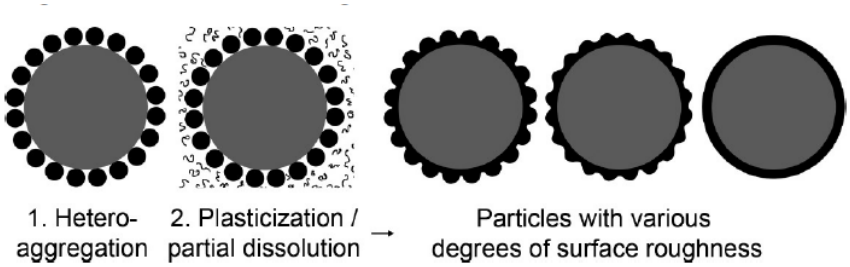

Figure 5. 4: Generation of colloidal particles with different degree of surface roughness. [24]

Above we have reviewed and discussed the ability of unmodified silica particles to stabilise oil in water Pickering emulsions, and silica surface modification through physical adsorption and chemical anchoring to modify the surface roughness. The following section will discuss the synthesis of Si/Pt composites.

5.4 Synthesis of Si/Pt composites

As described in chapter 4, Pt-NPs were synthesised with an average mean diameter size of 2.9 nm (+/-0.4). Colloidal silica with a diameter of 100nm was used to prepare the composites. Si/Pt composites were prepared with different amounts of coverage of the Si surface, as described in chapter 3.2.8 and table 5.1. Figure 5.6 describes the process of depositing Pt-NPs stabilised by PVP onto silica particles resulting in Si/Pt composites, subsequently the composites will be used as colloidal stabilisers for oil-in-water emulsions (Pickering emulsions). Colloidal silica was chosen to form the composites as it is well documented for stabilising oil in water and water in oil emulsions including alkanes.[6, 14, 25] The Pt-NPs on the surface of the silica composites will catalyse and provide a nucleation site for electroless deposition of gold.[26]

PVP is an amphiphilic polymer which is readily soluble in water and many non-aqueous solvents, PVP exhibits this behaviour from the presence of a highly polar amide group within the pyrollidone ring and apolar methylene and methane groups in the ring along the polymer backbone.[27]

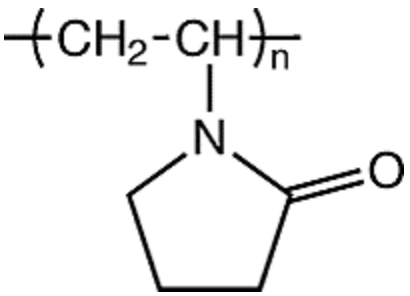

Figure 5. 5: Repeat unit of PVP chain.

It is well documented PVP is able to strongly adsorb on silica surfaces through hydrogen bonding, between the carbonyl groups of PVP molecules and the silanol groups on silica. [28-30]

In the following section it will be demonstrated the adsorption of Pt-NPs onto the silica surface to form Si/Pt composites which will subsequently be used to stabilise oil in water Pickering emulsions. Figure 5.6 demonstrates the overall process of synthesising Si/Pt composite stabilised emulsions gold coated.

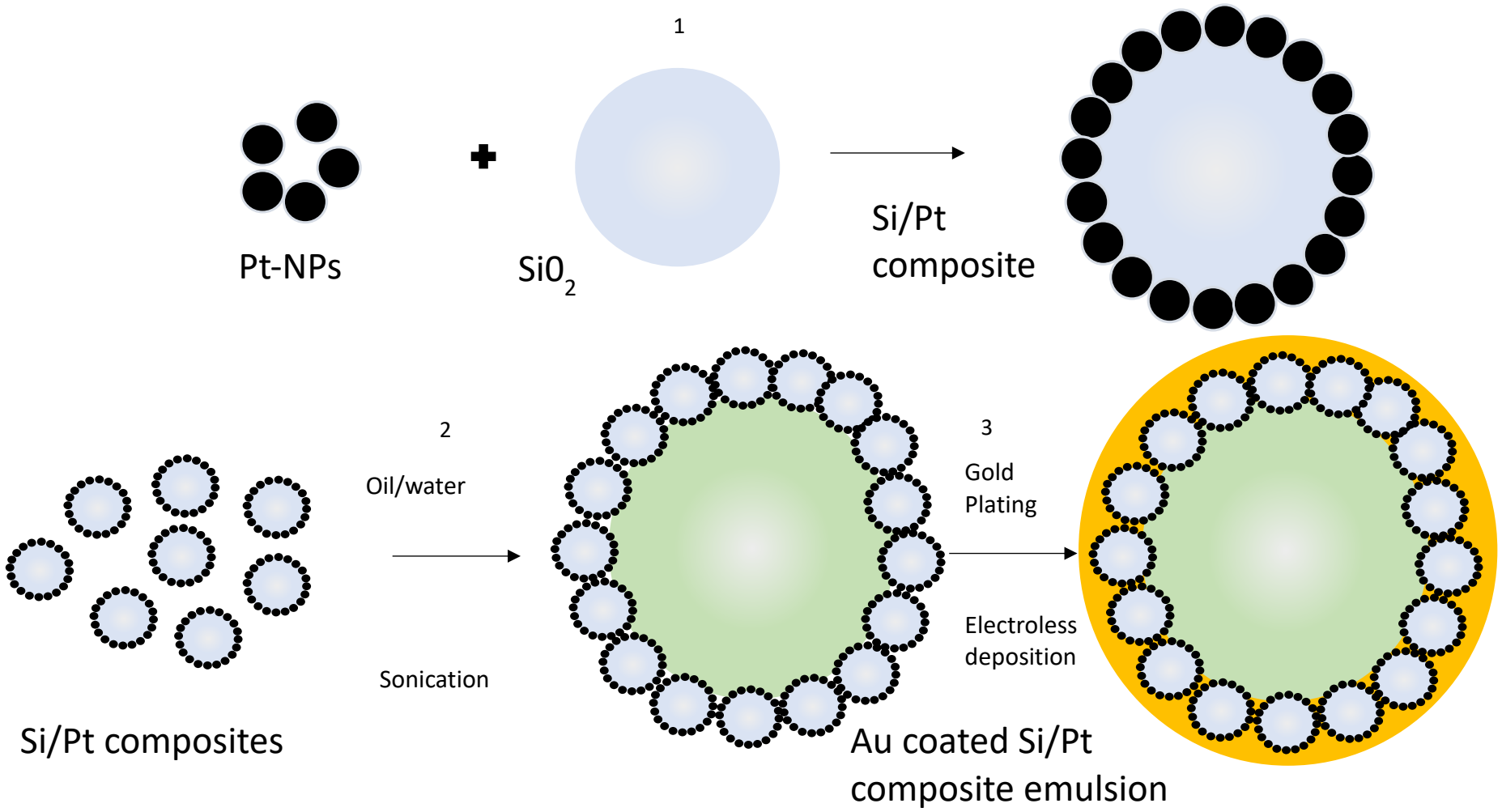

Figure 5. 6: Schematic representation of 1. Formation of Si/Pt composite, 2. Stabilisation of oil-water emulsion with Si/Pt composite, 3. Gold growth on Si/Pt composite stabilised emulsion.

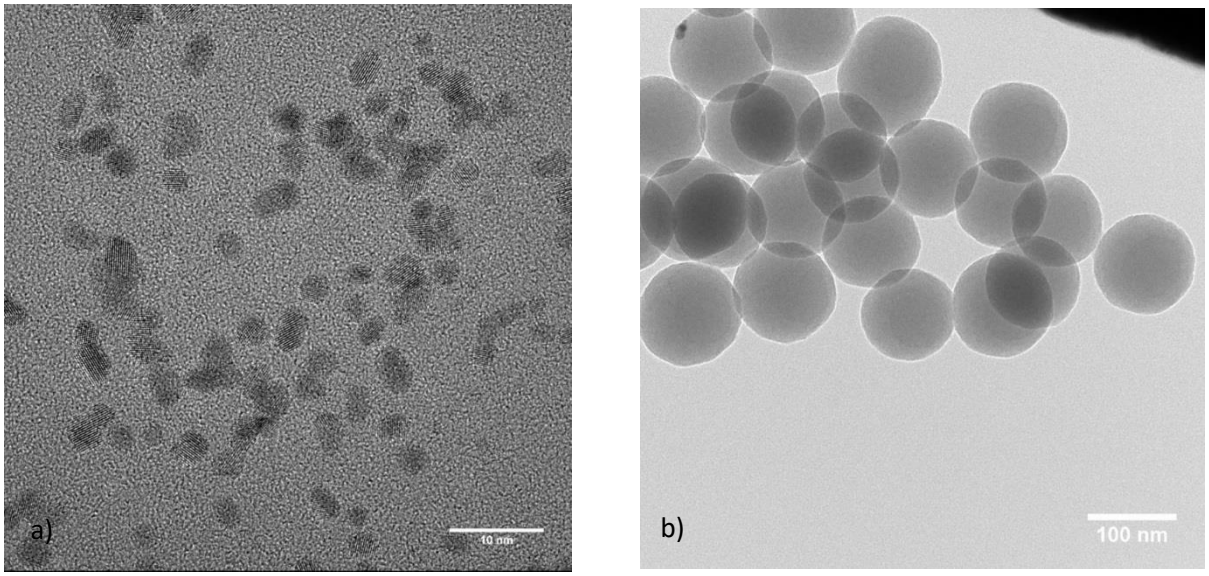

Figure 5. 7: Transmission electron micrograph of a) Pt-NPs deposited on TEM grids using the following conditions: (5.6 mM) $PtCl_6H_2$, (1.1 mM) $NaBH_4$ and (0.0067wt% 40kDa) PVP, b) colloidal silica particles (100nm) deposited on TEM grids.

Table 5. 1: Experimental conditions for formation of Si/Pt composites

Sample No.	Silica (g)	Pt-NPs (ml)	Total Theoretical surface area Pt-NPs can cover ($x10^{18}nm^3$)	Total Theoretical surface area Pt-PVP NPs can cover ($x10^{20}nm^3$)	Maximum surface coverage of Si (%) by Pt-NPs
1	0.1	3.3	0.23	0.14	10
2	0.1	8.25	0.575	0.34	25
3	0.1	16.5	1.15	0.68	50
4	0.1	33	2.3	1.35	100

Four concentrations of Pt-NPs were adsorbed onto the silica surface resulting in Si/Pt composites. Initially the total theoretical surface area of silica 100nm (0.1g) particles was calculated to be 2.3 $x10^{18}$ nm^2. Based on the average mean diameter size of the Pt-NPs of 2.9 nm (+/-0.4), and not taking into account the hydrodynamic diameter of the Pt-NPs, Si/Pt composites were prepared with different amount of theoretical surface coverage, as described in table 5.1. All the calculations quoted are theoretical and do not represent actual measurements as described in chapter 3.7.6.

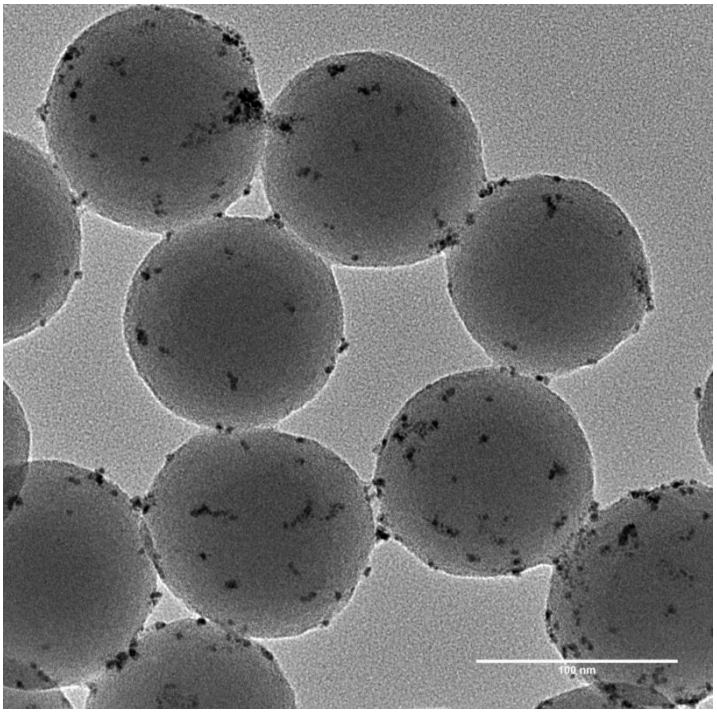

Figure 5. 8: Transmission electron micrograph of Si/Pt composites deposited on TEM grids. Pt-NPs 2.9nm (+/-0.4), Silica 100nm, theoretical surface coverage of silica by Pt-NPs 10%.

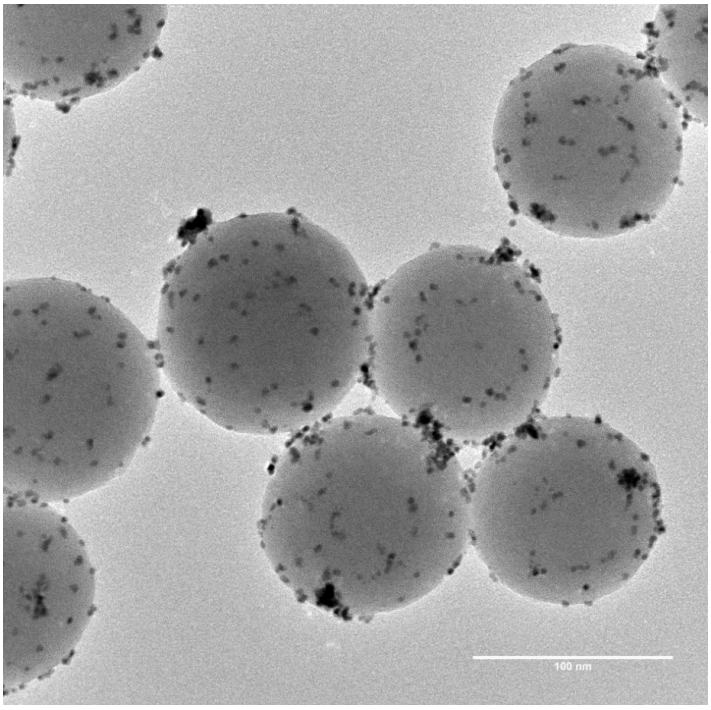

Figure 5. 9: Transmission electron micrographs of Si/Pt composites deposited on TEM grids. Pt-NPs 2.9nm (+/-0.4), Silica 100nm, theoretical surface coverage of silica by Pt-NPs 25%.

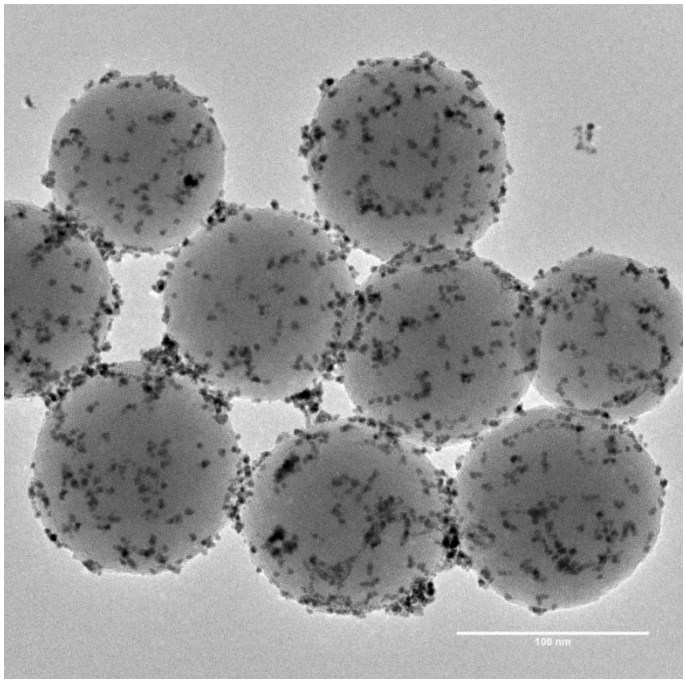

Figure 5. 10: Transmission electron micrographs of Si/Pt composites deposited on TEM grids. Pt-NPs 2.9nm (+/-0.4), Silica 100nm, theoretical surface coverage of silica by Pt-NPs 50%.

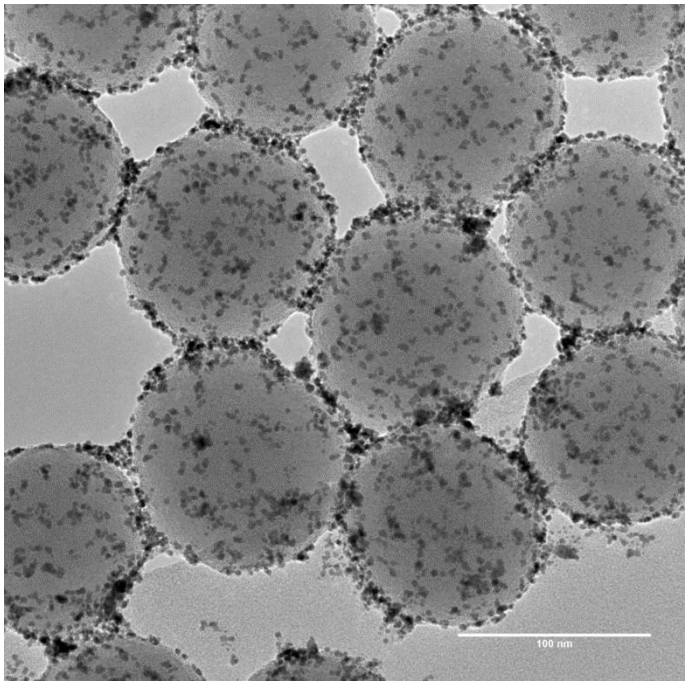

Figure 5. 11: Transmission electron micrograph of Si/Pt composites deposited on TEM grids 24 hours after deposition. Pt-NPs 2.9nm (+/-0.4), Silica 100nm, theoretical surface coverage of silica by Pt-NPs 100%.

From figure 5.9-5.11 it is evident the Pt-NPs aggregated on the surface of silica as the concentration is increased. Initial analysis of the Pt-NPs in the bulk demonstrated no signs of aggregation. As the Pt-PVP NPs were in excess in term of surface coverage of the silica surface, upon centrifuging the composites to separate the Pt-PVP NPs from the Si/Pt composites could result in the excess Pt-PVP NPs aggregating and depositing under force on the silica surface. This trend is evident from figure 5.9-5.11 with an increase in Pt-PVP NPs resulted in an increase of the NPs on the silica surface.

From figure 5.9-5.11 the surface coverage of silica with Pt-NPs is not in line with theoretical coverage calculations, this was due to steric repulsion of the PVP stabilising the Pt-NPs, which prevents Pt-NPs aligning on the surface of silica in a closely packed manner. It is also visually notable Pt-NPs adsorbed on the surface of silica as single Pt-NPs and also clusters of Pt-NPs, with increasing Pt-NP adsorption also resulted in an increase of surface roughness. To quantify the actual amount of Pt-NPs adsorbed on silica, UV-Vis spectroscopy was utilised. Si/Pt composites were centrifuged and separated from the continuous phase which was analysed for Pt-NP concentration, the resulting data is shown in table 5.2.

Table 5. 2: Theoretical surface coverage of Si particles with Pt-NPs and actual surface coverage of Si particles with Pt-NPs, calculated from UV-Vis data (chapter 3.3.3). Error bars represent R^2 from calibration curve.

Si-Pt PVP NP composite No.	Silica (g)	Pt-NPs (ml)	Theoretical Pt (g)	Total surface coverage of silica % (theoretical)	Actual surface coverage of silica % (measure UV-Vis)
1	0.1	3.3	0.0076	10	9.4 +/- 0.1
2	0.1	8.25	0.0189	25	12.8 +/-0.1
3	0.1	16.5	0.0379	50	23 +/- 0.1
4	0.1	33	0.0759	100	41.7 +/- 0.2

As the concentration of Pt-NPs was increased the deposition of Pt-NPs on the silica particles also increased as demonstrated in table 5.2. At the highest concentration of Pt-NPs which would theoretically cover 100% of the Si surface actually resulted in only 41.7% of the Si surface coverage. The calculations from the UV-vis data are in accordance with the TEM images of the Si/Pt composites as demonstrated in figure 5.9- 5.11.

Many techniques have been used to synthesise metal-silica composites, most techniques include the synthesis of metal nanoparticles onto the surface of silica, but these techniques lead to the formation of clusters of metal nanoparticles, the control of the size of the metal nanoparticles is limited and also control is limited of the deposition onto the silica surface.[25, 31, 32] It is very important to control the size of metal nanoparticles as increasing their size would require more mass of the metal leading to increased costs and hence less surface coverage compared to smaller nanoparticles. Also the catalytic activity of the Pt-NPs is due to the size of the particle and this would ware of with increased size. The purpose of the Pt-NPs is to provide a site for the deposition of a secondary metal gold, so again the size is important, as smaller nanoparticles provide more coverage of the surface and more deposition sites for the secondary metal, resulting in complete metal shells. Therefore, it is very important to control the size of the Pt-NPs and where the deposition takes place.

To overcome the issues of metal nanoparticle aggregation and where the adsorption took place, Pt-NPs were synthesised as shown in figure 5.7 a, stabilised with PVP. The Pt-NPs were subsequently mixed with silica to immobilise the Pt-NPs onto the surface of silica through adsorption, by using this technique we were able to overcome the aggregation of direct metal nanoparticle growth on the surface of silica and also control the adsorption of Pt-NPs concentration on the silica surface as shown in figure 5.9-5.11.

The following section will describe the stabilisation of oil in water emulsions (hexadecane) with Si/Pt composites. The Si/Pt composites were initially centrifuged and re-dispersed until no free Pt-NPs remained in the continuous phase.

5.4.1 Si/Pt composite stabilised emulsions

Si/Pt composites were used to stabilise Pickering emulsions. Hexadecane (1ml (corresponding to an oil volume fraction ϕ 0.1) was added to Si/Pt composites (9ml) and homogenised at 40% amplitude for 1 minute. The resulting data of the emulsion size distribution is shown in figure 5.12.

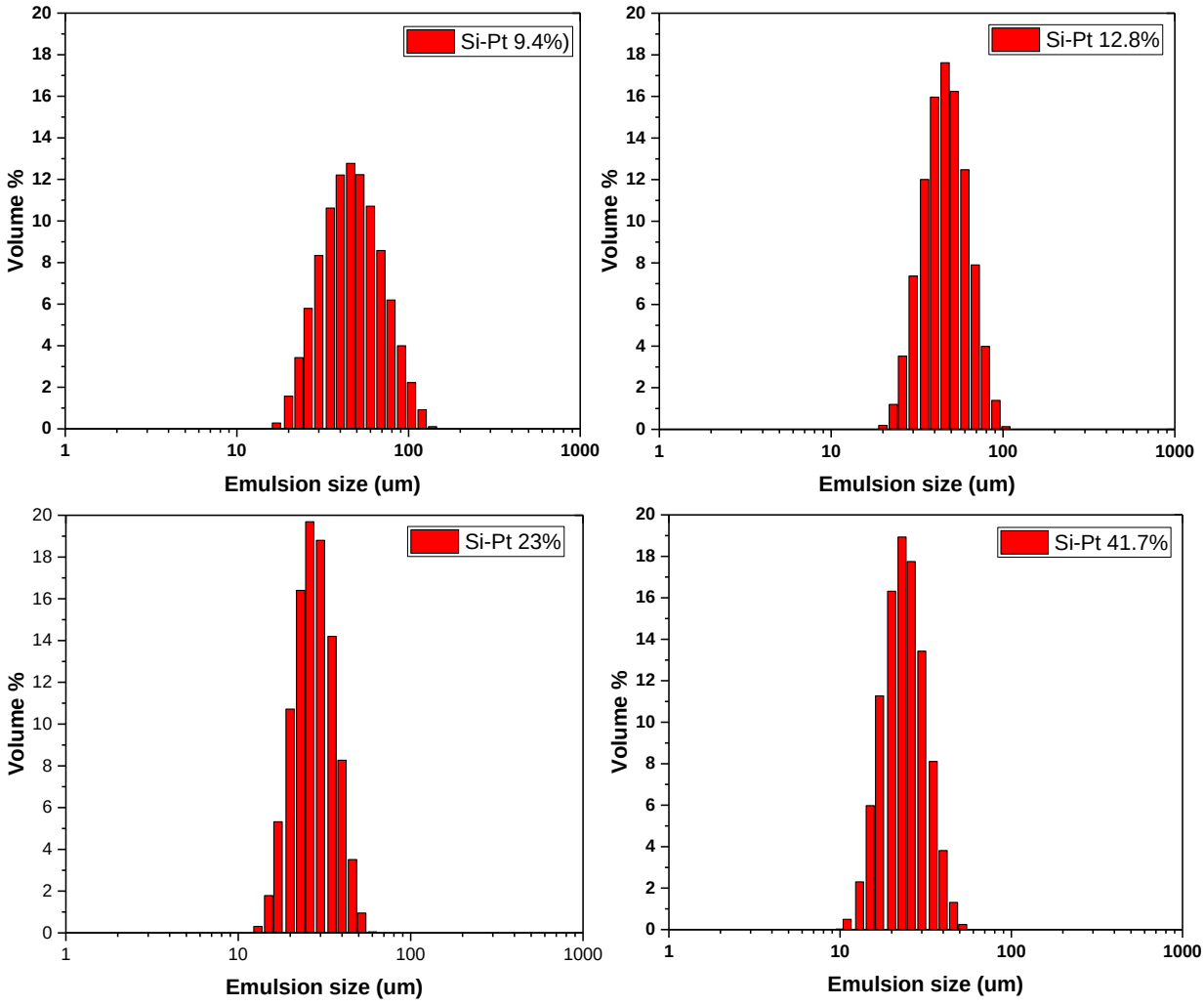

Figure 5. 12: Si/Pt composite (0.1 wt %) stabilised emulsion size distribution (hexadecane oil volume fraction ϕ 0.1). Si/Pt composites demonstrating different levels of wettability by increasing in terms of hydrophobicity (Si/Pt 9.4 %< Si/Pt 12.8 %< Si/Pt 23 %< Si/Pt 41.7 %< increasing hydrophobicity).

Figure 5.12 demonstrates the emulsion droplet size distribution of oil-water emulsion (hexadecane oil volume fraction ϕ 0.1) stabilised with Si/Pt composites with different coverages of the surface with Pt-NPs (9.4, 12.8, 23 and 41.7%), the concentration of silica was kept constant (0.1g). As the Si surface coverage by Pt was increased from 9.4 to 41.7% the emulsion size distribution decreased resulting in a smaller and more mono dispersed emulsion distribution. This can be explained in terms of wettability of the Si/Pt composites as demonstrated in figure 5.13, it is demonstrated as the surface of Si was increased with Pt coverage the three phase contact angle (water contact angle) increased, demonstrating the wettability of the particle in terms of hydrophobicity, hence the Si/Pt composites increasing in terms of hydrophobicity. This effect can be explained in terms of the Cassie-Baxter and Wenzel state, as the Pt-NP adsorption increased on the silica surface the roughness of the surface also increased, hence affecting the wettability of the particles as demonstrated in figure 5.3 A and B, this effect was also demonstrated by Bjorkegren, *et al.,.*[16]

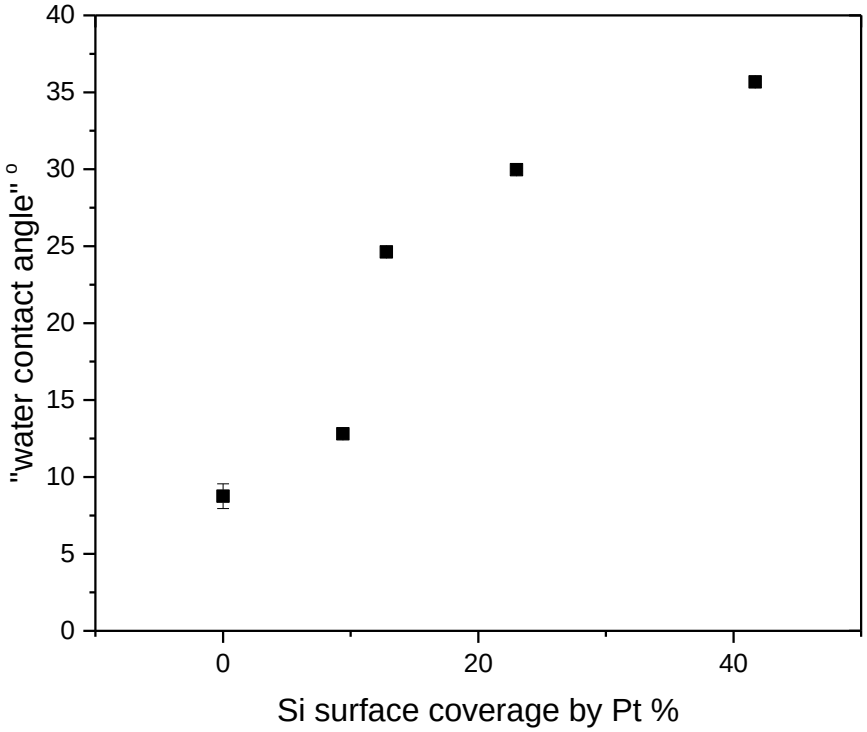

Figure 5. 13: Three phase water contact angle (water/Si-Pt/air) measurements of Si/Pt composites with different degree of surface coverage of Si (0, 9.4, 12.8, 23 and 41.7%). Error bars represent the standard deviation of the mean (3 measurements) but are too small to be distinguished on the data points at 9.4% Pt coverage and above.

It was not possible to measure the actual oil/water/solid (Pt-Si composites) contact angle, due to the small size of the Si/Pt composites, also when it was attempted to measure the water contact angle on a glass slide coated in a Si/Pt composite in an oil phase (hexadecane) this resulted in the Si/Pt coating on the glass slide not remaining stable. We were able to determine the trend of hydrophobicity of the Si/Pt composite by measuring the solid/water/air contact angle as described in method (chapter 3.4.2). Grate, *et al.,* demonstrated the use of this method, by modifying the surfaces of silicon wafers with silanes and measuring the air-water and oil-water contact angle. Also in the study Grate, *et al.,* [33] demonstrated the linear correlation between measured air-water and oil-water contact angles (figure 5.14). This analysis represents a pseudo

quantitative assessment of the wettability of the particle surface on the modified glass plate and not the Si/Pt composite directly. The trend should be similar to the three phase contact angle (oil/water/solid). As we were not able to measure the oil/water/solid contact angle we can make the assumption both systems would behave in a similar way after reviewing Grate, *et al.,*[33] study. Also as the system was controlled we can assume the effects seen were due to the wettability of the Si/Pt composites.

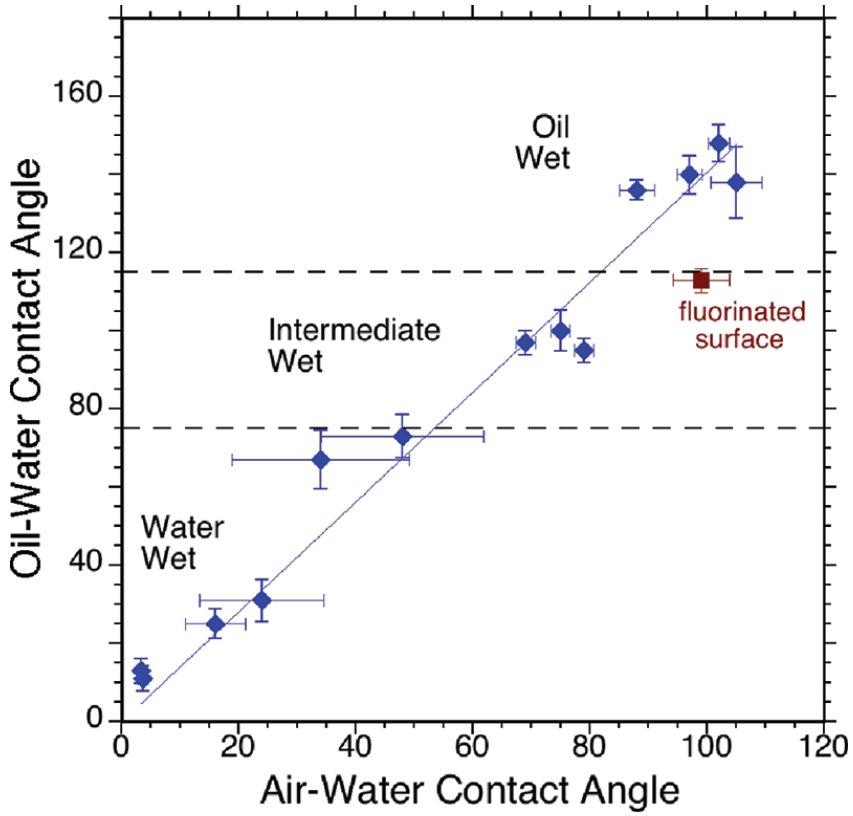

Figure 5. 14: Correlation of oil-water and air-water contact angles for silica and silanized-silica (diamond marker), and fluorinated surface (square marker).[33]

From figure 5.13 as the water contact angle increased, this demonstrated the increase of hydrophobicity of the Si/Pt composite. Figure 5.12 demonstrated the increase in the hydrophobicity of the Si/Pt composite resulted in the emulsion size distribution decreasing with the more hydrophobic particles. This was also demonstrated by Horozov and Binks, where hydrophobic silica particles resulted in smaller emulsion

size distributions compared to less hydrophobic silica particles which were five times larger when comparing the average emulsion size. [6]

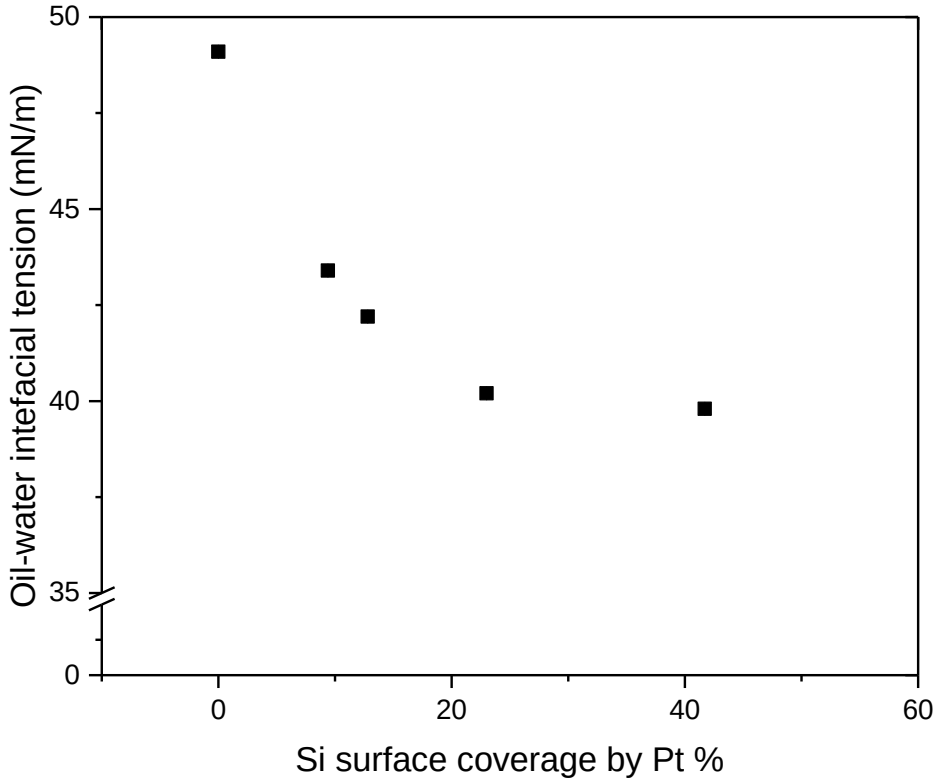

Figure 5. 15: Interfacial tension of hexadecane droplets in Si/Pt aqueous suspensions (0.1 wt%) with different degree of surface coverage of Si with Pt-NPs (0, 9.4, 12.8, 23 and 41.7%) measured as a function of time. The interfacial surface tension of hexadecane/water was measured at 49 mN/m (Lit value 53.5).[34] Error bars represent standard deviation of the mean (3 measurements) but are too small to be distinguished on the data points.

Figure 5.15 demonstrates the oil/water interfacial tension (hexadecane), the hexadecane/water interfacial tension was measure at 49 mN/m which was very close to the literature value of 53.5mN/m.[34] As the hydrophobicity of the Si/Pt composite

increased the interfacial tension of the oil/water decreased. This can be explained in terms of the wettability of the Si/Pt composites demonstrated in figure 5.13, as the hydrophobicity increased of the Si/Pt composites the more hydrophobic particles have more of a tendency to partition to the oil/water interface then less hydrophobic particles. The particles will diffuse at the same rate, but hydrophobic particle adsorption is favoured over hydrophilic particles, therefore the hydrophobic particles adsorb more efficiently at the interface, due to more adsorption events per contact. As hydrophobic particle adsorption is favoured over hydrophilic particles at the interface, more hydrophobic particles (silica with higher Pt-NP covering the surface, rougher surface) will adsorb at the interface, this would also result in a decrease in un-occupied interfacial surface area (more interface occupied by particles/more cross-section area) hence resulting in a decrease in interfacial surface tension. As the hydrophobic particles (silica with higher Pt-NP covering the surface, rougher surface) will adsorb more efficiently at the interface, it will also result in a decrease in emulsion droplet size as demonstrated in figure 5.12.

From equation 5.2 the detachment energy ΔE is affected by, a the particle radius, y_{ow} oil-water interfacial tension and θ the three phase contact angle. For our system the radius of the particles is kept constant and the oil-water interfacial tension (Hexadecane) is 49 (mN/m), the only parameter changing is the three phase contact angle (wettability), we are not able to measure the oil/water/solid contact angle due to the size and concentration of the Si/Pt composites, therefore we are not able to calculate the actual detachment energy for our particles but we are able to determine the detachment energy pattern from measuring the water/solid/air contact angle. As we demonstrated in figure 5.13 the Si/Pt composites increasing in hydrophobicity due

to the higher water contact angle, from equation 5.2 as the contact angle increases (between 0-90^{o}) this will result in the detachment energy to increase for our Si/Pt composites, as the particle will adsorb deeper into the oil-phase with increasing hydrophobicity (occupying more cross-section area of the interface).

Table 5. 3: Total emulsion surface area (measured figure 5.12, bin limits) and the corresponding theoretical shell thickness, while mass of gold 15.8mg and hexadecane oil volume fraction ϕ 0.1 kept constant.

Sample	Mass of gold (mg)	Total emulsion surface area (measured) (x10^{17} nm^2)	Theoretical shell thickness (nm)
Si-Pt 9.4%	15.8	3.71	43.9
Si-Pt 12.8%	15.8	3.79	43.0
Si-Pt 23.0%	15.8	5.46	29.9
Si-Pt 41.7%	15.8	6.25	26.1

Table 5.3 represents the total emulsion surface area (nm^2) calculated from the emulsion size distribution (figure 5.12, bin limits) measured using the mastersizer. The hexadecane oil volume fraction was kept constant at ϕ 0.1. From figure 5.12 as the emulsion size distribution decreased in size this resulted in an increase in the total emulsion surface area due to smaller emulsion droplets as more hydrophobic particles occupied more interface. From the total emulsion surface area as the gold concentration was kept constant we were able to calculate the theoretical thickness of the gold shells on the Si/Pt composite stabilised emulsions. With the increasing total emulsion surface area would result in a decrease in the shell thickness.

In the previous discussion only the Pt-NP surface coverage variable was discussed affecting the wettability of the Si/Pt composite. The PVP adsorb onto the Pt-NP could also be a variable affecting the wettability of the Si/Pt composite, as it could adsorb onto the silica surface. As we are using the minimum amount of PVP required to

stabilise the Pt-NP (chapter 4.4) making sure no excess PVP is present, we assume the effect of PVP is negligible. It has been demonstrated individually two components PVP and silica exhibited very little potential to partition at the air−water interface, and as such, stable foams could not be generated. In contrast, combining the two components to form silica−PVP core−shell nanocomposites led to good “foamability” and long term foam stability.[35, 36]

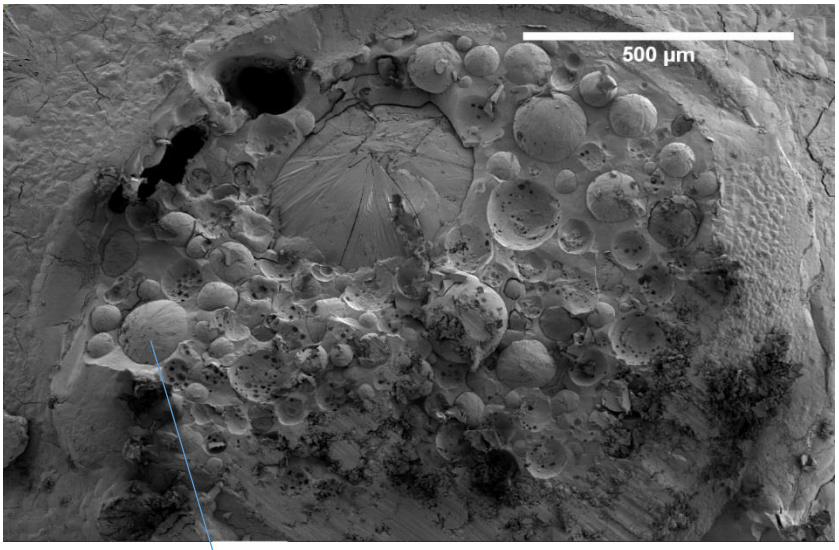

Figure 5. 16; CryoSEM micrographs of Si/Pt (41.7%) stabilised emulsions (9ml) and hexadecane oil volume fraction ϕ 0.1.

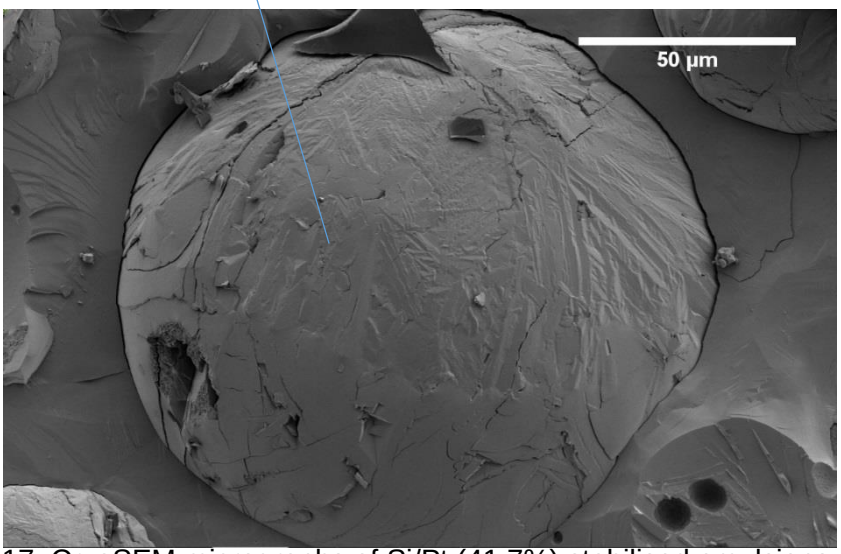

Figure 5. 17; CryoSEM micrographs of Si/Pt (41.7%) stabilised emulsions (9ml) and hexadecane oil volume fraction ϕ 0.1.

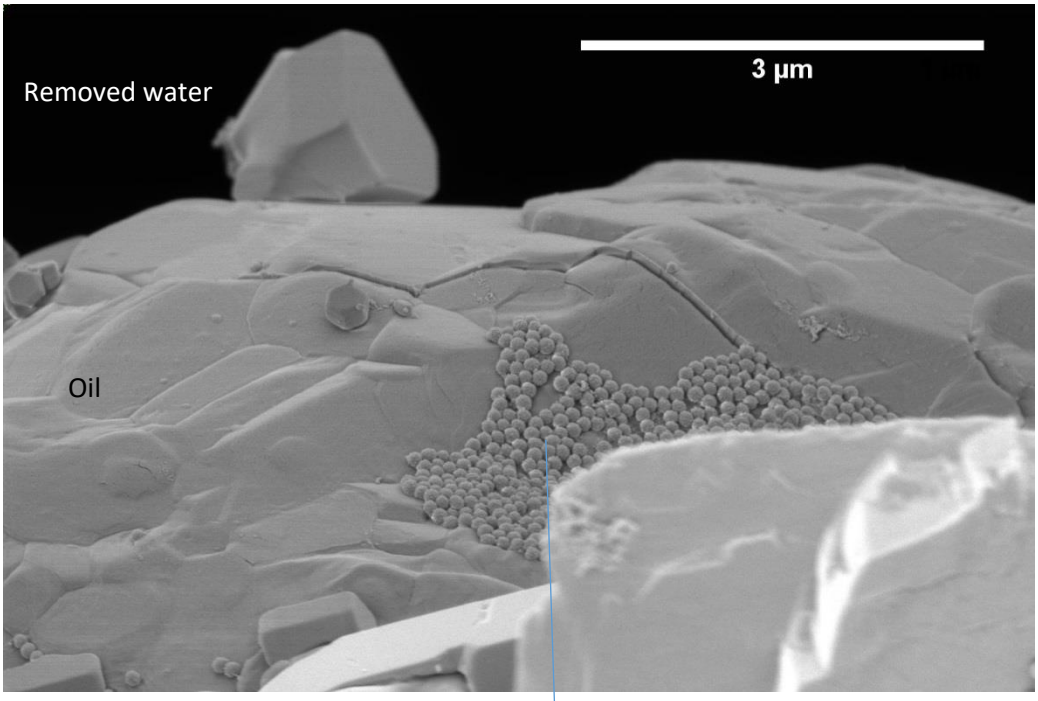

Figure 5. 18; CryoSEM micrographs of Si/Pt (41.7%) stabilised emulsions (9ml) and hexadecane oil volume fraction ϕ 0.1

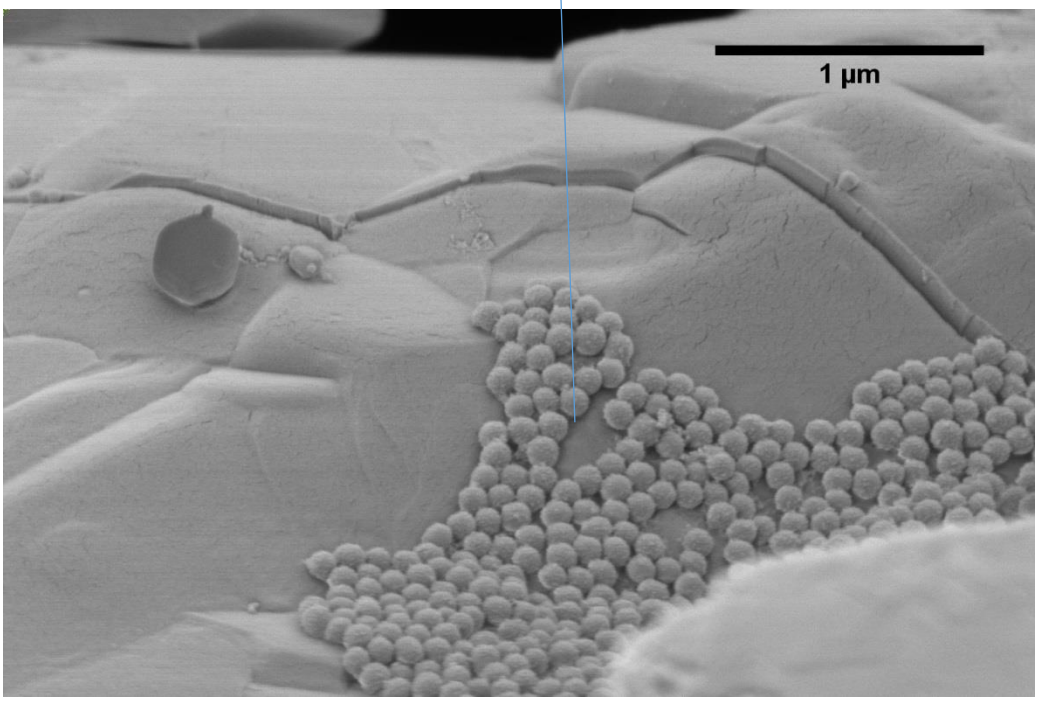

Figure 5. 19; CryoSEM micrographs of Si/Pt (41.7%) stabilised emulsions (9ml) and hexadecane oil volume fraction ϕ 0.1

SEM images were recorded in cryo conditions to analyse the 3D structure of the emulsions via focused ion beam (FIB). Once the sample is frozen, the sample is fractured exposing some of the emulsions and subsequently coated with platinum to reduce charging while in the SEM. The FIB can directly mill the frozen sample surface, via the sputtering of ions and therefore cut through the frozen sample to create a cross section from which the Si/Pt composite at the interface can be analysed.

The resulting micrographs for Si/Pt composite stabilised emulsion with hexadecane (1ml) can be observed from figure 5.16 - 5.19. Figure 5.16 and 5.17 demonstrate the fracturing of the surface of a Si/Pt stabilised emulsion which has creamed. It can also be observed where the emulsion droplets are still intact and where with fracturing have been removed leaving behind dimples. Figure 18 and 5.19 demonstrates the Si/Pt composite at the interface, most of the Si/Pt composite particles are removed from the interface during the fracturing process but some remain, it is observed a single mono layer of Si/Pt composite is present at the interface and no aggregation takes place.

By adsorption of Pt-NPs via PVP onto the surface of silica we were able to form Si/Pt composites which subsequently stabilised oil in water emulsion. Due to the size of the Si/Pt composites (~100nm) and hydrophobicity, the Si/Pt composites adsorbed efficiently at the interface compared to Pt-NPs used in chapter 4, resulting in stable emulsions. Also by using Si/Pt composites we were able to increase the core loading from an oil volume fraction of ϕ 0.04 for Pt-NP stabilised emulsions (chapter 4) to 0.1 ϕ, resulting in an increase of 150%.

5.4.2 Metal coating of Pt-Si stabilised emulsion

In the previous section we demonstrated the stabilisation of oil in water emulsion with Si/Pt composites. Furthermore, we will demonstrate the catalytic activity of the Pt-NPs on the surface of the Silica in terms of catalysing the growth of gold and also providing a site for the deposition of the gold. [26, 37] The four different emulsions stabilised with Si/Pt composites were coated with gold (1ml $HAuCl_4$ 40mM, 1ml 60mM H_20_2, 5ml 0.2 wt% PVP 40kDa) resulting in gold coated Si/Pt emulsions (chapter 3.2.12) as demonstrated in figure 5.20 and 5.21. It can be seen from figure 5.20 and 5.21 the size of the gold coated emulsions agrees with the trends in the emulsion size distribution represented in figure 5.12, which demonstrates the emulsion size decreases with the increase in hydrophobicity of the Si/Pt composite.

Figure 5.20 and 5.21 demonstrates the optical micrographs of Si/Pt composite stabilised emulsions, gold coated, under reflected and transmitted light. It is observed from figure 5.20 a-d, the microcapsules appear cracked due to the larger size of the microcapsules, resulting from the cover slip applying pressure to the larger microcapsules. All the microcapsules appear to be coated in a continuous metal gold film without any aggregation or destabilisation of the microcapsules.

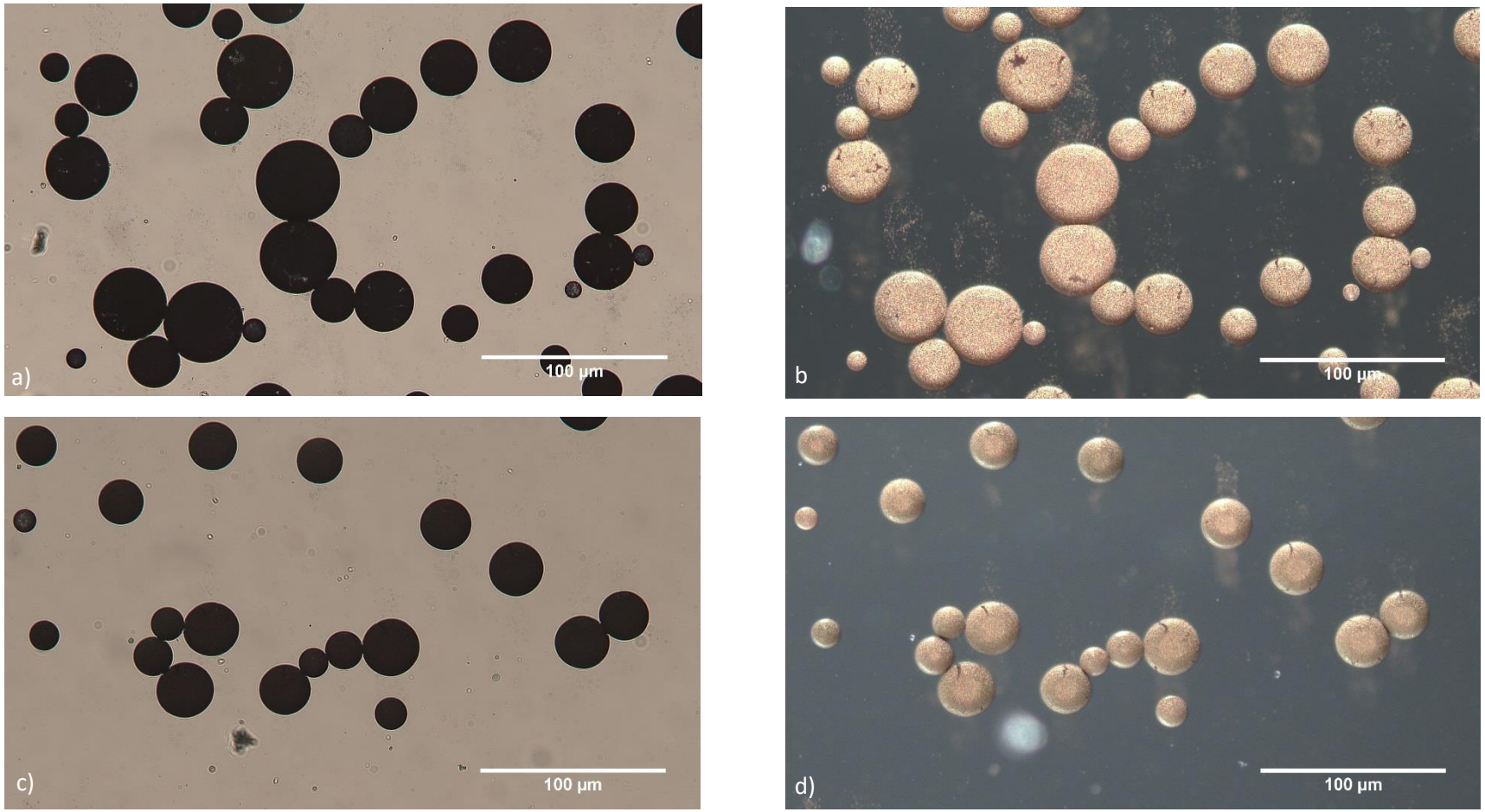

Figure 5. 20: Optical micrographs of Si/Pt stabilised emulsions, gold coated. a) Si/Pt composite (9.4%) gold microcapsules, transmitted light, b) Si/Pt composite (9.4%) gold microcapsules, reflected light, c) Si/Pt composite (12.8%) gold microcapsules, transmitted light, d) Si/Pt composite (12.8%) gold microcapsules, reflected light.

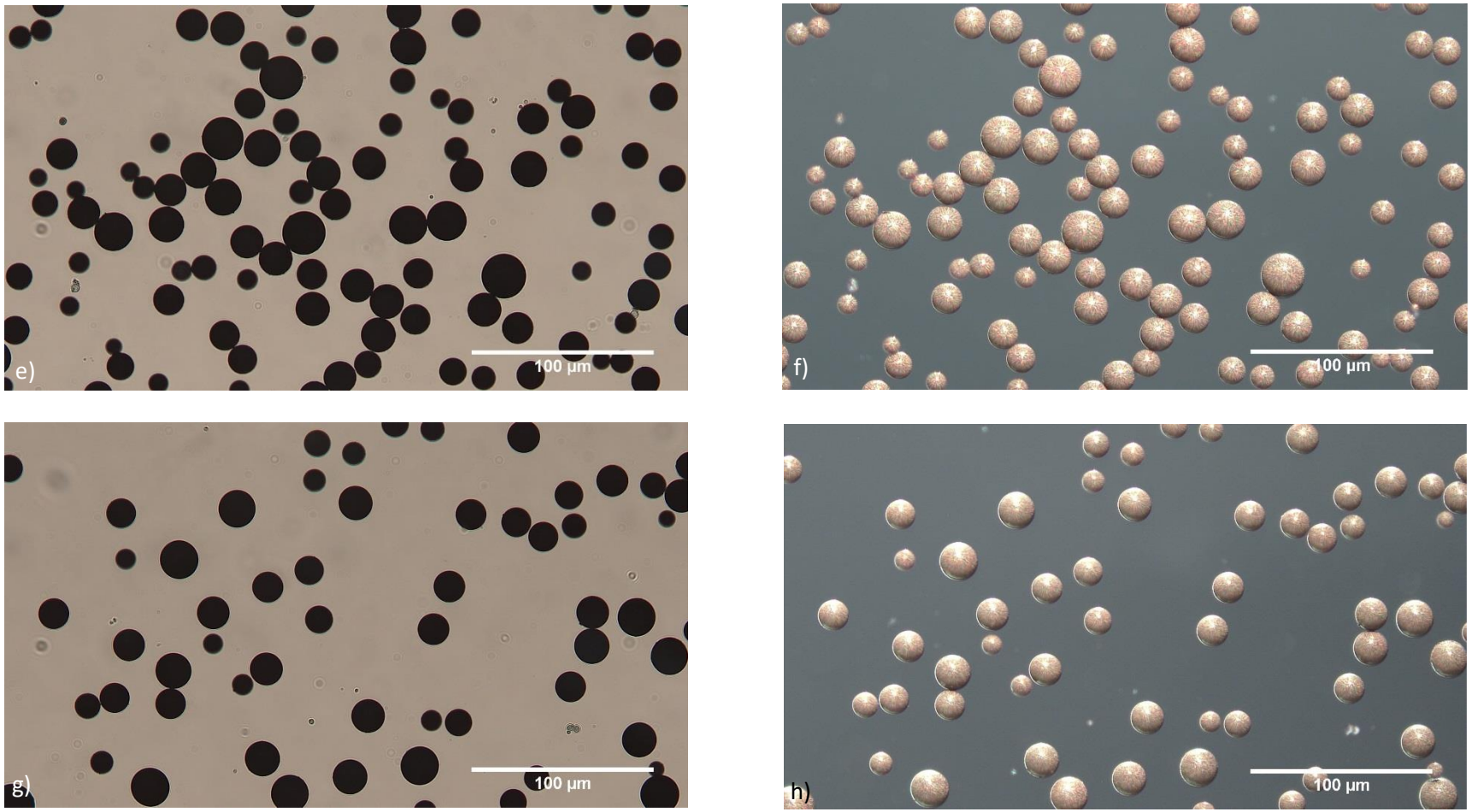

Figure 5. 21: Optical micrographs of Si/Pt stabilised emulsions, gold coated. a) Si/Pt composite (23%) gold microcapsules, transmitted light, b) Si/Pt composite (23%) gold microcapsules, reflected light, c) Si/Pt composite (41.7%) gold microcapsules, transmitted light, d) Si/Pt composite (41.7%) gold microcapsules, reflected light.

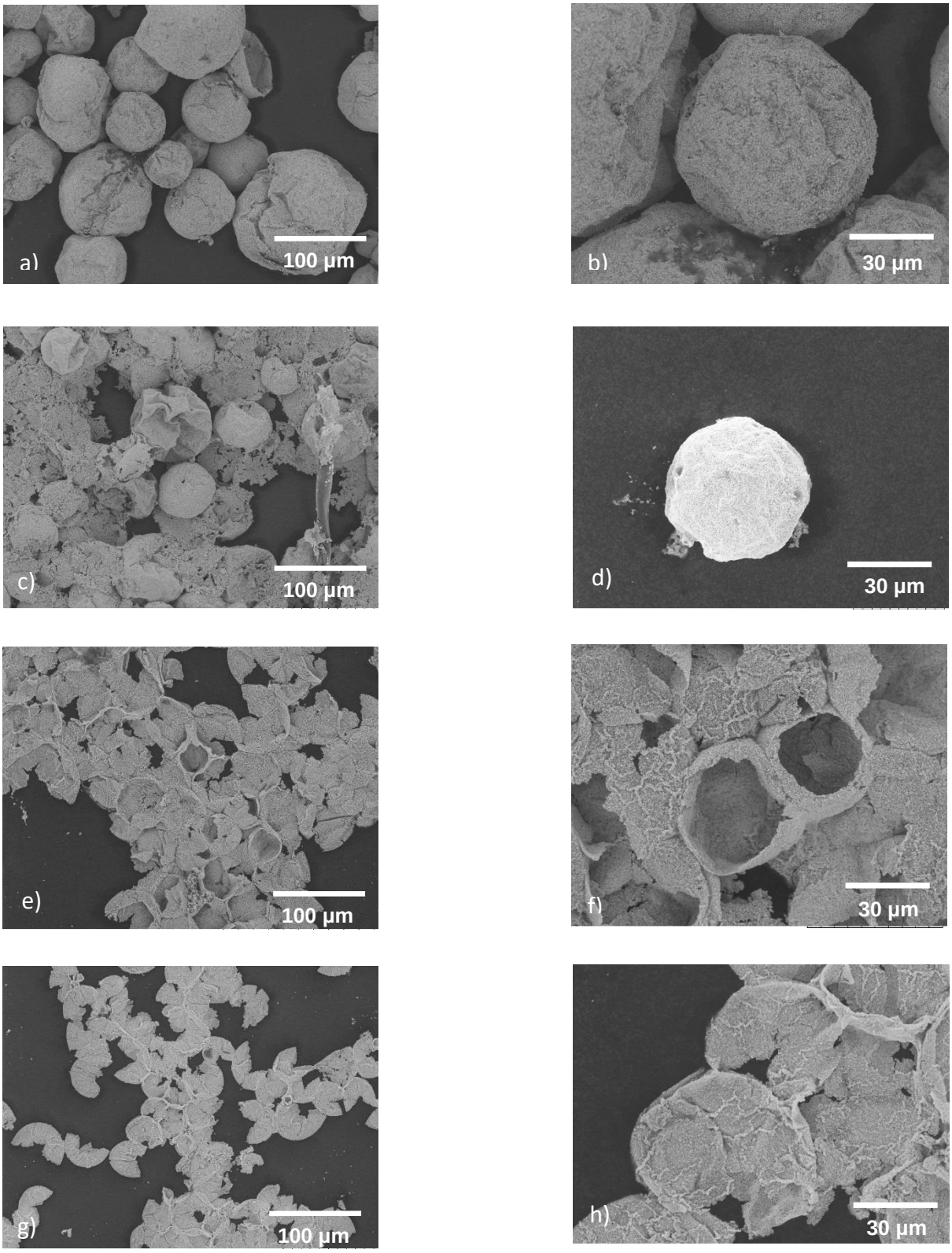

Figure 5. 22: Bench top Scanning Electron micrographs of gold microcapsules stabilised with Si/Pt composites, a, b) Si/Pt composite (9.4%) gold microcapsules, c, d) Si/Pt composite (12.8%) gold microcapsules, e, f) Si/Pt composite (23%) gold microcapsules and g, h) Si/Pt composite (41.7%) gold microcapsules.

Figure 5.22 demonstrates SEM images of the gold coated microcapsules, stabilised with 9.4, 12.8, 23 and 41.7% Si/Pt composites. With decreasing emulsion size resulted in an increase in the total surface area as illustrated in table 5.3. As the gold concentration was kept constant this resulted in a decrease in the theoretical shell thickness, this is evident in the SEM images as the larger microcapsules figure 5.22 a-d remain stable under drying and SEM vacuum (thicker shells, 43.9 and 43 nm) whereas the smaller microcapsules did not remain intact under drying and SEM vacuum (thinner shells 29.9 and 26.1nm).

As we assume the Si/Pt composites align in a close hexagonal packing arrangement at the oil water interface, the total surface area of the packing gaps in between the Si/Pt composites was calculated to be 1072.4nm^2, which equates to a maximum distance of 16.4nm growth of gold from the surface to the centre to completely cover the packing gaps (chapter 3.7.7). From table 5.3 the thinnest theoretical shell was 26.1nm which would sufficiently cover the gaps in between the silica particles. The following chapter will demonstrate the permeability of the microcapsule shells, if the packing gaps between the Si/Pt composites have not been completely covered the microcapsules would lose the core (hexadecane) when exposed to a continuous phase which can completely solubilise the core.

5.4.3 Demonstrating Impermeability

In the previous section we demonstrated the ability of Pt-NPs to adsorb onto the surface of silica resulting in Si/Pt composites which stabilised oil in water emulsion and were subsequently covered in a gold shell.

In this section we will demonstrate the retention of the hexadecane core of the microcapsule and also demonstrate permeability of the microcapsule shell. The microcapsules were placed in a 4:1 (volume ratio) ethanol/water continuous phase, this was done as the hexadecane core is completely soluble in ethanol and any hexadecane residue present or released from the microcapsules would be solubilised in the ethanol. Microcapsules were dispersed in an ethanol/water 4:1 ratio and kept suspended at 40^{o}C for 30 days. The microcapsules samples were taken at different time intervals and centrifuged to remove the microcapsules; the resulting sample was measured for hexadecane concentration using gas chromatography (GC). After 30 days the microcapsules were sonicated to break the microcapsules and measured for Hexadecane, this was done to demonstrate the microcapsules core contained Hexadecane. The resulting data from this experiment is shown in figure 5.23.

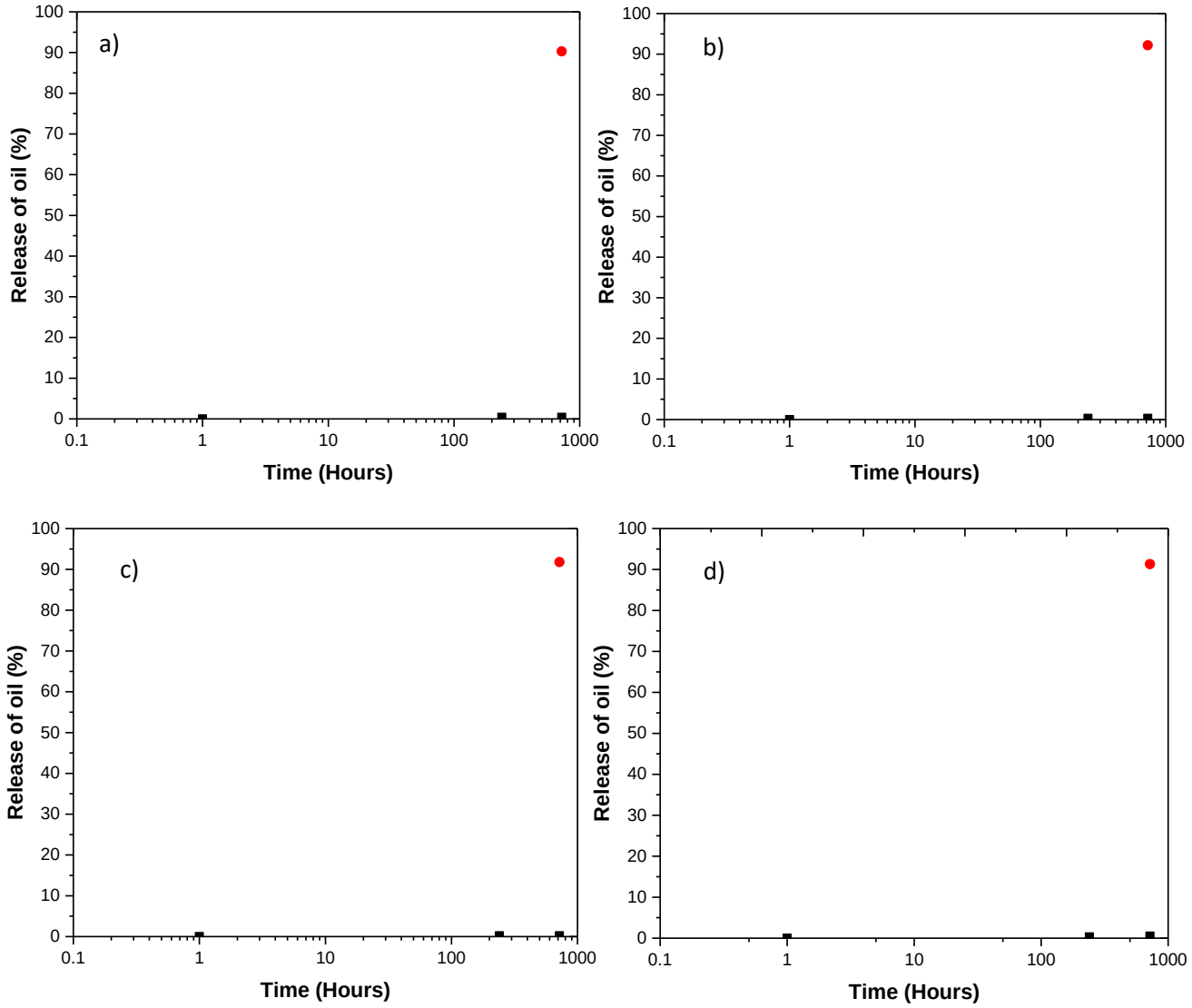

Figure 5. 23: Release of oil core from microcapsules, a) Si/Pt (9.4%) stabilised gold microcapsules, b) Si/Pt (12.8%) stabilised gold microcapsules, c) Si/Pt (23%) stabilised gold microcapsules and d) Si/Pt (41.7%) stabilised gold microcapsules, over time in a 4:1 ethanol/water continuous phase at 40^{o}C. Black square represents Hexadecane release after 1 Hour, release after 10 days and release after 30 days and red circle shows complete release after microcapsules are sonicated to break metal shells (1 min 40% amplitude).

Figure 5.23 demonstrates the microcapsules are able to fully retain the hexadecane core for over 30 days, demonstrating a continuous impermeable gold shell on the

emulsion droplets. After 30 days the microcapsules were sonicated to break the shells and the hexadecane concentration was measured and ~90% of the initial hexadecane core was recovered. The remaining 10% of the hexadecane not recovered was most likely to have been lost during the emulsification and wash process and also some of the microcapsule may remain intact after sonication, hence retaining the hexadecane in the core.

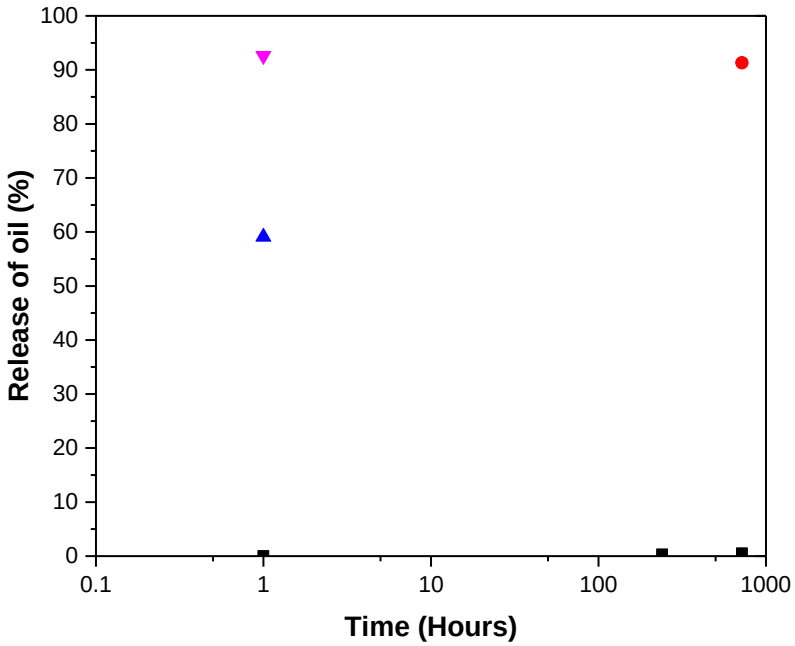

Figure 5. 24: Release of oil core from microcapsules, Si/Pt (41.7%) stabilised gold microcapsules and emulsion, over time in a 4:1 ethanol/water continuous phase at 40°C. Black square represents Hexadecane release from microcapsules after 1 Hour, release after 10 days and release after 30 days and red circle shows release measured after microcapsules are sonicated to break metal shells (1 min 40% amplitude), blue triangle represents release of Si/Pt stabilised emulsion after 1 Hour and purple triangle represents complete release of emulsion after sonicated to break emulsions after 1 hour (1 min 40% amplitude).

Figure 5.24 demonstrates the emulsions stabilised with Si/Pt (41.7%) composite was able to retain 40% of the hexadecane after 1 hour in a (4:1) ethanol/water continuous

phase. This demonstrated the composites also play a part in retaining the hexadecane core but more analysis is required over time to justify a conclusion on Si/Pt composite retention abilities. The Si/Pt emulsion was also sonicated to measure full release of the emulsion core, 92.6% of the hexadecane core was recovered which is similar to the levels recovered from the microcapsules.

5.5 Conclusion

In this chapter we have demonstrated the adsorption of Pt-NPs onto the surface of Silica resulting in Si/Pt composites. The composites stabilised an oil in water emulsion by adsorbing onto the interface and forming stable emulsions, which were subsequently covered in gold shells, via electroless deposition due to the ability of Pt-NPs on the surface to catalyse the reaction and provide a nucleation/deposition site for gold growth. By using Si/Pt composites we were able to increase the hexadecane core loading by 150% compared to emulsion stabilised with Pt-NPs (chapter 4). We also demonstrated the ability of the microcapsules to completely retain the core (hexadecane) for over 30 days at 40^{o}C in an ethanol/water (4:1) continuous phase resulting in a complete impermeable metal shell.

We successfully removed the use of nanoparticle intermediates by adsorbing Pt-NPs onto the surface of Si and removed any excess Pt-NPs by centrifuging the composite and removing the continuous phase as the composites settled out and were re-dispersed in water. With combining Si and Pt-NPs we were able to utilise the ability of Pt-NPs to catalyse the growth of gold and also increase the microcapsule size and loading compared to microcapsule synthesised in chapter 4 with Pt-NPs.

5.6 References

1. Binks, B.P., *Colloidal particles at liquid interfaces.* Physical Chemistry Chemical Physics, 2007. **9**(48): p. 6298-6299.
2. Stocco, A., et al., *Aqueous foams stabilized solely by particles.* Soft Matter, 2011. **7**(4): p. 1260-1267.
3. Aveyard, R., B.P. Binks, and J.H. Clint, *Emulsions stabilised solely by colloidal particles.* Advances in Colloid and Interface Science, 2003. **100**: p. 503-546.
4. Binks, B.P., *Particles as surfactants - similarities and differences.* Current Opinion in Colloid & Interface Science, 2002. **7**(1-2): p. 21-41.
5. Dickinson, E., *Use of nanoparticles and microparticles in the formation and stabilization of food emulsions.* Trends in Food Science & Technology, 2012. **24**(1): p. 4-12.
6. Horozov, T.S. and B.P. Binks, *Particle-stabilized emulsions: a bilayer or a bridging monolayer?* Angew Chem Int Ed Engl, 2006. **45**(5): p. 773-6.
7. Tambe, D.E. and M.M. Sharma, *The Effect of Colloidal Particles on Fluid-Fluid Interfacial Properties and Emulsion Stability.* Advances in Colloid and Interface Science, 1994. **52**: p. 1-63.
8. Xu, J., et al., *Janus-like Pickering emulsions and their controllable coalescence.* Chemical Communications, 2013. **49**(92): p. 10871-10873.
9. Binks, B.P. and M. Kirkland, *Interfacial structure of solid-stabilised emulsions studied by scanning electron microscopy.* Physical Chemistry Chemical Physics, 2002. **4**(15): p. 3727-3733.
10. Horozov, T.S., et al., *Particle zips: Vertical emulsion films with particle monolayers at their surfaces.* Langmuir, 2005. **21**(6): p. 2330-2341.
11. Vignati, E., R. Piazza, and T.P. Lockhart, *Pickering emulsions: Interfacial tension, colloidal layer morphology, and trapped-particle motion.* Langmuir, 2003. **19**(17): p. 6650-6656.
12. Kaganyuk, M. and A. Mohraz, *Non-monotonic dependence of Pickering emulsion gel rheology on particle volume fraction.* Soft Matter, 2017. **13**(13): p. 2513-2522.
13. Ridel, L., et al., *Pickering emulsions stabilized by charged nanoparticles.* Soft Matter, 2016. **12**(36): p. 7564-7576.
14. Frelichowska, J., M.A. Bolzinger, and Y. Chevalier, *Pickering emulsions with bare silica.* Colloids and Surfaces a-Physicochemical and Engineering Aspects, 2009. **343**(1-3): p. 70-74.

15. Giacomello, A., et al., *Cassie-Baxter and Wenzel states on a nanostructured surface: phase diagram, metastabilities, and transition mechanism by atomistic free energy calculations.* Langmuir, 2012. **28**(29): p. 10764-72.
16. Bjorkegren, S., et al., *Hydrophilic and hydrophobic modifications of colloidal silica particles for Pickering emulsions.* J Colloid Interface Sci, 2017. **487**: p. 250-257.
17. Xiao, M., et al., *Tailoring the Wettability of Colloidal Particles for Pickering Emulsions via Surface Modification and Roughness.* Front Chem, 2018. **6**: p. 225.
18. Frith, W.J., et al., *Formation, stability, and rheology of particle stabilized emulsions: Influence of multivalent cations.* Industrial & Engineering Chemistry Research, 2008. **47**(17): p. 6434-6444.
19. Haase, M.F., et al., *Encapsulation of Amphoteric Substances in a pH-Sensitive Pickering Emulsion.* Journal of Physical Chemistry C, 2010. **114**(41): p. 17304-17310.
20. Binks, B.P. and D.Z. Yin, *Pickering emulsions stabilized by hydrophilic nanoparticles: in situ surface modification by oil.* Soft Matter, 2016. **12**(32): p. 6858-6867.
21. Yang, H.Q., T. Zhou, and W.J. Zhang, *A Strategy for Separating and Recycling Solid Catalysts Based on the pH-Triggered Pickering-Emulsion Inversion.* Angewandte Chemie-International Edition, 2013. **52**(29): p. 7455-7459.
22. Nonomura, Y., S. Komura, and K. Tsujii, *Adsorption of microstructured particles at liquid-liquid interfaces.* Journal of Physical Chemistry B, 2006. **110**(26): p. 13124-13129.
23. Zanini, M., et al., *Universal emulsion stabilization from the arrested adsorption of rough particles at liquid-liquid interfaces.* Nature Communications, 2017. **8**.
24. San-Miguel, A. and S.H. Behrens, *Influence of Nanoscale Particle Roughness on the Stability of Pickering Emulsions.* Langmuir, 2012. **28**(33): p. 12038-12043.
25. Smith, G.N., et al., *Surfactants with colloids: adsorption or absorption?* J Colloid Interface Sci, 2015. **449**: p. 205-14.
26. Horiuchi, S. and Y. Nakao, *Platinum colloid catalyzed etchingless gold electroless plating with strong adhesion to polymers.* Surface & Coatings Technology, 2010. **204**(23): p. 3811-3817.
27. Smith, J.N., J. Meadows, and P.A. Williams, *Adsorption of polyvinylpyrrolidone onto polystyrene latices and the effect on colloid stability.* Langmuir, 1996. **12**(16): p. 3773-3778.
28. Pattanaik, M. and S.K. Bhaumik, *Adsorption behaviour of polyvinyl pyrrolidone on oxide surfaces.* Materials Letters, 2000. **44**(6): p. 352-360.
29. Robinson, S. and P.A. Williams, *Inhibition of protein adsorption onto silica by polyvinylpyrrolidone.* Langmuir, 2002. **18**(23): p. 8743-8748.

30. Zhang, Q., et al., *Permeable silica shell through surface-protected etching.* Nano Letters, 2008. **8**(9): p. 2867-2871.
31. Lyons, O.D., et al., *Synthesis, Characterization, and Reaction Studies of a PVP-Capped Platinum Nanocatalyst Immobilized on Silica.* Langmuir, 2010. **26**(21): p. 16481-16485.
32. Zidki, T., et al., *The effect of the nano-silica support on the catalytic reduction of water by gold, silver and platinum nanoparticles - nanocomposite reactivity.* Physical Chemistry Chemical Physics, 2014. **16**(29): p. 15422-15429.
33. Grate, J.W., et al., *Correlation of oil-water and air-water contact angles of diverse silanized surfaces and relationship to fluid interfacial tensions.* Langmuir, 2012. **28**(18): p. 7182-8.
34. Wu, D.M. and V. Hornof, *Dynamic interfacial tension in hexadecane water systems containing ready-made and in-situ-formed surfactants.* Chemical Engineering Communications, 1999. **172**: p. 85-106.
35. Manga, M.S., et al., *Measurements of Submicron Particle Adsorption and Particle Film Elasticity at Oil-Water Interfaces.* Langmuir, 2016. **32**(17): p. 4125-4133.
36. Yu, K., et al., *Foaming Behavior of Polymer-Coated Colloids: The Need for Thick Liquid Films.* Langmuir, 2017. **33**(26): p. 6528-6539.
37. Hitchcock, J.P., et al., *Long-Term Retention of Small, Volatile Molecular Species within Metallic Microcapsules.* ACS Appl Mater Interfaces, 2015. **7**(27): p. 14808-15.

6 Silver electroless plating of PDA polymer microcapsules without the use of metal nanoparticle catalyst

6.1 Synopsis

This chapter focuses on the synthesis and characterisation of colloidal silica stabilised emulsions, subsequently coated with polydopamine (PDA), thus resulting in core-shell microcapsules where the shell is a binary mixture of polymer and particles. The PDA surface is used to deposit a silver shell on the surface of these structures via electroless reduction of silver ions initially adsorbed to the PDA microcapsule shells. As the previous methods described in chapter 4 and 5 utilised Pt-NPs to synthesise metal coated microcapsules, this chapter will focus on utilising PDA for silver electroless plating without the use of nanoparticles in the system, due to the regulatory issues associated with the use of nanoparticles. The novelty of this work is the demonstration of the deposition of PDA onto liquid emulsion droplets followed by silver deposition via electroless plating, whereas the literature mostly consists of PDA deposition onto solid surfaces followed by silver plating.

6.2 Polymerisation mechanism of dopamine

The polymerisation mechanism of dopamine in solution is still not fully understood, nevertheless, a general scheme can be drawn. The proposed mechanism for the self-polymerisation of dopamine is shown in figure 6.2. The mandatory requirements for the reaction to proceed are a basic medium (Tris-HCl buffer solution 10mM, pH=8.5) and an O_2 rich environment. The initial reaction involves the slow oxidation of dopamine (A) to dopamine quinone (C), via dopamine semiquinone (B). Dopamine quinone (C) rapidly undergoes cyclisation through a Michael type cycloaddition forming leucodopaminechrome (D). The oxidation and subsequent rearrangement of

leucodopaminechrome (D) results in the formation of 5,6-Dihydroxyindoline DHI (E) and its oxidised product 5,6-indolequinone (F). 5,6-Dihydroxyindoline DHI (E) and 5,6-indolequinone (F) are the building block of PDA, and many chemical pathways are proposed leading to PDA through covalent polymerization and non-covalent self-assembly. [1-10]

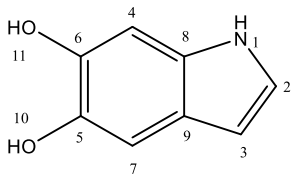

Figure 6. 1: Structure of 5,6-Dihydroxyindoline DHI, with numbering.

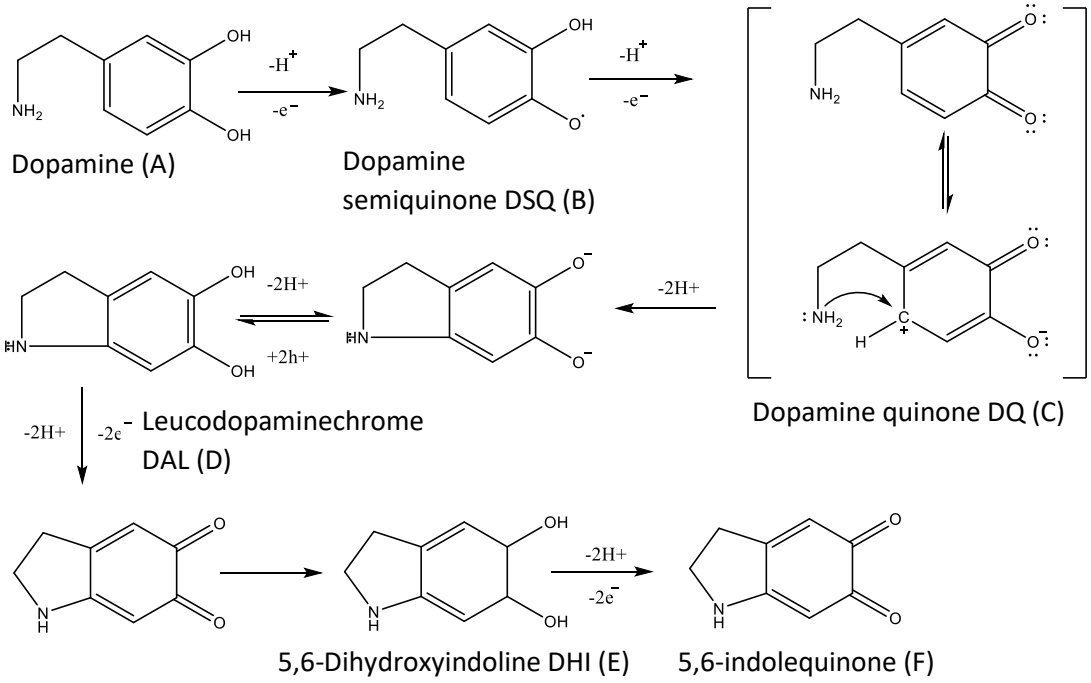

Figure 6. 2: Dopamine self-assembly (Tris buffer pH~8.5) proposed mechanism (A-F).

Okuda, *et al.,* proposed the formation of a linear polymer through covalent bonds governed by electron-transfer-controlled reaction. It is suggested the process involves the nucleophilic attack of DHI (C3) to one of the two-electron-oxidants (C4, C7) as an electrophile, resulting in DHI homotrimers (3 and 4). This is followed by the

nucleophilic attack of the C4 position (3) to the C4 position (4) leading to the formation of PDA (figure 6.3). [4, 9-11]

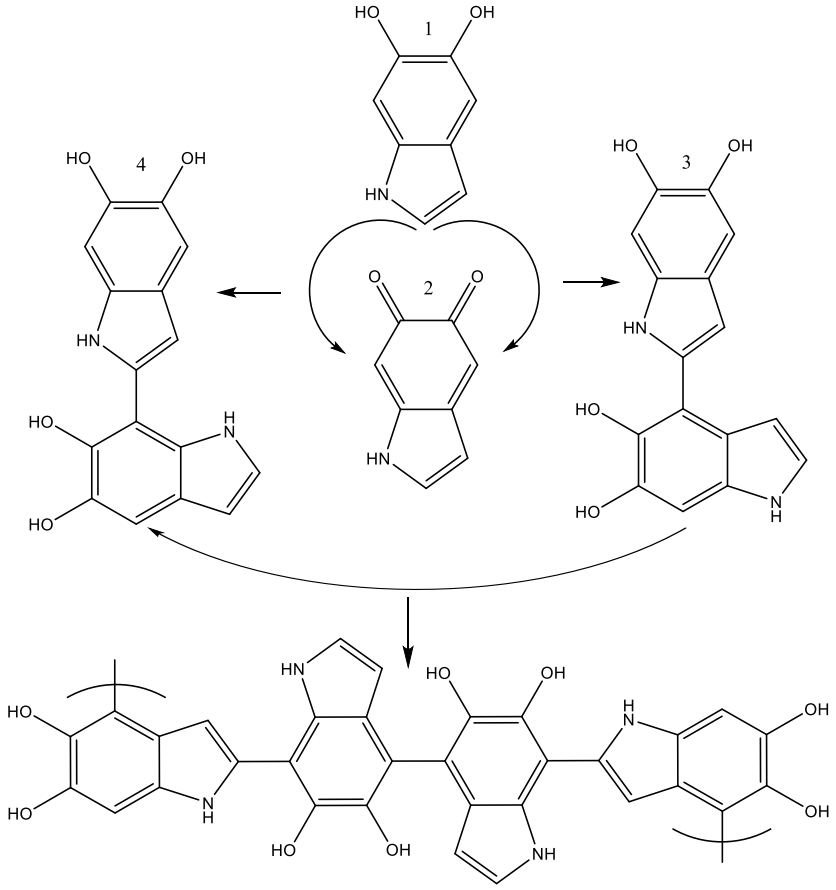

Figure 6. 3: Dopamine self-polymerisation, (Tris buffer pH~8.5) PDA proposed polymer structure.

Della Vecchia, *et al.,* proposed the formation of PDA as a supramolecular aggregate of monomers (consisting primarily of 5,6-dihydroxyindoline (E) and its dione derivative 5,6-indolequinone (F), held together through a combination of charge transfer, π - stacking, and hydrogen-bonding interactions (figure 6.4).[12]

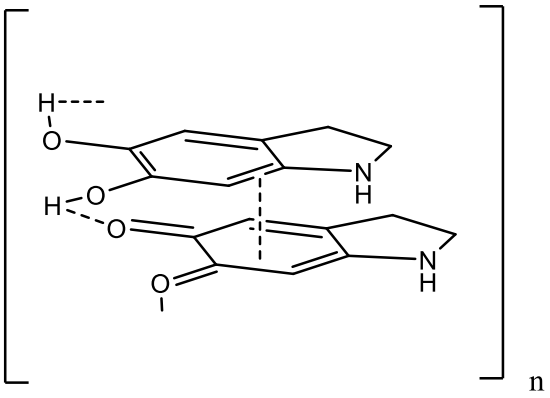

Figure 6. 4: PDA structure held together through a combination of charge transfer, π - stacking, and hydrogen-bonding interactions. [12]

PDA formation has also been proposed through combined covalent bonding and self-assembly via a combination of charge transfer, π- π stacking and H bonds (figure 6.5). [7, 13-16]

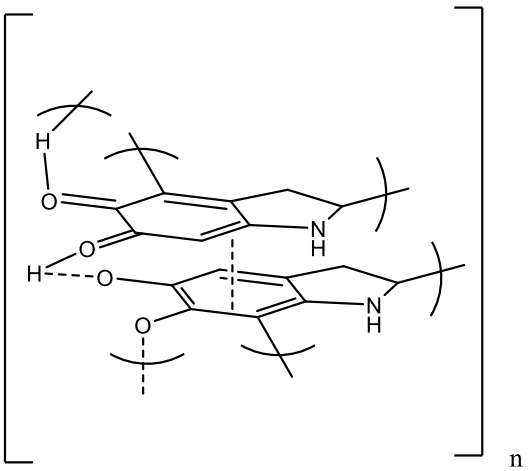

Figure 6. 5: PDA structure proposed through combined covalent bonding and self-assembly via a combination of charge transfer, π- π stacking and H bonds.

Once self-polymerised, PDA is able to deposit on inorganic and organic materials through strong covalent and non-covalent interactions with substrates.[3] PDA is able to deposit and bind to the silica through strong hydrogen-bonding between the catechol groups and the silanol groups on the silica surface.[17]

6.3 PDA deposition onto substrates

The following section will consist of a review on deposition of PDA onto solid substrates. Lee, *et al.,* demonstrated the coating of inorganic and organic materials with PDA by dip coating the objects in an aqueous solution of dopamine, resulting in the self-polymerisation of dopamine to PDA. The metal binding ability of the catechols group present in the PDA coating were exploited to deposit metal coatings via electroless plating. The PDA coated objects were coated in silver and copper films.[3] Luo, *et al.,* demonstrated the self-polymerisation of dopamine by synthesizing PDA sub-micrometer spheres. The metal binding ability of the catechols groups were exploited to deposit silver nanoparticles on the PDA spheres resulting in Ag-PDA spheres.[18] Wang, *et al.,* utilized the ability of dopamine to self-polymerise and deposit on inorganic and organic substrates by depositing thin uniform layers of PDA on silica, aluminum and poly styrene microspheres. The ability of the catechols group on the PDA surface was utilized as a chelating agent for silver ions and as a reducing agent for the formation of catalytic sites, resulting in Si-PDA-Ag, Al-PDA-Ag and PS-PDA-Ag core shell microspheres. The silver coating was deposited via electroless plating, glucose was used as the reducing agent.[4, 10, 19] Al-shannaq, *et al.,* demonstrated the deposition of silver onto PMMA microcapsules, through activation of the surface by PDA deposition, followed by dipping the PDA PMMA microcapsules in a silver plating bath.[20]

The ability of dopamine to self-polymerise and deposit on organic and inorganic materials could be utilized to synthesis PDA microcapsules, which inherently could be used by exploiting the ability of the catechols group to chelate/complex silver ions, reducing the silver ions on the surface of PDA, resulting in silver coated PDA microcapsules. All the papers reviewed include the deposition of PDA onto solid

substrates or polymer microcapsules. We will describe a method of depositing PDA onto emulsion droplets resulting in PDA microcapsules which will subsequently be silver coated.

6.3.1 Preparation of poly dopamine silica composites

Dopamine has recently attracted large attention due to its ability to self-polymerise and form thin layers on organic and inorganic materials.[3] Furthermore the metal-binding ability of the catechols and nitrogen containing groups in the resulting PDA coating are useful for reducing Ag ions to $Ag^{(0)}$ on the surface of PDA.[4]

As a preliminary experiment, PDA silica composites were synthesised to demonstrate the dopamine ability to bind and self-polymerise on silica particles, which resulted in the self-polymerization of dopamine on the surface of silica resulting in PDA silica composites.

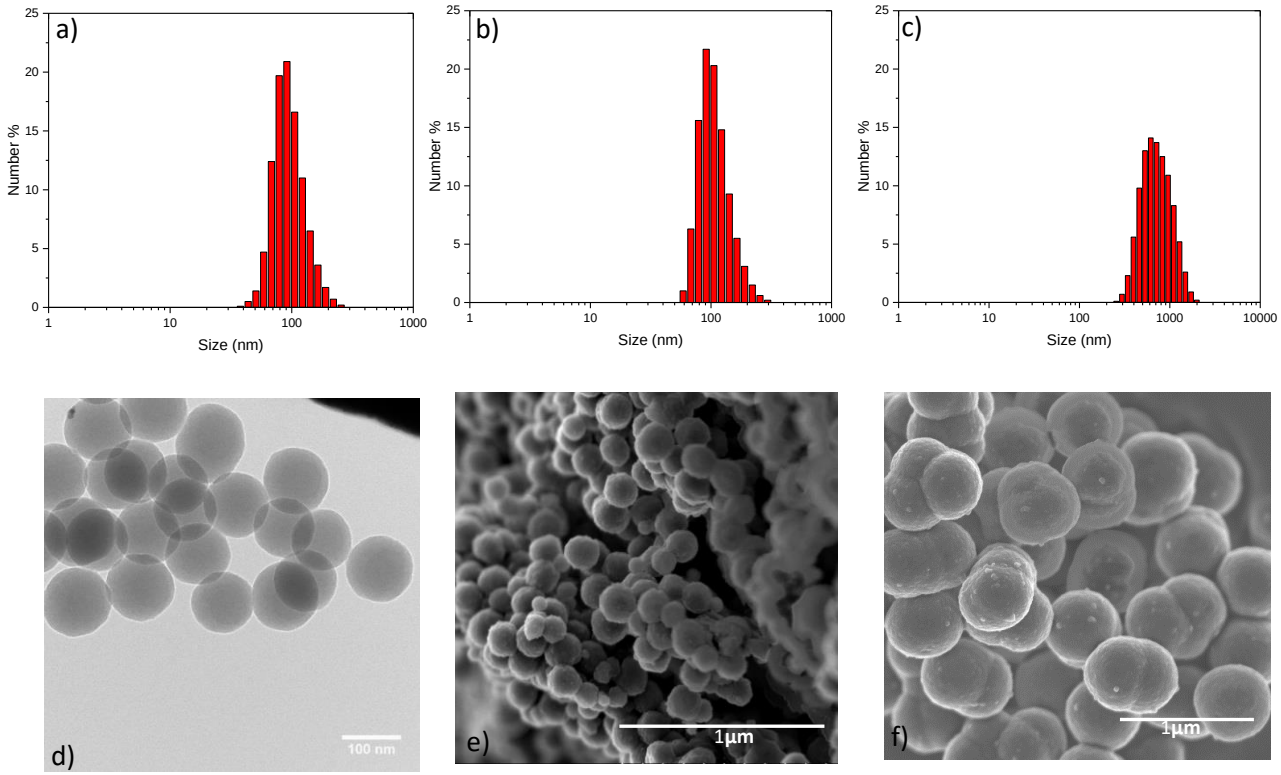

Figure 6. 6; a-c) Average particle size distribution (zetasizer), a) bare colloidal silica particles (nominal diameter from supplier is 100nm, theoretical total surface area 2.3 $x10^{18}$ nm^2), b)

PDA coated silica particles (mass of dopamine/total surface area 0.04 g/m^2), c) PDA coated silica particles (mass of dopamine/total surface area 0.22 g/m^2), d) Transmission electron micrograph of colloidal silica particles (Nominal diameter from supplier is 100nm, (0.1g) theoretical total surface area 2.3 x10^{18} nm^2), e, f) Scanning Electron Micrographs of PDA coated silica particles, e) PDA coated silica particles (mass of dopamine/total surface area 0.04 g/m^2), f) PDA coated silica particles (mass of dopamine/total surface area 0.22 g/m^2).

Figure 6.6 a and d -demonstrate the bare colloidal silica particles (nominal diameter from supplier is 100nm, (0.1g) theoretical total surface area 2.3 x10^{18} nm^2) and the average particle size distribution. Silica particles covered in PDA 0.04 g/m^2 resulted in individual PDA Si composites (non-aggregated) which had a very thin layer of PDA deposited on the surface as demonstrated in figure 5.2 b and e. Silica particles covered in PDA 0.22 g/m^2 resulted in the merging of the composites (aggregating) as they grew, this was due to the excess dopamine available as demonstrated in figure 6.6 c and f. The merging of the silica composites at 0.22 g/m^2 of PDA may result in thick microcapsule shells when trying to coat emulsion droplets in PDA to form PDA microcapsules. The PDA concentrations for coating emulsion droplets would range between ~0.09 and 0.22 g/m^2.

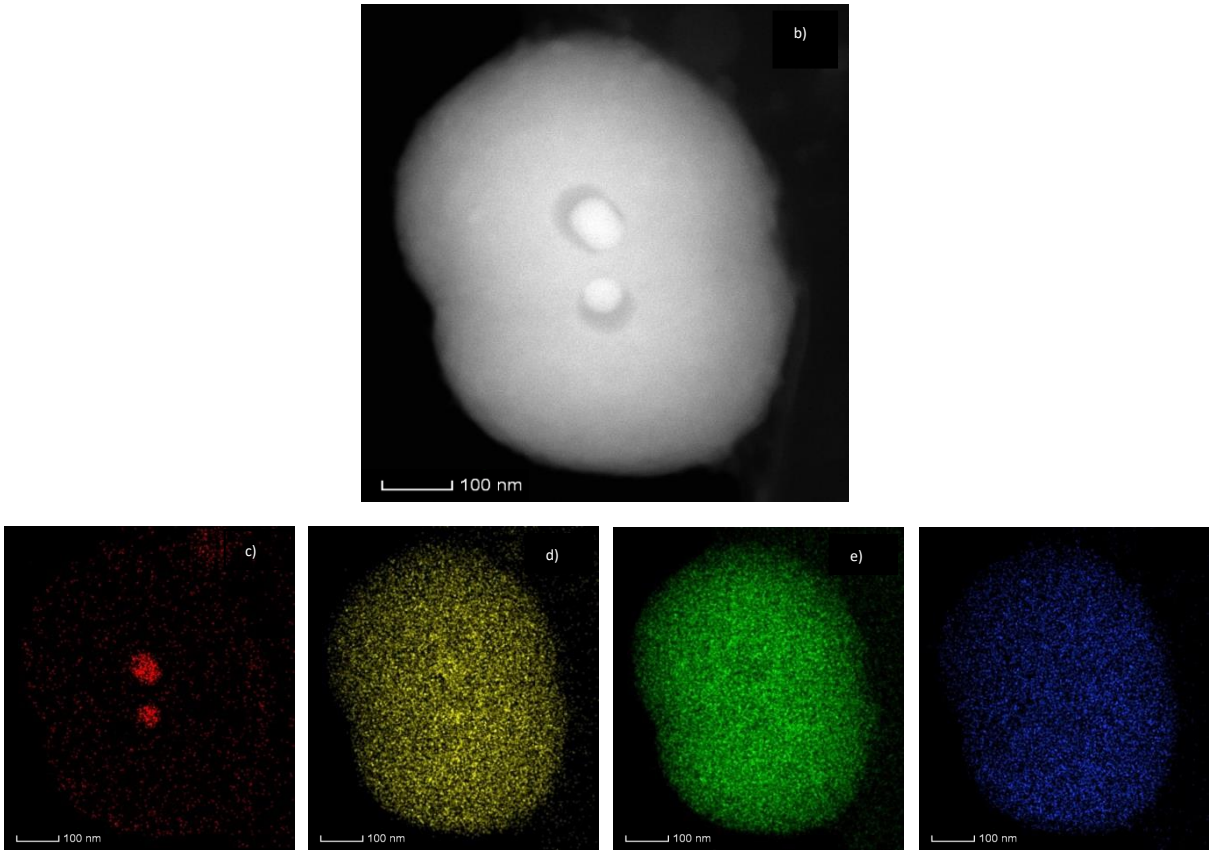

Figure 6. 7: Transmission electron micrographs/EDX analysis of PDA Si composite (mass of dopamine/total surface area 0.22 g/m^2) with corresponding false-color elemental distribution, a) PDA Si, b) silica, c) carbon, d) nitrogen and e) oxygen.

Figure 6.7 demonstrates the merging of PDA Si composites (mass of dopamine/total surface area 0.22 g/m^2) due to the excess PDA. Figure 6.7a demonstrates PDA Si particles merged together to form a large PDA multi Si composite, this was confirmed from EDX mapping as demonstrated in figure 6.7b-e, which demonstrates the deposition of PDA on the silica particles. Figure 6.6 c and f and figure 6.7 demonstrate the aggregation of PDA Si composites and also the difference in thickness between the silica diameter (100nm) and the PDA Si composite (~550nm).

Initially we demonstrated the deposition of PDA onto silica particles at two different concentrations (mass of dopamine/total surface area 0.04 and 0.22 g/m^2), which resulted in a thin PDA film deposition on the silica surface and also a very thick PDA film deposition which resulted in aggregation of the PDA Si composites respectively. In the following section we shall demonstrate the deposition of PDA on colloidal silica stabilised Pickering emulsions, resulting in PDA-coated colloidosome microcapsules.

6.3.2 Synthesis of PDA microcapsules stabilised via silica (Pickering emulsions)

Silica stabilised oil in water Pickering emulsions were prepared with different concentrations of silica particles (1, 3 and 5wt %), the hexadecane concentration was varied at 0.2 and 1ml (corresponding to an oil volume fraction ϕ of 0.02 and 0.11) resulting in oil in water Pickering emulsions.

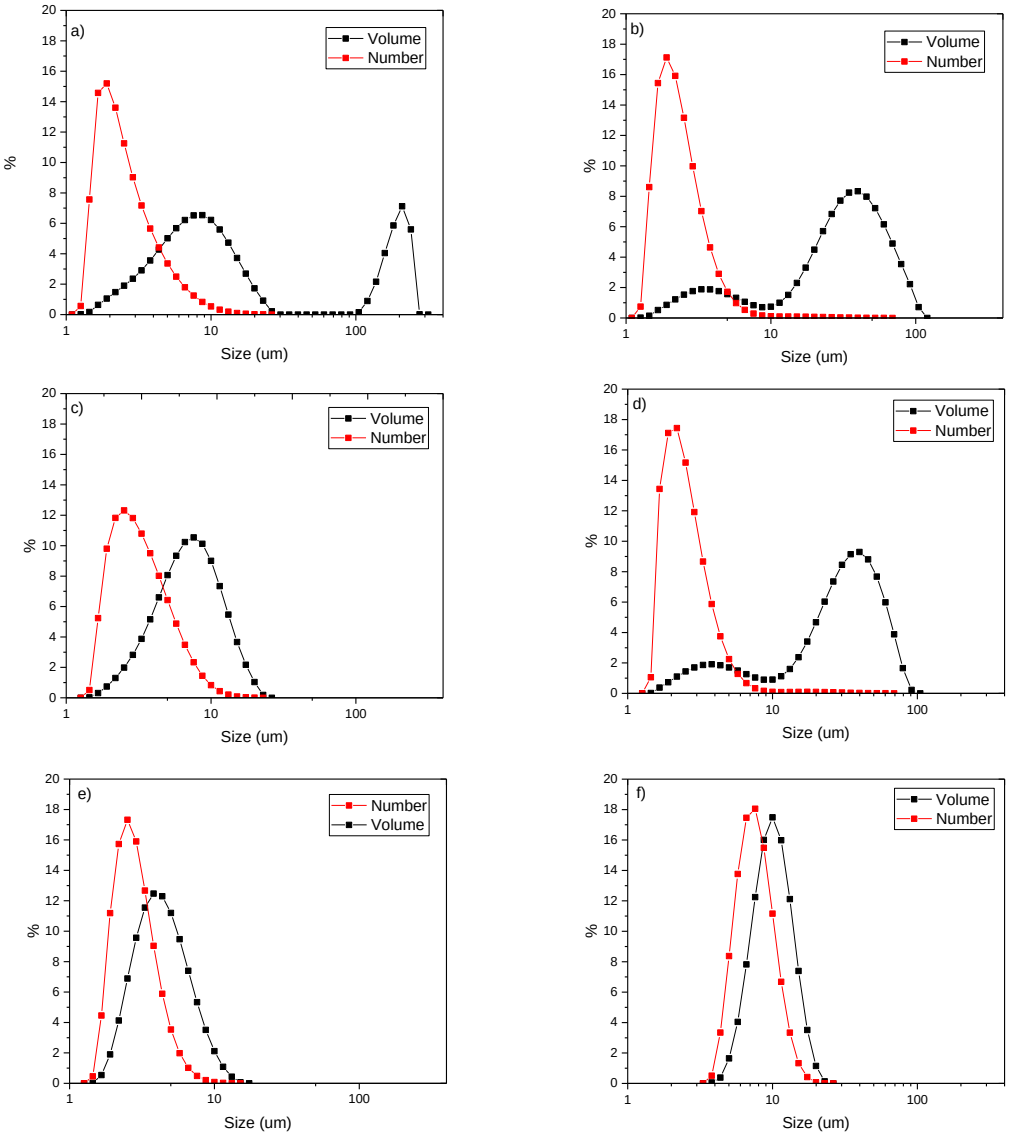

Figure 6. 8: Emulsion droplet size distributions measured using the mastersizer for a range of emulsions stabilised by silica particles with, a) 1 Wt% silica and oil volume fraction ϕ 0.02 hexadecane, b) 1 Wt% silica and oil volume fraction ϕ 0.11 hexadecane, c) 3 Wt% silica and oil volume fraction ϕ 0.02 hexadecane, d) 3 Wt% silica and oil volume fraction ϕ 0.11

hexadecane, e) 5 Wt% silica and oil volume fraction ϕ 0.02 hexadecane and f) 5 Wt% silica and oil volume fraction ϕ 0.11 hexadecane..

Figure 6.8 demonstrates the emulsion size distribution of the Pickering emulsions prepared using silica (1, 3 and 5wt %) and hexadecane (oil volume fraction ϕ 0.02 and 0.11). The emulsion stabilised with 5wt % silica and oil volume fraction ϕ 0.11, was chosen for dopamine deposition to synthesise PDA microcapsules due to a mono disperse emulsion size distribution, where the volume and number measured size distribution correlated with each other. The higher concentration of silica was able to stabilise more interface than the lower concentrations of silica as more particles are present and can accommodate more interface, resulting in a mono disperse emulsion size distribution.

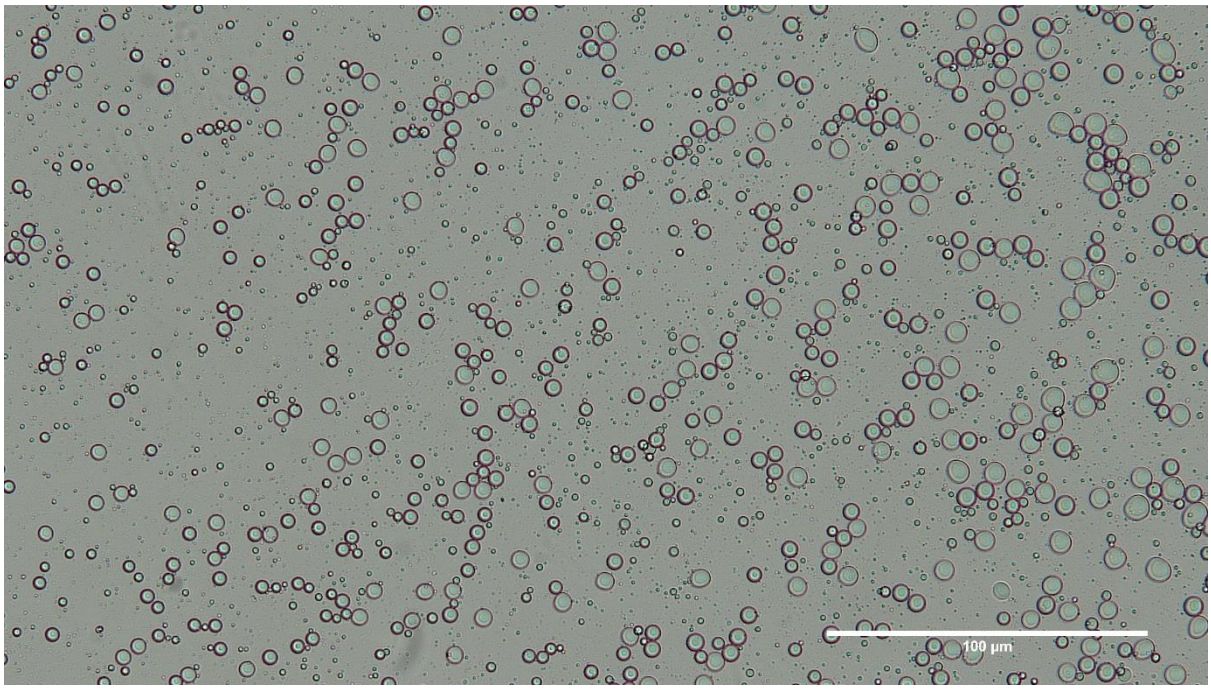

Figure 6. 9: Optical micrograph of a Pickering emulsion sample prepared from hexadecane (1ml, oil volume fraction ϕ 0.11) and silica (5 Wt%) suspension (figure 5.8 f).

Figure 6.9 represents the emulsion demonstrated in figure 6.8 f.

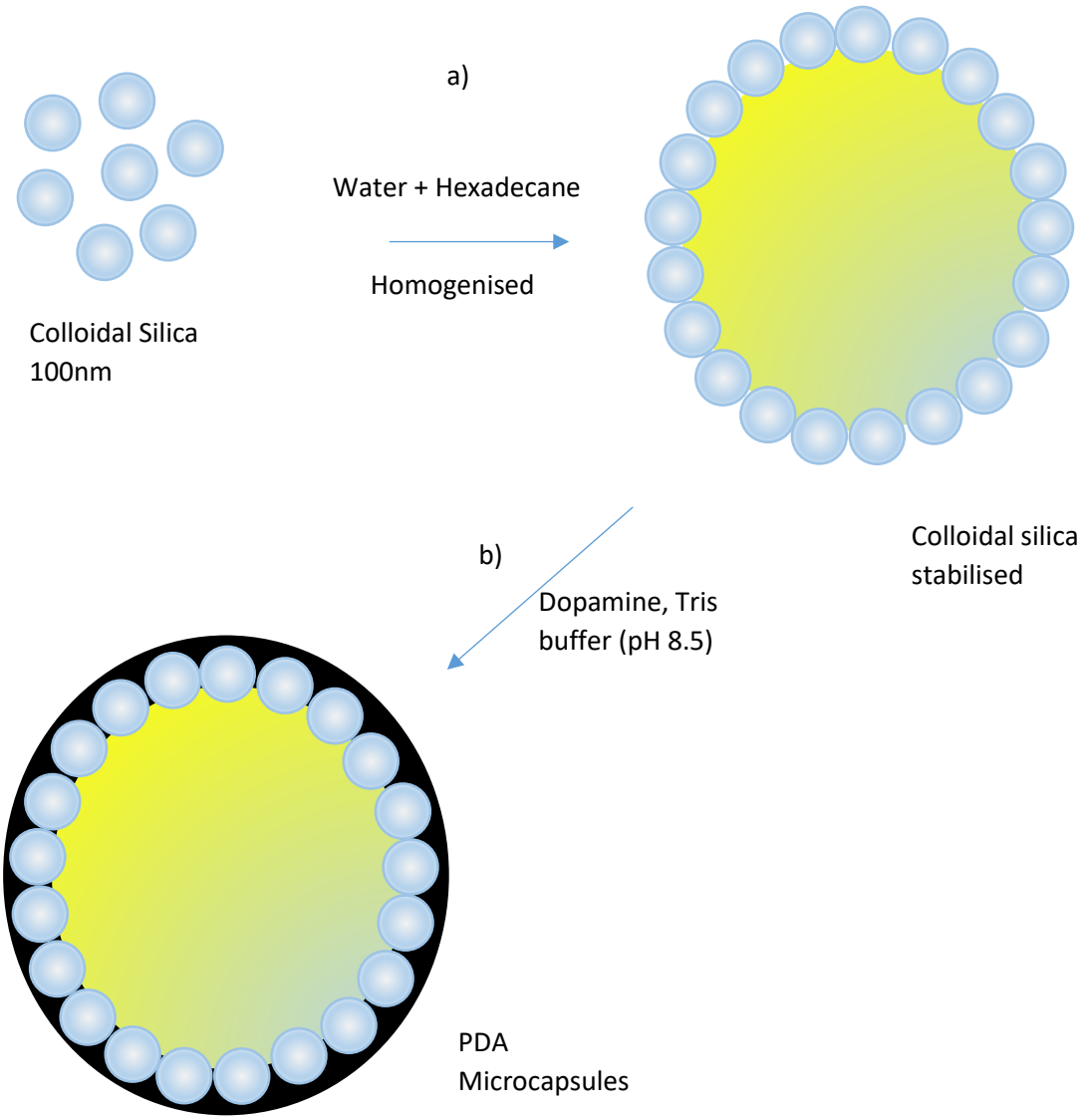

Figure 6. 10: Schematic representation of, a) stabilisation of oil in water Pickering emulsion by silica particles and b) resulting PDA-coated colloidosome microcapsules after self-polymerisation of dopamine onto the surface of the silica-stabilised emulsions.

Figure 6.10 demonstrates the process of stabilising oil in water Pickering emulsions with colloidal silica particles, followed by the self-polymerisation and deposition of dopamine on to the Pickering emulsions, resulting in PDA microcapsules.

The silica-stabilised emulsions were coated with three different concentrations of dopamine (mass of dopamine/total emulsion surface area 0.09, 0.19, and 0.28 g/m^2), all concentrations of dopamine above 0.09 g/m^2 resulted in the aggregation of the PDA microcapsules. This was due to high concentration of dopamine to total emulsion surface area (> 0.09 mg/m^2) and was also demonstrated in figure 6.6 c) and f) where the concentration of dopamine/total surface area 0.22 g/m^2, resulted in the aggregation of PDA Si composites.

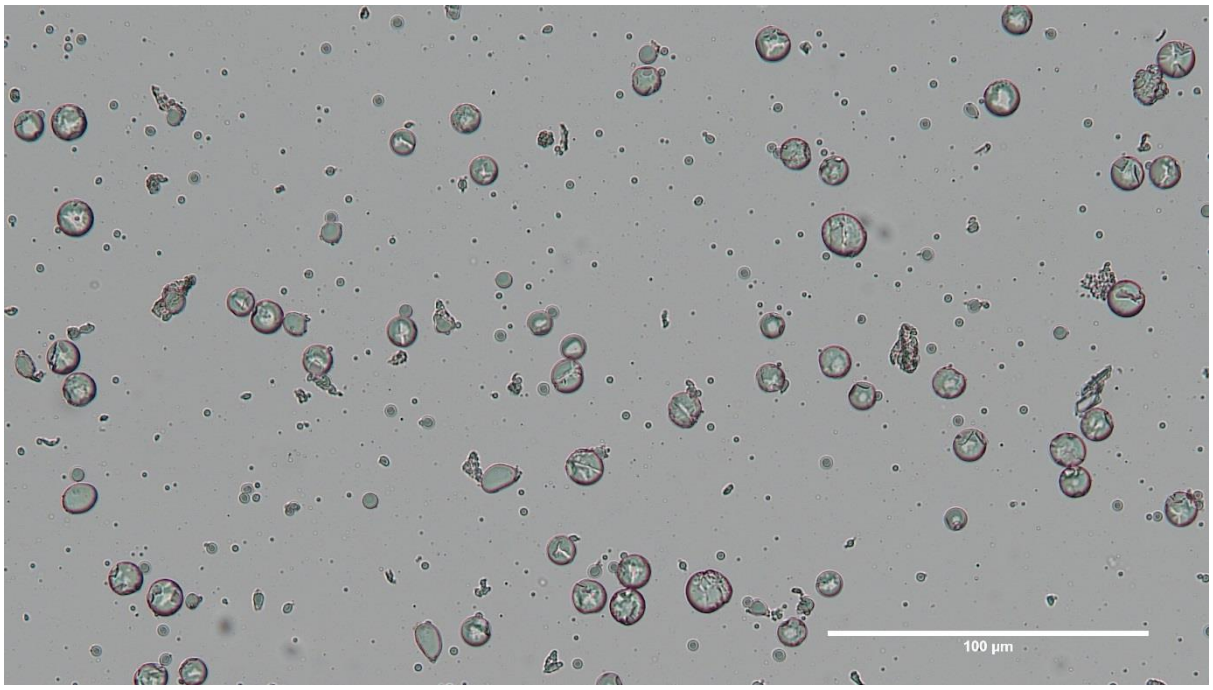

Figure 6. 11: Optical micrograph of PDA microcapsules (5 Wt% silica, hexadecane 1ml (oil volume fraction ϕ 0.11) (mass of dopamine/total emulsion surface area 0.09 g/m^2)).

From figure 6.11 the PDA microcapsules appear stable and spherical and no aggregation of the microcapsules is visible. Excess PDA films are visible in the continuous phase which have not deposited on the surface of the colloidal silica stabilised emulsions.

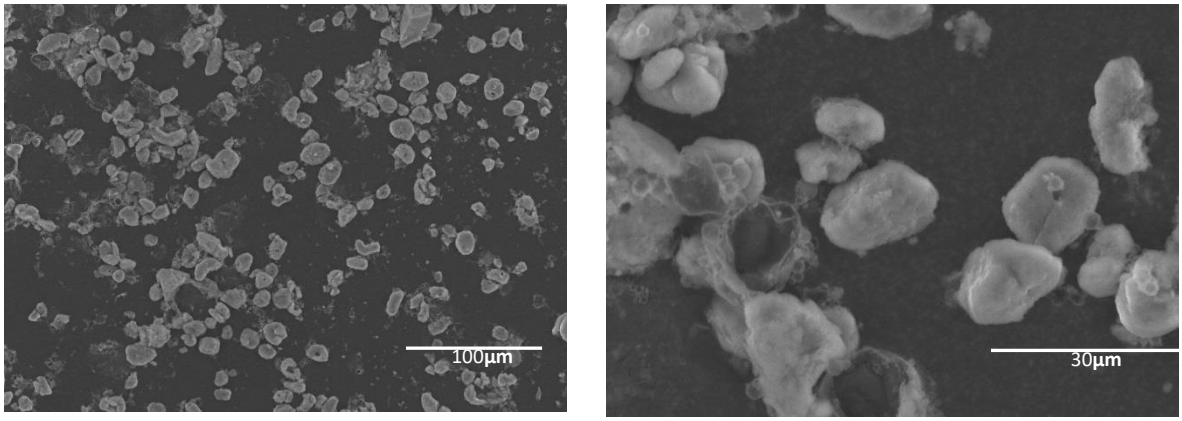

Figure 6. 12: Scanning Electron micrographs of PDA microcapsules (5 Wt% silica, hexadecane 1ml (oil volume fraction ϕ 0.11) (mass of dopamine/total emulsion surface area 0.09 g/m^2)).

Figure 6.12 demonstrates the different morphologies of PDA microcapsules at two different magnifications. From analysing the images, the microcapsules no longer remain spherical and uptake deformed morphologies. Also from analysing the images the deposition of dopamine on the emulsion templates does not seem homogenously distributed and excess PDA is present in the continuous phase. When comparing the dopamine concentration to the total silica surface area (figure 6.6 a and d (mass of dopamine/total particle surface area 0.04 g/m^2) and total emulsion surface area, (mass of dopamine/total emulsion surface area 0.09 g/m^2) respectively, twice as much dopamine concentration is used for depositing on the emulsions compared to depositing on the silica particles, therefore resulting in excess PDA present in the continuous phase of the PDA microcapsules. The change in morphologies of the PDA microcapsules could be due to the vacuum pressure in the SEM. Upon drying the microcapsules could shrink and change morphology, also the excess PDA in the system upon drying could randomly deposit on the PDA microcapsules resulting in a change in morphology.

It was attempted to analyse the thickness of PDA on the emulsion droplets via TGA but due to the calcination of silica over a temperature range 150-1050^{o}C and hexadecane evaporation we were not able to distinguish between the calcination of silica, evaporation of hexadecane and decomposition of PDA. Instead we could theoretically calculate the shell thickness based on the measured total emulsion surface area (figure 6.8 f), mass of dopamine and density of dopamine, assuming all the dopamine deposited on the emulsion surface. The PDA microcapsule theoretical shell thickness was calculated at 58nm assuming all the dopamine deposited on the emulsion droplets (table 6.1).

Table 6. 1: Theoretical PDA shell thickness on emulsion droplets

	Mass of dopamine/total emulsion surface area g/m^2	Total emulsion surface area nm^2 x10^{18}	Theoretical shell thickness nm
PDA microcapsules	0.09	1.08	58

6.3.3 Silver electroless plating of PDA Microcapsules

PDA microcapsules synthesised with 0.09 g/m^2 (mass of dopamine/total emulsion surface area), 5wt % silica containing hexadecane (1ml, oil volume fraction ϕ 0.11) were coated with silver by adding to a silver plating bath 5 ml ($[Ag(NH_3)_2]^+$, 10 and 20mM). PDA microcapsules synthesised with 0.09 g/m^2 (mass of dopamine/total emulsion surface area) were chosen as they contained the highest concentration of PDA without aggregating. The metal-binding ability of catechol and nitrogen-containing groups present in the PDA structure were exploited to immobilize silver complex diamine ions on the PDA surface, by strong coordination of the metal ions to

the catechol and nitrogen-containing groups on the PDA surface through absorption.[4, 10]

The plating bath solution consisted of silver diamine complex ions which complexed with PDA. The initial plating solution contained silver nitrate and a small amount of ammonium hydroxide. As the ammonium hydroxide solution was added, the reactive solution first turned a muddy brown due to the formation of a silver(I) oxide precipitate as described in reaction equation 6.1:

$$2Ag^{+}\,(aq) + 2OH^{-}\,(aq) \longrightarrow Ag_2O\,(s) + H_2O\,(l) \qquad 6.1$$

The ammonium hydroxide is a source of ammonia, as well as ammonium and hydroxide ions. Further addition of the ammonium hydroxide solution led to the solution clearing through the formation of the colourless silver diamine complex ion as described in reaction equation 6.2:

$$Ag_2O\,(s) + 4NH_3\,(aq) + H_2O\,(l) \longrightarrow 2[Ag(NH_3)_2]^{+}\,(aq) + 2OH^{-}\,(aq) \qquad 6.2$$

Upon reduction of the silver ions on the PDA surface, silver nanoparticles could be absorbed by catechol and nitrogen-containing groups, resulting in the formation of solid silver on the PDA surface (due to the high redox potential of silver ions), resulting in a silver film on the PDA microcapsules.[4]

The chemical reduction of silver diamine complex ion by glucose proceeds via the following overall reaction in aqueous solution resulting in silver growth on the PDA surface (reaction equation 6.3). 6.3

$$(C_5H_{11}O_5)\text{-}CHO\ (aq) + 2[Ag(NH_3)_2]^+(aq) + 2OH^-(aq) \leftrightarrow (C_5H_{11}O_5)\text{-}COOH\ (aq) + 2Ag\ (s) + 4NH_3(aq) + H_2O\ (l)$$

Glucose was chosen as it is a mild reducing agent and would ensure a controlled shell growth of silver on PDA. In chapter 4 and 5 the Pt catalyst was present at the oil water interface, where the deposition of the gold was required resulting in the formation of a continuous gold film. Therefore, in chapter 4 and 5 hydrogen peroxide was used as the reducing agent, as the rate of reduction did not matter as the catalysis was at the interface, providing a nucleation/deposition site, therefore resulting in the deposition at the interface. Whereas in the reduction of silver required a weaker reducing agent as the silver metal reduction was insensitive to the surface of PDA, as the silver diamine ions complex at the surface and are also present in the continuous phase. The use of a stronger reducing agent resulted in the reduction on the surface as well as in the continuous phase, whereas when glucose was used as the reducing agent the silver diamine ions had more time to choose where to react or deposit resulting in the silver depositing more efficiently on the surface of PDA microcapsules.

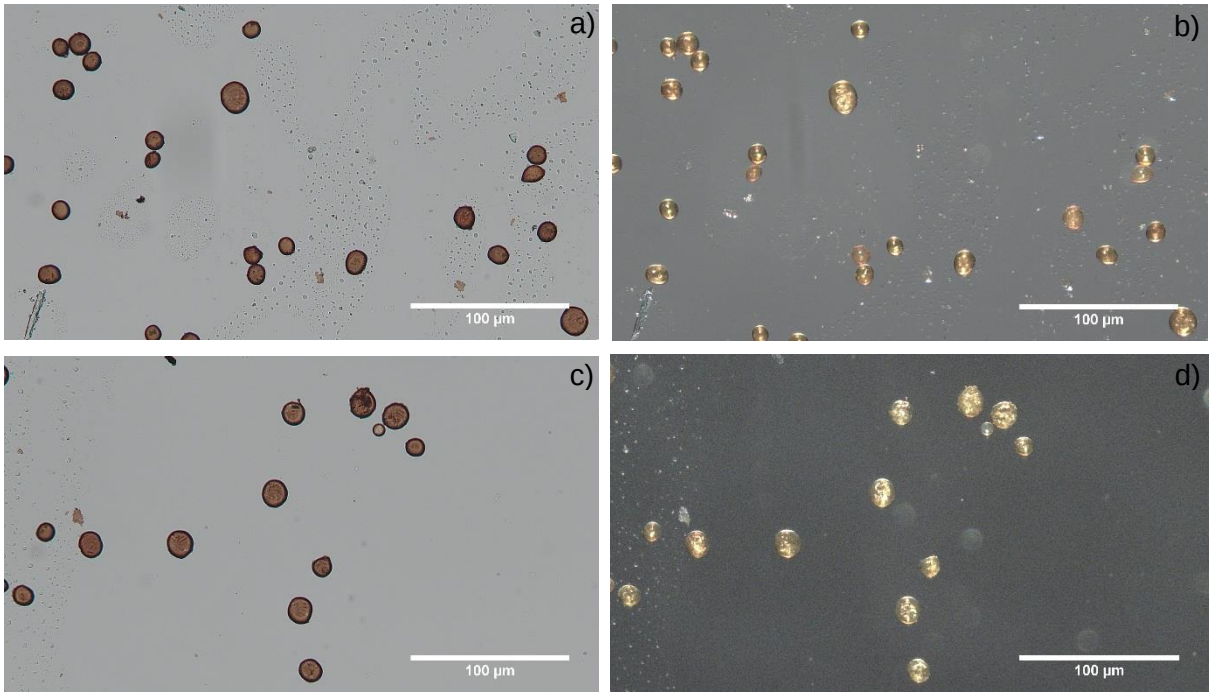

Figure 6. 13: Optical micrographs of silver-coated PDA microcapsules in aqueous suspension. Film deposition conditions are 10mM, $[Ag(NH_3)_2]^+$ for microcapsules shown in a) and b) and are 20mM, $[Ag(NH_3)_2]^+$ for microcapsules shown in c) and d), a) and c) show micrographs obtained in transmitted light and b) and d) show micrographs obtained in reflected light.

The PDA microcapsules were coated in silver as is visible in figure 6.13. The silver coated PDA microcapsules appear opaque and darker compared to PDA microcapsules demonstrated in figure 6.11 and also retain the spherical shape as demonstrated in figure 6.11.

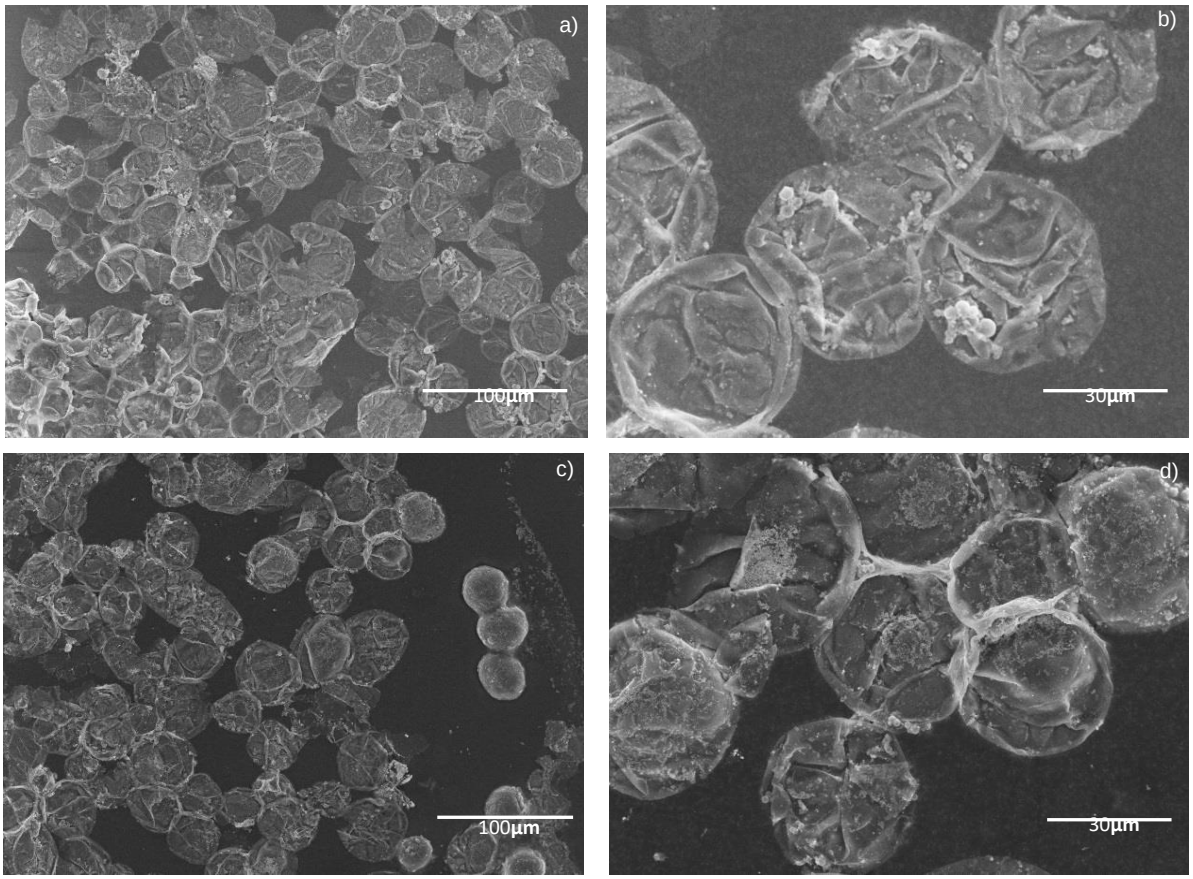

Figure 6. 14: Scanning Electron Micrographs of silver-coated PDA microcapsules. Film deposition conditions are 10mM, $[Ag(NH_3)_2]^+$ for microcapsules shown in a) and b) and are 20mM, $[Ag(NH_3)_2]^+$ for microcapsules shown in c) and d.

Silver coated PDA microcapsules appear stable when dried and under vacuum. Shell wrinkling was visible and this could be attributed to the shrinking of the microcapsules upon drying.[21]

SEM images were recorded in cryo conditions to analyse the 3D structure of the emulsions via focused ion beam (FIB). Once the sample is frozen, the sample is fractured exposing some of the emulsions and subsequently coated with platinum to reduce charging while in the SEM. The FIB can directly mill the frozen sample surface, via the sputtering of ions and therefore cut through the frozen sample to create a cross section from which the Si/Pt composite at the interface can be analysed.

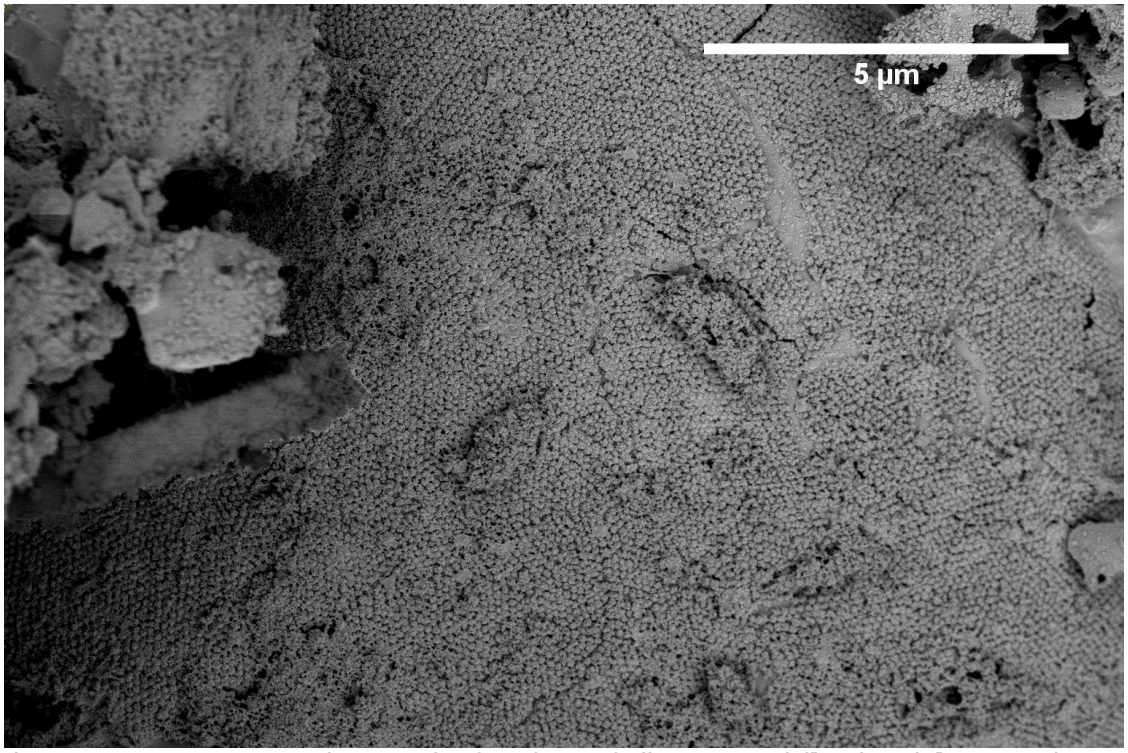

Figure 6. 15: CryoSEM micrograph of surface of silver coated ($[Ag(NH_3)_2]^+$, 10mM) PDA Microcapsule.

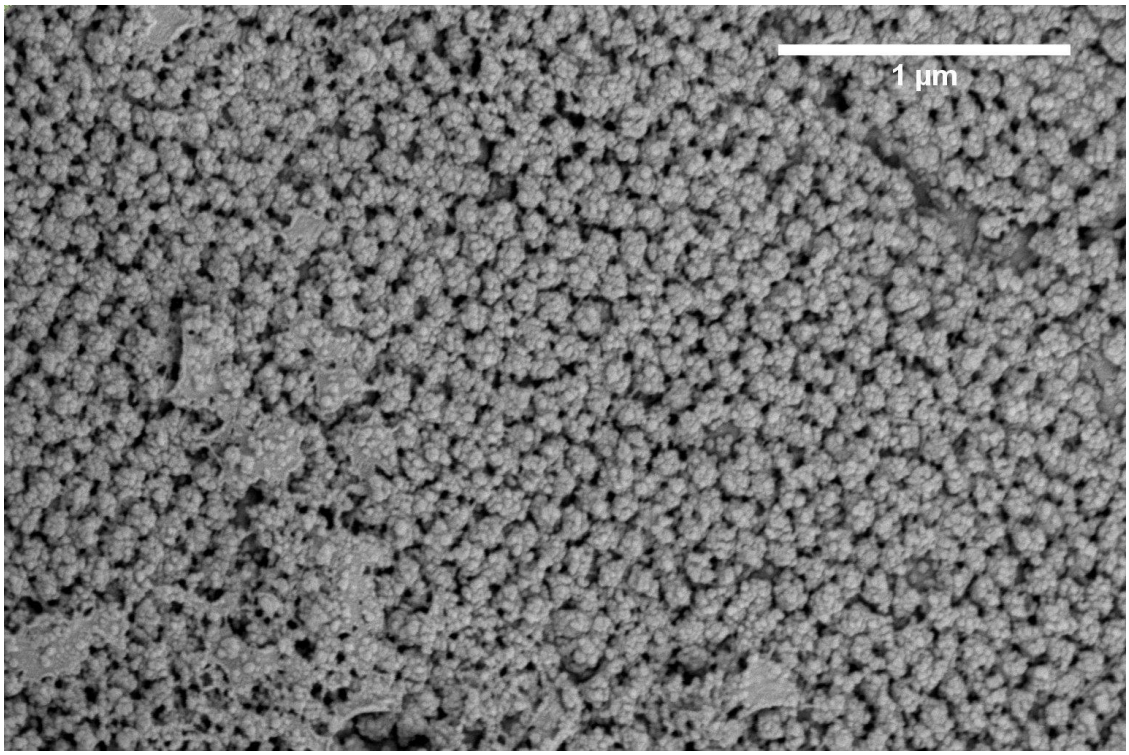

Figure 6. 16: CryoSEM micrograph of surface of silver coated ($[Ag(NH_3)_2]^+$, 10mM) PDA Microcapsule.

Figure 6.16 and 6.17 demonstrate the surface structure of the silver deposited on PDA microcapsules at different magnifications. From analysing figure 6.16 and 6.17 it is visible the surface of silver coated PDA microcapsules is not of a continuous film of silver, pin holes are visible which will result in the content of the core leaking out due to the permeability of the silver PDA microcapsule shell.

Table 6. 2: Total emulsion surface area (measured figure 6.8 f, bin limits) and the corresponding theoretical shell thickness, while mass of silver varied at 5.4 and 10.8mg and hexadecane oil volume fraction ϕ 0.11 kept constant.

	Mass of silver (mg)	Total emulsion surface area $nm^2 x10^{18}$	Theoretical shell thickness nm
Silver coated PDA microcapsules	10.8mg	1.08	10
Silver coated PDA microcapsules	21.6	1.08	19

From table 6.2 it is noted the theoretical shell thickness are 10 and 19nms for 10.8 and 21.6mg of silver respectively. As the reduction and deposition of silver is not completely controlled at the surface of the PDA microcapsules, some silver is lost in the continuous phase, hence resulting in the theoretical shell further decreasing in thickness. In the following section we will demonstrate the retention properties of the microcapsules when exposed to a continuous phase of ethanol/water (4:1).

6.3.4 Demonstrating Permeability

We demonstrated the ability of dopamine to self-polymerise and deposit onto colloidal silica stabilised oil in water Pickering emulsion resulting in PDA microcapsules which were subsequently coated in silver resulting in silver PDA microcapsules.

In this section we will demonstrate the retention of the hexadecane core of the microcapsules and also the permeability of the microcapsule shell. The microcapsules were placed in a 4:1 (volume ratio) ethanol/water continuous phase, this was done as the hexadecane core is completely soluble in ethanol and any hexadecane residue present or released from the microcapsules would be solubilised in the ethanol. Microcapsules were dispersed in an ethanol/water 4:1 ratio and kept suspended at 40^{o}C for 30 days. The microcapsules samples were taken at different time intervals and centrifuged to remove the microcapsules; the resulting sample was measured for hexadecane concentration using gas chromatography (GC). After 30 days the microcapsules were sonicated to break the microcapsules and measured for hexadecane, this was done to demonstrate the microcapsules contained hexadecane. The resulting data from this experiment is shown in figure 6.17.

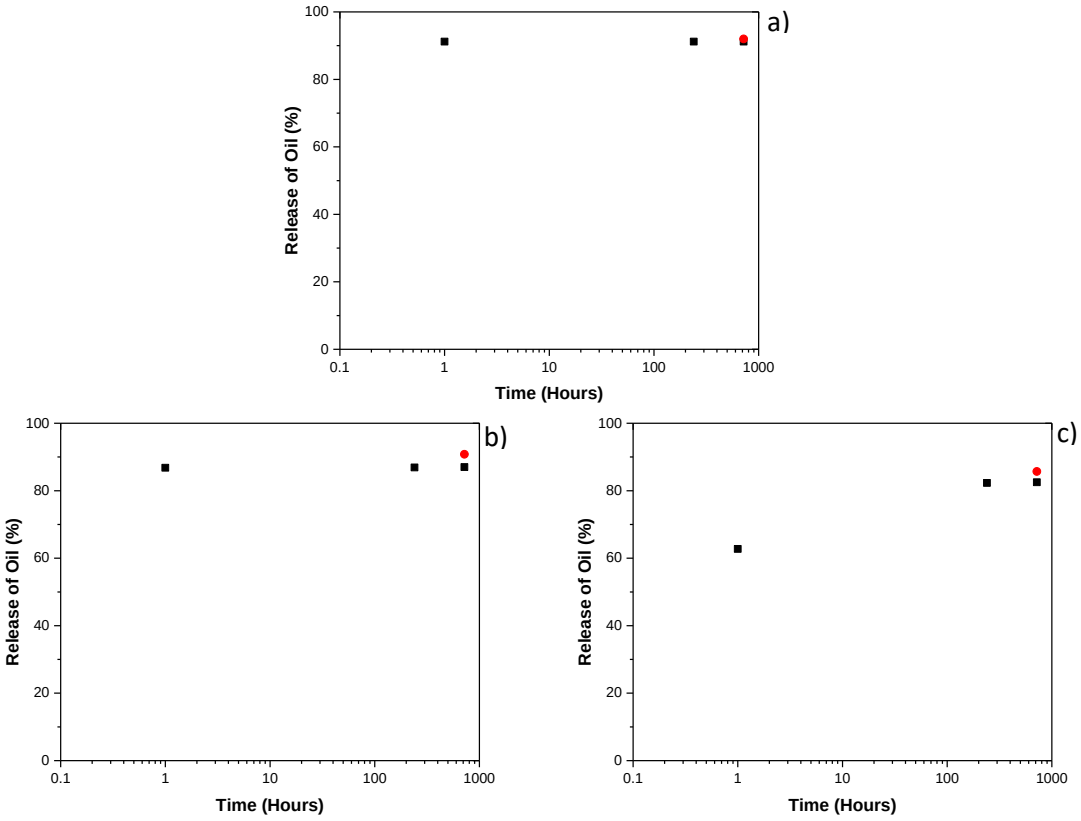

Figure 6. 17: Release of oil core from microcapsules, a) PDA microcapsules, b) Ag PDA ($[Ag(NH_3)_2]^+$, 10mM) microcapsules and c) Ag PDA ($[Ag(NH_3)_2]^+$, 20mM) microcapsules. Black square represents Hexadecane release after 1 Hour, release after 10 days and release after 30 days and red circle shows complete release after microcapsules are sonicated to break metal shells (1 min 40% amplitude).

As expected the PDA microcapsules released most of the core when exposed to a continuous phase of ethanol/water (4:1) due to the porosity of polymer shell and also the solubility of the polymer shell (PDA) in ethanol.[22] The silver ($[Ag(NH_3)_2]^+$, 10mM) coated PDA microcapsules also released most of the core after 1 hour when exposed to a continuous phase of ethanol/water (4:1), this was due to the in-sufficient coverage

of the PDA surface with silver as demonstrated in figure 6.15 and 6.16 where pin holes are visible on the surface on the microcapsules. The silver ($[Ag(NH_3)_2]^+$, 20mM) coated PDA microcapsules retained some of the core when exposed to an ethanol/water continuous phase after 1 hour, but released most of the oil core at day 10. Neither of the silver shells on the PDA microcapsules were able to form an impermeable continuous shell around the PDA microcapsules and retain the core.

The method of depositing silver onto PDA microcapsules is less efficient compared to methods in chapter 4 and 5 of depositing gold onto Pt-NP and Si/Pt stabilised emulsion. This was due to the controlled deposition of the metal shell at the interface and surface of silica at the interface in chapter 4 and 5 respectively due to the Pt-NP catalyst residing at the interface, whereas in this method the silver deposition is insensitive to the PDA surface, requiring a mild reducing agent, hence resulting in increased reaction times. Also this method performs less well as silver is reduced in the continuous phase, hence resulting in waste materials. The silver deposition also does not result in a continuous impermeable shell as demonstrated in figure 6.17. This could be due to the reduction of silver in the continuous phase resulting in thinner shells than illustrated in table 6.2.

6.4 Conclusion

In this chapter we have demonstrated the ability of dopamine to deposit on single silica particles and also silica stabilised Pickering emulsions resulting in PDA Si composites and PDA microcapsules respectively. The PDA microcapsules were subsequently coated in a silver shell, by utilising the catechol and nitrogen containing groups on the PDA surface to reduce the silver ions to silver on the PDA surface resulting in Ag PDA microcapsules. We demonstrated ~40% retention of the Ag ($[Ag(NH_3)_2]^+$, 20mM) PDA microcapsule core for up to 1 hour at 40^{o}C in an ethanol/water (4:1) continuous phase. The novelty of this work is the demonstration of the deposition of PDA onto liquid emulsion droplets followed by silver deposition via electroless plating, whereas the literature mainly consists of PDA deposition onto solid surfaces followed by silver plating.

We successfully removed the use of Pt-NPs and Si-Pt composites from our system for the synthesis of metal coated microcapsules by utilising PDA and directly depositing silver onto the PDA surface without the use of catalyst. This procedure has drastically reduced the cost of synthesising metal coated microcapsules, but we have not been able to demonstrate the retention of the core by forming an impermeable, uniform and complete continuous silver shell around the PDA microcapsules.

6.5 References

1. Ball, V., *Polydopamine films and particles with catalytic activity.* Catalysis Today, 2018. **301**: p. 196-203.
2. Ito, S., *A chemist's view of melanogenesis.* Pigment Cell Research, 2003. **16**(3): p. 230-236.
3. Lee, H., S.M. Dellatore, W.M. Miller, and P.B. Messersmith, *Mussel-inspired surface chemistry for multifunctional coatings.* Science, 2007. **318**(5849): p. 426-30.
4. Wang, W.C., A.N. Zhang, L. Liu, M. Tian, and L.Q. Zhang, *Dopamine-Induced Surface Functionalization for the Preparation of Al-Ag Bimetallic Microspheres.* Journal of the Electrochemical Society, 2011. **158**(4): p. D228-D233.
5. Yin, X.B. and D.Y. Liu, *Polydopamine-based permanent coating capillary electrochromatography for auxin determination.* Journal of Chromatography A, 2008. **1212**(1-2): p. 130-136.
6. d'Ischia, M., A. Napolitano, and A. Pezzella, *5,6-Dihydroxyindole Chemistry: Unexplored Opportunities Beyond Eumelanin.* European Journal of Organic Chemistry, 2011(28): p. 5501-5516.
7. Hong, S., Y.S. Na, S. Choi, I.T. Song, W.Y. Kim, and H. Lee, *Non-Covalent Self-Assembly and Covalent Polymerization Co-Contribute to Polydopamine Formation.* Advanced Functional Materials, 2012. **22**(22): p. 4711-4717.
8. Chen, C.T., C. Chuang, J.S. Cao, V. Ball, D. Ruch, and M.J. Buehler, *Excitonic effects from geometric order and disorder explain broadband optical absorption in eumelanin.* Nature Communications, 2014. **5**.
9. Perrot, D., C. Croutxe-Barghorn, and X. Allonas, *Towards mussel-like on-demand coatings: light-triggered polymerization of dopamine through a photoinduced pH jump.* Polymer Chemistry, 2016. **7**(15): p. 2635-2638.
10. Wang, W., Y. Jiang, Y. Liao, M. Tian, H. Zou, and L. Zhang, *Fabrication of silver-coated silica microspheres through mussel-inspired surface functionalization.* J Colloid Interface Sci, 2011. **358**(2): p. 567-74.
11. Okuda, H., K. Wakamatsu, S. Ito, and T. Sota, *Possible Oxidative Polymerization Mechanism of 5,6-Dihydroxyindole from A Initio Calculations.* Journal of Physical Chemistry A, 2008. **112**(44): p. 11213-11222.
12. Della Vecchia, N.F., R. Avolio, M. Alfe, M.E. Errico, A. Napolitano, and M. d'Ischia, *Building-Block Diversity in Polydopamine Underpins a Multifunctional Eumelanin-Type Platform Tunable Through a Quinone Control Point.* Advanced Functional Materials, 2013. **23**(10): p. 1331-1340.

13. Postma, A., Y. Yan, Y.J. Wang, A.N. Zelikin, E. Tjipto, and F. Caruso, *Self-Polymerization of Dopamine as a Versatile and Robust Technique to Prepare Polymer Capsules.* Chemistry of Materials, 2009. **21**(14): p. 3042-3044.
14. Wang, W., Y. Jiang, S. Wen, L. Liu, and L. Zhang, *Preparation and characterization of polystyrene/Ag core-shell microspheres--a bio-inspired poly(dopamine) approach.* J Colloid Interface Sci, 2012. **368**(1): p. 241-9.
15. Dreyer, D.R., D.J. Miller, B.D. Freeman, D.R. Paul, and C.W. Bielawski, *Elucidating the Structure of Poly(dopamine).* Langmuir, 2012. **28**(15): p. 6428-6435.
16. Dreyer, D.R., D.J. Miller, B.D. Freeman, D.R. Paul, and C.W. Bielawski, *Perspectives on poly(dopamine).* Chemical Science, 2013. **4**(10): p. 3796-3802.
17. Qu, Y.N., R.L. Huang, W. Qi, R.X. Su, and Z.M. He, *Interfacial Polymerization of Dopamine in a Pickering Emulsion: Synthesis of Cross-Linkable Colloidosomes and Enzyme Immobilization at Oil/Water Interfaces.* Acs Applied Materials & Interfaces, 2015. **7**(27): p. 14954-14964.
18. Luo, H.Y., C.W. Gu, W.H. Zheng, F. Dai, X.L. Wang, and Z. Zheng, *Facile synthesis of novel size-controlled antibacterial hybrid spheres using silver nanoparticles loaded with poly-dopamine spheres.* Rsc Advances, 2015. **5**(18): p. 13470-13477.
19. Wang, W.C., Y. Jiang, Y. Liao, M. Tian, H. Zou, and L.Q. Zhang, *Fabrication of silver-coated silica microspheres through mussel-inspired surface functionalization.* Journal of Colloid and Interface Science, 2011. **358**(2): p. 567-574.
20. Al-Shannaq, R., J. Kurdi, S. Al-Muhtaseb, and M. Farid, *Innovative method of metal coating of microcapsules containing phase change materials.* Solar Energy, 2016. **129**: p. 54-64.
21. Rosenberg, M., I.J. Kopelman, and Y. Talmon, *A Scanning Electron-Microscopy Study of Microencapsulation.* Journal of Food Science, 1985. **50**(1): p. 139-144.
22. You, I., H. Jeon, K. Lee, M. Do, Y.C. Seo, H.A. Lee, and H. Lee, *Polydopamine coating in organic solvent for material-independent immobilization of water-insoluble molecules and avoidance of substrate hydrolysis.* Journal of Industrial and Engineering Chemistry, 2017. **46**: p. 379-385.

7 Comparison of microencapsulation methods of PCM for thermal energy storage and release

7.1 Synopsis

This chapter will focus on comparing the heat transfer properties of metal-shell microcapsules produced with the three different methods presented in the previous chapters, for the subsequent use of the microcapsule cores as an encapsulated phase change material (PCM). Initially, background information about the characteristics and uses of PCMs and microencapsulated PCMs (MEPCMs) are given in order to fully introduce the concepts necessary to fully understand the results obtained here. Subsequently, the various MEPCMs synthesised in the previous chapters are specifically studied to understand their potential benefits for latent heat storage and transfer, supercooling, encapsulation efficiency and thermal conductivity. The work in this chapter builds upon recent literature studies that have also incorporated metals (in most cases as metal nanoparticles with only rare examples of full metal films) to microcapsule shells in order to improve the heat transfer properties of microencapsulated PCMs. The novel methods for preparing full impermeable metal shells directly onto emulsion droplets presented in this work are tested in this chapter with high core loadings, enhanced thermal conductivity and encapsulation efficiency demonstrated for such microcapsules.

7.2 Introduction

In 2016, the household/residential sector represented 25.4% of the final energy consumption in the EU. Household energy uses include, space and water heating, space cooling, cooking, lighting and electrical appliances and other end-uses, which mainly cover uses of energy by households outside the dwellings themselves. The largest energy consumption aspects within the residential sector (64.7%) were

attributed to the heating of homes, followed by electricity used for lighting and electrical appliances (13.8%).[1]

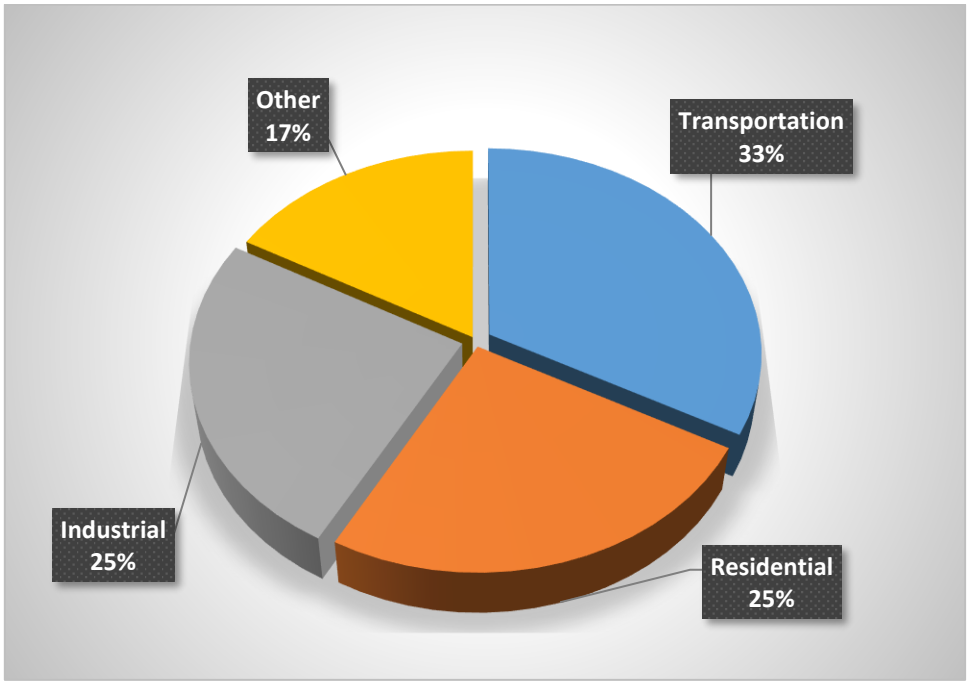

Figure 7. 1: EU energy consumption 2016 for corresponding sectors - 25% industrial energy consumption, 33% transportation energy consumption, 25 residential energy consumption and 17% other energy consumption.[2]

Recent projections predict energy consumption will rise by 48% in 2040.[3] To reduce energy production and meet the consumption requirements, better energy storage is required. Solar thermal systems are industrially mature and utilise a major part of the sun's thermal energy during the day, but during low or no solar radiation hours not enough thermal backup is stored to continue operating.[3] One particular solution to continue operating at all hours and minimise energy consumption in the residential sector is the use of microencapsulated phase change materials (MEPCMs) incorporated into building materials. To reduce energy consumption in residential buildings MEPCMs need to control the internal room temperature (indoor thermal comfort) by providing heating and cooling capabilities.[4] However, before these

systems can be implemented fully, several challenges still need to be addressed, in particular the suitability of encapsulation processes for a cost-effective production of efficient MEPCM systems and the efficiency of heat transfer through the microcapsule shells, which are typically constructed of polymeric/non-conductive materials. It is these two challenges in particular that this thesis addresses overall and that this chapter tests in particular.

7.3 Background

This section of the chapter introduces the general concepts of heat storage and how phase change materials allow for enhancing this process for potential industrial applications. It then focuses on the general notion of microencapsulated PCMs and their main characteristics.

7.3.1 Heat storage and phase change materials

Heat storage can be categorised into three different types, sensible heat storage, latent heat storage and chemical heat storage that are first introduced below.

7.3.1.1 Sensible Heat Storage (SHS)

Sensible heat storage (SHS) is the simplest method. It is based on storing thermal energy by heating or cooling a liquid or solid storage medium. The most popular, cheapest and commercial SHS medium is water, which has a number of residential and industrial applications, such as use of hot-water tanks for thermal energy storage. Water SHS main advantages are its low cost and very low risk as compared to using toxic materials. The factors affecting heat stored depend on the specific heat of the medium, temperature change and amount of the storage material. [2]

7.3.1.2 Chemical heat storage (CHS)

Chemical heat storage (CHS) is the energy absorbed and released from breaking and reforming molecular bonds in reversible chemical reactions. The amount of heat stored for CHS depends on the mass of the storage material, the endothermic heat of reaction and the degree of conversion. [5]

7.3.1.3 Latent heat storage (LHS)

Latent heat storage (LHS) is the heat absorbed or released when a storage material undergoes a phase change (for example solid to liquid, liquid to gas or the opposite phase changes). LHS materials are known as PCMs due to their ability to absorb and release thermal energy with a change in physical state. Thermal energy is stored in the phase-change process (occurring at a defined temperature) and is directly proportional to the latent heat of the phase change material. LHS systems using PCM can be utilised as an effective way of storing and releasing thermal energy. The main applications of LHS materials include incorporation into building materials such as:

- Gypsum boards
- Plaster
- Concrete
- Wall covering materials [3]

Incorporating LHS materials into building applications reduces the energy required for heating and cooling buildings, as the LHS materials provide thermal energy into the buildings while solidifying when the temperature is reduced and, reversely, absorb thermal energy from the building while melting as the temperature increases.

7.3.2 Phase Change Materials (PCMs)

Phase change materials (PCMs) are important materials that are able to absorb, store and release large amounts of latent heat over a defined temperature range when undergoing phase change (melting and solidifying at well-defined temperature ranges). PCMs are known to possess 5-14 times more heat per unit volume than sensible storage materials such as water, masonry or rock.[6, 7]

PCMs can be classified into two groups, organic and inorganic phase change materials. Organic PCMs consist of paraffins (straight chain alkanes) and non-paraffins such as esters, fatty acids, alcohols and glycols. Inorganic PCMs consist of salt hydrates and metallics.[5]

7.3.3 Organic PCMs

Organic paraffins release large amounts of latent heat upon crystallization. The heating and melting point of the paraffins can vary as a function of chain length. Indeed, increasing the chain length results in an increase in the melting point and also an increase in the latent heat of fusion, as demonstrated in table 7.1. Organic paraffins are safe to handle, cost effective, non-corrosive, chemically insert, stable below 500°C and exhibit low supercooling. However, the disadvantages of organic paraffins include low thermal conductivity and not being compatible with plastics and flammable.[5, 8, 9]

Non-organic paraffins when compared to organic paraffins demonstrate higher heat of fusion and no supercooling. However, typically their limitations outweigh the advantages, such as high costs, mildly corrosive, low thermal conductivity and instability at high temperatures.[10-12]

No. of carbon atoms	Melting point (°C)	Latent heat of fusion (KJ/Kg)
14	5.5	228
15	10	205
16	16.7	237
17	21.7	213
18	28.0	244
19	32.0	222
20	36.7	246
21	40.2	200
22	44.0	249
23	47.5	232
24	50.6	255
25	49.4	238
26	56.3	256
27	58.8	236
28	61.6	253
29	63.4	240
30	65.4	251
31	68.0	242
32	69.5	170
33	73.9	268
34	75.9	269

Table 7. 1: Latent heat of fusion and melting point for varying chain length of alkanes (PCM). [6, 7]

7.3.4 Inorganic PCMs

Inorganic PCMs, salt hydrates (e.g. calcium chloride hexahydrate, sodium sulfate decahydrate, sodium acetate) are regarded as alloys of inorganic salts and water forming a typical crystalline solid. Salt hydrates are one of the most important and extensively studied group of PCMs. This is due to their unique combination of interesting properties, such as high latent heat of fusion per unit volume, high thermal conductivity (almost double that of paraffins), small volume changes on melting, compatible with plastics and relatively inexpensive. Salt hydrates are not without their problems, including high degree of supercooling, phase segregation and corrosion.[5, 12]

7.3.5 Metallic PCMs

Metallic PCMs are low melting metals, which have not been extensively studied due to their high density and low availability of temperature range. Metallic PCMs do exhibit the highest thermal conductivity when compared to other PCMs.[5]

7.3.6 Justification of the PCMs used in this work

From evaluating PCMs, paraffins were chosen as the most beneficial PCMs for use in building materials to reduce energy consumption in the residential sector, because of their properties, including high latent heat, good availability of working temperature (room temperature), cost-effectiveness, non-corrosive, chemically insert, stable below 500°C and low supercooling. As paraffin PCMs are liquids and incorporating (and handling) liquids within building materials is difficult. Thus, to overcome this challenge, paraffin PCMs will be encapsulated resulting in microencapsulated PCMs (MEPCMs) which will be easier to handle and incorporate into building materials. Hexadecane was chosen as the PCM (latent heat of fusion 237 KJ/Kg, melting point 18°C).[5]

7.3.7 Requirements for microencapsulation of PCMs

For encapsulating PCMs, certain criteria have to be met to enable successful uptake of the concept by industry, including achieving suitable thermo-physical, kinetic and chemical properties.[3, 5, 8, 13]

Thermal properties:

- Suitable phase-transition temperature - the operating temperature of heating/cooling needs to match the transition temperature, the optimum home temperature is 18-21°C, therefore the PCM melting and freezing range should be 18-21°C,

- High latent heat of transition - to minimise size of heat store (microcapsule size), less material required for high energy output,
- Good heat transfer - high thermal conductivity, so energy can be transferred efficiently to the surroundings. [5]

Physical properties:

- Phase stability during freezing/melting,
- High density - smaller size of storage container (microcapsule size), small volume change and low vapour pressure - reduce containment problems.[14]

Kinetic properties:

- No supercooling or limited supercooling - supercooling results in the liquid PCMs to stay in the liquid state when its temperature is reduced to below its freezing point without freezing (solid). One of the applications of phase change energy storage is temperature control i.e. heat is extracted within a fixed temperature range. With supercooling, the objective is compromised, since the temperature of the PCM goes below the nominal phase change temperature range during heat extraction.
- Sufficient crystallisation rate - quick phase transition, liquid to solid and vice-versa.[12]

Chemical properties:

- Long-term chemical stability,
- Compatibility with encapsulation materials,
- Non-toxic and non-flammable.[5]

PCMs also need to be economically viable, abundant and readily available.[5]

Microencapsulation of PCMs is desired as it would improve handling and incorporation of PCMs into building materials. Also the shell would prevent the leakage and contamination of the PCMs upon melting. As PCMs are an effective way of storing thermal energy, incorporating MEPCMs into building materials would reduce energy usage for cooling and heating tendencies in residential buildings due to the relatively high energy storage and release capacities.

7.3.8 Properties of Microencapsulated PCMs (MEPCMs)

The desired properties of the shell material for encapsulating PCMs are enhanced mechanical properties, increased stability of PCMs, increased thermal conductivity of the thermal energy and enhanced thermal stability.

The working principle of MicroEncapsulated Phase Change Materials (MEPCMs) can be explained as follows: as heat is applied to a solid MEPCM, temperature of the microcapsule increases until the PCM (core) becomes liquid (melts). During this phase, the MEPCM stores a significant amount of heat energy (thermal energy). As the temperature is subsequently reduced below its melting point, the PCM in the microcapsule core starts the transformation to the solid state (freezes), resulting in the stored heat energy (thermal energy) being released to the surroundings. MEPCMs incorporated in building materials would reduce the room temperature by absorbing the heat energy from the room by melting and would increase the room temperature by releasing stored thermal energy by freezing. Figure 6.1 demonstrates the working principle of MEPCMs.

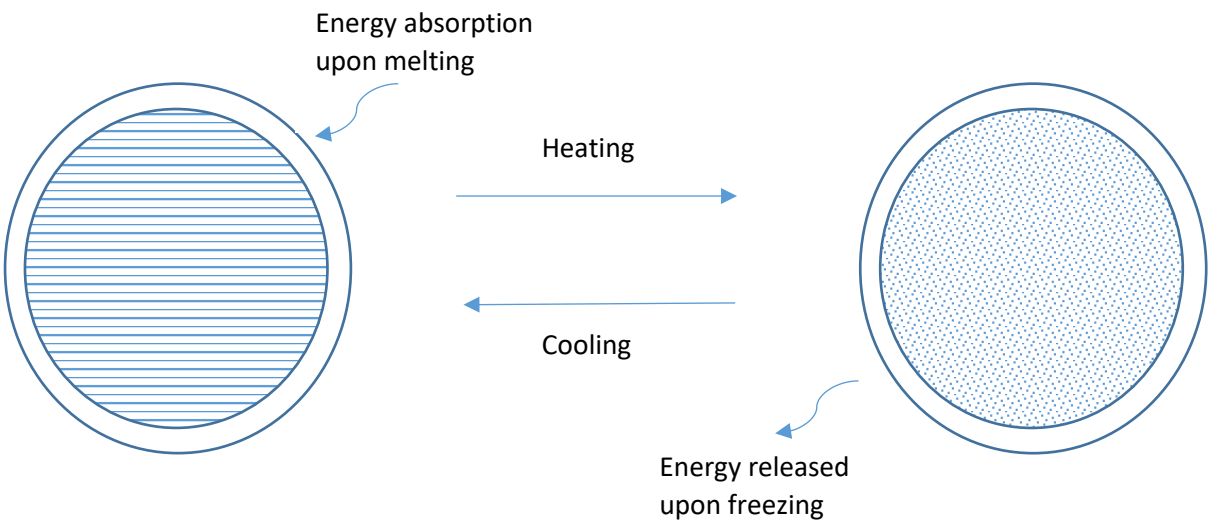

Figure 7. 2: Working principle of thermal energy storage and release in MEPCMs: as the temperature increases, PCM in the core of the microcapsule absorb thermal energy (through the melting process) and as the temperature decreases, the PCM in the core releases thermal energy (through the freezing process).

7.3.9 Recent progress in developing microencapsulated PCMs with high heat transfer properties.

Several research papers have demonstrated the possibility of synthesising microcapsules containing PCMs, discussing the properties of PCMs and MEPCMs for example latent heat and supercooling and also investigating the properties of shell materials for example mechanical stability, thermal conductivity and thermal stability. In the following section a review of the recent literature will be carried out, exploring the properties of MEPCMs and evaluating the choices made in previous studies for the PCM and shell material.

Initially polymer (organic) shells encapsulating organic PCMs will be discussed, followed by inorganic and metal shells for encapsulating organic PCMs.

7.3.10 Organic Polymer shells

Organic polymers have been widely used as materials to encapsulate PMCs such as poly(methylmethacrylate) (PMMA), melamine-formaldehyde resin and polyuria. Generally, polymeric shells used to encapsulate PCMs, resulted in various degrees of encapsulation efficiency but typically led to an increase in thermal stability and low conductivity of the shell.[6, 15, 16] Indeed, polymeric materials are commonly utilised as shells because they have good sealing ability, good chemical and thermal stability.

For example, Su, *et al.* demonstrated the encapsulation of n-octadecane (PCM) with methyl methacrylate (MMA) and methacrylic acid (MAA) through in-situ suspension polymerization method for use as MEPCMs in residential buildings for thermal comfort. The DSC thermograms and recorded thermal properties of n-octadecane and MEPCMs (n-octadecane) within this previous study are demonstrated in table 7.2.

Su, *et al.,* concluded that encapsulating PCM with polymeric shells (organic shells) results in enhanced thermal stability of the PCM, and an increase in encapsulation efficiency but supercooling was observed in the MEPCMs. As the encapsulation efficiency cannot be greater than 100% but this is a result reported by these authors, these data should be read with caution.[16]

Table 7. 2: Properties of n-octadecane and MEPCMs with PMMA-MAA shells with varying shell ratios.[16]

Samples	MMA: MAA Ratio	Melting point (°C)	Latent heat (KJ/Kg)	Core material (wt%)	Encapsulation efficiency (%)
n-Octadecane	--	24.12	216	--	--
PMMA-MAA1	1 : 0.25	23.68	170	79.8%	114%
PMMA-MAA2	1 : 0.67	22.56	164	77.0%	110%
PMMA-MAA3	1 : 1	22.92	150	70.4%	101%

Zhang and Wang, studied the effect of encapsulating PCM (n-octadecane) with polyurea shells with different monomer ratios through interfacial polycondensation. In the study it was concluded that the encapsulation efficiency of the MEPCMs (73-87.4%) compared to n-octadecane varied with different monomer ratios. The encapsulation process resulted in an increase in the thermal stability of the MEPCMs.[6]

Sari, *et al.,* studied the effect of encapsulating n-octacosane with PMMA via an emulsion polymerisation process. It was concluded that the PMMA MEPCMs, had a 43% encapsulation efficiency and observed that after 5000 cycles of heating and cooling the average latent heat varied only by 7.5%, thus demonstrating good thermal stability for these PMMA MEPCMs.[15]

The three articles reviewed above, all used polymeric shells to encapsulate PCMs and it is worth highlighting that mixed results were obtained in terms of supercooling and

thermal stability. All the MEPCMs had good encapsulation efficiency, but all the polymeric MEPCMs were concluded to have low thermal conductivity due to the non-conductive polymeric shell.

7.3.11 Inorganic shells

Advantages of using inorganic shells for encapsulating PCMs have been reported in the literature, including beneficial properties for fire resistance, chemical and thermal stability and compatibility with other materials.[12] Zhang, *et al.,* synthesised microencapsulated n-octadecane with silica shell via a sol-gel process to enhance the thermal conductivity of the MEPCMs. The study demonstrated high encapsulation efficiency, high thermal conductivity and phase change performance. The thermal conductivity increased with an increase in the shell ratio to PCM, resulting in a decrease in the encapsulation efficiency.[17] Yu, *et al.,* synthesised microencapsulated n-octadecane with calcium carbonate shell via self-assemble precipitation reaction to enhance the thermal conductivity of the MEPCMs. An increase in thermal conductivity resulted in a low encapsulation efficiency (21.89-40.04%).[18] Li, *et al.,* synthesised paraffin microcapsules coated with a silica shell via in situ emulsion interfacial hydrolysis and polycondensation of tetraethyl orthosilicate (TEOS). The MEPCMs exhibited good thermal stability and very low encapsulation efficiency (31.7%), supercooling was also observed.[19] Zhang, Yu, and Li, demonstrated an increase in thermal conductivity by utilising inorganic shells to encapsulate PCMs. By increasing the thermal conductivity resulted in a decrease in the encapsulation efficiency, which resulted in a lower latent heat.

7.3.12 Hybrid Shells

Yang, *et al.,* utilised hybrid shells to encapsulate PCMs, silicon nitride was uniformly dispersed in a PMMA shell encapsulating n-octadecane. The hybrid shell resulted in enhance thermal properties and improved mechanical strength, but supercooling was exhibited in the MEPCMs.[20] Yin, *et al.,* synthesised hexadecane microcapsules coated in $Si0_2$-poly(methyl methacrylate) hybrid shell, initiated via atom transfer radical polymerization (SI-ATRP). The MEPCMs when compared to hexadecane resulted in supercooling and also broadening of the heat flow peak (DSC), demonstrating low thermal conductivity.[21]

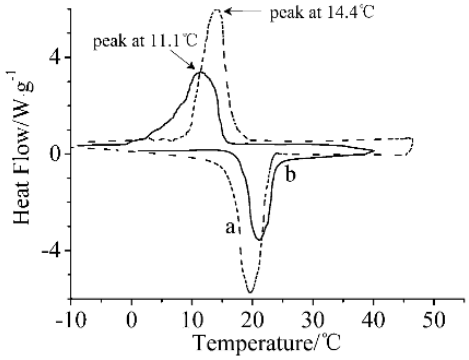

Figure 7. 3: DSC thermograms of hexadecane and MEPCMs ($Si0_2$-poly(methyl methacrylate) hybrid shell. The dotted line represents hexadecane and the black line represents the MEPCM.[21]

7.3.13 Metal shells

Metals are a valuable and potential option to encapsulate PCM as they possess excellent thermal and mechanical properties.[22] Encapsulating PCMs effectively with metal shells is challenging. Most of the literature incorporates organic or inorganic

shells followed by metal plating. Not much literature has been reported on encapsulating PCMs with metal shells.

Yalin, *et al*., utilised metal coatings (silver) on silica nanocapsules, followed by electroless plating in Tollens reagent. It was concluded silver silica MEPCMs resulting in higher thermal conductivity, increased thermal stability and low supercooling.[23]

Qingwen, *et al*., incorporated silver nanoparticles into an aminoplast wall encapsulating bromo-hexadecane as the PCM. Incorporation of the silver nanoparticles into the shell resulted in an increase in the thermal stability of the MEPCMs.[24]

Al-shannaq, *et al.,* studied the effect of polymer MEPCMs against metal coated polymer MEPCMs to enhance the thermal conductivity of MEPCMs. PMMA MEPCMs and silver coated PMMA MEPCMs by activating the surface of the PMMA MEPCMs with PDA were compared. It was concluded metal coated polymer MEPCMs had lower encapsulation efficiency than polymer MEPCMs but the thermal conductivity was enhanced by using a metal coating. Metal coated MEPCM had lower encapsulation efficiency due to the metals high density and the incorporation of the PMMA and PDA shell, which reduced the actual PCM mass in the MEPCM. Also no supercooling was observed with metal MEPCMs.[25]

This chapter will investigate two different methods for preparing metal-shell microcapsules (chapter 4 and 5), both of which are new to the literature and neither of which have been used to encapsulate PCMs and therefore never been tested for their heat transport properties.

7.4 Results and discussion

The two different types of MEPCMs will be analysed for latent heat storage and transfer, supercooling, encapsulation efficiency and thermal conductivity characterised by the width of the melting/freezing peak from the DSC. The two different MEPCMs are as follows:

1. Pt-NP stabilised emulsions (hexadecane) gold coated (chapter 4)
2. Si/Pt composite stabilised emulsions (hexadecane) gold coated (chapter 5)

PDA microcapsules silver coated analysis was not carried out as the microcapsules were not impermeable as demonstrated in chapter 6. As to obtain clean data as possible and make sure any changes noticed in the DSC data were attributed to the variables tested only, hence requiring any trace of PCM non-encapsulated removed by thorough cleaning of the obtained microcapsules with ethanol. Upon washing the PDA microcapsules with ethanol would result in the encapsulated PCM to leach out of the microcapsules, resulting in an unknown composition of the shell to core.

The encapsulation efficiency E can be calculated by the phase change enthalpies obtained from the DSC thermograms according to equation 7.1:

$$E = \frac{\Delta H_{m,Micro-PCMs}}{\Delta H_{m,PCM}} + \frac{\Delta H_{c,Micro-PCMs}}{\Delta H_{c,PCM}} x100 \qquad 7.1$$

where $\Delta H_{m,Micro-PCMs}$ is the latent heat of fusion of the microencapsulated hexadecane;

$\Delta H_{c,Micro-PCMs}$ is the enthalpy of crystallization of the microencapsulated hexadecane;

$\Delta H_{m,PCM}$ is the latent heat of fusion of pure hexadecane;

$\Delta H_{c,PCM}$ is the enthalpy of crystallization of pure hexadecane.

The encapsulation ratio R (wt% of PCM in the microcapsules) can be determined using the latent heat from the DSC results as shown in equation 7.2:

$$R = \frac{\Delta H_{m,Micro-PCMs}}{\Delta H_{m,PCM}} x100 \qquad 7.2$$

where $\Delta H_{m,Micro-PCMs}$ is the latent heat of fusion of the microencapsulated hexadecane;

$\Delta H_{m,PCM}$ is the latent heat of fusion of hexadecane.

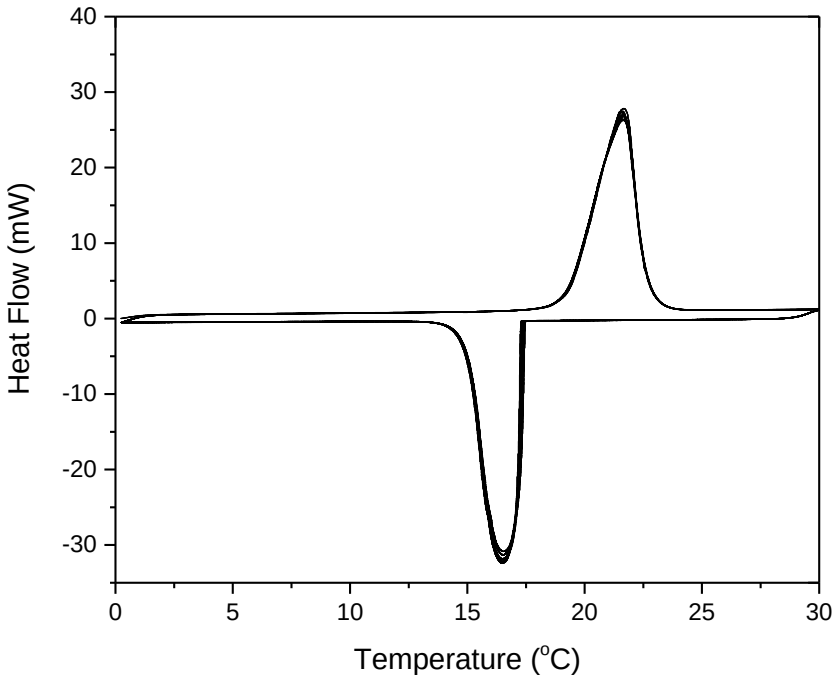

Figure 7. 4: DSC thermogram of pure hexadecane, in stainless steel pan with lid analysed using the DSC, 50 cycles of heating and cooling, heating/cooling ramp 2°C/min (0-30°C).

Figure 6.4 presents 50 thermal cycles of heating and cooling for pure hexadecane, where no noticeable difference were observed in the melting (16.6 °C) and freezing (21.7 °C) point of hexadecane after 50 cycles. The freezing and melting points of hexadecane make it suitable for encapsulation for use in residential buildings.

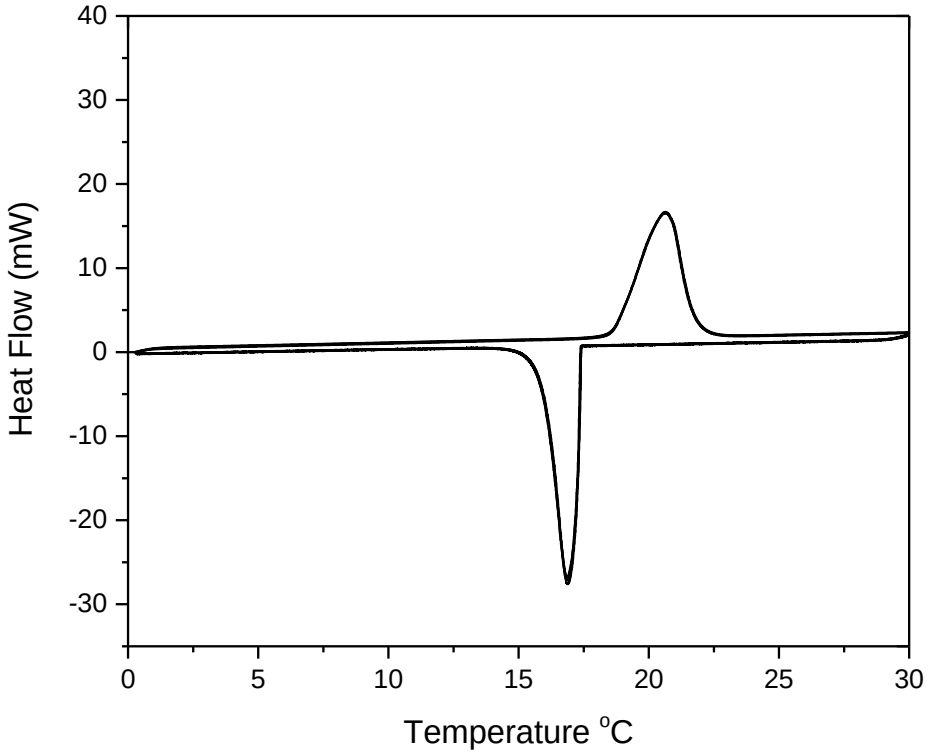

Figure 7. 5: DSC thermogram of gold coated Pt-NP stabilised emulsions, in stainless steel pan with lid analysed using the DSC, 50 cycles of heating and cooling, heating/cooling ramp 2°C/min (0-30°C).

Figure 7.5 presents 50 thermal cycles of heating and cooling of gold coated Pt-NP microcapsules (MEPCMs). No change is observed in terms of melting (20.5°C) and freezing (16.9°C) point of the PCM as compared to that recorded for pure hexadecane. However, a slight change was observed in the latent heat of fusion and the enthalpy of crystallization of the microencapsulated hexadecane. Figure 7.5 demonstrates the suitability of the MEPCMs for application in residential buildings.

7.4.1 Gold coated Pt-NP PVP stabilised emulsions (MEPCMs)

The following section will demonstrate the comparison of hexadecane against MEPCMs (gold coated Pt-NP stabilised emulsions containing hexadecane). The difference in gold shell thickness will also be analysed for comparing hexadecane and MEPCMs. The DSC thermograms in figure 7.6 represent the results obtained for different weights analysed samples so are not directly comparable but data normalised by the mass of hexadecane present in the samples are presented in table 7.3 and 7.4.

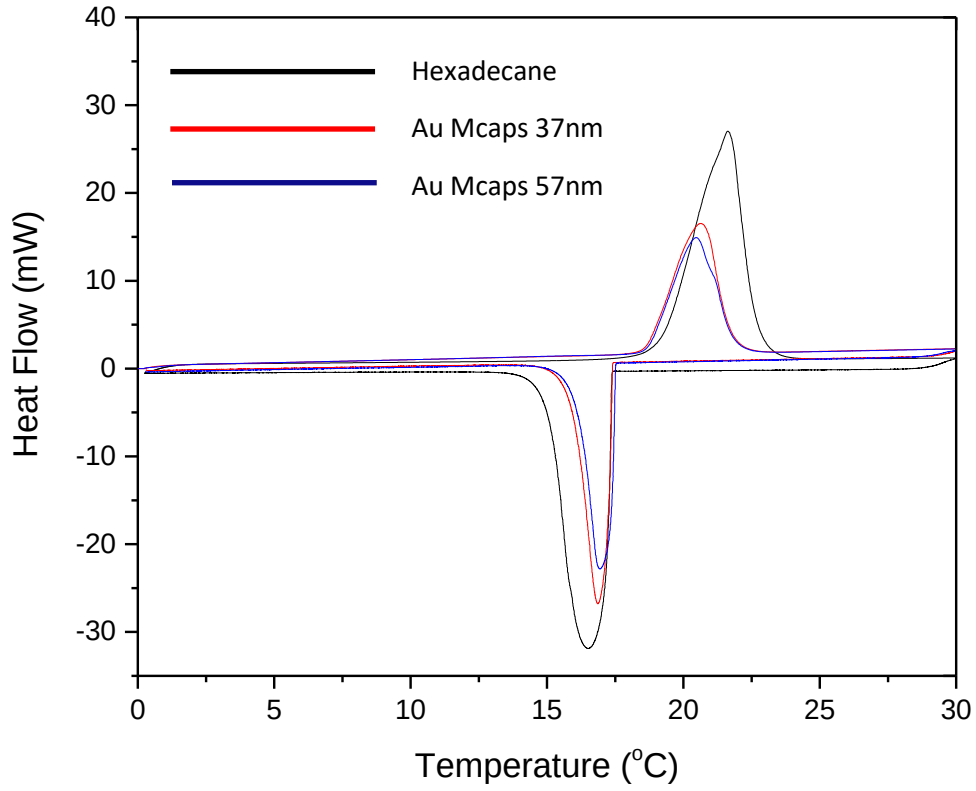

Figure 7. 6: DSC thermograms of hexadecane and dry MEPCMs (37 and 57nm shell thickness) in stainless steel pan with lid analysed using the DSC (temp range 0-30°C, heating and cooling rate 2°C/min), hexadecane oil volume fraction ϕ of 0.04.

Table 7. 3: Thermal properties of hexadecane (PCM) and MEPCMs (gold coated Pt-NP stabilised emulsions). The data for the MEPCMs is normalised based on the mass of the MEPCMs (including shell and PCM mass).

Sample/shell thickness	T_m (°C)	ΔH_M (J/g)	T_c (°C)	ΔH_c $(\mathrm{J/g})$
Hexadecane	21.7	194.8	16.6	199.9
Au Mcaps 37nm	20.6	107.9	16.9	107.5
Au Mcaps 57nm	20.5	81.1	16.9	82.1

Table 7.4 represents the properties of the MEPCMs at different shell thickness. The theoretical oil core % represents the volume of the PCM used for the synthesis of the MEPCMs and the TGA measure oil core % is the actual volume of hexadecane in the microcapsules obtained from the TGA data analysis (chapter 4). The encapsulation ratio and efficiency are explained in equation 7.1 and 7.2.

Table 7. 4: Properties of MEPCMs (gold coated Pt-NP stabilised emulsions).

Sample/shell thickness	Theoretical oil core %	TGA measured Oil core %	Encapsulation Ratio (%)	Encapsulation Efficiency (%)
Au Mcaps 37nm	54.6	51.2	55.3	54.6
Au Mcaps 57nm	44.3	41.0	41.6	41.3

From analysing figure 7.6, table 7.3 and 7.4, the latent heat of fusion (melting) and enthalpy of crystallization of hexadecane were determined to be 194.8 J/g and 199.9 J/g respectively. These values are slightly lower than those indicated in the literature,

which may be a result of impurities in the purchased sample.[5] However, the data confirm the excellent ability of hexadecane to store and release thermal energy.

The MEPCMs Au Mcaps (37nm) latent heat of fusion (melting) and enthalpy of crystallization (freezing) were determined to be 107.9 J/g and 81.1 J/g. The MEPCMs Au Mcaps (57nm) latent heat of fusion (melting) and enthalpy of crystallization (freezing) were determined to be 107.5 J/g and 82.1 J/g. The latent heat of fusion and enthalpy of crystallisation decreased due to the incorporation of the metal gold shell, which reduces the proportion of hexadecane in the sample. The decrease in the enthalpy of crystallisation was also observed by Zhang Yu and Li and explained in terms of reduction of the proportion of the hexadecane in the sample, but no correlation was made between the theoretical or actual loading of the PCM in the sample, with the results obtained.[17-19]

The results obtained are consistent with the theoretical percentage of oil core estimated in the previous chapters, via TGA measured oil core % (chapter 4), encapsulation ratio% (the amount of PCM) and the encapsulation efficiency. Indicating the gold shell did not affect the latent heat of fusion and enthalpy of crystallisation of the encapsulated hexadecane. The increase of the metal shell thickness did not appear to adversely affect the measured latent heat of fusion and enthalpy of crystallisation for the microencapsulated samples. However, an increase in the shell thickness for these samples resulted, as expected, in a decrease in the encapsulation efficiency. Indeed, as the core hexadecane mass ratio was reduced, the measured encapsulation ratio also reduced.

Supercooling for pure hexadecane was recorded to be 5.1°C (difference between melting and freezing temperatures). Encapsulating the hexadecane resulted in a

reduction of this supercooling, Au Mcaps (37nm) supercooling was reduced to 3.7°C and for Au Mcaps (57nm) supercooling was reduced to 3.6°C. The gold shells resulted in the reduction of supercooling and also enhanced the thermal conductivity by narrowing the DSC curve obtained as compared to the curve obtained for pure hexadecane. A sharp and narrow DSC curve indicates good thermal conductivity. The narrowing of the DSC curves demonstrated the faster transfer of thermal energy as a result of the high conductivity of the metal shell.

This was also demonstrated by Al-shannaq, *et al.,* when investigating silver coatings on PMMA MEPCMs. The silver coated PMMA MEPCMs enhanced the thermal conductivity and reduced supercooling when compared to PMMA MEPCMs, but this resulted in the PCM loading decreasing from 77% for PMMA MEPCMs to 50% for silver coated PMMA MEPCMs, no comparison in data was made to the raw PCM.[25] In our system and the system described by Al-shannaq, *et al.,* both resulted in enhanced thermal conductivity and reduced supercooling. The process described by Al-shannaq, *et al.,* includes the synthesis of PMMA microcapsules followed by activation of the PMMA microcapsules with dopamine and then the subsequent coating of the PMMA microcapsules with silver. Whereas our system simply consists of stabilising an oil in water emulsion with Pt-NPs followed by electroless gold plating. Not only does our system bring the benefits on enhanced thermal conductivity and reduced super cooling but also simplicity in the process for synthesising MEPCMs.

From table 7.4 the DSC, TGA (chapter 4), theoretical and GC data (chapter 4) of the gold shell microcapsules are in good agreement. The GC data confirms the encapsulation and retention of the hexadecane core while the DSC data, encapsulation ratio and efficiency % confirm the hexadecane oil core % by analysing the latent heat of fusion and enthalpy of crystallisation and confirming the similarity between the encapsulation ratio %, encapsulation efficiency%, theoretical and TGA measured oil core, demonstrating all round reliability and data agreement.

7.4.2 Gold coated Pt-Si stabilised emulsions (MEPCMs)

The following section will demonstrate the comparison of hexadecane against MEPCMs (gold coated Si/Pt composite stabilised emulsions containing hexadecane). The effect of the size and core loading of MEPCMs will also be analysed for comparing against hexadecane. The DSC thermograms in figure 7.7 represent the results obtained for different weights analysed samples so are not directly comparable but data normalised by the mass of hexadecane present in the samples are presented in table 7.5 and 7.6.

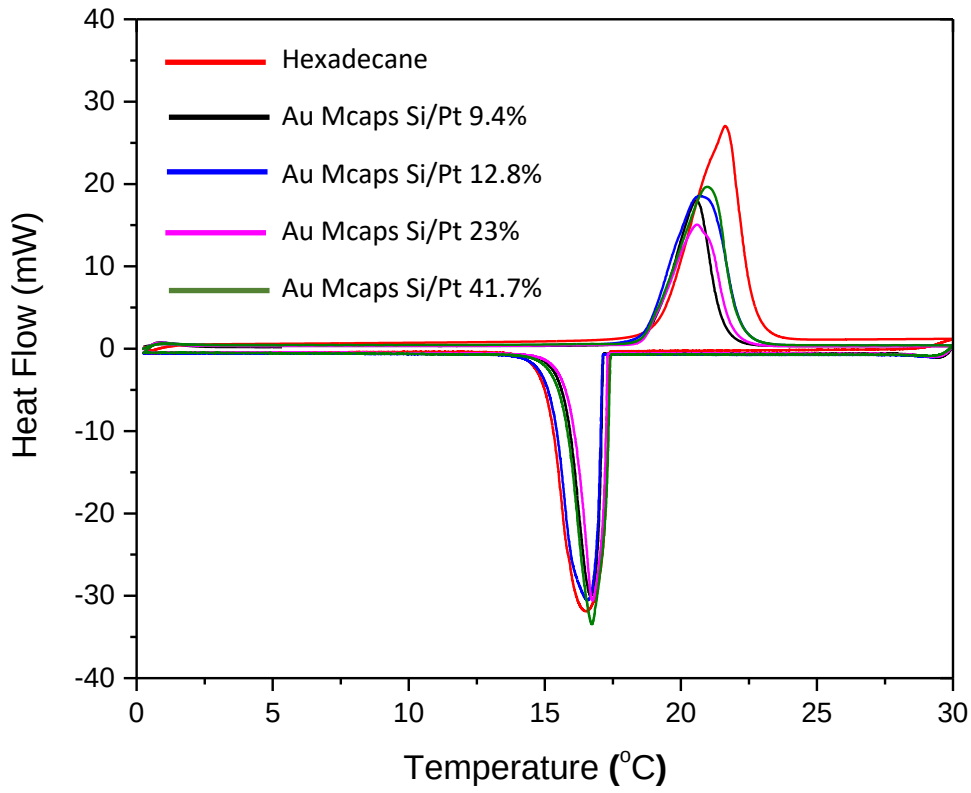

Figure 7. 7: DSC thermograms of hexadecane and dry MEPCMs (Au Mcaps Si/Pt 9.4, 12.8, 23 and 41.7%) in stainless steel pan with lid analysed using the DSC (temp range 0-30°C, heating and cooling rate 2 °C/min), hexadecane oil volume fraction ϕ of 0.1.

Table 7. 5: Thermal Properties of hexadecane (PCM) and MEPCMs (gold coated Si/Pt composite stabilised emulsions). The data for the MEPCMs is normalised based on the mass of the MEPCMs (including shell and PCM mass).

Sample	T_m (°C)	ΔH_M (J/g)	T_c (°C)	ΔH_c $(\mathrm{J/g})$
Hexadecane	21.7	194.8	16.6	199.9
Au Si/Pt (9.4%) Mcaps	20.6	108.8	16.7	110.9
Au Si/Pt (12.8%) Mcaps	20.7	108.4	17.1	110.7
Au Si/Pt (23.0%) Mcaps	20.6	120.4	16.8	120.3
Au Si/Pt (41.7%) Mcaps	21.0	120.7	16.7	120.9

In chapter 5 we demonstrated the coverage of silica surface with Pt-NPs at different surface coverages %. The different surface coverage of silica with Pt-NPs resulted in difference in the wettability of the Si/Pt composites. The wettability was measured in terms of the water contact angle, which increased as the silica surface was covered with more Pt-NPs. As the water contact angle (chapter 5, figure 5.12) increased this resulted in the average emulsions size distribution (figure 7.8) of the Pickering emulsion stabilised with the Si/Pt composites to reduce. Table 7.5 and 7.6 illustrate the properties of hexadecane with gold coated Si/Pt stabilised emulsions (MEPCMs).

Table 7. 6: Properties of MEPCMs (gold coated Si/Pt composite stabilised emulsions).

Sample	Theoretical Oil Core %	Encapsulation Ratio (%)	Encapsulation Efficiency (%)
Au Pt-Si (9.4%) Mcaps (10%HD)	70.6	55.9	55.7
Au Pt-Si (12.8%) Mcaps (10%HD)	70.6	55.6	55.5
Au Pt-Si (23.0%) Mcaps (10%HD)	70.6	61.8	61.0
Au Pt-Si (41.7%) Mcaps (10%HD)	70.6	62.0	61.2

Figure 7.8 and table 7.7 demonstrate the comparison of the size of the Si/Pt composite stabilised emulsions and their total emulsion droplet surface area and theoretical shell thickness. By comparing table 7.5 and 7.6 with figure 7.8 and table 7.7, a comparison can be made between the emulsion droplet size, shell thickness affecting the latent heat of fusion, enthalpy of crystallisation, supercooling and thermal stability.

As the emulsion size decreased, this resulted in an increase in the total surface area of the emulsion droplets, as the gold concentration was kept constant this resulted in thinner shells depositing on the smaller emulsions due to larger surface area (table 6.7). As the emulsion size distributions are similar for Si-Pt 9.4% with Si-Pt 12.8% and Si-Pt 23% with Si-Pt 41.7%, the theoretical shell thickness are also similar.

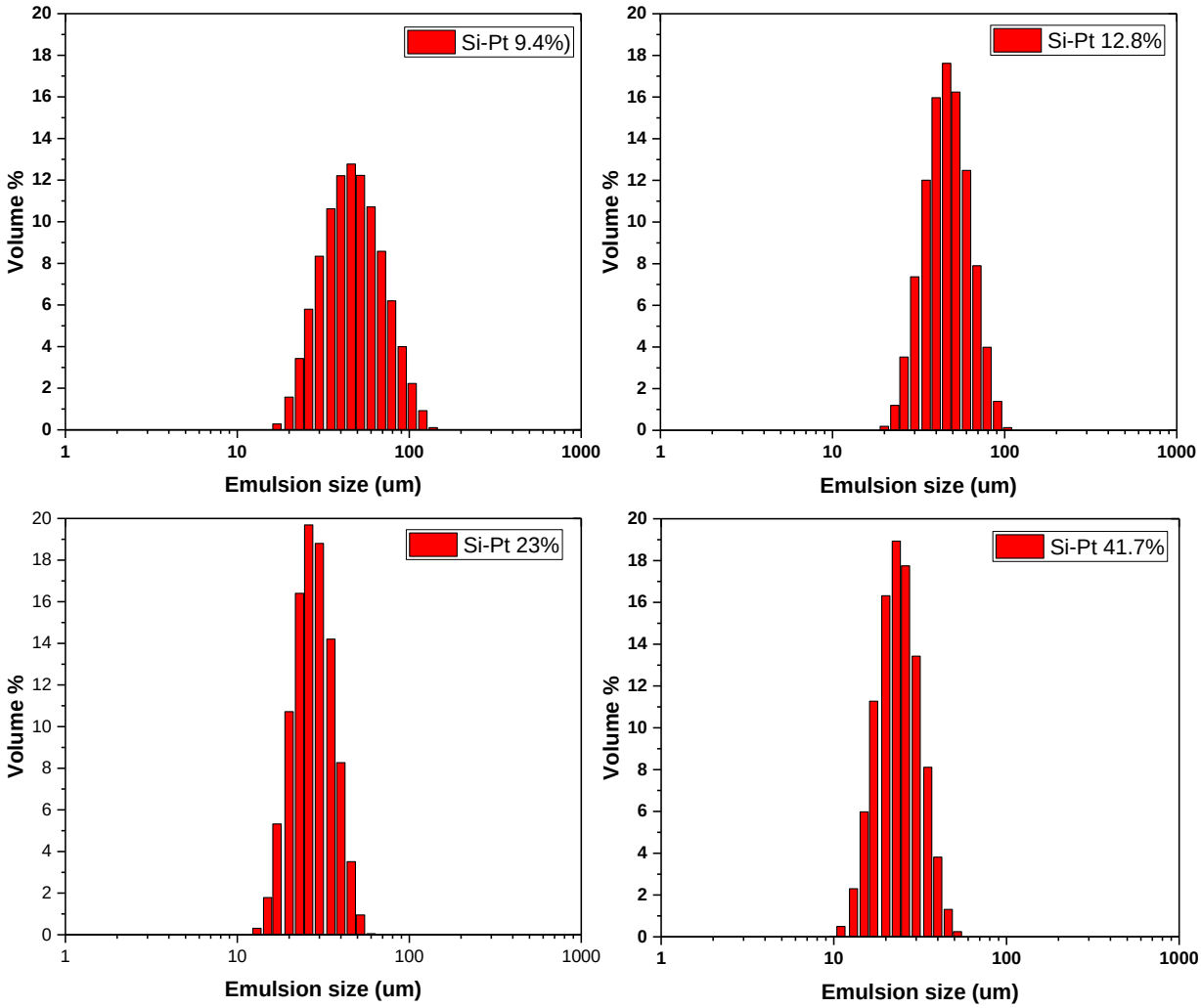

Figure 7. 8: Si-Pt composite 0.1 wt % (Si-Pt 9.4, 12.8 23.0 and 41.7%) stabilised emulsion size distribution (hexadecane oil volume fraction ϕ 0.1 kept constant).

Table 7. 7: Total emulsion surface area (measured figure 6.8, bin limits) and the corresponding theoretical shell thickness, while mass of gold 15.8mg and hexadecane oil volume fraction ϕ 0.1 kept constant.

Sample	Mass of gold (mg)	Total emulsion surface area (measured) ($x10^{17}$ nm^2)	Theoretical shell thickness (nm)
Si-Pt 9.4%	15.8	3.71	44
Si-Pt 12.8%	15.8	3.79	43
Si-Pt 23.0%	15.8	5.46	30
Si-Pt 41.7%	15.8	6.25	26

The encapsulation efficiency% was increased from 55.7 and 55.5% for Si/Pt 9.4 and 12.8% microcapsules to 61 and 61.2% for Si/Pt 23 and 41.7% microcapsules respectively. This could be explained in terms of smaller microcapsules and thinner shells resulted in the transfer of thermal energy more efficiently due to smaller transfer distance whereas larger microcapsules with thicker shells resulted in the reduced efficiency of transfer of thermal energy due to the larger transfer distance.

All the microcapsules incorporating silica into the microcapsules resulted in the reduction of the encapsulation efficiency% and encapsulation ratio%, compared to the theoretical oil core % as silica is non-conductive and would prevent the transfer of thermal energy by forming a physical barrier between the PCM (core) and the gold shell (thermal conductor).

The supercooling of hexadecane was recorded at 5.1°C (difference between melting and freezing), with encapsulating the hexadecane resulted in the reduction of supercooling, for Si/Pt 9.4, 12.8, 23 and 41.7% microcapsules to 3.9, 3.6, 3.8 and 4.3°C respectively. The gold shells resulted in the reduction of supercooling and also enhanced the thermal conductivity by narrowing the DSC curve obtained compared to

the hexadecane curve which is broader. A sharp and narrow DSC curve indicates good thermal conductivity. The narrowing of the DSC curves demonstrated the faster transfer of thermal energy due to the conductivity of the metal shell.

As described in the previous section the Pt-NP stabilised MEPCMs, and the Si/Pt stabilised MEPCMs enhanced thermal conductivity and decreased supercooling, but the incorporation of silica reduced the encapsulation efficiency. Compared to the literature procedure this process brings simplicity in terms of the synthesis of the MEPCMs, requiring the stabilisation of oil in water emulsion by Si/Pt composites followed by electroless gold plating.

7.4.3 Gold coated Pt-Si stabilised emulsions (MEPCMs)

The following section will demonstrate the comparison of hexadecane against MEPCMs (gold coated Si/Pt composite stabilised emulsions containing hexadecane), with varying the hexadecane oil volume fraction ϕ (PCM core). The DSC thermograms in figure 7.9 represent the results obtained for different weights analysed samples so are not directly comparable but data normalised by the mass of hexadecane present in the samples are presented in table 6.9 and 6.10.

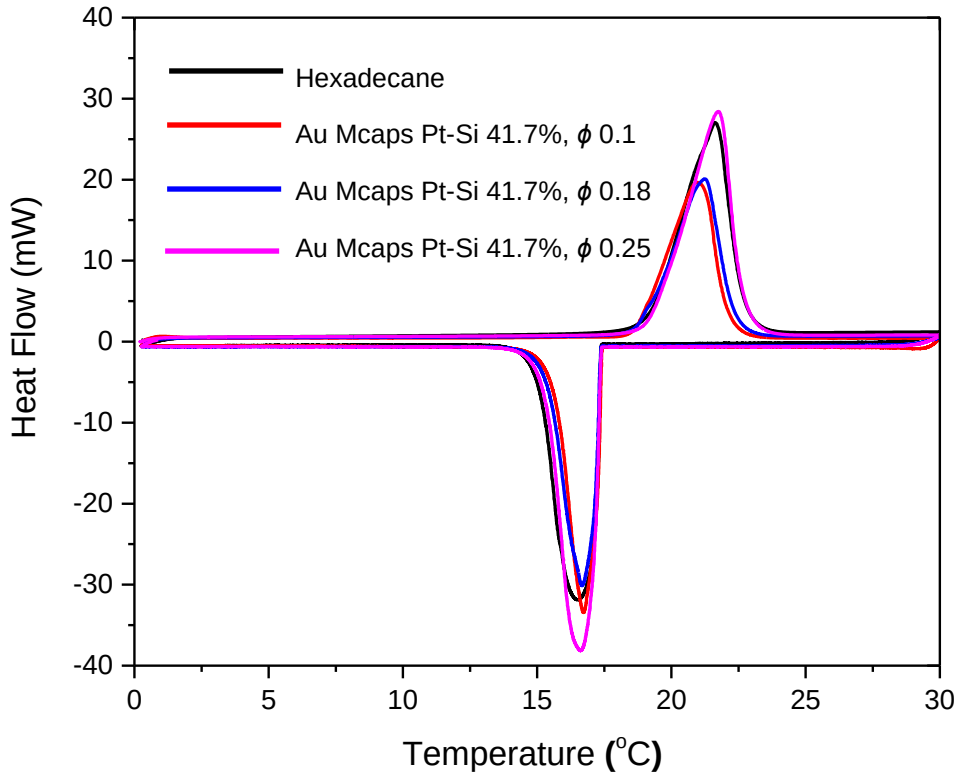

Figure 7. 9: DSC thermograms of hexadecane and dry MEPCMs (Au Mcaps Pt-Si 41.7%) with varying hexadecane oil volume fraction ϕ 0.1, 0.18 and 0.25 in stainless steel pan with lid analysed using the DSC (temp range 0-30°C, heating and cooling rate 2 °C/min).

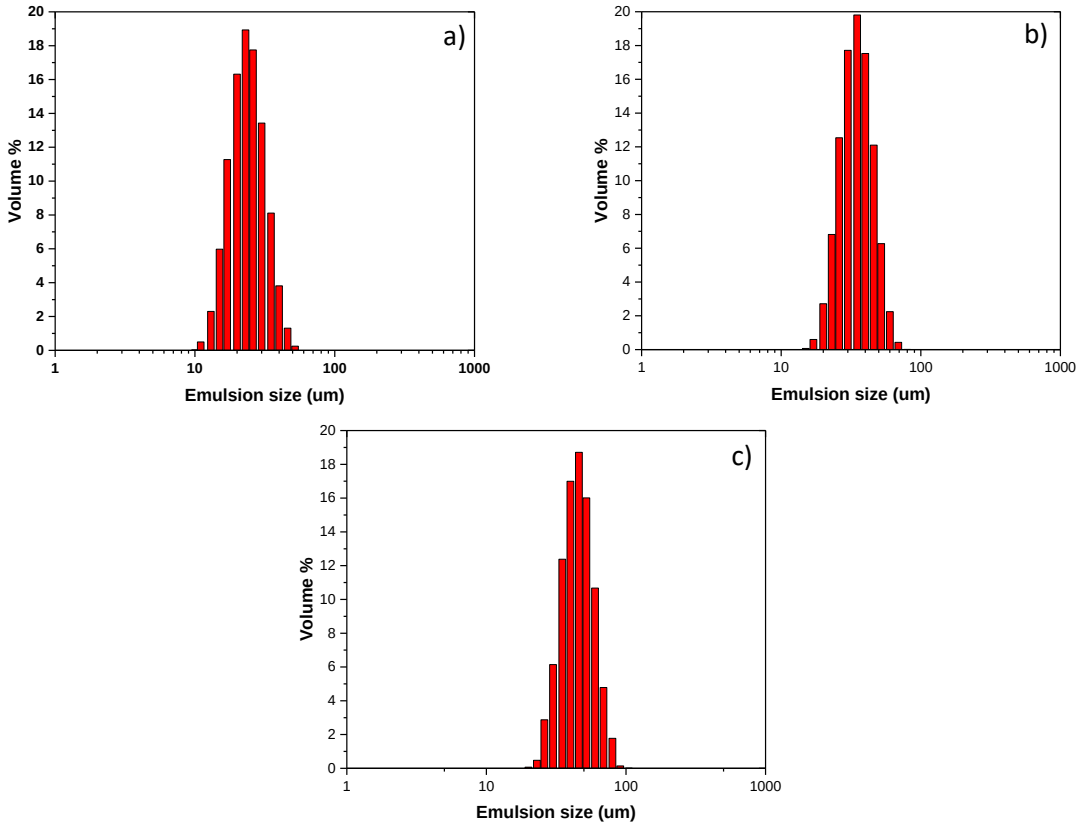

Figure 7. 10: Si/Pt composite 0.1 wt % (Si-Pt 41.7%) stabilised emulsion size distribution (hexadecane oil volume fraction ϕ a- 0.1, b- 0.18 and c- 0.25).

Table 7. 8: Total emulsion surface area (measured figure 6.10, bin limits) and the corresponding theoretical shell thickness, while mass of gold 15.8mg and varying hexadecane oil volume fraction ϕ 0.1, 0.18 and 2.5.

Sample	Hexadecane Oil volume fraction ϕ	Mass of gold (mg)	Total emulsion surface area (measured) ($x10^{17}$ nm^2)	Theoretical shell thickness (nm)
Si-Pt 41.7%	0.1	15.8	6.25	26
Si-Pt 41.7%	0.18	15.8	4.24	43
Si-Pt 41.7%	0.25	15.8	3.00	59

The Pt-Si 41.7% composite was used to stabilise oil in water emulsions with varying hexadecane (oil volume fraction ϕ 0.1, 0.18 and 0.25) the emulsion size distribution is demonstrated in figure 7.10. The emulsion droplets were coated in gold shells (1ml $HAuCl_4$). As only the hexadecane oil volume fraction was varied and the Si/Pt concentration (0.1wt%) and gold concentration was kept constant we would assume the total emulsion surface area and shell thickness would remain constant over the different emulsions size distributions, this was not the case as demonstrated in figure 7.10. The system behaving this way could be due to coalescence in the system as the oil volume fraction was increased, this would also effect the kinetics of the emulsification process and may require more energy for the breakdown of larger emulsion droplets. With the emulsion droplet size increase, resulted in a reduction of the total emulsion surface area resulting in thicker shells (table 7.9), this trend was not expected but we were able to increase the core loading.

Table 7. 9: Properties of hexadecane (PCM) and MEPCMs (gold coated Pt/Si composite 41.7%) stabilised emulsions with varying the concentration of hexadecane oil volume frcation (ϕ 0.1, 0.18 and 0.25). The data for the MEPCMs is normalised based on the mass of the MEPCMs (including shell and PCM mass).

Sample/ oil volume fraction	T_m (°C)	ΔH_M (J/g)	T_c (°C)	ΔH_c (J/g)
Hexadecane	21.7	194.8	16.6	199.9
Au Pt/Si (41.7%) Mcaps (ϕ 0.1)	21.0	120.7	16.7	120.9
Au Pt/Si (41.7%) Mcaps (ϕ 0.18)	21.3	139.7	16.7	145.4
Au Pt/Si (41.7%) Mcaps (ϕ 0.25)	21.7	163.8	16.6	169.3

Table 7. 10: Properties of MEPCMs (gold coated Si/Pt composite stabilised emulsions with varying oil volume fraction).

Sample/oil volume fraction	Theoretical Oil Core %	Encapsulation Ratio (%)	Encapsulation Efficiency (%)
Au Pt/Si (41.7%) Mcaps (ϕ 0.1)	70.6	55.9	61.2
Au Pt/Si (41.7%) Mcaps (ϕ 0.18)	82.8	71.7	72.2
Au Pt/Si (41.7%) Mcaps (ϕ 0.25)	87.8	84.1	84.0

With increasing the hexadecane oil volume fraction resulted in an increase in the encapsulation efficiency from 61.2% (ϕ 0.1) to 84.4% (ϕ 0.25). Also with increasing the hexadecane oil volume fraction resulted in the encapsulation efficiency, encapsulation ratio % and theoretical oil core all being in good agreement. The encapsulation efficiency is based on the phase change enthalpy, increasing the oil volume fraction results in an increase in phase change enthalpy, hence which results in a greater encapsulation efficiency (equation 7.1). The supercooling was reduced to 4.3 and 4.6°C for ϕ 0.1 and ϕ 0.18 oil volume fraction and 5.1°C for ϕ 0.25 oil volume fraction which was the same for hexadecane without encapsulation. At the lower oil volume fraction of hexadecane ϕ 0.1 and ϕ 0.18 resulted in enhanced thermal conductivity by narrowing the DSC curve obtained compared to the pure hexadecane curve which is broader (figure 7.9). For the oil volume fraction of ϕ 0.25, the thermal conductivity was not effected and matched that of hexadecane without encapsulation. Increasing the hexadecane concentration resulted in an increase in encapsulation efficiency, reduced supercooling and increased thermal conductivity up until ϕ 0.18 oil volume fraction.

By increasing the oil volume fraction we were able to drastically increase the encapsulation efficiency over 70% with enhanced thermal conductivity and reduced supercooling. The method of stabilising oil in water emulsion with Pt-NPs followed by gold plaiting had an encapsulation efficiency of ~50% and also from the literature AL-shannaq, *et al.,* also had demonstrated an encapsulation efficiency of 50%.[25] This method does not only provide enhanced thermal conductivity and reduced supercooling but also encapsulation efficiencies above 70%, combined with the simple preparation procedure of synthesising the MEPCMs.

7.5 Conclusion

By depositing gold shells on Pt-NP and Si/Pt stabilised emulsion we demonstrated encapsulation efficiency, encapsulation ratios%, theoretical oil core % and TGA measured oil core % all in good agreement, which demonstrated the shells did not affect the latent heat of fusion and enthalpy of crystallization of the PCMs. By comparing the MEPCMs with pure hexadecane we also demonstrated reduced supercooling and enhanced thermal conductivity. The MEPCMs with gold shells are suitable for use in building materials for home comfort, which would reduce energy consumption.

The metals shells offer an advantage in encapsulating PCMs, by storing and releasing large amounts of thermal energy, demonstrating reduced supercooling, and enhanced thermal stability and conductivity. The disadvantage associated with metal shells, the density of metals reduced the core PCM loading, resulting in lower encapsulation efficiency's. To overcome this, we have demonstrated the stabilisation of oil in water emulsions with Si/Pt composites which are able to encapsulate far higher oil volume fractions than Pt-NP stabilised oil in water emulsions.

The novelty of this work is the demonstration of metal coated PCMs directly onto emulsion droplets, without the initial incorporation of organic or inorganic shell, resulting in higher core loadings, enhanced thermal conductivity and encapsulation efficiency.

7.6 References

1. Energy Statistics Explained. *Energy consumption in households*. 2018, September 3.
2. Eurostat Statistics Explained. *Archive:Consumption of energy*. 2018, September 2018; Available from: https://ec.europa.eu/eurostat/statistics-explained/index.php?title=Archive:Consumption_of_energy.
3. Sarbu, I. and C. Sebarchievici, *A Comprehensive Review of Thermal Energy Storage.* Sustainability, 2018. **10**(1).
4. Berthou, Y., et al., *Full scale experimentation on a new translucent passive solar wall combining silica aerogels and phase change materials.* Solar Energy, 2015. **115**: p. 733-742.
5. Sharma, A., et al., *Review on thermal energy storage with phase change materials and applications.* Renewable & Sustainable Energy Reviews, 2009. **13**(2): p. 318-345.
6. Zhang, H.Z. and X.D. Wang, *Synthesis and properties of microencapsulated n-octadecane with polyurea shells containing different soft segments for heat energy storage and thermal regulation.* Solar Energy Materials and Solar Cells, 2009. **93**(8): p. 1366-1376.
7. Tzvetkov, G. and R.H. Fink, *Temperature-dependent X-ray microspectroscopy of phase-change core-shell micropsules.* Scripta Materialia, 2008. **59**(3): p. 348-351.
8. Abhat, A., *Low-Temperature Latent-Heat Thermal-Energy Storage - Heat-Storage Materials.* Solar Energy, 1983. **30**(4): p. 313-332.
9. Himran, S., A. Suwono, and G.A. Mansoori, *Characterization of Alkanes and Paraffin Waxes for Application as Phase-Change Energy-Storage Medium.* Energy Sources, 1994. **16**(1): p. 117-128.
10. Feldman, D., M.M. Shapiro, and D. Banu, *Organic-Phase Change Materials for Thermal-Energy Storage.* Solar Energy Materials, 1986. **13**(1): p. 1-10.

11. Hasan, A. and A.A. Sayigh, *Some Fatty-Acids as Phase-Change Thermal-Energy Storage Materials.* Renewable Energy, 1994. **4**(1): p. 69-76.
12. Lin, Y.X., et al., *Review on thermal conductivity enhancement, thermal properties and applications of phase change materials in thermal energy storage.* Renewable & Sustainable Energy Reviews, 2018. **82**: p. 2730-2742.
13. Sharma, S.D., et al., *Design, development and performance evaluation of a latent heat storage unit for evening cooking in a solar cooker.* Energy Conversion and Management, 2000. **41**(14): p. 1497-1508.
14. Kumar, A. and S.K. Shukla, *A Review on Thermal Energy Storage Unit for Solar Thermal Power Plant Application.* International Conference on Technologies and Materials for Renewable Energy, Environment and Sustainability -Tmrees15, 2015. **74**: p. 462-469.
15. Sari, A., et al., *Microencapsulated n-octacosane as phase change material for thermal energy storage.* Solar Energy, 2009. **83**(10): p. 1757-1763.
16. Su, W.G., et al., *Preparation of microencapsulated phase change materials (MEPCM) for thermal energy storage.* Improving Residential Energy Efficiency International Conference, Iree 2017, 2017. **121**: p. 95-101.
17. Zhang, H.Z., X.D. Wang, and D.Z. Wu, *Silica encapsulation of n-octadecane via sol-gel process: A novel microencapsulated phase-change material with enhanced thermal conductivity and performance.* Journal of Colloid and Interface Science, 2010. **343**(1): p. 246-255.
18. Yu, S.Y., X.D. Wang, and D.Z. Wu, *Microencapsulation of n-octadecane phase change material with calcium carbonate shell for enhancement of thermal conductivity and*

serving durability: Synthesis, microstructure, and performance evaluation. Applied Energy, 2014. **114**: p. 632-643.

19. Li, B.X., et al., *Fabrication and Properties of Microencapsulated Paraffin@SiO2 Phase Change Composite for Thermal Energy Storage.* Acs Sustainable Chemistry & Engineering, 2013. **1**(3): p. 374-380.
20. Yang, Y.Y., et al., *Polymethyl methacrylate based phase change microencapsulation for solar energy storage with silicon nitride.* Solar Energy, 2015. **115**: p. 289-296.
21. Yin, D.Z., et al., *Microencapsulation of hexadecane by surface-initiated atom transfer radical polymerization on a Pickering stabilizer.* New Journal of Chemistry, 2015. **39**(1): p. 85-89.
22. Singh, K.G.K., et al., *Microencapsulation of Paraffin Wax Microspheres with Silver.* Defence Science Journal, 2018. **68**(2): p. 218-224.
23. Zhu, Y.L., et al., *Novel metal coated nanoencapsulated phase change materials with high thermal conductivity for thermal energy storage.* Solar Energy Materials and Solar Cells, 2018. **176**: p. 212-221.
24. Song, Q.W., et al., *Thermal stability of composite phase change material microcapsules incorporated with silver nano-particles.* Polymer, 2007. **48**(11): p. 3317-3323.
25. Al-Shannaq, R., et al., *Innovative method of metal coating of microcapsules containing phase change materials.* Solar Energy, 2016. **129**: p. 54-64.

8 Conclusion and future work

8.1 Conclusion

It has been successfully demonstrated the synthesis of platinum nanoparticles stabilised with PVP, resulting in Pt-NPs. The adsorption of the Pt-NPs onto the surface of colloidal silica, resulting in Si-Pt composites. Pt-NPs, Si-Pt composites and colloidal silica particles were utilised to stabilise oil in water Pickering emulsions.

The Pt-NPs and Si-Pt composite stabilised emulsions were subsequently coated in gold by utilising the ability of Pt-NPs at the oil/water interface and on the surface of colloidal silica at the oil/water interface to act as a catalyst and also provide a nucleation and deposition site for metal film growth via electroless plating resulting in gold coated emulsion droplets.

The ability of dopamine to self-polymerise and deposit on solid surfaces was utilised to deposit PDA on colloidal silica stabilised oil in water emulsions resulting in PDA microcapsules. The PDA microcapsules were subsequently coated in a silver shell, by utilising the catechol and nitrogen containing groups on the PDA surface to reduce the silver ions to silver on the PDA surface resulting in silver coated PDA microcapsules. As the silver reduction was insensitive to the PDA surface a mild reducing agent (glucose) was used, resulting in increased reaction times. Even with the use of a mild reducing agent still resulted in some of the silver reducing in the continuous phase and aggregating.

The gold coated, Pt-NPs and Si-Pt composite stabilised oil in water emulsion droplets, demonstrated complete retention of the core (hexadecane) and complete impermeability of the gold shell when introduced to a continuous phase of ethanol/water (volume ratio 4:1) which could completely solubilise the hexadecane core, for over 30 days at 40^{o}C. Silver coated PDA microcapsules, released most of the hexadecane core after 1 hour when introduced to a continuous phase of ethanol/water (volume ratio 4:1) due to the in-sufficient coverage of the PDA surface with silver. By utilising the ability of Pt-NPs to act as a catalyst and also provide a nucleation and deposition site for metal film growth via electroless deposition, continuous impermeable gold films were deposited on Pt-NP and Si/Pt composite stabilised emulsion droplets.

The gold coated, Pt-NP and Si/Pt composite stabilised emulsion droplets were analysed for their abilities to encapsulate PCM (hexadecane) and tested for thermal energy storage/release, supercooling, encapsulation efficiency and thermal conductivity. The gold coated emulsion droplets demonstrated good thermal energy storage and release, good encapsulation efficiency, reduced supercoiling and enhanced thermal conductivity. The silver coated PDA microcapsules were not analysed as the microcapsules were permeable.

Gold coated, Pt-NP and Si/Pt composite stabilised emulsions can be utilised for completely retaining low molecular weight actives in a continuous phase where the active is completely soluble. These microcapsules can be utilised for fragrance delivery in perfumes. The gold coated Pt-NP and Si-Pt composite stabilised emulsions

can also be utilised for encapsulating PCM (hexadecane) for heat storage and transfer in building applications, to reduce energy consumption for home comfort.

8.2 Future work

From chapter 4 the gold coated microcapsules can be applied to other applications besides from fragrance retention and delivery, to drug retention and delivery. As existing microencapsulation methods tend to be leaky due to the porosity of polymer shells, our gold films are able to form a continuous impermeable barrier, completely retaining the core. As gold is inert, the microcapsules can be utilised for encapsulating drugs and the targeted delivery of the microcapsules to a specific target site by utilising a magnetic. As the microcapsule shell is thin we may require thicker shells to apply a magnetic force for target delivery. In this case cheaper metal pairings may be required for thicker shells, rather than platinum and gold to reduce the costs of thicker shells. Once the microcapsules have reached their target site ultra-sound can be applied for breaking the microcapsules as we demonstrated the ability of ultra-sound to break the metal coated microcapsules, and release the payload at the target site.

Chapter 5 demonstrated the use of Si/Pt composites to stabilise emulsion encapsulating high volumes of PCMs through direct deposition of a secondary metal film. As we demonstrated the ability of the microcapsules for thermal energy storage and release, the microcapsules could be incorporated into building materials and analysed in real application scenarios for heat storage and release.

Silver reduction on PDA microcapsule surface did not result in a continuous impermeable metal film. Further work is required to understanding the silver reduction process to synthesis a complete continuous impermeable metal film. The parameters effecting dopamine polymerisation and deposition need to be analysed and tested to understand the mechanism of PDA synthesis, deposition and adhesion to silica surface. Varying thickness of silver shells are required to deposit on PDA microcapsules to analyse the effect of thicker shells on permeability.

9 Appendix

9.1 **Pt-PVP NP TEM**

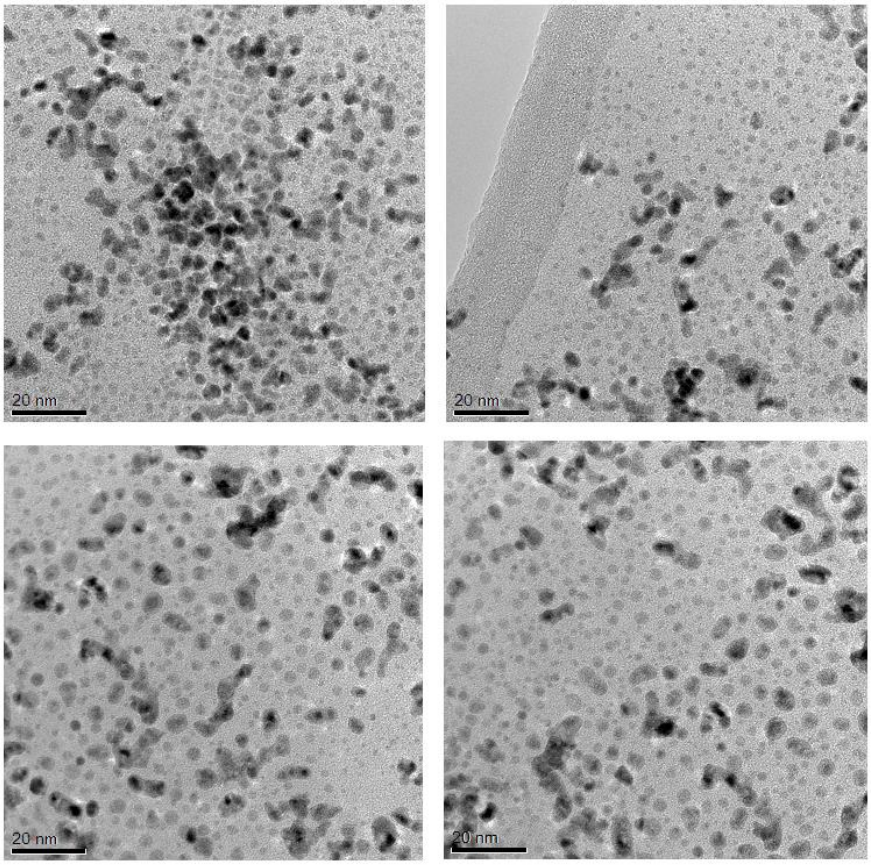

Figure 9. 1:Transmission electron micrographs of Pt-NPs deposited on TEM grids 24 hours after synthesis conducted using the following conditions: (5.6 mM) $PtCl_6H_2$, (1.1 mM) $NaBH_4$ and (0.0067wt% 10kDa) PVP.

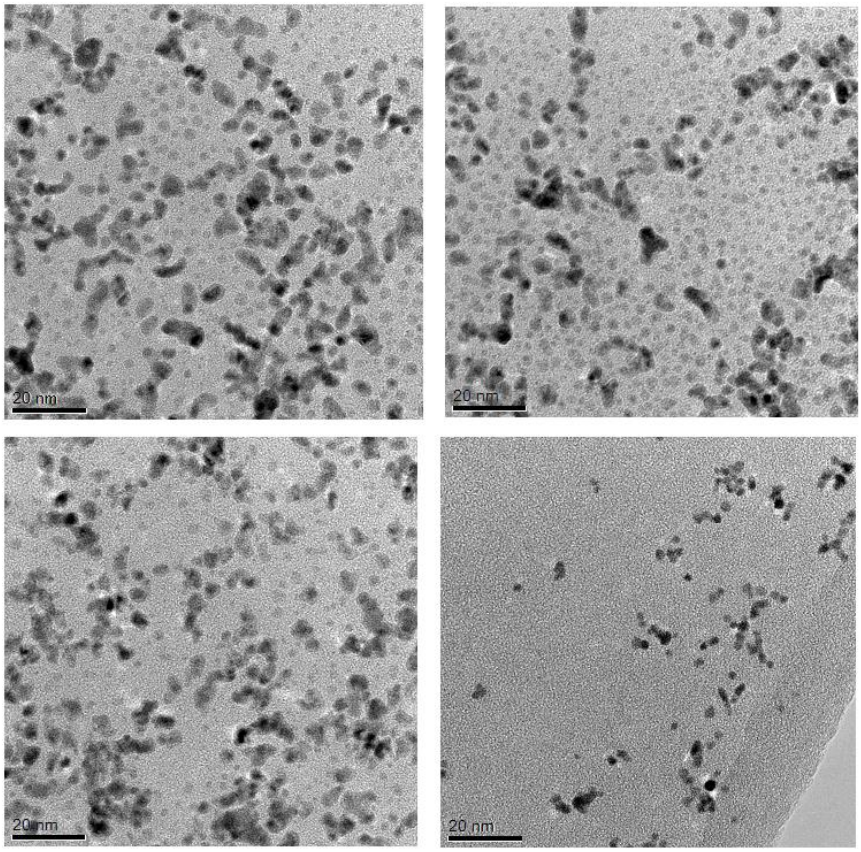

Figure 9. 2:Transmission electron micrographs of Pt-NPs deposited on TEM grids 24 hours after synthesis conducted using the following conditions: (5.6 mM) $PtCl_6H_2$, (1.1 mM) $NaBH_4$ and (0.0067wt% 40kDa) PVP.

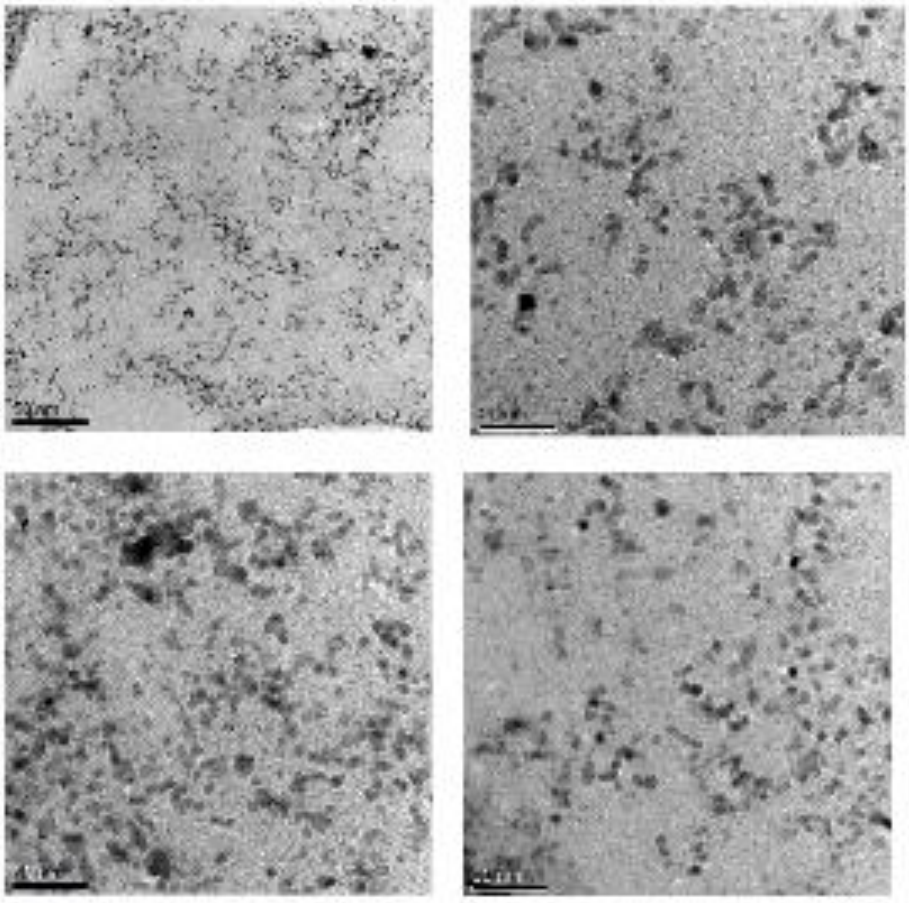

Figure 9. 3: Transmission electron micrographs of Pt-NPs deposited on TEM grids 24 hours after synthesis conducted using the following conditions: (5.6 mM) $PtCl_6H_2$, (1.1 mM) $NaBH_4$ and (0.0067wt% 10kDa) PVP.

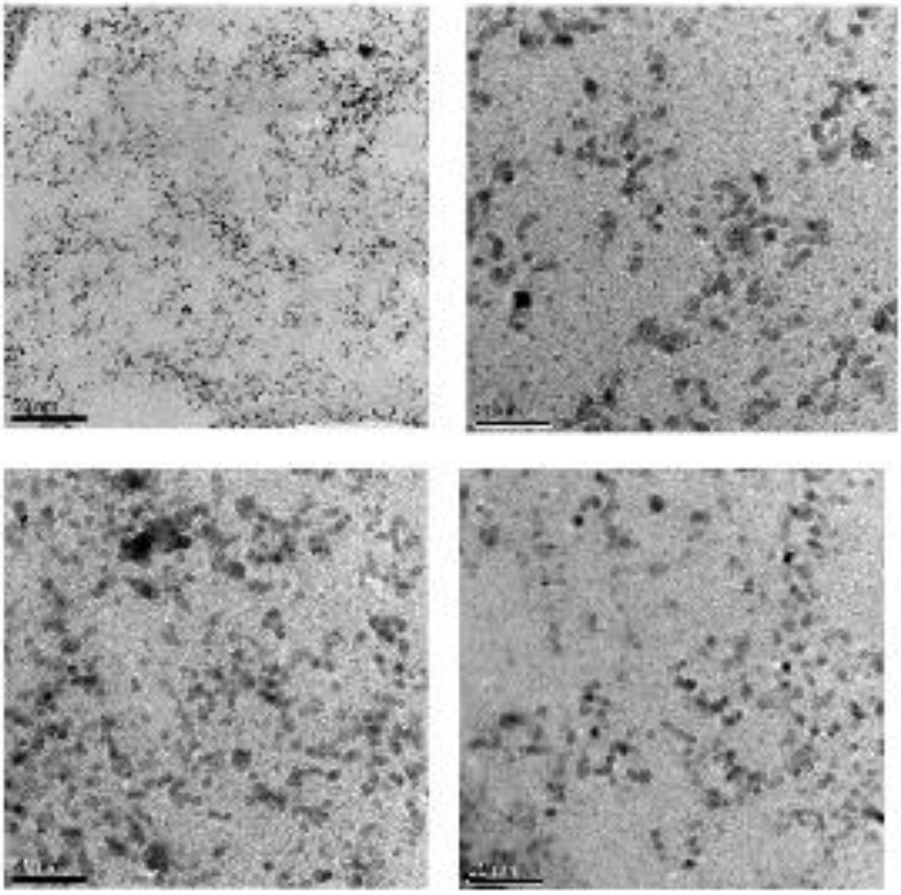

Figure 9. 4: Transmission electron micrographs of Pt-NPs deposited on TEM grids 24 hours after synthesis conducted using the following conditions: (5.6 mM) $PtCl_6H_2$, (1.1 mM) $NaBH_4$ and (0.0067wt% 10kDa) PVP.

9.2 UV-Vis spectroscopy

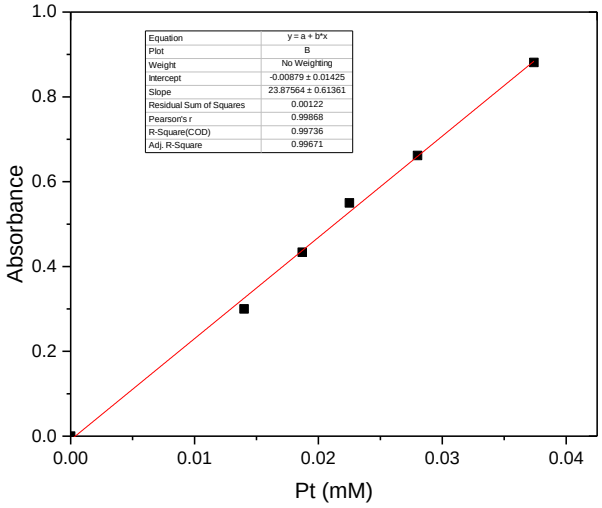

Figure 9. 5: UV-Vis Absorbance calibration as a function of Pt-NP concentration.

Table 9. 1: UV-Vis absorbance of free remaining Pt-NPs

Sample	Silica (g)	Pt PVP NPs (ml)	UV-Vis absorbance of free remaining Pt-NPs
1	0.1	3.3	0.01633
2	0.1	8.25	0.647609
3	0.1	16.5	0.562654 (x2)
4	0.1	33	0.624649 (x2)